



UNIVERSITAT DE
BARCELONA

Characterization of the proteome and palmitoylome alterations induced by palmitic and oleic acids in OSCC cells

Uxue Urdiroz Urricelqui

ADVERTIMENT. La consulta d'aquesta tesi queda condicionada a l'acceptació de les següents condicions d'ús: La difusió d'aquesta tesi per mitjà del servei TDX (www.tdx.cat) i a través del Dipòsit Digital de la UB (diposit.ub.edu) ha estat autoritzada pels titulars dels drets de propietat intel·lectual únicament per a usos privats emmarcats en activitats d'investigació i docència. No s'autoritza la seva reproducció amb finalitats de lucre ni la seva difusió i posada a disposició des d'un lloc aliè al servei TDX ni al Dipòsit Digital de la UB. No s'autoritza la presentació del seu contingut en una finestra o marc aliè a TDX o al Dipòsit Digital de la UB (framing). Aquesta reserva de drets afecta tant al resum de presentació de la tesi com als seus continguts. En la utilització o cita de parts de la tesi és obligat indicar el nom de la persona autora.

ADVERTENCIA. La consulta de esta tesis queda condicionada a la aceptación de las siguientes condiciones de uso: La difusión de esta tesis por medio del servicio TDR (www.tdx.cat) y a través del Repositorio Digital de la UB (diposit.ub.edu) ha sido autorizada por los titulares de los derechos de propiedad intelectual únicamente para usos privados enmarcados en actividades de investigación y docencia. No se autoriza su reproducción con finalidades de lucro ni su difusión y puesta a disposición desde un sitio ajeno al servicio TDR o al Repositorio Digital de la UB. No se autoriza la presentación de su contenido en una ventana o marco ajeno a TDR o al Repositorio Digital de la UB (framing). Esta reserva de derechos afecta tanto al resumen de presentación de la tesis como a sus contenidos. En la utilización o cita de partes de la tesis es obligado indicar el nombre de la persona autora.

WARNING. On having consulted this thesis you're accepting the following use conditions: Spreading this thesis by the TDX (www.tdx.cat) service and by the UB Digital Repository (diposit.ub.edu) has been authorized by the titular of the intellectual property rights only for private uses placed in investigation and teaching activities. Reproduction with lucrative aims is not authorized nor its spreading and availability from a site foreign to the TDX service or to the UB Digital Repository. Introducing its content in a window or frame foreign to the TDX service or to the UB Digital Repository is not authorized (framing). Those rights affect to the presentation summary of the thesis as well as to its contents. In the using or citation of parts of the thesis it's obliged to indicate the name of the author.

Universitat de Barcelona

Facultat de farmàcia i ciències de l'alimentació

Characterization of the proteome and palmitoylome alterations induced by palmitic and oleic acids in OSCC cells

Uxue Urdiroz Urricelqui

Programa de doctorado en Biomedicina

Diciembre de 2021



UNIVERSITAT DE
BARCELONA

Facultat de Farmàcia
i Ciències de l'Alimentació

Programa de doctorado en Biomedicina
Facultat de farmàcia i ciències de l'alimentació

Institut de Recerca Biomèdica de Barcelona (IRB Barcelona)

Characterization of the proteome and palmitoylome alterations induced by palmitic and oleic acids in OSCC cells

Memòria presentada per Uxue Urdiroz Urricelqui per optar al grau de
doctora per la Universitat de Barcelona

Uxue Urdiroz Urricelqui

Director:
Salvador Aznar Benitah

Co-director:
Miguel Martin Perez

Tutor: Antonio Zorzano Olarte

**Antonio
Zorzano** Digitally signed
by Antonio
Zorzano
Date: 2021.12.14
10:08:02 +01'00'

 UNIVERSITAT DE
BARCELONA

Facultat de Farmàcia
i Ciències de l'Alimentació

Diciembre de 2021

ABSTRACT

The role of lipid metabolism in cancer progression is currently being re-evaluated. Recent studies from our laboratory show that the metastatic potential of cancer cells is increased upon palmitic acid (PA) treatment in cell culture or a PA-enriched diet in mice. In contrast, the same experiments but using oleic acid (OA) appeared to decrease the metastatic capacity, suggesting that distinct dietary fatty acids (FAs) can have distinct effects on tumour cells. The pro-metastatic effects of PA appear to be mediated by an epigenetic memory, via unknown mechanisms. To characterize how PA primes cancer cells to a pro-metastatic state, we used proteomics-based methodologies to analyze the cellular signaling elicited by PA and OA. In cell culture, we observed that the proteome of oral squamous cell carcinoma (OSCC) cell lines changes in opposite directions when treated with PA or OA. In stark contrast, analyzing the proteome of tumour cells growing orthotopically in mice fed a palm oil-enriched (e.g., PA-enriched) or an olive oil-enriched (e.g., OA-enriched) diet revealed that both diets have similar effects, although the magnitude of the induced changes is more prominent in the PA-enriched diet. This could reflect the fact that the dietary oils (palm and olive) are composite of FAs, rather than pure FAs. Nonetheless, several distinctions are still present. One of the top categories specifically upregulated by a PA-enriched diet is the post-translational modification of protein S-palmitoylation: the DHHC protein acyl transferases are upregulated by the diet, and their gene expression is enhanced, by PA treatment in culture and in lymph node metastases as compared to primary tumours. The palmitoylome of a pro-metastatic OSCC cell line is enriched in proteins involved in membrane functions such as cell motility or cell adhesion. Interestingly, cells treated with PA showed an increase in the palmitoylation state of the proteome as compared to those treated with OA or control. Of note, we found that [REDACTED] has increased levels of palmitoylation after PA treatment. We determined that [REDACTED] is the predominantly palmitoylated [REDACTED] in OSCC, while the [REDACTED] were palmitoylated to the same degree in melanoma cells, and we identified [REDACTED] as the S-palmitoylated residue of [REDACTED]. Subcellular fractionation and cell imaging experiments suggest that this residue is not involved in the [REDACTED] [REDACTED] or in the tethering of the [REDACTED]; thus, the functionality of [REDACTED] palmitoylation remains to be elucidated.

RESUMEN

El papel que juega el metabolismo lipídico en la progresión del cáncer está siendo revisado. Estudios recientes de nuestro laboratorio demuestran que el tratamiento con ácido palmítico (AP) de células en cultivo o una dieta rica en AP en ratones incrementan la capacidad metastática de las células cancerosas. Sin embargo, los mismos experimentos realizados con ácido oleico (AO) disminuyen la capacidad metastática, lo cual sugiere que cada ácido graso (AG) de nuestra dieta tiene un efecto diferente en las células tumorales. El efecto pro-metastático del AP es mediado por una memoria epigenética, pero su mecanismo no se ha comprendido completamente todavía. Para caracterizar el mecanismo por el cual el AP induce un estado pro-metastático en las células, decidimos estudiar mediante análisis proteicos los cambios en la señalización celular provocados por el AP y el AO. Observamos que el proteoma de las líneas celulares de carcinoma oral de células escamosas (COCE) cambia en direcciones opuestas en respuesta a los tratamientos con AP o AO en cultivo. Por el contrario, el análisis del proteoma de células tumorales creciendo ortotópicamente en animales alimentados con dietas enriquecidas con aceite de palma (rico en AP) o aceite de oliva (rico en AO) mostró que ambas dietas inducen cambios similares, aunque la magnitud de dichas alteraciones es mayor en la dieta rica en AP. Esta diferencia podría ser causada por el hecho de que los aceites de la dieta (palmítico y oleico) están compuestos por diversos AG, no son AG puros. A pesar de ello, observamos ciertas diferencias en los cambios inducidos por cada dieta. Una de las principales categorías específicamente incrementadas con la dieta rica en AP fue la S-palmitoilación: las acil-proteína transferasas DHHC son aumentadas por esta dieta y su expresión génica incrementa con el tratamiento con AP en cultivo y en las metástasis en nódulos linfáticos en comparación con los tumores primarios. El estudio del palmitoiloma de células COCE pro-metastáticas, indicó que está enriquecido en proteínas involucradas en funciones de la membrana celular como movilidad o adhesión celular. Pudimos observar que las células tratadas con AP muestran un aumento en el nivel de palmitoilación de su proteoma comparadas con las tratadas con AO o las células control. Descubrimos [REDACTED] entre las proteínas cuya palmitoilación aumenta con AP, lo cual podría ser un hecho de especial relevancia dado su papel [REDACTED]. Determinamos que [REDACTED] predominantemente palmitoilada en COCE, mientras que las células de melanoma muestran una estequiometría de palmitoilación similar entre [REDACTED], e identificamos [REDACTED] como el residuo S-palmitoilado en la [REDACTED]. Experimentos de fraccionamiento celular y microscopía sugieren que este residuo no está implicado ni en [REDACTED] ni en la interacción [REDACTED], por lo que queda todavía por dilucidar cual es la función de la palmitoilación de [REDACTED]

TABLE OF CONTENTS

TABLES AND FIGURES	1
LIST OF ABBREVIATIONS	5
INTRODUCTION	13
1 Cancer & lipid metabolism	15
1.1 Head and neck squamous cell carcinomas (HNSCC)	15
1.2 The hallmarks of cancer	16
1.2.1 Tissue invasion and metastasis	17
1.2.2 Deregulation of cellular energetics as an emerging hallmark of cancer	20
1.3 Lipid metabolism and cancer	22
1.3.1 Lipids & lipid metabolism, a general view	22
1.3.1.1 Lipids	22
1.3.1.2 Lipid metabolism	23
1.3.2 Influence of the lipid metabolism in the metastatic cascade	27
1.3.2.1 Alterations of the lipid metabolism within the cancer cell	27
1.3.2.2 Alterations of the lipid metabolism within the main cells of the TME	32
1.3.3 Lipid metabolism in the resistance to therapy	34
1.3.4 Targeting lipid metabolism	36
2 Lipid modifications of proteins	39
2.1 Protein S-acylation (S-palmitoylation)	42
2.1.1 Protein acyl transferases (PATs)	42
2.1.1.1 Protein structure	43
2.1.1.2 Substrate specificity	44
2.1.1.3 Acyl-CoA specificity	45
2.1.2 Protein thioesterases	49
2.1.2.1 APT1/2	49
2.1.2.2 PPT1/2	50
2.1.2.3 ABHD17	50
2.1.3 Functions of protein palmitoylation	51
2.1.3.1 Membrane association and protein trafficking	51
2.1.3.2 Signaling and regulation of protein function	53
2.1.4 Regulation of protein palmitoylation	54
2.1.5 Protein palmitoylation and cancer	56
2.1.6 Targeting protein palmitoylation	58
3	63
3.1 Chromatin & epigenetics	63
3.2	64
3.2.1	64
3.2.1.1 Genetic and proteomic characteristics of	65
3.2.1.2 Genomic location and function of	66
3.2.2 and cancer	67
3.2.2.1 mutations	67
3.2.2.2 Alteration of	68
3.3 PTMs	69
3.3.1 PTMs on the domain	69
3.3.2 acylation	71

3.3.2.1	██████████ acylation	72
3.3.2.2	Metabolic regulation of ██████████ acylation	72
BACKGROUND, HYPOTHESIS AND OBJECTIVES		75
MATERIALS & METHODS		79
1	Cell culture	81
1.1	Stable isotope labelling by amino acids in cell culture (SILAC)	81
1.2	FA stimulation	83
1.3	Retroviral particle generation and infection ██████████ overexpression	83
1.4	Cell viability	83
2	Treatments preparation	84
3	██████████ overexpression construct design	84
4	Animal studies	85
4.1	PT generation and follow up	85
4.2	Metastasis quantification	85
4.3	Dietary intervention	85
5	Single cell preparation from tumours	87
6	Fluorescence activated cell sorting (FACS)	87
7	Immunofluorescence staining	88
8	Protein and peptide sample preparation	88
8.1	Protein extraction	88
8.2	Click-chemistry	90
8.3	Chloroform-methanol precipitation of proteins	90
8.4	Enrichment of palmitoylated proteins	91
8.5	Protein alkylation and reduction	91
8.6	Tryptic digestion of protein	91
8.7	Peptides desalting	92
8.7.1	Sep-Pak columns	92
8.7.2	StageTip	92
8.8	Deep reverse-phase basic fractionation of the proteome	92
9	Liquid chromatography-mass spectrometry (LC-MS) analysis	93
9.1	In culture SILAC-based proteomic analysis (Thermo Scientific Q Exactive)	93
9.1.1	LC-MS/MS method	93
9.1.2	MS data analysis	93
9.2	In vivo LFQ-based proteomic analysis (Bruker timsTOF Pro)	94
9.2.1	LC-MS/MS method	94
9.2.2	MS data analysis	94
10	Immunoprecipitation	95
11	In gel fluorescence detection and Western Blot	95

11.1	SDS-polyacrylamide gel electrophoresis (SDS-PAGE)	95
11.2	In-gel fluorescence detection	95
11.3	Western blot	95
11.3.1	HRP inactivation	96
11.3.2	Harsh stripping	96
12	<i>Real-time quantitative PCR (RT-qPCR)</i>	97
13	<i>Statistical analyses</i>	97
14	<i>Antibodies</i>	98
RESULTS		99
1	<i>Changes in the proteome induced by dietary PA and OA in OSCC</i>	101
1.1	Changes in the proteome of OSCC cells induced by cell culture treatment with PA and OA	101
1.1.1	Proteomic changes induced in SCC-25	101
1.1.2	Comparison of the response induced by PA and OA in two different OSCC cell lines: SCC-25 and VDH-15	104
1.2	Changes in the proteome of SCC-25 induced by PA- and OA-enriched diets in mice	105
2	<i>Palmitoylome studies</i>	111
2.1	Phenotypic characterization of 17-ODYA in OSCC	112
2.1.1	Incorporation of 17-ODYA into proteins	112
2.1.2	Metastatic phenotype induced by 17-ODYA treatment	114
2.1.3	Proteomic changes induced by 17-ODYA	118
2.2	Palmitoylome of metastatic SCC-25	119
2.3	Validation of palmitoylated proteins	123
2.4	Changes in protein palmitoylation induced by PA and OA treatments	125
3	<i>Characterization of [REDACTED] palmitoylation</i>	129
3.1	Validation of the palmitoylation of [REDACTED]	129
3.2	Identification of the S-palmitoylated Cys residue	130
3.3	Function of [REDACTED] palmitoylation at [REDACTED]	133
3.3.1	[REDACTED] is not implicated in its [REDACTED]	133
3.3.2	[REDACTED] is not implicated in the [REDACTED] localization of [REDACTED]	135
DISCUSSION		137
1	<i>Changes in the proteome induced by dietary PA and OA in OSCC</i>	139
1.1	Dietary PA vs OA in healthy and cancer cells	139
1.2	Cell culture vs animal studies	142
1.3	Dietary interventions in cancer	143
2	<i>Palmitoylome studies</i>	145
2.1	Variability within palmitoylome studies	148
2.1.1	Metabolic labelling vs chemical labelling	149
3	<i>[REDACTED] palmitoylation</i>	151

3.1	Palmitoylation of the	151
3.2	S-palmitoylation of	151
3.3	Functions of	153
3.3.1	Structural functions of	153
3.3.2	Implication of in the	155
CONCLUSIONS		159
REFERENCES		163

TABLES AND FIGURES

Tables

Introduction

Lipid modifications on proteins

- Table I2.1. Summary of the different types of fatty-acylations that proteins can undergo. *(Page 40)*
- Table I2.2 A & B. Detail of the structural characteristics, location and examples of substrates of each DHHC-PAT. *(Pages 47-48)*
- Table I2.3 Described inhibitors of protein thioesterases. *(Page 60)*

Materials & Methods

- Table M&M1. Isotopes used for SILAC experiments. *(Page 82)*
- Table M&M2. Protein, carbohydrate and lipid composition of each experimental diet. *(Page 86)*
- Table M&M3. Origin of the fat and percentage of PA and OA contained in each diet. *(Page 86)*
- Table M&M4. Antibodies used. *(Page 98)*

Figures


Introduction

Cancer & lipid metabolism

- Figure I1.1. The hallmarks of cancer. *(Page 16)*
- Figure I1.2. The metastatic cascade. *(Page 19)*
- Figure I1.3. Projected rates of obesity in the OECD. *(Page 21)*
- Figure I1.4. PA and OA chemical structure. *(Page 23)*
- Figure I1.5. Overview of the major lipid metabolism pathways. *(Page 25)*
- Figure I1.6. Only PA can boost the metastatic capacity of OSCC cells. *(Page 28)*
- Figure I1.7. Influence of lipid metabolism in the metastatic cascade. *(Page 29)*
- Figure I1.8. Influence of metabolism in the functionality of the immune cells within the TME. *(Page 34)*

Lipid modifications on proteins

- Figure I2.1. Examples of structures of DHHC-PATs. *(Page 43)*
- Figure I2.2. Phylogenetic tree of DHHC-PATs. *(Page 44)*
- Figure I2.3. Detail of the S-acylation reaction. *(Page 46)*
- Figure I2.4. CD36 acylation/deacylation cycle. *(Page 55)*

- Figure I3.1. Chromatin condensation. *(Page 63)*
- Figure 3.2. Alignment of the amino acid sequences of human  *(Page 65)*

- Figure I3.3. Classification of Lys acyl groups. *(Page 71)*

Materials & Methods

- Figure M&M1. SILAC proteomics. *(Page 82)*

Results

Changes in the proteome induced by dietary PA and OA in OSCC

- Figure R1.1. CD36 changes induced by PA and OA in SCC-25. *(Page 101)*
- Figure R1.2. PA and OA treatments induce an opposite proteomic response in SCC-25. *(Page 102)*
- Figure R1.3. Proteome and transcriptome changes correlate in PA treated cells. *(Page 103)*
- Figure R1.4. Similar results are obtained with a second OSCC cell line: VDH-15. *(Page 105)*
- Figure R1.5. Mouse OSCC dietary model scheme and sorting strategy. *(Page 106)*
- Figure R1.6. PA- and OA-enriched HFDs do not induce opposite responses. *(Page 107)*
- Figure R1.7. Protein palmitoylation and DHHC-PATs are upregulated in SCC-25 upon PA-enriched diet mice feeding. *(Page 108)*
- Figure R1.8. ZDHHCs gene expression is upregulated by PA cell culture treatment and in the LN metastases in mice. *(Page 109)*

Palmitoylome studies

- Figure R2.1. 17-ODYA and the metabolic labelling of palmitoylated proteins. *(Page 111)*
- Figure R2.2. 17-ODYA is incorporated into proteins in a dose and time dependent manner. *(Page 113)*
- Figure R2.3. 17-ODYA is incorporated into proteins by the same enzymatic machinery than PA and can compete with it. *(Page 114)*
- Figure R2.4. 17-ODYA toxicity and CD36 induction capacity. *(Page 115)*
- Figure R2.5. PA and 17-ODYA induce tumour cell aggressiveness to similar extent. *(Page 117)*
- Figure R2.6. PA and 17-ODYA generate similar proteomic response. *(Page 118)*
- Figure R2.7. Four days 17-ODYA treatment palmitoylates the same proteins with higher intensity. *(Page 119)*
- Figure R2.8. Enrichment of palmitoylated proteins in metastatic SCC-25. *(Page 121)*
- Figure R2.9. Enriched categories within the palmitoylated proteins. *(Page 122)*
- Figure R2.10. Western blot validation of palmitoylated proteins. *(Page 123)*
- Figure R2.11. Analysis of the palmitoylome of SCC-25 upon PA and OA treatments. *(Page 125)*
- Figure R2.12. Proteins more palmitoylated upon PA treatment. *(Page 127)*

Characterization of [REDACTED] palmitoylation

- Figure R3.1. Validation of the palmitoylation of [REDACTED]. *(Page 129)*
- Figure R3.2. Expression of exogenous [REDACTED]. *(Page 132)*

- Figure R3.3. [REDACTED] is the palmitoylated residue [REDACTED]. (Page 133)
- Figure R3.4. [REDACTED] does not interfere with and it is not necessary for [REDACTED]. (Page 134)
- Figure R3.5. [REDACTED] is not implicated in [REDACTED] localization. (Page 136)

Discussion

Palmitoylome studies

- Figure D2.1 Metabolic labelling vs chemical labelling. (Page 149)

[REDACTED] palmitoylation

- Figure D3.1. [REDACTED] structure. (Page 153)
- Figure D3.2. [REDACTED]. (Page 154)

LIST OF ABBREVIATIONS

2-BP: 2-bromopalmitate
17-ODYA: 17-octadecynoic acid
AA: acetic acid
ABHC17A: α/β hydrolase-domain containing 17 proteins A
ABHC17B: α/β hydrolase-domain containing 17 proteins B
ABHC17C: α/β hydrolase-domain containing 17 proteins C
ABE: acyl-biotin exchange
ac: acetyl
ACACA: acetyl-CoA carboxylase 1
ACACB: acetyl-CoA carboxylase 2
ACLY: ATP-citrate lyase
ACN: acetonitrile
acyl-CoA: acyl-coenzyme A
ACSL1: long-chain acyl-CoA synthetase
ACSS2: acetyl-CoA synthetase short chain 2
ADP: adenosine diphosphate
ALA: α -linolenic acid
Alk-C13: 12-tridecynoic acid
Alk-C14: 13-tetradecynoic acid
Alk-C16: 15-hexadecynoic acid
Alk-C18: 17-octadecynoic acid
AML: acute myeloid leukemia
ANK: ankyrin repeat
ANOVA: analysis of variance
APT1: acyl-protein thioesterase 1 (also known as LYPLA1)
APT 2: acyl-protein thioesterase 2 (also known as LYPLA2)
ARPC1A: actin-related protein 2/3 complex subunit 1A
ARPC1B: actin-related protein 2/3 complex subunit 1B
ARPC2: actin-related protein 2/3 complex subunit 2
ARPC4: actin-related protein 2/3 complex subunit 4
ATF6: activating transcription factor 6
ATP: adenosine triphosphate
ATRX: alpha-thalassemia/mental retardation X-linked syndrome protein
B2M: beta-2-microglobulin
BC: breast cancer
bhb: β -hydroxybutyryl
BPE: bovine pituitary extract
BRG1: Brahma related gene-1
BSA: bovine serum albumin
bu: butyryl
CACT: carnitine acylcarnitine translocase
CAF: cancer associated fibroblast
CAF-1: chromatin assembly factor 1
CAV1: caveolin 1
CD9: cluster of differentiation 9

CD4: cluster of differentiation 4
CD8: cluster of differentiation 8
CD36: cluster of differentiation 36
CD44: cluster of differentiation 44
CD45: cluster of differentiation 45
CD151: cluster of differentiation 151
CENP-A: centromere-specific variant CenH3
CPT1: carnitine palmitoyl transferase 1
CPT2: carnitine palmitoyl transferase 2
CQ: chloroquine
cr: crotonyl
CRC: colorectal cancer
CRD: cysteine rich domain
CSC: cancer stem cell
CT: control
CTC: circulating tumour cell
C-terminal: carboxy terminal
Cyt.: cytoplasm
DAG: diacylglycerol
DAXX: death domain associated protein
DC: dendritic cell
DDA: data dependent acquisition
DEGS1: dihydroceramide desaturase 1
DGAT2: diacylglycerol O-acyltransferase
DHHC: aspartate-histidine-histidine-cysteine
Disp: dispatched
DMEM: Dulbecco's Modified Eagle Medium
DMSO: dimethyl sulfoxide
DNM1: dynamin
DNMT3A: DNA methyltransferase 3 alpha
DRM: detergent-resistant membranes
DSC3: desmocollin-3
DSP: desmoplakin
DTT: DL-Dithiothreitol
Dvl2: dishevelled segment polarity protein 2
ECM: extracellular matrix
EGF: epidermal growth factor
EGFR: epidermal growth factor receptor
EGR2: early growth response 2
EIF4A3: eukaryotic translation initiation factor 4A3
ELAVL1: ELAV like RNA binding protein 1
ELOVL: elongation of very long chain fatty acids proteins
EMA: European Medicines Agency
EMEM: Eagle's Minimum Essential Medium
EMT: epithelial to mesenchymal transition
endo.: endogenous
eNOS: endothelial nitric oxide synthase

EPA: eicosapentaenoic acid
ER: endoplasmic reticulum
ERN1: endoplasmic Reticulum to Nucleus Signaling 1
ERP29: endoplasmic reticulum resident protein 29
ERP44: endoplasmic reticulum resident protein 44
ERP72: endoplasmic reticulum resident protein 72
EWI-F: Glu-Trp-Ile (EWI) motif-containing protein
exo.: exogenous
FA: fatty acid
FABP: fatty acid binding protein
FACS: fluorescence activated cell sorting
FADH₂: flavin adenine dinucleotide
FADS2: fatty acid desaturase 2
FAO: fatty acid β -oxidation
FASN: fatty acid synthase
FATP: fatty acid transport proteins
FBS: fetal bovine serum
fc: fold change
FDA: US Food and Drug Administration
FDR: false discovery rate
FKBP12: FKBP prolyl isomerase 1A
FSC: forward scatter
GAP-43: growth associated protein 43
GFP: green fluorescent protein
glu: glutarylation
GLUL: glutamine synthetase
GO: gene ontology
GOAT: ghrelin O-acyltransferase
GOBP: gene ontology biological process
GOCC: gene ontology cellular component
GPC19: golgi localized membrane protein 19
GPI: glycosylphosphatidylinositol
GPX4: glutathione peroxidase 4
GSH: glutathione
GTP: guanosine triphosphate
H.: heavy
H2Kd: MHC class I
HAT: histone acetyltransferases
HCC: hepatocellular carcinoma
HDFP: hexadecylfluorophosphonate
hDHHC20: human DHHC 20
hEGF: human EGF
HEK293T: human embryonic kidney 293, SV40 large T antigen
HFD: high fat diet
Hhat: hedgehog acyltransferase
hib: 2-hydroxyisobutyryl
HIP14: huntingtin interacting protein

HIRA: histone regulator A
HLA-A: class I histocompatibility antigen, A alpha chain
HLA-C: class I histocompatibility antigen, C alpha chain
HMGCR: 3-hydroxy-3-methylglutaryl-CoA reductase
HNSCC: head and neck squamous cell carcinomas
HPV: human papilloma virus
HRP: horseradish peroxidase
HSPA5: heat shock protein family A (Hsp70) member 5
HTT: huntingtin
IDH: isocitrate dehydrogenase
IFI16: interferon gamma induced protein 16
IFI30: interferon gamma induced protein 30
IFI35: interferon induced protein 35
IFIT1: interferon induced protein with tetratricopeptide repeats 1
IFIT2: interferon induced protein with tetratricopeptide repeats 2
IFIT3: interferon induced protein with tetratricopeptide repeats 3
IFITM1: interferon induced transmembrane protein 1
IFN: interferon
IL-1 α : interleukin 1 alpha
IL-1 β : interleukin 1 beta
IL-3: interleukin 3
IL-8: interleukin 8
insol.: insoluble
IP: immunoprecipitation
IT: intra-tongue
ITGA6: integrin subunit alpha 6
ITGB1: integrin subunit beta 1
ITGB4: integrin subunit beta 4
ITGB6: integrin subunit beta 6
JAK2: Janus kinase 2
JNK: C-Jun N-terminal kinase 1 (also known as MAPK8)
KD: knock down
KEGG: Kyoto encyclopedia of genes and genomes
KO: knock out
KFSM: Keratinocyte Serum-Free growth medium
L.: light
LA: linoleic acid
LAT: Linker for activation of T cells
LC-MS: liquid chromatography - mass spectrometry
LD: lipid droplets
LDL: low density lipoproteins
LFQ: label free quantification
LGAL1: galectin 1
LGAL3: galectin 3
LGAL7: galectin 7
LIPG: lipase G
LN: lymph node

LPCAT1: lysophosphatidylcholine acyltransferase 1
LSC: leukemic stem cell
Luc: luciferase
LYPLA1: lysophospholipase 1
LYPLA 2: lysophospholipase 2
M.: medium
ma: malonylation
MAFP: methyl arachidonyl fluorophosphonate
MAM: mitochondrial-associated membrane
MAPK: mitogen activated protein kinase
MBOAT: membrane bound O-acyl transferase
MC1R: melanocortin-1 receptor
MCAM: melanoma cell adhesion molecule
MDSC: myeloid-derived suppressor cells
me: methyl
MET: mesenchymal to epithelial transition
MHCI: major histocompatibility complex class I
MIC: metastasis-initiating cell
Microtub.: microtubules
MITF: microphthalmia-associated transcription factor
Mito.: mitochondria
MMP14: matrix metalloproteinase 14
MRD: minimal residual disease
MS: mass spectrometry
MUFA: Monounsaturated fatty acid
NADH: nicotinamide adenine dinucleotide
NADPH: nicotinamide adenine dinucleotide phosphate
NANOG: nanog homeobox
NAT10: N-acetyltransferase
NEM: N-ethylmaleimide
NET: neutrophil extracellular DNA-traps
NF- κ B: nuclear factor kappa B
NK: natural killer
NLRP: NOD-like receptor protein
NMT: N-myristoyl transferase
NSG: NOD Scid gamma (NOD.Cg-Prkdcscid Il2rgtm1Wjl/SzJ)
N-terminal: amino-terminal
OA: oleic acid
OAS1: 2'-5'-oligoadenylate synthetase 1
OAS2: 2'-5'-oligoadenylate synthetase 2
OAS3: 2'-5'-oligoadenylate synthetase 3
OD: 17-ODYA
OE: overexpression
OECD: Organization for Economic Co-operation and Development
ON: overnight
OSCC: oral squamous cell carcinoma
OXPHOS: oxidative phosphorylation

PA: palmitic acid
PaCCT: palmitoyl transferase conserved C terminus
PAGE: polyacrylamide gel electrophoresis
PASEF: parallel accumulation serial fragmentation
PAT: protein acyl transferase
PBS: phosphate-buffered saline
PC: phosphatidyl choline
PCA: principal component analysis
PD-1 :programmed cell death protein 1
PDAC: pancreatic ductal adenocarcinoma
PDE δ : phosphodiesterase 6D
PD-L1: programmed cell death ligand 1
PERK: protein kinase R-like endoplasmic reticulum kinase
ph: phosphor
PHD: double plant homeodomain
PI: protease inhibitor
PI3K: phosphatidylinositol-4,5-biphosphate 3 kinase
PIP₃: phosphatidylinositol-3,4,5-triphosphate
PKC δ : protein kinase C delta
PKP1: plakophilin-1
PKP3: plakophilin-3
PM: plasma membrane
PMSF: phenylmethylsulphonyl fluoride
pr: propionyl
PRC1: polycomb repressive complex 1
PRC 2: polycomb repressive complex 2
PRDX2: peroxiredoxin 2
PRDX5: peroxiredoxin 5
P/S: penicillin-streptomycin
PSD-95: postsynaptic density protein 95
PSMB8: proteasome subunit beta type 8
PSME1: proteasome activator subunit 1
PSME2: proteasome activator subunit 2
Porc. porcupine
PPAR β : peroxisome proliferator activated receptor beta
PPAR δ : peroxisome proliferator activated receptor delta
PPT1: palmitoyl-protein thioesterases 1
PPT 2: palmitoyl-protein thioesterases 2
PT: primary tumour
PTEN: phosphatase and tensin homolog
PTM: post-translational modification
PUFA: polyunsaturated fatty acid
PYCARD: PYD And CARD Domain Containing
REAM: reduced expression associated with metastasis (*ZDHHC2*)
RNS: reactive nitrogen species
ROI: region of interest
ROS: reactive oxygen species

RPL10A: ribosomal protein L10A
RSP14: ribosomal protein S 14A
RT: room temperature
RT-qPCR: real-time quantitative PCR
RXRG: retinoid X receptor gamma
SA: stearic acid
SCD1: stearoyl-CoA desaturase 1
SCRIB: scribble planar cell polarity protein
SD: standard deviation
Set1A: SET domain-containing protein 1
SFA: saturated fatty acid
SHH: Sonic hedgehog
SILAC: Stable isotope labelling by amino acids in cell culture
SIRT1: sirtuin 1
SIRT2: sirtuin 2
SIRT3: sirtuin 3
SIRT5: sirtuin 5
SIRT7: sirtuin 7
SLBP: stem-loop binding protein
SMARCA4: SWI/SNF related, matrix associated, actin dependent regulator of chromatin, subfamily A member 4
SNAP23: synaptosome associated protein 23
SNAP25: synaptosome associated protein 25
SOD1: Cu,Zn-superoxide dismutase
SOD2: superoxide dismutase 2
sol.: soluble
SPF: specific-pathogen-free
SSC: side scatter
STAT3: signal transducer and activator of transcription 3
STIM1: stromal interaction molecule 1
STING: stimulator of interferon genes
SYK: spleen tyrosine kinase
T2DM: type 2 diabetes mellitus
TAG: Triacylglycerol
TAM: tumour associated macrophage
TAMRA: 5-Carboxytetramethylrhodamine
TBST: Tris-buffered saline with Tween-20
TBTA: Tris[(1-benzyl-1H-1,2,3-triazol-4-yl)methyl]amine
TCA: tricarboxylic acid
TCEP: tris(2-carboxyethyl)phosphine
TCR: T cell antigen receptor
TEAD: TEA domain transcription factor
T_{eff}: effector T cells
T_{ex}: exhausted T cells
TF: transcription factor
TFA: trifluoroacetic acid
TGFβ: transforming growth factor beta

TIL: tumour infiltrating lymphocyte
TIMS: trapped ion mobility spectrometry
TLR2: toll like receptor 2
TLR4: toll like receptor 4
TME: tumour microenvironment
T_{mem}: T memory cells
TMX: thioredoxin related transmembrane protein 1
TNF α : tumour necrosis factor alpha
T_{reg}: T regulatory cells
VAMP2: vesicle associated membrane protein 2
VLDL: very-low-density lipoproteins
VSV: vesicular stomatitis virus
WB: western blot
WHO: World Health Organization
WT: wild type
YAP: Yes1-associated transcriptional regulator
ZEB: Zinc finger E-box binding homeobox

α -amino acids are named using the trivial name or symbols accepted by the International Union of Pure and Applied Chemistry:

Alanine: Ala, A *	Leucine: Leu, L *
Arginine: Arg, R *	Lysine: Lys, K *
Asparagine: Asn, N	Methionine: Met, M *
Aspartic acid: Asp, D *	Phenylalanine: Phe, F
Cysteine: Cys, C *	Proline: Pro, P*
Glutamic acid: Glu, E *	Serine: Ser, S *
Glutamine: Gln, Q*	Threonine: Thr, T *
Glycine: Gly, G *	Tryptophan: Trp, W
Histidine: His, H *	Tyrosine: Tyr, Y *
Isoleucine: Ile, I*	Valine: Val, V*

* α -amino acids mentioned in the thesis.

INTRODUCTION

1 Cancer & lipid metabolism

The World Health Organization (WHO) defines cancer as a genetic disease based on the excessive and uncontrolled proliferation of some cells that can eventually spread to parts of the body different from their tissue of origin and form metastases. It is the second cause of death worldwide, after cardiovascular diseases, accounting for 9 million deaths in 2018; according to certain predictions, it will become the first one by 2060 (Mattiuzzi and Lippi, 2019). Depending on the cell of origin, there are more than 100 different types of cancer, which are often considered as independent diseases due to the disparities between each malignant tumour type in terms of incidence, etiology, biology or treatment. In this thesis, we used oral squamous cell carcinoma (OSCC) cell lines (a type of cancer included in the group of head and neck squamous cell carcinomas; HNSCC) for all experiments as a cancer model.

1.1 Head and neck squamous cell carcinomas (HNSCC)

HNSCCs comprise a variety of malignant tumours that arise within the cavities of these anatomical parts, which are usually grouped together due to their etiological, epidemiological and molecular similarities. It is estimated that more than 90% of head and neck cancers are HNSCC, arising from the cells of the squamous epithelium lining the mucosal surfaces of the oral cavity, pharynx, larynx and sinonasal tract (Johnson et al., 2020; Markopoulos, 2012). HNSCC is the 6th most common cancer group worldwide and, according to the global Cancer Observatory, its incidence continues to rise (Johnson et al., 2020). The prevalence of HNSCC varies between countries mainly due to its etiology and the geographical and cultural differences in the consumption of certain substances. The main common risk factors of HNSCC around the world are tobacco and alcohol consumption. Nevertheless, in countries of south east Asia, like India, where HNSCC accounts for around 45% of the diagnosed cancers, the disease is also associated to chewing areca nut products (Johnson et al., 2020). In the United States and western Europe, the incidence of this cancer is lower and only 1% to 4% of diagnosed cancers are HNSCC. Nonetheless, this incidence is worryingly increasing due to its association with certain oncogenic strains of human papilloma virus (HPV) and the expansion of this pathogen (Stein et al., 2016; Johnson et al., 2020).

HNSCC are usually diagnosed in advanced stages due to the lack of clinical symptoms or wrong diagnosis (Markopoulos, 2012). Lymph node (LN) metastases are present in 80% of the patients with advanced disease (Markopoulos, 2012) and are associated to the size of primary tumour (PT) and the presence of distant metastases, mainly in the lungs (Farooq and Bugshan, 2020). The 5-year survival rate for those patients with an advanced HNSCC is 12% (Markopoulos, 2012). For HNSCC, as for most of cancers, there is still a need to develop effective treatments against the metastatic disease.

1.2 The hallmarks of cancer

Cancer is an unquestionable complex disease, with great differences between cancer types and there is also tremendous heterogeneity within the malignant tumours of the same origin. The tumours of each cancer type are usually further subclassified in molecular subtypes depending on specific biomarkers or mutations that have an impact on the prognosis and treatment of the patients (Prat et al., 2015; Fontana et al., 2019; Rudin et al., 2019).

In 2000, Douglas Hanahan and Robert A. Weinberg defined the hallmarks of cancer as 6 principles common to most cancers to conciliate the complexity detected in the laboratories and clinics (**Figure I1.1**) (Hanahan and Weinberg, 2000). They observed that cancers, regardless of their cell of origin, mutations or molecular classification, share a few common and acquired functional capabilities. Cancer cells present **self-sufficiency in growth signals** that combined with the **insensitivity to anti-growth signals** and the **limitless replicative potential**, allow them to proliferate and form the PT ignoring all

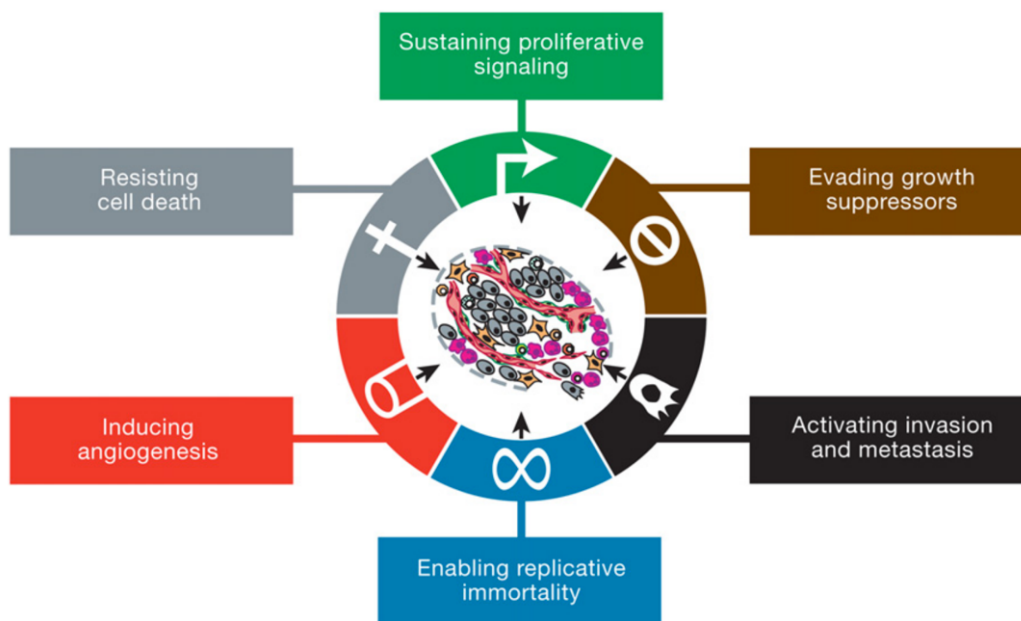


Figure I1.1. The hallmarks of cancer. From Hanahan and Weinberg, 2011
The six hallmark capabilities of tumour cells exposed in 2000.

extracellular or intracellular signals that control the size of healthy tissues (**Figure I1.1**). On top of that, they develop mechanisms to **evade apoptosis**, which allows them to cope with the accumulation of mutations, the metabolic stress generated by the excessive proliferation, the response of the immune system or even the anti-tumour treatments. Once the tumour reaches certain size, the diffusion of nutrients and oxygen through the interstitial liquid is no longer sufficient and cancer cells need to **induce angiogenesis** or perform vessel co-option (Kuczynski et al., 2019). Finally, all malignant

tumours acquire the capacity to **invade the tissue and metastasize** to distant organs (**Figure I1.1**). I will focus on this last hallmark, as it is the one responsible for the death of most cancer patients.

1.2.1 Tissue invasion and metastasis

Metastasis is the process by which cancer cells spread from the PT to a secondary site within the host's body and is the cause of 90% of cancer deaths. While surgical resection and adjuvant therapy can cure localized PTs, once tumour cells have metastasize, cancer is considered a systemic disease and remains largely incurable (Gupta and Massagué, 2006; Massagué and Ganesh, 2021). The vast majority of patients diagnosed with metastatic cancer die within the 5 years after diagnosis (Siegel et al., 2020).

To metastasize, cancer cells need to go through a complex and highly challenging process via different steps and known as the **metastatic cascade** (**Figure I1.2**) (Lambert et al., 2017). This process is highly inefficient, and the vast majority of cells leaving the PT fail to colonize distant organs (Fares et al., 2020). To be able to perform all the different steps of the metastatic cascade, cancer cells need to acquire specific functions or phenotypes and adapt to new environmental stresses. The cells responsible for cancer dissemination and the most important processes occurring during the metastatic cascade are briefly described bellow.

Metastasis–initiating cells (MICs)

The cancer stem cell (CSC) hypothesis states that malignant tumours are generated by the accumulation of oncogenic mutations in normal adult stem or by transit-amplifying cells that become CSCs (Tan et al., 2006). These CSCs give rise to the rest of tumour cells and can regenerate the tumour after therapy or when transplanted into a secondary recipient (Tan et al., 2006). Metastatic colonization is driven by stem-like tumour cells, known as “metastasis–initiating cells” (MICs) that are not necessary CSCs. These MICs have the capacity to generate a secondary tumour but they present a phenotype similar to that of a regenerative adult stem cell, which enables them to disseminate (Ganesh et al., 2020).

Invasion and migration

Invasion is the first step of the metastatic cascade. MICs need to degrade the basal membrane surrounding the PT, remodel the ECM and migrate towards the blood or lymphatic vessels surrounding the tumour (Lambert et al., 2017). The conversion of an epithelial cell into a motile, individually infiltrating cell requires a massive phenotypic change that has been intensively studied (Paňková et al., 2010). There are two different types of migration: ameboid and mesenchymal; however, the second one is the more

general and has been deeply studied due to its implications in metastasis and chemotherapy resistance (Brabletz et al., 2018).

The epithelial-to-mesenchymal transition (EMT) is a physiological process used by epithelial stem cells to move to distant locations during wound healing or gastrulation (Koike et al., 2020; Massagué and Ganesh, 2021). In those situations, specific EMT-related transcription factors (TFs) (mainly of the Snail, ZEB [Zinc finger E-box binding homeobox] or TWIST families) repress epithelial genes and upregulate the expression of mesenchymal components, inducing the phenotypic transformation of the cell (Paňková et al., 2010; Brabletz et al., 2018). Once the cell arrives at its destination, it returns to an epithelial state through the mesenchymal-to-epithelial transition (MET) (Ribatti et al., 2020). Many malignant tumour cells hijack this transcriptional program which endows them with the required plasticity to follow and survive the metastatic cascade and still be able to reactivate proliferation in the distant organ for the outgrowth of the metastasis (Ribatti et al., 2020).

Cellular stress during tumour cell dissemination

During tumour formation, and especially in metastatic dissemination, cancer cells have to deal with many different stressors. Two metastasis-specific stresses particularly relevant for epithelial tumours are the loss of cell-cell and cell-ECM contact and the dissemination through an iron-rich environment.

In healthy epithelial tissues, cells sense their location through interaction with the ECM and neighboring cells. **Anoikis** is the apoptotic process activated by specific signals that are triggered when those interactions are altered or lost (Gilmore, 2005). In later stages of cancer progression, metastatic cells detach from the PT and have to survive in suspension in the lumen of lymphatic or vascular vessels or in cavities such as the abdominal avoiding anoikis.

The itinerary or route of dissemination (e.g., blood or lymphatic vessels, perineural, perivascular) that a tumour cell takes depends mainly on the tumour type, being the hematogenous and lymphatic circulations the most common tracks of dissemination (Massagué and Ganesh, 2021). Cells disseminating through blood are the ones facing the second metastasis-specific stress: a completely new environment particularly rich in free iron. This excess of iron can lead to the intracellular accumulation of massive amounts of ROS (reactive oxygen species) that if not properly quenched can induce **ferroptosis**. Ferroptosis is a recently described type of cell death characterized by the intracellular accumulation of iron that ultimately leads to membrane phospholipid peroxidation (Jiang et al., 2021). During dissemination, tumour cells need to be able to cope with the excess of ROS to avoid ferroptosis or to bypass the bloodstream.

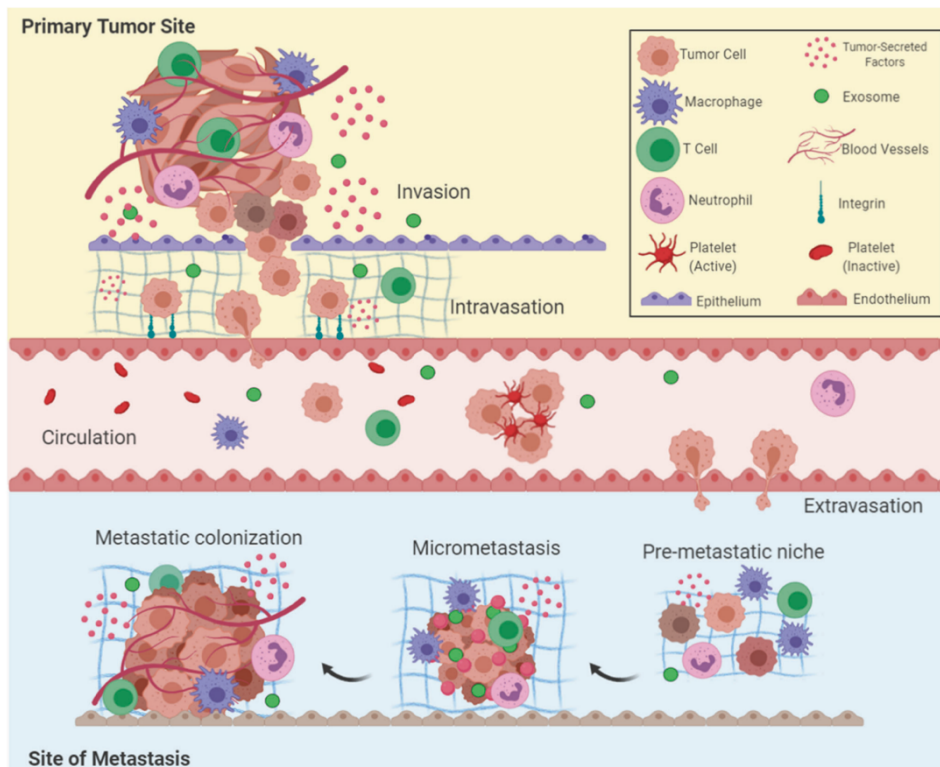


Figure I1.2. The metastatic cascade. From Fares et al., 2020.

Tumour cells within the PT invade the surrounding tissue and intravasate into blood or lymph vessels. They are disseminated through circulation and extravasate in distant organs. Upon extravasation, MICs have to adapt to the pre-metastatic niche to be able to grow first micro-metastases. With time, these micro-metastases manage to modulate the immune response and induce angiogenesis or co-opt preexisting blood vessels to progress and generate macro-metastases. During the whole process of tumour progression cancer cells interact with the cells that compose the tumour microenvironment.

Extravasation and organ tropism

Circulating tumour cells (CTCs) are randomly trapped in the capillaries of distant organs within seconds or minutes of intravasation. Nevertheless, only a few cancer types (e.g., small cell lung cancer or melanoma) can generate metastases in multiple distant sites without showing an organ predilection. Most tumour types present which is known as metastatic organotropism, which is the preference to metastasize to particular organs. Organ tropism depends on two factors: the ability of the tumour cell to reach that tissue and the ability of the MIC to grow in that organ (Lambert et al., 2017; Massagué and Ganesh, 2021).

Dormancy and the metastatic outgrowth

Once MICs arrive to a distant site, they enter into an environment completely different from that of the PT. They need to be able to adapt to the new microenvironment and nutrients available before growing a metastasis; prior to this, they usually enter

dormancy. Metastatic dormancy can go through two different and complementary scenarios. On the one hand, disseminated MICs might exit temporarily the cell cycle in a cell-autonomous manner. This quiescence can be stimulated by inhibitory signals within the metastatic microenvironment (Prunier et al., 2019) or it can even be initiated by MICs through inhibition of mitogenic signals (Malladi et al., 2016). Quiescence enables immune evasion, chemotherapy resistance and survival until an appropriate microenvironment is generated. On the other hand, dormancy can be induced by cell-extrinsic limitations. A small secondary tumour mass can enter dormancy due to insufficient nutrient or oxygen diffusion and lack of angiogenesis (Risson et al., 2020). Also, the immune surveillance of the distant organ can detect the proliferative MICs and attack them generating a dynamic equilibrium of micro-metastasis growth and destruction (Risson et al., 2020). Immune evasion and the metabolic adaptation of MICs to the metastatic niche can elicit metastatic outgrowth.

1.2.2 Deregulation of cellular energetics as an emerging hallmark of cancer

In 2011, in light of new discoveries, the hallmarks of cancer were revisited, and two emerging functional capabilities were added: **evading immune destruction** and **reprogramming energy metabolism** (Hanahan and Weinberg, 2011). This last hallmark is of especial relevance since it implies a greater complexity of cancer biology but, at the same time, opens up a wide range of potential therapeutic targets. Otto Warburg was the first scientist who realized that tumour cells presented an anomalous metabolism (Warburg, 1927, 1956). Even under aerobic conditions, proliferative cancer cells tend to direct their glucose metabolism towards glycolysis and lactic fermentation, in what he called “aerobic glycolysis” and is also known as “the Warburg effect” (Warburg, 1927, 1956). Glucose fermentation is around 18-folds less efficient than mitochondrial oxidative phosphorylation (OXPHOS) in terms of energy production but in return it is 10- to 100- times faster (Liberti et al., 2016). To compensate this energetic loss, cancer cells dramatically increase glucose uptake (DeBerardinis et al., 2008). As a consequence of this metabolic switch, the cell gets different glycolytic intermediates that can be used in various biosynthetic pathways to sustain proliferation and, at the same time, it can survive even under hypoxic conditions (DeBerardinis et al., 2008; Liberti et al., 2016).

In the last decade, different studies have revealed the importance of other metabolic pathways in the progression of the disease (Bergers and Fendt, 2021; Elia et al., 2018). During tumour evolution, cancer cells cope with different metabolic challenges (e.g., hypoxia, oxidative stress, migration, metastatic colonization, chemotherapy) by adapting their metabolism to their needs and the nutrients available (Bergers and Fendt, 2021; Elia et al., 2018). Metabolic alterations associated with the progression of cancer have been described in the pyruvate and lactate metabolism (Caneba et al., 2012; Tasdogan et al., 2020), in the metabolism of different amino acids such as glutamine or

proline (Loayza-Puch et al., 2016; Yang et al., 2014), and in the lipid metabolism (Broadfield et al., 2021b; Pascual et al., 2017). In fact, lipid metabolism rewiring is one of the most common and worrying metabolic alterations in cancer, given that it is especially associated to tumour aggressiveness (Broadfield et al., 2021b; Martin-Perez et al., 2021). Additionally, changes in the lifestyle of modern societies are leading to higher consumption of fatty diets, reduced physical activity and an increasingly overweight/obese population, which could generate more aggressive tumours in the future.

According to the Organization for Economic Co-operation and Development (OECD), 25% of adults are clinically obese, and 60% of the population is considered overweight (OECD, 2017). Furthermore, the percentage of obese population is projected to rise even more in the next decade (Figure I1.3). Worryingly, obesity is associated with higher incidence of many different tumour types, including esophagus adenocarcinoma, CRC, pancreatic ductal adenocarcinoma (PDAC), and gastric cancer (Lauby-Secretan et al., 2016), and it is also an independent risk factor for the development of distant metastasis, resistance to therapy and death in breast cancer (BC) (Ewertz et al., 2011).

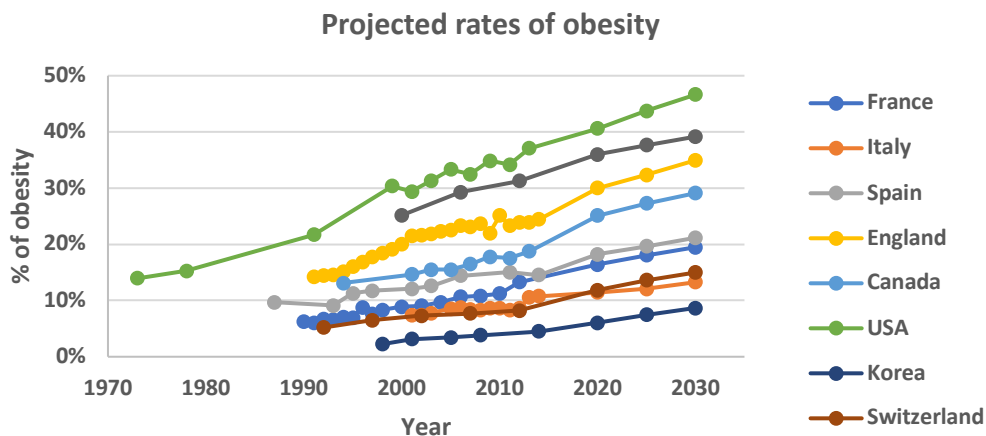


Figure I1.3. Projected rates of obesity in the OECD countries. Figure taken from OECD obesity update 2017 (OECD, 2017). The percentage of obese population is predicted to increase in all the studied countries in the following ten years.

Lipid metabolism alterations can be observed even before the development of the PTs (Broadfield et al., 2021a; Marino et al., 2020) but they have been described to be particularly relevant in the latest stages of cancer. When tumour cells metastasize and become resistant to therapy, they tend to upregulate lipid uptake from the microenvironment, oxidation or synthesis (Broadfield, L. A. et al, 2021b; Martin-Perez et al., 2021).

1.3 Lipid metabolism and cancer

1.3.1 Lipids & lipid metabolism, a general view

1.3.1.1 Lipids

Lipids are a complex group of molecules insoluble in water but soluble in organic solvents that vary in their structure and function within the cell (Snaebjornsson et al., 2020). There is a great variety of lipid molecules in eukaryotic cells but the most important categories for the purpose of this thesis are the following five (Fahy et al., 2005):

- **Fatty acids (FAs)** are the building blocks of most lipids. They are formed by different number of concatenated methylene groups bound to a final carboxyl group. The saturation status of a FA determines its physicochemical properties and thus, its biological functions (Snaebjornsson et al., 2020). They can be subclassified as:
 - **Saturated FAs (SFAs)**, which have only single bonds between the carbon atoms of the hydrocarbon chain (e.g., palmitic acid (PA) (16:0)) (**Figure I1.4**).
 - **Monounsaturated FAs (MUFAs)**, which contain one double bond between carbon atoms (e.g., oleic acid (OA) (18:1)) (**Figure I1.4**).
 - **Polyunsaturated FAs (PUFAs)**, with more than one double bond (e.g., eicosapentaenoic acid (EPA) (22:5n3); arachidonic acid (20:4)) (Fahy et al., 2005).
- **Triacylglycerols (TAGs) or triglycerides** are energy storage molecules formed by the esterification of three FAs to a glycerol moiety (Fahy, E. et al, 2005). They are packaged in lipid droplets (LD) inside the cell and used in periods of nutrient deprivation as a source of FAs for energy generation or membrane biosynthesis (Olzmann, J. A. et al, 2019).
- **Glycerophospholipids or phospholipids** are the main amphipathic components of all the bilayer membranes in the cell. They are typically built by a glycerol molecule esterified with one or two FAs, the hydrophobic fraction of the molecule; and a phosphatidic acid, the hydrophilic part (Hishikawa et al., 2014). There are different types of glycerophospholipids depending on the particular FAs bound to the glycerol moiety and the different polar heads bound to the phosphatidic group (e.g., phosphatidyl choline (PC)) (Hishikawa et al., 2014).
- **Sphingolipids** are a really complex family of lipids that share a common backbone molecular base, sphingosine, formed by a long-chain FA bound to a

serine amino acid (Fahy et al., 2005). They are structural components of membranes and act as bioactive regulatory lipids (Hannun et al., 2018).

- **Sterols.** The main sterols in mammalian cells are cholesterol and its derivatives, formed by four hydrocarbon rings (Fahy et al., 2005). They can act as signaling molecules or hormones but also as important components of the cellular membranes (Snaebjornsson et al., 2020).

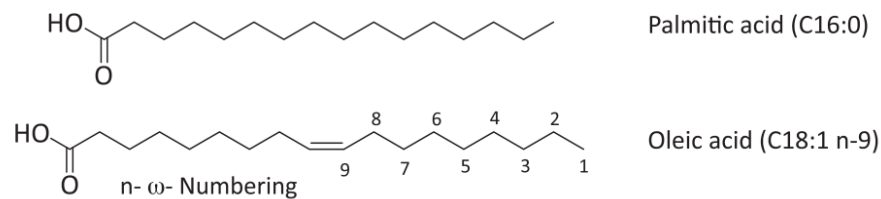


Figure I1.4. PA and OA chemical structure. From Palomer et al., 2018.

Scheme of the molecular structure of saturated palmitic acid (C16:0) and monounsaturated oleic acid (OA) (C18:1). The carbon-carbon double bond of OA is located at the omega-9 (ω) position (C18:1 n-9).

1.3.1.2 Lipid metabolism

What we term “lipid metabolism” in fact comprises many different pathways. Only the pathways most relevant to this thesis are described here.

- **Lipid uptake**

FAs can enter the cell by simple diffusion but transport by membrane fat receptors is predominant. The main FA transporters are the CD36 (cluster of differentiation 36), and FABP (fatty acid binding protein) and FATP (fatty acid transport proteins) families of proteins (**Figure I1.5**) (Houten and Wanders, 2010). Apart from free lipid metabolites, these transporters can also bind low- and very-low-density lipoproteins (LDL and VLDL) that provide lipids to the cancer cell (Broadfield et al., 2021b). Upon entrance, FAs are esterified into acyl-CoAs (acyl-coenzyme A) by FATPs, which also have acyl-CoA synthetase activity, or by ACSL (long-chain acyl-CoA synthetases) or ACSS2 (acetyl-CoA synthetase short chain 2), and then they can be used in biosynthetic pathways or oxidized through fatty acid β -oxidation (FAO) to obtain energy and generate other metabolites (**Figure I1.5**).

- **Fatty acid β -oxidation (FAO)**

FAO can occur in the mitochondria as well as in the peroxisome, although with important differences between both systems. Peroxisomal lipid oxidation is performed by different enzymes than the mitochondrial one and preferentially acts as a chain-shortening pathway that does not degrade FAs completely. Lipids oxidized in the peroxisome are mainly very-long-chain FAs (>20C) or more complex lipids like branched FAs or lipids derived from PUFAS (e.g., eicosanoids) (Poirier et al., 2006). In the mitochondria, FAO is coupled to OXPHOS, thus it is more energetically efficient. FAs are broken into acetyl-CoA molecules for their entrance into the tricarboxylic acid (TCA) cycle. As the mitochondrial membrane is not permeable to long-chain FAs, such as PA or OA, they have to be translocated by the carnitine shuttle, formed by: CPT1 (carnitine palmitoyl transferase 1) the rate-limiting enzyme of FAO; CACT (carnitine acylcarnitine translocase); and CPT2 (carnitine palmitoyl transferase 2) (Figure I1.5) (Houten and Wanders, 2010). β -oxidation cycle consists on 4 consecutive enzymatic reactions. In each cycle, two carbons of the acyl-CoA carbon chain are released as acetyl-CoA and one NADH (nicotinamide adenine dinucleotide) and another FADH₂ (flavin adenine dinucleotide) molecules are generated. The shortened acyl-CoA enters again the β -oxidation cycle until it is fully degraded. The generated acetyl-CoA molecules can enter the TCA cycle and the electron carriers NADH and FADH₂ can deliver the electrons to the electron transport chain to produce energy in form of ATP (adenosine triphosphate) through OXPHOS (Houten and Wanders, 2010).

- **TCA cycle and OXPHOS**

The TCA cycle (or Krebs cycle) is an eight-reactions cycle in which three NADH, one FADH₂, one GTP (guanosine triphosphate) or one ATP and two CO₂ are generated from one acetyl-CoA molecule. NADH and FADH₂ molecules can then transfer their electrons to the electron transport chain to generate up to 12 ATPs (Akram, 2014). The TCA cycle is not necessarily fed by acetyl-CoA, other metabolites might enter the cycle at different points to be oxidized. This cycle receives metabolic intermediates to be oxidized for energy production but at the same time has an important role in anabolic metabolism; thus, it is considered an amphibolic pathway (Da Poian and Castanho, 2016). Some of the metabolic intermediates might be withdrawn from the TCA cycle to be used as precursors in biosynthetic pathways. Citrate is used for lipogenesis (Figure I1.5), oxaloacetate is used for gluconeogenesis and it is the precursor of nucleotides and α -ketoglutarate and oxaloacetate are required for the synthesis of various amino acids (Da Poian and Castanho, 2016). α -ketoglutarate is a particularly relevant intermediate for the redox homeostasis of the cell. It is an antioxidant

molecule itself as well as a fundamental precursor of glutamic acid, one of the three amino acids that compose glutathione (GSH) (Liu et al., 2018).

OXPHOS is the main mechanism for ATP synthesis in most human cells, and it occurs in the inner mitochondrial membrane. It comprises all the different steps in the transport of electrons, from the electron carrier coenzymes NADH and FADH₂ to O₂, which is reduced to H₂O (Figure I1.5) (Da Poian and Castanho, 2016). Electron transfer through the respiratory chain is coupled to proton pumping from the mitochondrial matrix into the intermembrane space. The proton gradient generated between the matrix and the intermembrane space is

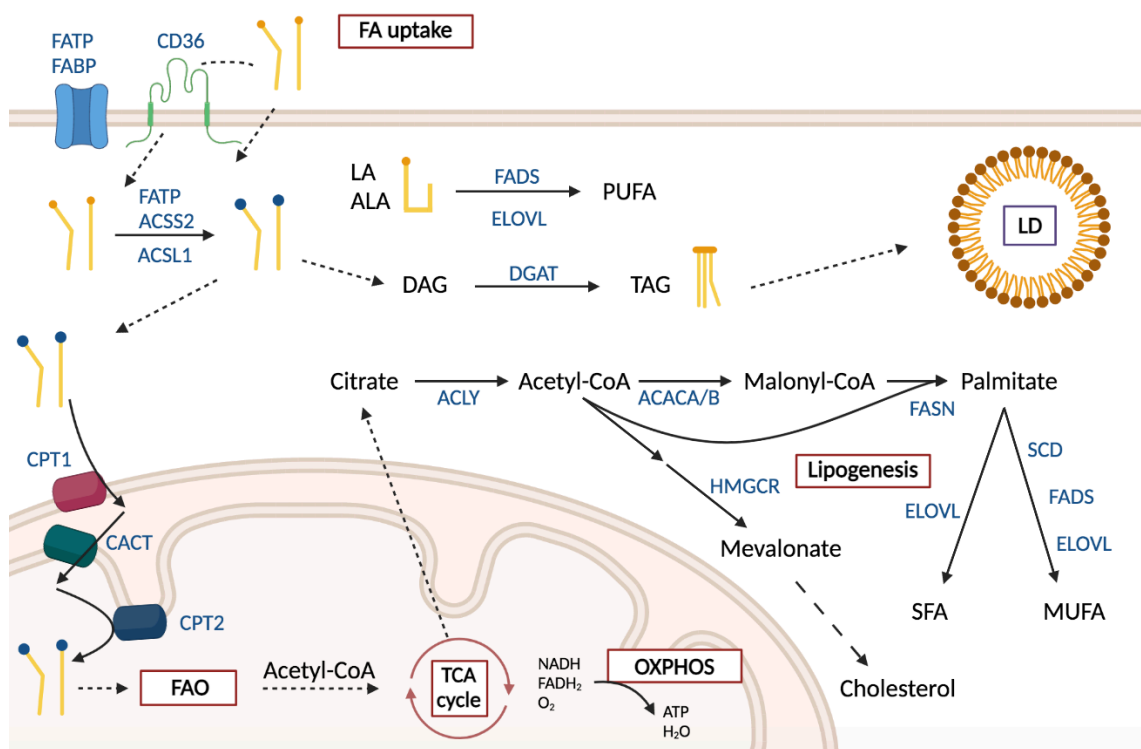


Figure I1.5. Overview of the major lipid metabolism pathways. Inspired by Broadfield et al., 2021b. FAs can enter the cell via passive diffusion or through translocases like CD36, FATPs and FABPs. Once inside the cell FAs are esterified to acyl-CoAs by FATPs, ACSL1 or ACS2. CoA (Coenzyme A) is represented by a blue circle. Acyl-CoAs are transported into the mitochondria by the carnitine shutter (CPT1, CACT and CPT2) where they enter FAO. Acetyl-CoAs generated upon FAO are transferred to the TCA cycle. Electrons from NADH and FADH₂ dinucleotides are used in OXPHOS for ATP generation and O₂ reduction into H₂O. Citrate generated during TCA cycle can exit the mitochondria as a first step in *de novo* lipogenesis. Acetyl-CoA, the main building-block for FA and cholesterol synthesis is generated from citrate by ACLY. Acetyl-CoA is then carboxylated by ACACA or ACACB generating malonyl-CoA, which is used by FASN for palmitate generation. Palmitate is then desaturated by SCD and FADS generating MUFAs. Palmitate or MUFAs can be elongated by ELOVL. Mevalonate is generated by HMGCR in the rate-limiting step of cholesterol synthesis. Acyl-CoAs can also be used for TAG synthesis. DGAT is the enzyme responsible for the addition of the last FA to the DAG. TAGs are then stored in LDs. Essential FAs (LA and ALA) are elongated by ELOVL and desaturated by FADS for the generation of different PUFAs. Created with BioRender.com

the electrical potential that drives ATP synthesis from ADP (adenosine diphosphate) (Da Poian and Castanho, 2016).

- **De novo lipogenesis**

De novo lipogenesis usually occurs in hepatocytes and adipocytes, although all body cells are capable of synthesizing lipids. There are two essential FAs that cannot be synthesized by the cell and must be consumed in the diet: α -linolenic acid (ALA) (18:3) and linoleic acid (LA) (18:2). The rest of the FAs are synthesized in the cytosol (Da Poian and Castanho, 2016). Citrate from the TCA cycle can be exported to the cytosol via citrate transporter (**Figure I1.5**). Once in the cytosol, ACLY (ATP-citrate lyase) converts citrate into acetyl-CoA and oxaloacetate. Alternatively, acetyl-CoA can be generated from acetate. Cytosolic acetyl-CoA is carboxylated to malonyl-CoA, the main substrate of FA synthesis, by ACACA and ACACB (acetyl-CoA carboxylases 1 and 2 respectively) in the rate-limiting step of FA synthesis. From here, FA synthesis consists of the incorporation of acetyl units into malonyl-CoA to generate palmitate, a reaction catalyzed by FASN (fatty acid synthase) (**Figure I1.5**) (Da Poian and Castanho, 2016).

PA is a saturated FA of 16 carbons (16:0) but it can be further modified to give longer or unsaturated FAs. ELOVLs (elongation of very long-chain fatty acids proteins) are the enzymes responsible for increasing the carbon chain length from PA to stearic acid (SA) (18:0) and so on (Broadfield et al., 2021b). On the other hand, desaturation to MUFAs can be driven by SCD1 (stearoyl-CoA desaturase), which gives palmitoleate (16:1n7) or oleate/OA from PA and SA, respectively; or by FADS2 (fatty acid desaturase 2), that generates sapienate (16:1 Δ 6) from PA (**Figure I1.5**) (Broadfield et al., 2021b). PUFAs synthesis requires the elongation and desaturation of essential LA and ALA but the rate of generation in normal conditions is very low (Broadfield et al., 2021b).

Synthesized FAs can be then incorporated into phospholipids, sphingolipids or TAGs. The different phospholipids are synthesized from a diacylglycerol precursor through different pathways at the ER or mitochondria cytosolic membranes. From there, they are distributed to the cell membranes via lipid transfer proteins or vesicles (Vance, 2014). Sphingolipids are synthesized by several different enzymes located within the secretory pathway. First, serine is conjugated with a FA-CoA generating a sphingosine, which is further N-acylated with a second FA-CoA to produce a ceramide. Ceramides undergo specific modifications at the “head-group” and they finally travel towards the plasma membrane (PM) as sphingolipids (Breslow and Weissman, 2010). For the synthesis of TAGs, three different FAs are esterified to one glycerol molecule. The addition of the last FA is catalyzed by DGATs (diacylglycerol O-

acyltransferases) and afterwards TAGs are stored in LD, phospholipid enveloped vesicles (**Figure I1.5**) (Broadfield et al., 2021b).

Finally, cholesterol synthesis takes place in the cytosol and uses cytosolic acetyl-CoA. HMGCR (3-hydroxy-3-methylglutaryl-CoA reductase), is the rate-limiting enzyme in this pathway and produces mevalonate. Mevalonate, similar to what happens with palmitate, can undergo further modifications to produce different cholesterol derivatives (**Figure I1.5**) (Broadfield et al., 2021b).

1.3.2 Influence of the lipid metabolism in the metastatic cascade

Cancer progression has been believed to be driven by accumulation of mutations that provide the tumour cells with different capabilities that eventually culminate in metastasis (Merlo et al., 2006). Nonetheless, epidemiologic studies have failed to identify metastasis-specific mutations. Genomes of metastatic lesions showed similar mutational landscape and driver mutations as their PTs (Reiter et al., 2018; Priestley et al., 2019). This suggests that cancer cells manage to adapt to the different challenges imposed by the metastatic cascade through non-mutational means, in other words, by epigenetic, transcriptional and metabolic alterations. Lipid metabolism is used by the tumour cells for adaptation in different moments of the metastatic cascade.

Alterations of the lipid metabolism can happen within the tumour cell but also within the different cells of the tumour microenvironment (TME) and in all cases favor the aggressiveness of the tumour. The TME is composed by all the different nutrients, signaling molecules, ECM and non-tumour cells that are present in the tumour tissue and interact with the cancer cells. Tumour cells manage to manipulate the different cells of the TME for their own benefit by different means and one of them is upregulating their lipid metabolism. The main alterations of the lipid metabolism affecting the tumour cell or the cells of the TME are described in the following sections.

1.3.2.1 Alterations of the lipid metabolism within the cancer cell

Lipid metabolism can be used to favor all the different steps of the metastatic cascade, from MICs generation to metastatic outgrowth.

MICs and lipid metabolism

A few years ago, our laboratory described for the first time the cells responsible for the metastasis formation in OSCC, melanoma and BC (Pascual et al., 2017). These MICs were characterized by the presence of CD44 (cluster of differentiation 44)-stem cell marker and CD36 receptor in their PM. Interestingly, they also presented an enhanced lipid metabolism. CD36 is a scavenger receptor that can bind long-chain FAs, oxo-LDLs, thrombospondin-1 and pathogen-associated molecules, among others (Tian et al.,

2020). In the context of MICs, CD36's main function consists of internalizing long-chain FAs that boost the metastatic capacity of the cell (Pascual et al., 2017).

Cell culture treatment of different cancer cell lines with PA is able to enhance CD36 expression, and thus the metastatic capacity of the cells when injected in mice (Pascual et al., 2017) (Figure I1.6). In line with these results, mice bearing a PT and fed a HFD based on lard develop more and bigger metastases than those eating a control diet, due to the increase in the percentage of MICs (CD44^{bright}, CD36+) within the PT (Pascual et al., 2017). Strikingly, not all the FAs can boost the metastatic capacity of the cells. Upon cell culture treatment with OA or LA, tumour cells downregulate CD36 expression and when injected, the metastatic burden is decreased compared to controls. Indeed, PT-bearing animals fed with a fatty diet enriched in PA present a higher incidence of metastases than control mice, but this is not the case for those mice eating an OA-enriched fatty diet (Pascual et al., 2021).

The influence of HFD on the CSC pool and the metastasis formation was also observed in CRC (Wang et al., 2019c). In a murine model of CRC, HFD induces the activation of PPAR δ (peroxisome proliferator activated receptor delta), which in turn activates Nanog expression and thus, the CSC pool expansion in the PT (Figure I1.7). This CSC expansion leads to the induction of liver metastasis formation, probably due to the increase in the number of MICs within the PT (Wang et al., 2019c).

Lipid metabolism in EMT, tumour cell migration and infiltration

Different studies have shown the relevance of the lipid metabolism during tumour invasion and EMT. While migrating and invading, tumour cells upregulate FA uptake and oxidation. CD36 expression is associated with esophageal cell carcinoma aggressiveness and induces tumour cell migration in culture (Yoshida et al., 2021). In gastric cancer, CD36 expression in patient samples is associated with poor prognosis (Yang et al., 2020b). In fact, CD36 can promote the nuclear localization of c-Myc, which in turn can activate the EMT program through GSK-3 β / β -catenin pathway (Wang et al., 2021). Activation of FAO by CPT1A also enhances the expression of the EMT markers and activates gastric cancer cell invasion (Wang et al., 2020b). In HCC, the downregulation of STIM1 (stromal interaction molecule 1) leads to the activation of the CaMKII/AKT/GSK-3 β and FAO pathways. As a consequence, Snail-1 is stabilized and the

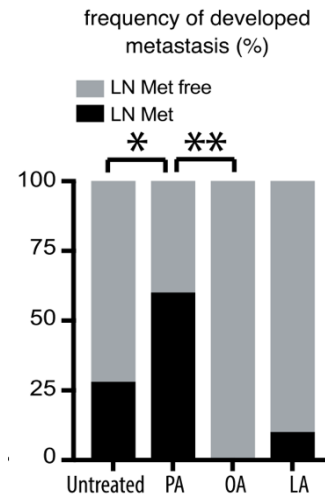


Figure I1.6. Only PA can boost the metastatic capacity of OSCC cells.

From Pascual et al., 2021
Frequency of developed LN metastases upon four days cell culture treatment of OSCC cells with 300 μ M PA, 50 μ M OA or 50 μ M LA. Two-tailed Fisher's exact test *p-value<0.05, **p-value<0.01.

metastatic capacity is boosted (Zhao et al., 2020). CD36 expression has also been linked to EMT in this cancer type (Figure I1.7) (Nath et al., 2015).

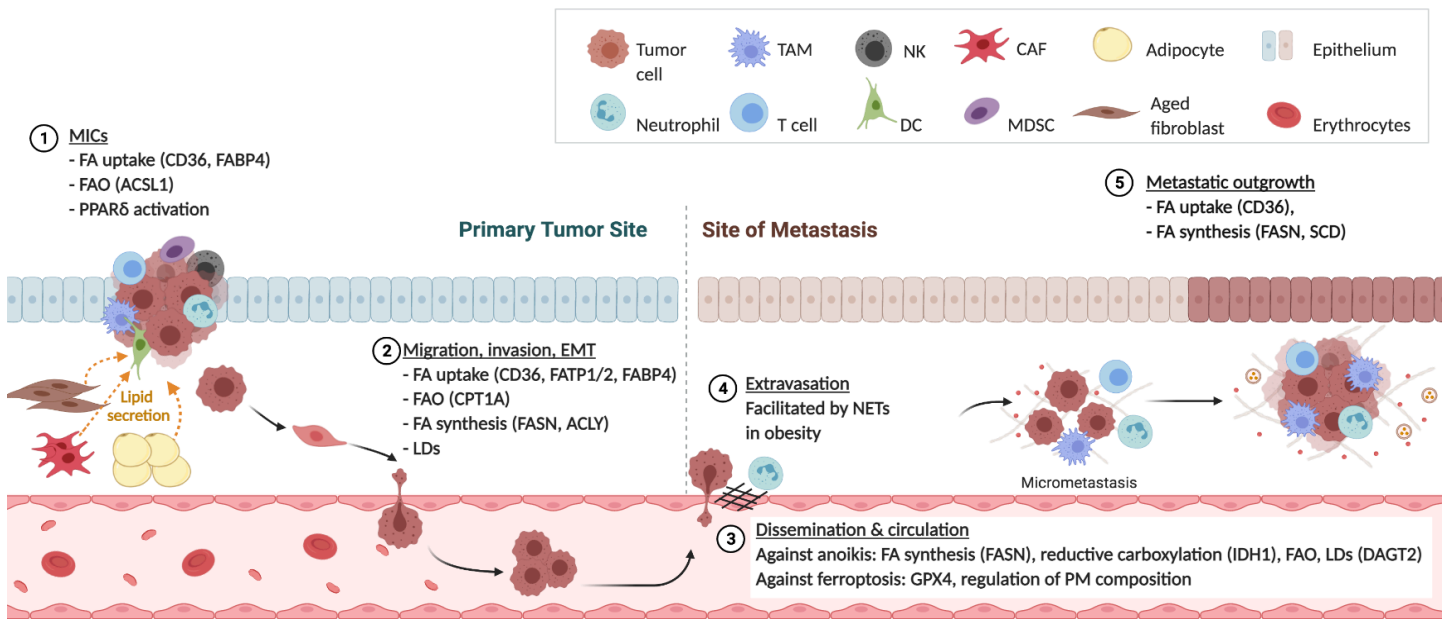


Figure I1.7. Influence of lipid metabolism in the metastatic cascade.

The figure represents a scheme of the five main steps of the metastatic cascade. The lipid metabolism pathways described in this thesis affecting each process are highlighted. MICs activate PPAR δ , upregulate FA uptake via CD36 and FABP4 and enhance FAO. During EMT, migration and invasion, tumour cells can upregulate FA uptake and oxidation but also FA synthesis and LD accumulation. The lipids uptaken by cancer cells can be secreted by adipocytes, CAFs or aged fibroblasts within the TME. During dissemination and circulation tumour cells fight anoikis inducing EGFR signaling via ROS generation. The excess of ROS is quenched by FA synthesis and reductive carboxylation, by FAO activation or by LD formation. Ferroptosis is avoided via GPX4 upregulation or PM composition alteration. Tumour cell extravasation can be boosted by NETs generated upon obesity-induced neutrophilia in the lungs. FA synthesis and uptake are upregulated for the metastatic outgrowth in certain organs. Created with BioRender.com.

Upregulation of the FA synthesis can also be implicated in tumour cell invasion (Figure I1.7). In cervical cancer, induction of *de novo* lipogenesis is associated with LN metastasis and can induce migration and invasion of tumour cells in cell culture (Guo. et al., 2019; Xu et al., 2020). FASN and lipid metabolism upregulation also correlate with intrahepatic cholangiocarcinoma aggressiveness (Zhang et al., 2020). Similarly, ACLY (the rate-limiting enzyme in lipid synthesis) favors migration and invasion of CRC cells (Wen et al., 2019).

Implication of the lipid metabolism in the survival to lethal stressors in dissemination and circulation

Cancer cells have to deal with oncogenic signaling pathways, alterations in the metabolism and phenotype of the cell, and external stressors, such as changes in the

microenvironment, immunity and therapy, all of which can lead to the accumulation of ROS. Increased lipid metabolism is necessary in metastatic cells for energy production and PM synthesis but it also has a role in stress tolerance. (Broadfield et al., 2021b). Lipid metabolism and cellular lipid composition can be regulated by the cancer cell for the maintenance of the redox homeostasis (Broadfield et al., 2021b).

ROS levels within the tumour cell increase massively in the two main stresses that tumour cells face during dissemination (i.e., anoikis due to loss of epithelial interactions and ferroptosis due to circulation in an iron-rich environment). Thus, the tumour cell needs to be able to adapt to these conditions or buffer their apparition in order to survive.

The main survival mechanism used by malignant cells to escape anoikis is via ROS production, which is used for second messenger signaling that activates Src and EGFR (epidermal growth factor receptor) (Giannoni et al., 2008). In this situation, tumour cells use the lipid metabolism to properly modulate the amount of ROS in order avoid an excess of damage that could compromise their viability. Some cells upregulate FASN to produce the reductive power necessary to quench the excess of ROS via IDH (isocitrate dehydrogenase) dependent reductive carboxylation (**Figure I1.7**) (Bueno et al., 2019); others, activate FAO to gain that reductive power through intermediate metabolites (Qiao et al., 2020; Sawyer et al., 2020; Zhao et al., 2020). LDs can also be used to cope with oxidative stress. These organelles serve as lipid storage depots that can fuel the cell spreading (Rozeveld et al., 2020) but also have a function in ROS modulation (**Figure I1.7**) (Corbet et al., 2020). In fact, HFD can induce peritoneal and lung metastases in gastric cancer via upregulation of DGAT2, one of the enzymes in charge of TAG synthesis and LD expansion. DGAT2 silencing decreases LD formation, activates anoikis, and inhibits metastasis (Li et al., 2020).

Ferroptosis-associated lipid peroxidation starts in the cell with the removal of a double bond between two carbons in a PUFA moiety of a phospholipid. This generates a phospholipid radical that, if not converted to an alcohol by GPX4 (glutathione peroxidase 4), can react with other PUFAS within the membrane and generate a chain reaction that ends up with the breakdown of the membrane integrity (**Figure I1.7**) (Jiang et al., 2021). Not all FA moieties within cell membranes are equally sensitive to lipid peroxidation, with SFA and MUFA being less reactive than PUFA; thus, cancer cells try to regulate their lipid composition to survive this type of cell death (**Figure I1.7**) (Jiang et al., 2021). Interestingly, melanoma cells that disseminate through the lymphatic system prior to accessing blood are less sensitive to ferroptosis thanks to the OA they uptake from the lymph (Ubellacker et al., 2020). On the other hand, certain lymphomas get protection from ferroptosis through the accumulation of squalene, an intermediate metabolite of the cholesterol synthesis. The accumulation of this polyunsaturated lipid

seems to protect membrane PUFAs from lipid peroxidation although the concrete mechanism remains to be elucidated (Garcia-Bermudez et al., 2019).

Alterations in the plasma membrane composition during metastasis

During metastasis, cancer cells tend to alter the lipid composition of their membranes in different ways. Melanoma cells with low MITF (microphthalmia-associated transcription factor) and more invasive phenotype downregulate the lipogenic enzyme SCD1. The inhibition of SCD1 causes an increase in the ratio SFA/MUFA in the membranes that favors EMT, inflammation and metastasis (Vivas-García et al., 2020). In CRC, an elevated arachidonic acid/eicosapentaenoic acid ratio can also induce inflammation and metastasis formation (Tutino et al., 2019). Alterations of the membrane lipid composition can impact oncogenic growth factor signaling pathways and even determine cell states. In glioblastoma, mutant EGFR signaling alters the lipid membrane composition of cancer cells via LPCAT1 (lysophosphatidylcholine acyltransferase 1). LPCAT1 activity increases the saturation of the membrane PCs, which favors EGFR signaling in a positive feedback loop (Bi et al., 2019). Puzzlingly, another study published at the same time showed that ELOVL2 and long-chain PUFAs are fundamental for EGFR signaling and glioblastoma CSC survival (Gimple et al., 2019). More studies will be required to elucidate if this striking difference is given by the state of differentiation of the cell or if both enzymes are required to compensate the biological effect of each other. Too many saturated FAs within the PM could lead to a rigid membrane, and this excess of saturation could be compensated by long-chain PUFAs.

Lipid metabolism in the route of dissemination, organ tropism and metastatic outgrowth

The capacity of tumour cells to adapt their lipid metabolism is important for the selection of the route of dissemination. While cancer cells that choose the hematogenous dissemination need to be ready to cope with ferroptosis, those that enter the lymphatic system have to adapt to the new microenvironment and upregulate FAO (Lee et al., 2019). Cancer cells that arrive to the LN undergo a YAP (Yes1-associated transcriptional regulator)-dependent metabolic shift towards FAO using the different lipids within the node microenvironment as substrates (Lee et al., 2019).

On the other hand, lipid metabolic pathways are particularly relevant for the metastatic outgrowth in specific organs. Some recently published studies evidence the relevance of lipid metabolism for the metastatic outgrowth of BC cells specifically in the brain (Ferraro et al., 2021; Jin et al., 2020). Brain metastatic BC cells upregulate FA synthesis via FASN overexpression to compensate the decreased availability of lipid nutrients in this organ (**Figure I1.7**). This metabolic adaptation is specific of the brain metastasis and does not happen in liver or bone, where the metabolic requirements are others (Ferraro et al., 2021). In a different study, the biochemical composition of BC cells with bone or

lung tropism was analyzed in cell culture. The study proved that the cells that preferentially colonize the lung present an enhanced lipid metabolism compared to those that metastasize to the bone (**Figure I1.7**) (Marro et al., 2018). Metastatic tumour cells in the different organs depend on lipid metabolism to different extent being the brain ones the more addicted to lipids followed by the lung ones.

1.3.2.2 Alterations of the lipid metabolism within the main cells of the TME

Cancer cells exploit the TME cells, for instance by hijacking the normal function of some cells (e.g., adipocytes), or by altering the physiological activity of others (e.g., with fibroblasts or many immune compartment cells). The metabolism of cancer cells alters the composition of the TME, which affects the cells living within that microenvironment. Apart from the signaling molecules that tumour cells may secrete, an excess of lipids within the PT or in circulation affects the stromal cells that compose the TME, and especially the immune compartment cells. Changes in the lipid metabolism can induce a switch of the cells in the stroma towards a pro-tumorigenic phenotype.

Adipocytes

Tumour cells uptake lipids present in the TME or that come in circulation. However, in some cases, the source of lipids for the cancer cell are the cells of the TME. In most occasions the donors of those lipids are the adipocytes surrounding the tumour (**Figure I1.7**). Lipid metabolism within the adipocytes is not altered but the cancer cell takes advantage of these natural fat reservoirs. Melanoma cells can directly take FAs from subcutaneous adipocytes via FATP1, which supports tumour growth and invasion (Zhang et al., 2018). In ovarian cancer, omental adipocytes can attract tumour cells via IL-8 (interleukin 8). When the adipocytes contact the tumour cells, they activate lipolysis and secrete FAs that ovarian cancer cells take through CD36 (Ladanyi et al., 2018) or FABP4 (Nieman et al., 2011) and use for further invasion (Ladanyi et al., 2018; Nieman et al., 2011). Exactly the same happens in BC, CD36 (Zaoui et al., 2019) or FABP4 (Kim et al., 2020) are upregulated upon interaction with adipocytes. The induction of these FA receptors upregulates lipid uptake, LD formation and the migratory and invasive capacity of these cells (Kim et al., 2020; Zaoui et al., 2019).

Cancer-associated fibroblasts (CAFs)

CAFs present an altered metabolism characterized by the storage (Nardi et al., 2018) and secretion of abundant lipids (**Figure I1.7**) (Auciello et al., 2019; Gong et al., 2020). In CRC, CAFs can undergo a lipidomic reprogramming, upregulate FASN and accumulate and secrete FAs and phospholipids. CRC cells in turn can uptake those lipids through CD36 and this enhances their aggressiveness (Gong et al., 2020). The same happens in PDAC where CAFs, derived from stellate cells, secrete lysophosphatidilcholines to support the tumour growth (Auciello et al., 2019). Worryingly, this metabolic rewiring

towards a lipogenic state is not specific of CAFs and can also happen in normal aged fibroblasts (Alicea et al., 2020). Aged dermal fibroblasts increase the secretion of lipids, especially ceramides, compared to young fibroblasts (Figure I1.7). These lipids can be taken by melanoma cells through FATP2 and used for targeted therapy resistance (Alicea et al., 2020).

Immune compartment

The immune compartment of the TME is particularly sensitive to changes in the lipid metabolism (Figure I1.8). Cancer cells manage to evade immune surveillance by different means and one of them is the dysfunction of immune cells as a consequence of changes in the metabolites of the TME.

In normal conditions, metabolism can affect immune cells differentiation and function. Most anti-tumour cells of the immune compartment such as: effector T cells (Howie et al., 2018), natural killer cells (NKs) (Cong, 2020), M1 macrophages (Mehla and Singh, 2019) or N1 neutrophils (Injarabian et al., 2020) (Figure I1.8); rely on glycolysis and OXPHOS for their proper maturation and functioning. On the other hand, immunomodulatory (pro-tumour) cells like T regulatory (T_{reg}) cells (Kouidhi et al., 2017), M2 macrophages (Mehla and Singh, 2019) or myeloid-derived suppressor cells (MDSCs) (Hossain et al., 2015); are characterized by the upregulation of FAO (Figure I1.8).

The metabolic activity of tumour cells within the PT, generates an environment depleted of glucose and with a high concentration of lipids, which favors the accumulation of immunomodulatory cells and dampens immune surveillance. An increased concentration of lipids within the TME induces CD36 upregulation in CD8⁺ T cells and oxoLDL and cholesterol uptake, which leads to lipid peroxidation and T cell dysfunction or even ferroptosis (Ma et al., 2021; Manzo et al., 2020; Xu et al., 2021). Dendritic cells (DCs) within the TME accumulate lipid peroxidation byproducts that induce ER stress response and TAG biosynthesis. This lipid accumulation leads to DC dysfunction, decreased antigen cross-presentation and lack of anti-tumour T cell activation (Cao et al., 2014; Cubillos-Ruiz et al., 2015; Veglia et al., 2017). Accumulation of lipids in NK cells upon PT removal surgery via CD36 upregulation also decreases their cytotoxic capacity and can induce metastases formation (Tai et al., 2013; Niavarani et al., 2019).

On the other hand, intra-tumoural T_{reg} cells induce CD36 and PPAR β to enhance lipid uptake and FAO (Wang et al., 2020). These cells can also upregulate SREBPs (sterol regulatory element-binding proteins) to coordinate lipid synthesis and inhibitory receptor signaling upregulating FASN and PD-1 (programmed cell death protein 1) expression (Lim et al., 2021). Tumour-associated macrophages (TAMs) are characterized by CD36 expression (Su et al., 2020), LD accumulation (Wu et al., 2019) and an enhanced

FAO (Su et al., 2020; Zhang et al., 2018b). Similarly, MDSCs within the PT upregulate FATP1/2 or CD36, which leads to lipid accumulation, FAO activation and prostaglandin E₂ synthesis, increasing the immunosuppressive function of MDSCs and the tumour growth (Al-Khami et al., 2017; Veglia et al., 2019).

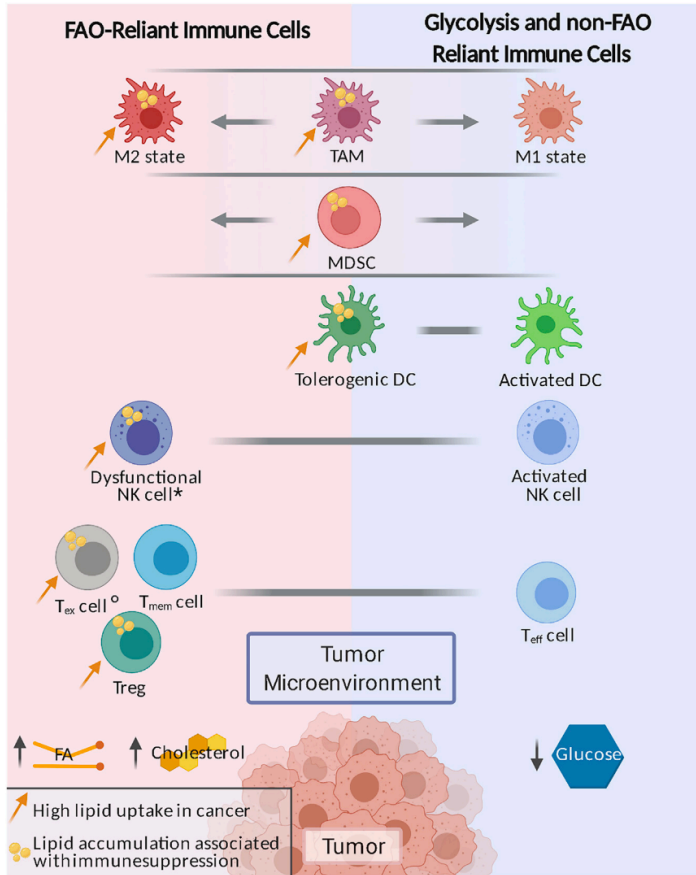


Figure 11.8. Influence of metabolism in the functionality of the immune cells within the TME. From Broadfield et al., 2021b. M1 macrophages, activated DCs and NKs and effector T cells (T_{eff}) rely on glycolysis for their proper functioning. Low glucose and high FA and cholesterol within the TME induce M2 macrophages or TAMs, MDSCs, tolerogenic DCs, dysfunctional NKs, T_{regs}, T memory cells (T_{mem}) and exhausted T cells (T_{ex}). In general, lipids within the TME induce a pro-tumour immune response.

Upon fatty diet feeding the amount of circulating fats increases dramatically, what further dampens immune surveillance. Worrying discoveries show that HFD itself can promote cancer development through exhaustion of CD8⁺ T cells (Kado et al., 2019). This type of diet can also inhibit CD4⁺ helper T cells activation (Guerrero-Ros et al., 2020) and induce DC dysfunction (Gao et al., 2015), while favoring MDSCs accumulation in circulation and within the PT (Clements et al., 2018; Hale et al., 2015). On the other hand, high adiposity associated with obesity induces neutrophilia (i.e. higher neutrophil count than in normal reference range) specifically in the lungs (Quail et al., 2017). Neutrophils accumulated in the lungs produce ROS and neutrophil extracellular DNA-traps (NETs), which generates vascular damage and favors BC cell extravasation and metastasis in the lung (Kaplan and Radic, 2012) (**Figure 11.7**).

1.3.3 Lipid metabolism in the resistance to therapy

Lipid metabolism underlies to a large extent how cancer cells cope with extreme stressors, such as therapy. Upregulation of lipid metabolism has been observed in both

chemotherapy and targeted therapy resistant cells. Chemotherapy-resistant acute myeloid leukemia (AML) cells display high levels of ROS and mitochondrial mass that correlate with enhanced OXPHOS. They also upregulate CD36 and increase FAO probably to get metabolic intermediates to modulate redox homeostasis (Farge et al., 2017). The same upregulation of CD36 is observed in chronic myeloid leukemia upon tyrosine kinase inhibitors (Landberg et al., 2018).

The mesenchymal state that cancer cells acquire through EMT is associated to treatment resistance (Staalduinen et al., 2018). Most mesenchymal resistant to therapy cells upregulate GPX4. ZEB1, one of the major EMT-TFs, controls uptake, accumulation and mobilization of lipids and regulates EMT-associated remodeling of PM. It is likely that there is a therapy resistance-associated upregulation of PM PUFA upon EMT. This excess of PUFA in the membranes would be compensated by GPX4 upregulation for ferroptosis prevention (Viswanathan et al., 2017).

In many occasions, resistance is associated with CSCs. Classical chemotherapeutic treatments kill rapidly proliferating cells, thus quiescent CSC are not affected by them. However, modern targeted therapies also seem to exert less damage on CSCs. A less differentiated phenotype probably confers higher metabolic plasticity to adapt and cope with aggressive treatments. This adaptation usually relies on lipid metabolism alterations. Sorafenib-resistant HCC cells are enriched in stem-like markers such as NANOG (Nanog Homeobox) or Oct4, and present upregulation of FA uptake through CD36 and synthesis via FASN (Bort et al., 2020). MAPK (mitogen activated protein kinase)-targeted therapy resistant BRAF-mutant melanoma cells present a neural crest stem cell transcriptional program and express CD36 (Rambow et al., 2018). Indeed, CD36 can be a good marker of the adaptation of melanoma cells to MAPK inhibitors and already resistant cells can present an enhanced FAO with PPAR α and CPT1A upregulation (Aloia et al., 2019; Rambow et al., 2018). Mesenchymal stem cells within the TME of HER2+ BC tumours could favor trastuzumab resistance through stemness induction and FAO upregulation (Han et al., 2020). Similarly, lapatinib acquired resistance depends on exogenous FA uptake via CD36 and enhanced metabolic plasticity (Feng et al., 2019).

Certain tumour types take advantage of other tissues or organs to gain resistance to therapy. In a murine model of chronic myeloid leukemia, leukemic stem cells (LSCs) invade gonadal adipose tissue. Within this niche, LSCs can induce adipose tissue lipolysis, upregulate CD36 and increase FA uptake and with this, therapy resistance (Ye et al., 2016). Due to the disseminated nature of the disease, LSCs also invade other organs, such as the liver, where they favor hepatocytes lipolysis via LIPG (lipase G) upregulation. Liver-derived PUFAs induce LSC expansion and liver damage induced by LSC infiltration,

leads to the release of chemotherapy degrading enzymes, which enhances therapy resistance (Ye et al., 2021).

1.3.4 Targeting lipid metabolism

Lipids are beneficial for tumour cell survival and aggressiveness, yet dependency of cancer cells on lipid metabolism makes it a promising target to stop cancer progression. Some of the main lipid pathways and targets that could be therapeutically targeted are described below.

FA uptake: CD36, FATPs, FABPs

Induction of FA uptake seems to be a general mechanism used by cancer cells to fuel their dissemination or therapy resistance and CD36 is one of the main receptors upregulated. In fact, chemical inhibition of CD36 or downregulation of its expression via shRNA reverses the mesenchymal and invasive phenotype of tumour cells in culture (Nath et al., 2015; Yoshida et al., 2021). Strikingly, blockage of lipid entrance through CD36 with JC63.1 anti-CD36 antibody can inhibit metastasis formation or decrease the metastatic burden in immunocompromised models of OSCC (Pascual et al., 2017) or CRC (Gong et al., 2020). CD36 is also used by tumour cells to overcome therapy; therefore, combinations of an anti-cancer treatment with CD36 inhibition should boost the drug efficiency. Indeed, imatinib-resistant CD36+ cells can be killed with CD36 targeting antibodies (Landberg et al., 2018). This scavenger receptor is also expressed within the immune compartment of the TME; hence CD36 inhibition could also boost immunosurveillance. Indeed, genetic ablation of CD36 in CD8+ T cells (Ma et al., 2021) or T_{regs} (Wang et al., 2020) increases anti-tumour immunity. This immune surveillance is further boosted in both cases when CD36 ablation is combined with anti-PD-1 therapy (Ma et al., 2021; Wang et al., 2020). Luckily, CD36 expression is relevant for tumour infiltrating T_{reg} cells but not for the circulating ones, thus its inhibition should not lead to autoimmune diseases (Wang et al., 2020).

Other FA transporters, such as FATP1 (Zhang et al., 2018), FATP2 (Alicea et al., 2020) and FABP4 (Nieman et al., 2011), are associated to cancer progression and should be considered as promising therapeutic targets as well. Additionally, considering the importance of FA uptake and lipid transporters in cancer progression and therapy resistance, the design of FA-like prodrugs could be an effective strategy to facilitate drug entry specifically in the cells of interest, decreasing side effects and drug toxicity (Jayawardhana et al., 2020)

FAO: CPT1A, ACSL1

Cells that upregulate lipid uptake usually present an enhanced FAO, which could also be targeted to hamper cancer progression. *CPT1A* KD decreases EMT and invasion (Wang

et al., 2020b) and can even induce anoikis (Sawyer et al., 2020). *ACSL1* KD also reduces FAO and LN metastatic capacity of OSCC cells (Pascual et al., 2017). In the immune compartment, inhibition of FAO specifically in MDSCs decreases their immunosuppressive function and delays tumour growth in a T cell dependent manner (Hossain et al., 2015). Further, etomoxir (CPT1A inhibitor) treatment could re-sensitize trastuzumab resistant cells by inhibiting FAO and reversing their stem phenotype (Han et al., 2020). Nevertheless, thanks to their metabolic plasticity, tumour cells can overcome FAO inhibition by glycolysis upregulation (Aloia et al., 2019).

Lipid desaturation: SCD1

SCD1 inhibition has been tested in some pre-clinical studies with promising results. Inhibition of SCD1 induces cell death by ER stress-induced apoptosis in glioblastoma (Pinkham et al., 2019) and by ferroptosis in ovarian cancer (Tesfay et al., 2016). *SCD1* KD also decreases EMT, migration and invasion of CRC cells (Ran et al., 2018). However, targeting SCD1 can produce self-defeating results as observed in melanoma, where SCD1 inhibition decreases cancer cell proliferation but induces a pro-inflammatory phenotype and metastasis (Vivas-García et al., 2020). Moreover, SCD1 chemical inhibition can be bypassed by the cells through an alternative FA desaturation pathway involving FADS2 (Vriens et al., 2019). Further studies are needed to clarify the concrete cancer types and circumstances in which SCD1 inhibition can be beneficial.

Ferroptosis: GPX4

Ferroptosis might have evolved as an anti-tumour mechanism: many tumour suppressors, such as p53, sensitize cells to ferroptosis. Unlike the rest of the cells of the body, cancer cells are particularly sensitive to lipid peroxidation; thus, they often have upregulated GPX4 to avoid ferroptosis (Jiang et al., 2021). This specificity makes GPX4 a highly interesting therapeutic target. Indeed, *GPX4* knock out (KO) significantly reduces the metastatic incidence in melanoma, although cancer cells disseminating through lymphatic vessels might not rely that much on this pathway (Ubellacker et al., 2020). Sensitization to ferroptosis can also be an interesting approach to overcome certain therapy resistances. Different mesenchymal cancer cells have an increased proportion of PUFAs within the PM that somehow helps them coping with therapy. This excess of PUFAs creates a dependency of those cells on targetable-GPX4 to avoid ferroptosis. Indeed, *GPX4* genetic ablation leads to tumour regression (Viswanathan et al., 2017). However, contrary to what happens with CD36, GPX4 systemic inhibition might give conflicting responses. Upon lipid accumulation, over expression of GPX4 in CD8+ T cells can prevent the ferroptotic death and restore their anti-tumour immunity (Xu et al., 2021). On the other hand, there are mechanisms independent of GPX4 that cancer cells can use to cope with lipid peroxidation upon GPX4 inhibition (Blomme et al., 2020; Garcia-Bermudez et al., 2019; Jiang et al., 2021).

Lipid synthesis: FASN, HMGCR

FASN also appears as an attractive target for cancer treatment given the implications of this enzyme in tumour progression. Chemical inhibition of FASN with G28UCM in a model of BC delays tumour apparition and infiltration (Bueno et al., 2019). Also, genetic ablation of *FASN* impairs BC metastatic outgrowth in the brain (Ferraro et al., 2021) and inhibition of this enzyme with orlistat in combination with cisplatin delays tumour growth in cisplatin-resistant ovarian cancer cells (Papaevangelou et al., 2018). Orlistat is an FDA (US Food and Drug Administration) and EMA (European Medicines Agency)-approved FASN inhibitor already used in the clinic for obesity treatment. It has shown very promising effects in pre-clinical studies, decreasing melanoma (Seguin et al., 2012) and OSCC (Agostini et al., 2014) metastatic burden. Other FASN inhibitors such as TVB-2640 have been developed and they are already being tested in clinical trials in combination with standard of care therapies (Broadfield et al., 2021b). Unfortunately, FASN inhibition can lead to CD36 upregulation as a compensatory mechanism. Combined FASN and CD36 inhibition might be required to overcome this resistance (Drury et al., 2020).

Other lipid metabolism-related drugs already being tested in clinical trials against cancer are statins. Statins inhibit HMGCR, the rate-limiting enzyme for cholesterol synthesis (Di Bello et al., 2020) and have shown promising results in pre-clinical studies in decreasing both tumour growth (Chou et al., 2019; Yin et al., 2018) and metastasis (Yin et al., 2018), as well as in re-sensitizing resistant cancer cells to different treatments (Feng et al., 2020; Yin et al., 2018).

To sum up, recent discoveries have emphasized the extreme relevance of lipid metabolism in cancer progression. Cancer cells use lipid metabolism as a mechanism of adaptation to the different challenging environments faced during the metastatic cascade. FA uptake and lipid metabolism provides tumour cells with energy and molecules used for membranes biosynthesis but it also helps them to modulate redox homeostasis. Regulating lipid metabolism, cancer cells can adapt the lipid membrane composition and generate metabolic intermediates to better tolerate the excess of ROS generated in the different stressing moments of tumour progression. This dependency of the most aggressive cancer cells on lipid metabolism, shapes it as an attractive target to stop tumour progression. Nevertheless, metastatic cancer cells are characterized by their plasticity and their capacity to accommodate to changes in the environment. Combinatory and aggressive treatments will probably be necessary to kill these tumour cells before adaptation occurs.

2 Lipid modifications of proteins

Of the many different types of lipid modifications of proteins, the most common one is protein acylation, which is the covalent modification of proteins with different acyl groups (usually FAs). Most acylated proteins are modified with the long-chain saturated FAs: myristate (14:0) and palmitate (16:0). However, shorter or unsaturated FAs can also be attached to proteins, such as propionic acid (3:0) and butyric acid (4:0) (Resh, 2016). At least five different types of acylation have been described depending on the site of modification and kind of linkage, summarized in **Table I2.1**.

Protein **N-myristoylation** is the irreversible covalent addition of myristate (14:0) to the amino-terminal (N-terminal) glycine of the protein with an amide linkage. This modification usually occurs co-translationally, right after cleavage of the initial methionine, although it can also happen post-translationally after exposition of an internal glycine (Resh, 2013; Resh, 2016; Smotrys and Linder, 2004; Udenwobele et al., 2017). N-myristoylation is catalyzed by NMT (N-myristoyl transferase) and it affects more than 150 proteins, including eNOS (endothelial nitric oxide synthase), Src family of kinases, and the $G_{i\alpha}$ family of protein signaling subunits (Udenwobele et al., 2017; Smotrys and Linder, 2014).

N-palmitoylation is the post-translational addition of a PA moiety to the N-terminal cysteine of a protein with an amide linkage. This modification was first observed in SHH (Sonic hedgehog) protein which has to be dually modified by cholesterol on its C-terminus and palmitate on its N-terminus in order to be properly secreted (Pepinsky et al., 1998; Resh, 2016). Hhat (Hedgehog acyltransferase) is a member of the MBOAT (membrane bound O-acyl transferase) family of proteins and is located in the ER. This enzyme is the responsible for N-palmitoylation of SHH as well as other members of the hedgehog family of proteins (Tukachinsky et al., 2012). Other proteins have been found to be N-palmitoylated in *Drosophila melanogaster*; however, to date, no further proteins have been described as N-palmitoylated in mammals (Resh, 2013; Resh, 2016).

Acylation at the ϵ -amino group of lysine is present in other secreted proteins. TNF α (tumour necrosis factor alpha) and IL-1 α (interleukin 1 alpha) precursors are myristoylated on lysines through an amide linkage probably to facilitate their traffic towards the PM (Stevenson et al., 1992; Stevenson et al., 1993). This post-translational modification (PTM) is not just present in secreted proteins. Histones are also acylated on their lysines by myristoyl groups or by shorter acyl groups, like propyl or butyryl (Chen et al., 2007; Kebede et al., 2017; Liu et al., 2009). The enzyme responsible for TNF α and IL-1 α myristoylation has not yet been identified, but p300 can acylate histones (Chen et al., 2007; Liu et al., 2009).

Acyl modification	Chemical structure	Acyl transferases	Erasers	Substrate examples
N-myristoylation (N-terminal Gly)		NMT	-	(>150) eNOS, Src, Gi α
N-palmitoylation (N-terminal Cys)		Hhat	-	SHH
ϵ-amino acylation (Lys)		p300	SIRT5	Histones
		-	SIRT6	TNF α
		-	-	IL1 α
O-acylation (Ser or Thr)		Porcn	Notum	Wnt
		GOAT	-	Ghrelin
		Lpcat1	-	Histone H4
S-acylation (Cys)		DHHCs	APT1/2 PPT1 ABHD17	>4000* Ras, CAV, CD44, TEAD, STAT3, CD36, Histone H3

Table I2.1. Summary of the different types of fatty-acylations that proteins can undergo.

The chemical structure of ϵ -amino acylation corresponds to an ϵ -amino myristoylation, the representation of O-acylation is an O-palmitoylation and the one for S-acylation is a S-palmitoylation, although different fatty acids can bind to proteins with these linkages. In the chemical representations: oxygen (O) atoms and their covalent bonds are pictured in red, nitrogen (N) atoms in blue and sulfur (S) ones in green. H represents hydrogen; C is carbon; AA represents the rest of the amino acids of the protein and R stands for “residue” that can differ depending on the amino acid of the linkage (Ser or Thr). Chemical structures were drawn using BioEddie tool from Chem Axon. – appears in the table when the acyl transferase or the eraser is unknown or does not exist. *According to SwissPalm database (Blanc M et al., 2015).

Certain sirtuins (SIRT), known as NAD-dependent deacetylases, can efficiently remove long-chain fatty acids from acylated lysine residues. For instance, the SIRT6 demyristoylates TNF α , allowing its secretion (Jiang et al., 2013). *In vitro* studies also show that interactions of SIRT6 with long-chain FAs enhances its low deacylase activity and that SIRT2 can also remove acylations from histone residues (Feldman et al., 2013; Liua et al., 2015; Teng et al., 2014).

Proteins are **O-acylated** when the FA is attached to either a serine or a threonine through an oxyester linkage. Wnt proteins are O-acylated by a monosaturated form of

palmitate, cis- Δ^9 palmitoleate (16:1ⁿ⁹) (Resh, 2016). This modification is catalyzed by Porcn (Porcupine), another ER resident member of the MBOAT acyltransferase family of proteins. This acylation allows the Wnt protein to travel to the PM and to interact with Wntless for its secretion, as well as to interact with its receptor Frizzled (Janda et al., 2012; Zeng et al., 2015). Palmitoleation of Wnt can be specifically removed by Notum, a conserved antagonist with carboxylesterase activity (Kakugawa et al., 2015). Ghrelin and histone H4 are other two examples of O-acylated proteins. Ghrelin is a secreted peptide hormone that can only bind its receptor when it is acylated. The enzyme in charge of Ghrelin's acylation is GOAT (Ghrelin O-acyltransferase), another MBOAT protein, which catalyzes the binding of an octanoate (8:0) molecule to Ghrelin's Ser3 (Yang et al., 2008). Although most circulating Ghrelin is not acylated, no deacylase has been described yet for it (Satou et al., 2012). Histone H4 can be O-palmitoylated by LPCAT1 on its Ser47. While its principal function of this cytoplasmic enzyme is the addition of saturated acyl-CoAs (mainly palmitoyl-CoA groups) to PM lysophospholipids, LPCAT1 is quite promiscuous and it could acylate proteins as well. O-palmitoylation of histone H4 can activate RNA polymerase II and enhance genome-wide transcription (Zou et al., 2011).

The last known type of protein acylation is **S-acylation** or **thioacylation**, which takes place on cysteine residues through a thioester linkage. Even though proteins can be S-acylated with different FAs, regardless of their length (usually 14C or longer) or saturation, the traditional term used in the literature for this modification is **S-palmitoylation**. As the traditional term states, palmitate (16:0) is the most common fatty acid present in S-acylated proteins, followed by palmitoleate (16:1), stearate (18:0) and oleate (18:1). (Smotrys and Linder, 2004; Tabaczar et al., 2017; Won et al., 2018).

To date, only the SHH proteins family has been described to be N-palmitoylated, and very few proteins have been found to be O-palmitoylated. In sharp contrast, there are more than 13,000 proteins in the human proteome predicted to be S-palmitoylated, with more than 4,500 already validated or described at least in one palmitoylome study according to SwissPalm database (Blanc M et al., 2015). Thus, S-palmitoylation is by far the most common lipid-based PTM and it will be discussed in more detail in the next section.

Although fatty acid acylations are the most common lipid modifications of proteins, other lipid PTMs such as prenylation or the attachment of the glycosylphosphatidylinositol (GPI) anchor, are fundamental for the biology of the cell. Protein **prenylation** consists of the covalent binding of farnesyl (15C) or geranylgeranyl (20C) isoprenoid groups to a cysteine at or near the C-terminus of the protein through a thio-ether linkage. Both types of prenylation enhance the interaction of the proteins with the membranes although farnesylation is not sufficiently hydrophobic to anchor the modified protein to the membrane. Farnesylated proteins such as H- or N-Ras

require a second lipid modification, such as palmitoylation, to form a stable membrane interaction (Resh M.D., 2013). The **GPI anchor** comprises a phosphatidylinositol, 1 glucosamine, 3 mannoses and a phosphoethanolamine bound to the carboxy terminal of the protein through an amide linkage. GPI-anchored proteins are usually localized at the extracellular cell surface in specific domains of the PM. There are at least 150 GPI-anchored proteins in humans (Resh M.D., 2013).

2.1 Protein S-acylation (S-palmitoylation)

S-apalmitoylation is the addition of a long-chain FA to a cysteine residue through a thioester linkage (traditionally known as palmitoylation), and thousands of proteins have been described with this PTM. S-palmitoylation is catalyzed by a family of protein acyl transferases (PATs) that contain zinc-finger and aspartate-histidine-histidine-cysteine (Asp-His-His-Cys, DHHC) domains, although high concentrations of PA can induce the non-enzymatic palmitoylation of accessible cysteines (Won et al., 2018). S-palmitoylation it is removed by different protein thioesterases (Tabaczar et al., 2017; Won et al., 2018; Korycka et al., 2012). Importantly, to date, S-palmitoylation is considered to be the only reversible lipid modification of proteins. It is true that certain erasers have been found for some specific acylated proteins like the ones previously mentioned. However, in the case of S-palmitoylation the mechanism of deacylation is more dynamic, general and less specific. Most S-palmitoylated proteins can undergo several rounds of palmitoylation and depalmitoylation during the protein's lifetime, which is used by the cell as a mechanism to regulate protein function and cell signaling. (Smotrys et al., 2004).

2.1.1 Protein acyl transferases (PATs)

There are few described cases of proteins that can undergo auto-palmitoylation or self-palmitoylation. Most of those proteins are the DHHC-PATs, in charge of the S-palmitoylation of all the rest of palmitoylated proteins, but other proteins like TEAD (TEA domain transcription factor) (Chan et al., 2016) and Bet3 (Kümmel et al., 2006) can also get autopalmitoylated. All these auto S-palmitoylated proteins present a similar structure with a hydrophobic pocket where the FA locates and an accessible cysteine residue that generates the thioester linkage (Chan et al., 2016; Kim et al., 2005; Rana et al., 2018).

There are 23 *ZDHHC* genes in the human genome (*ZDHHC1–ZDHHC24*, *ZDHHC10* is omitted) that encode 23 different DHHC-PATs (**Table I2.2**). Although protein palmitoylation was discovered in 1979, the enzymes responsible for this modification were not identified in *Saccharomyces cerevisiae* until 2002 (Lobo et al., 2002; Roth et

al., 2002) and it was only in 2018 when the crystal structure of the human DHHC20 (hDHHC20) was resolved (Rana et al., 2018).

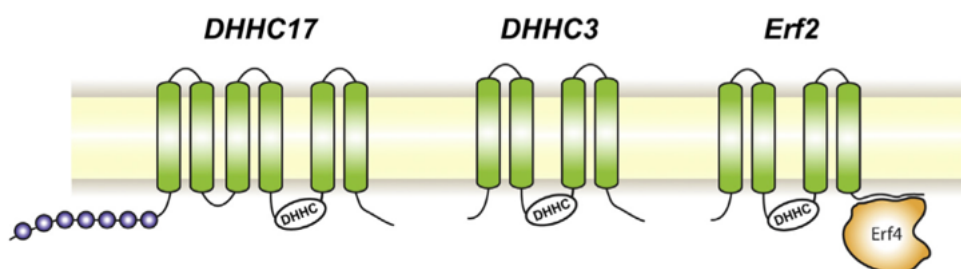


Figure I2.1. Examples of structures of DHHC-PATs. Adopted from Stix et al., 2020. Human DHHC17 and DHHC3 and yeast Erf2 are represented. DHHC17 has six transmembrane domains and an ankyrin repeat domain at the N-terminal. DHHC3 only presents four transmembrane helices and Erf2 needs to interact with Erf4 for its activity. In all cases the catalytic domain DHHC is located at the interface between PM and cytoplasm.

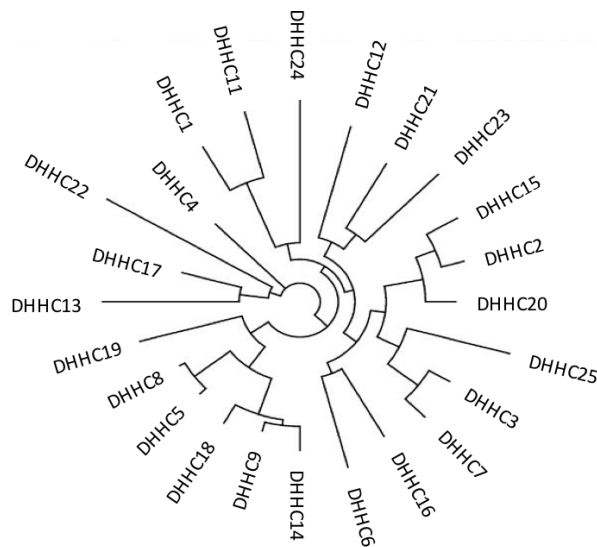
2.1.1.1 Protein structure

All PATs share some commonalities in their sequence of amino acids, and presumably in their structure, important for their function. **Figure I2.2** shows the phylogenetic tree of mouse DHHC-PATs based on the similarities of their catalytic domain. The first, and most important common feature is the active site. The catalytic domain of these transmembrane enzymes, is located at the interface between the cytoplasm and the membrane (**Figure I2.1**). It consists in the previously mentioned tetrapeptide: Asp-His-His-Cys (DHHC), surrounded by around 50 highly conserved amino acids rich in Cys and His. These two motives together form the DHHC cysteine rich domain (DHHC-CRD) and they are usually located between transmembrane domains 2 and 3 (Putilina et al., 1999; Rana et al., 2018; Stix et al., 2020; Tabaczar et al., 2017). This catalytic region contains two zinc-finger domains, which bind two Zn^{2+} ions that seem to have only a structural, and no catalytic, role (Gottlieb et al., 2015; Rana et al., 2018). Most DHHC enzymes also present a palmitoyl transferase conserved C terminus (PaCCT) that is fundamental for the enzymatic activity (González Montoro et al., 2009). All these enzymes also contain 4 or more transmembrane helices that generate a closed cavity where the FA is located for catalysis (**Figure I2.3**) (Stix et al., 2020).

PATs differ the most at their C- and N- termini, which are located in the cytosol. In these regions, some DHHCs contain protein-protein interaction domains that can affect the substrate recognition. DHHC13 and DHHC17 present an ankyrin repeat (ANK) domain at their N-terminus (**Figure I2.1**), while several other DHHC-PATs (DHHC3, 5, 7, 8, 14, 16, 17, 20 and 21) have a PDZ-binding motif and DHHC6 is predicted to have a SH3 domain

(Table I2.2) (Tabaczar et al., 2017; Stix et al., 2020). Some of these non-catalytic domains are important for the interaction with other non-substrate proteins that can regulate their activity. GPC19 (Golgi localized membrane protein 19) interacts with DHHC9 and is fundamental maintaining the activity and stability of the PAT (Swarthout et al., 2005). These non-catalytic domains can also be involved in the determination of the PAT location within the cellular organelles or in the regulation of the PAT activity (see the “Regulation of protein palmitoylation” section) (Gorleku et al., 2011).

Figure I2.2. Phylogenetic tree of DHHC-PATs. Adopted from Greaves and Chamberlain, 2011. Tree showing the evolutionary relationships of mouse DHHC-PATs based on the amino acid sequence of their DHHC-CR domain.



2.1.1.2 Substrate specificity

The substrate specificity of PATs is one of the most controversial aspects of their biology. Some studies argue that different DHHCs have overlapping activities and that a substrate can be palmitoylated by different PATs. DHHC9 was described as the enzyme responsible for H-Ras palmitoylation (Swarthout et al., 2005). However, others showed that upon DHHC9 KD, H-Ras protein was still palmitoylated and functional (Rocks et al., 2010). In fact, DHHC18 can also palmitoylate H-Ras *in vivo* (Fukata et al., 2004). Another example of protein palmitoylated by different PATs is PSD-95 (postsynaptic density protein 95), which can be palmitoylated by: DHHC2, 3, 7, 8, 15, and 17 (Fukata et al., 2004; Huang et al., 2004; Mukai et al., 2008; Ohno et al., 2012). There does not seem to be a well-defined consensus sequence of amino acids in the palmitoylated motifs (Smotrýs et al., 2004). Some authors suggest that the only requirements that any protein needs in order to be palmitoylated is having an accessible cysteine residue and being able to transiently locate at the Golgi membranes, where most PATs reside (Rocks et al., 2010).

In contrast, many studies claim that a specific DHHC is necessary for the S-palmitoylation of a particular protein, and when that enzyme is missing, the substrate is not longer palmitoylated. This is the case of STAT3 (signal transducer and activator of transcription 3), which is specifically palmitoylated by DHHC7. In the absence of DHHC7, STAT3 is no longer acylated and cannot travel to the PM to interact with JAK2 (Janus kinase 2) and promote T helper 17 cell differentiation (Zhang et al., 2020b). Similarly, R-Ras is palmitoylated by DHHC19, which is not able to acylate N-Ras, H-Ras or RhoB (Baumgart et al., 2010). This specificity can be determined in part by the differential non-catalytic domains of the DHHC enzymes (Huang et al., 2004; Huang et al., 2009), but also by the substrate structure. A point mutation in the cysteine-rich domain of SNAP23, making it similar to one of DHHC15's targets, is sufficient to induce its palmitoylation by DHHC15 (Greaves et al., 2010).

Thus, the specificity of DHHC-PATs for a particular substrate can depend on many different aspects. It is possible that some substrates are more promiscuous and can be acylated by many different enzymes, like PSD-95 (Fukata et al., 2004; Ohno et al., 2012), while others have a particular structure that can only be recognized by the PATs containing a specific protein-recognition domain (Huang et al., 2004). This specificity can also depend on the level of expression of each DHHC-PAT in a specific cell type as well as the intracellular location of that particular PAT. For example, PSD-95 can be palmitoylated by DHHC2, 15, 3, 7 and 17, all of them resident of the Golgi membrane. DHHC2 and 15 are phylogenetically very close and their structure is very similar (**Figure I2.2**), which can explain their shared affinity for PSD-95. The same happens with DHHC3 and 7 (**Table I2.2**). However, PSD-95 is not a known substrate of DHHC13, even though DHHC13 is very similar to DHHC17 (**Figure I2.2**), probably because DHHC13 is located at the ER and not at the Golgi, which can prevent its interaction with the substrate. Further, it is important to emphasize that even if two DHHC-PATs palmitoylate the same substrate, they can still have complementary and non-redundant functions. This is the case of DHHC4 and DHHC5 enzymes and CD36 palmitoylation (**Figure I2.4**). Both PATs are necessary for the location of CD36 at the PM. This complementation in the function can be explained by the different subcellular location of both PATs (**Table I2.2**). DHHC4, located at the Golgi, palmitoylates CD36 and induces its traffic towards the PM. There, DHHC5 maintains the palmitoylated state of CD36 until the receptor binds a FA (Wang et al., 2019d).

2.1.1.3 Acyl-CoA specificity

DHHCs usually S-acylate their substrates with PA (16:0) but they can also use palmitoleate (16:1), stearate (18:0), oleate (18:1) or other less-abundant long-chain FAs. The specificity for the FA might rely largely on each particular DHHC structure (Greaves et al., 2017; Jennings et al., 2012; Stix et al., 2020). Protein S-acylation occurs in a two-

step mechanism. First, PATs are autoacylated and then transfer the FA to their substrate (Stix et al., 2020) (Figure 12.3). Different DHHCs present distinct acyl-CoA preference for autoacylation *in vitro*; for instance, DHHC2 can equally bind different FAs of 14C or longer, while DHHC3 is limited to FAs up to ≤ 16 C. Further, autoacylation is the restrictive step that confers acyl-CoA specificity (Jennings et al., 2012).

Other studies have discovered that the preference of each DHHC for a specific FA is mainly determined by its transmembrane domain structure, which creates a cavity in the PM where the FA is located during the catalytic reaction (Figure 12.3). The residues directly facing the cavity are the ones limiting the size and saturation state of the FA. This structural limitation explains why DHHC3 and DHHC7 present different acyl-CoA affinity, despite being in the same phylogenetic group (Figure 12.2). DHHC7 prefers longer chain-FAs like palmitate (16:0) or stearate (18:0), but DHHC3 presents an isoleucine residue in its transmembrane domain 3 that limits its binding capacity to myristate (14:0) or palmitate (16:0) (Greaves et al., 2017). These observations were confirmed when the crystal structure of hDHHC20 got resolved (Rana et al., 2018).

Another source of complexity determining the specificity of DHHC-PATs for different FAs, can arise from the differential distribution of the diverse FA species within the membranes of the cell and the subcellular location of the PATs (Table 12.2) (Stix et al., 2020).

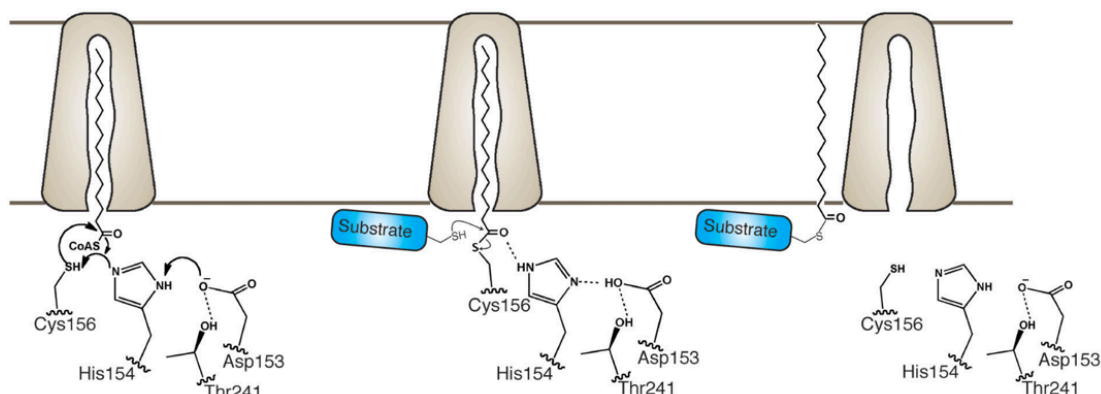


Figure 12.3. Detail of the S-acylation reaction. Adopted from Rana et al., 2018.

The transmembrane helices of PATs generate a cavity within the PM where the acyl-CoAs are located. Then, S-palmitoylation occurs through a “ping-pong” kinetic reaction. First, the DHHC-PAT gets autopalmitoylated and then, the enzyme transfers the FA to the substrate. Cys156 and His154 are the residues responsible for the catalysis.

Enzyme	Particular characteristic	Subcellular location	Examples of substrates and method of detection
DHHC1	-	ER/Cyt.	Ncdn (<i>in vitro</i>) (Oku et al., 2013)
DHHC2		ER and Golgi/ PM	PSD-95, GAP-43 (<i>in vivo</i> , OE) (Fukata et al., 2004) SNAP23, SNAP25b (<i>in vivo</i> , OE) (Greaves et al., 2010) eNOS (<i>in vivo</i> , OE) (Fernández-Hernando et al., 2006) CD9, CD151 (<i>in vivo</i> , OE) (Sharma et al., 2008) CKAP4 (P63) (<i>in vivo</i> , OE) (Zhang et al., 2008)
DHHC3 (GODZ)	- PDZ domain	Golgi/Golgi	PSD-95, GAP-43 (<i>in vivo</i> , OE) (Fukata et al., 2004) SNAP25b (<i>in vivo</i> , OE) (Fukata et al., 2004; Greaves et al., 2010) SNAP23 (<i>in vivo</i> , OE) (Greaves et al., 2010) Ncdn (<i>in vitro</i>) (Oku et al., 2013) eNOS (<i>in vivo</i> , OE) (Fernández-Hernando et al., 2006) GABBAA-γ2, AMPA-GluR1/2 (<i>in vivo</i> , OE) (Huang. et al., 2009) Gα (<i>in vivo</i> , OE) (Tsutsumi et al., 2009) ITGα6, ITGβ4 (<i>in vivo</i>) (Sharma et al., 2012)
DHHC4		Golgi/ -	CD36 (<i>in vivo</i> , animal model) (Wang et al., 2019d)
DHHC5	- PDZ domain - CCX7-13(S/T) domain - Regulated by: Fyn and Lyn	PM/PM and nucleoplasm	CD36 (<i>in vivo</i> , animal model) (Wang et al., 2019d) δ-Catenin (<i>in vivo</i> , OE) (Brigidi et al., 2014)
DHHC6	- SH3 domain (interacts with Selk through SH3) - CCX7-13(S/T) domain	ER/-	Calnexin (<i>in vivo</i>) (Lakkaraju et al., 2012) TFR1 (<i>in vivo</i>) (Senyilmaz et al., 2015) IP3R (<i>in vivo</i>) (Fredericks et al., 2014)
DHHC7	- PDZ domain	Golgi/Golgi	PSD-95, GAP-43, SNAP25b (<i>in vivo</i> , OE) (Fukata et al., 2004) STAT3 (<i>in vivo</i> , OE) (Zhang et al., 2020b) CAV1 (<i>in vivo</i> , OE) (Tonn et al., 2018) SNAP23 (<i>in vivo</i> , OE) (Greaves et al., 2010) Ncdn (<i>in vitro</i>) (Oku et al., 2013) eNOS (<i>in vivo</i> , OE) (Fernández-Hernando et al., 2006) Gα (<i>in vivo</i> , OE) (Tsutsumi et al., 2009) NCAM (<i>in vivo</i> , OE) (Ponimaskin et al., 2008) SCRIB (<i>in vivo</i> , OE) (Chen et al., 2016)
DHHC8	- PDZ domain - CCX7-13(S/T) domain	Golgi/ Nucleoplasm and Cyt.	PSD-93, PSD-95, SNAP25 (<i>in vivo</i> , OE) (Mukai et al., 2008) eNOS (<i>in vivo</i> , OE) (Fernández-Hernando et al., 2006) ABCA1 (<i>in vivo</i> , OE) (Singaraja et al., 2009)
DHHC9	- Interacts with GPC19	ER and Golgi/ ER, Golgi, Cyt.	H-/N-Ras (<i>in vitro</i>) (Swarthout et al., 2005)
DHHC11		ER/ Mito.	Ncdn (<i>in vitro</i>) (Oku et al., 2013)

Enzyme	Particular characteristic	Subcellular location	Examples of substrates and method of detection
DHHC12		ER and Golgi/ Nucleoplasm	CLND3 (<i>in vivo</i> , OE) (Yuan et al., 2020)
DHHC13 (HIP14L)	ANK domain	ER/Vesicles	HTT (<i>in vivo</i> , OE) (Huang et al., 2009) CTNND1, MCAT, ACAA2 (<i>in vivo</i> , OE) (Shen et al., 2017)
DHHC14	PDZ domain	ER/Nucleoli, Mito.	
DHHC15		Golgi/Nuclear speckles and Cyt.	PSD-95, GAP-43, SNAP25b (<i>in vivo</i> , OE) (Fukata et al., 2004)
DHHC16	PDZ domain	ER/ Nucleoplasm and Cyt.	
DHHC17 (HIP14)	ANK domain	Golgi/Golgi and vesicles	PSD-95, HTT (<i>in vitro</i>) (Huang et al., 2004) Lck (<i>in vivo</i> , OE) (Fukata et al., 2004) SNAP25b (<i>in vivo</i> , OE) (Fukata et al., 2004; Greaves et al., 2010) SNAP23 (<i>in vivo</i> , OE) (Greaves et al., 2010) H-Ras (<i>in vitro</i>) (Ducker et al., 2004)
DHHC18		Golgi/Microtub.	H-Ras, Lck (<i>in vivo</i> , OE) (Fukata et al., 2004) VAMP7, LAT (<i>in vitro</i>) (Morrison et al., 2020)
DHHC19		ER/-	R-Ras (<i>in vivo</i> , OE) (Baumgart et al., 2010) PDE10A (<i>in vivo</i> , OE) (Charych et al., 2010)
DHHC20	PDZ domain	PM/PM and vesicles	δ-Catenin (<i>in vivo</i> , OE) (Brigidi et al., 2014) EGFR (<i>in vivo</i>) (Runkle. et al., 2016)
DHHC21	PDZ domain	PM/ Golgi and Cyt.	eNOS (<i>in vivo</i> , OE) (Fernández-Hernando et al., 2006) CAV1 (<i>in vivo</i> , OE) (Tonn Eisinger et al., 2018) Lck (<i>in vivo</i> , OE) (Tsumumi et al., 2009) Fyn (<i>in vitro</i>) (Mill et al., 2009)
DHHC22		ER and Golgi/ PM	BK (<i>in vitro</i>) (Tian et al., 2012)
DHHC23		ER and PM/ Nucleoplasm	BK (<i>in vitro</i>) (Tian et al., 2012)
DHHC24		ER and PM/ Vesicles and Cyt.	Gp78 (<i>in vivo</i> , OE) (Fairbank et al., 2012)

Table I2.2 A & B. Detail of the structural characteristics, location and examples of substrates of each DHHC-PAT. The names of the DHHC enzymes are colored based on their phylogenetic proximity, further detailed in figure I2.2. Those PATs written with the same color are very close and present a similar structure. The ones that remain in black are not closely related to any other DHHC enzyme. For some enzymes no particular structural characteristics or substrates have been described. As for the location, in black location described in [Korycka et al., 2012](#) based on NCBI database; in dark red, location accepted by The Human Protein Atlas ([Thul et al., 2017](#)). Cyt. = cytoplasm; Mito. = mitochondria; ER = endoplasmic reticulum; PM = plasma membrane; Mitrotub. = microtubules; OE = overexpression.

2.1.2 Protein thioesterases

As it has been mentioned, protein S-palmitoylation is a reversible lipid modification of proteins. Protein thioesterases, also known as protein depalmitoylases, are the enzymes responsible for the removal of the thioester-linked long-chain FAs from the Cys residues of S-palmitoylated proteins. To date, three different enzyme families have been described to have protein thioesterase activity: APTs (acyl-protein thioesterases), PPTs (palmitoyl-protein thioesterases) and ABHD17s (α/β hydrolase-domain containing 17 proteins) ([Won et al., 2018](#)).

2.1.2.1 APT1/2

APT1 and 2 are also known as LYPLA1/2 (lysophospholipase 1 and 2). In addition to their protein thioesterase activity both enzymes can hydrolyze lysophospholipids ([Sugimoto et al., 1996](#)). On top of that, APT1 hydrolyzes other long-chain mono acyl-glycerol esters ([Won et al., 2018](#)) while APT2 hydrolyzes prostaglandin glycerol esters ([Manna et al., 2014](#)). Despite their protein structures being nearly identical, they show great specificity in the substrates they depalmitoylate and also have specific inhibitors: ML348 (APT1) and ML349 (APT2) (**Table R2.3**) ([Adibekian et al., 2012](#)). For example, APT2 is the enzyme responsible for SCRIB (scribble planar cell polarity protein) depalmitoylation ([Chen et al., 2016](#); [Hernandez et al., 2017](#)) while APT1 shows no activity against this protein. The opposite happens with CD36's acylation, which is only removed by APT1 ([Hao et al., 2020](#)). Nevertheless, APT1 and 2 also show certain redundancy in the depalmitoylation of some targets like HTT (huntingtin), whose deacylation is only abolished when both enzymes are inhibited at the same time ([Lin et al., 2015](#)).

Both enzymes are mainly located at the cytoplasm although they can also localize to internal membranes ([Vartak et al., 2014](#)), the PM ([Hirano et al., 2009](#); [Kong et al., 2013](#)) or even the mitochondria ([Kathayat et al., 2018](#)). Interestingly, APT1 and APT2 are both palmitoylated at their Cys2 residue, what allows their relocation to membranes,

although the specific DHHC responsible for this palmitoylation is still unknown. APT1 is the enzyme responsible for its own depalmitoylation and that of APT2 as well. The implications of this dynamic cycle of acylation and de-acylation and the cytoplasm-membrane trafficking of both proteins are still under discussion (Kong et al., 2013; Vartak et al., 2014).

2.1.2.2 PPT1/2

PPT1 and 2 are two long-chain FA hydrolases located at the lysosomes and late endosomes (Verkruyse et al., 1996). They probably play a role in autophagy and vesicular depalmitoylation prior to lysosomal degradation of S-acylated proteins but do not seem to affect PM proteins (Koster et al., 2019). Loss of function mutations in these enzymes have been related to neuronal lipid lipofuscinosis (Gupta et al., 2001) therefore, most of the research involving PPT1/2 has focused on their influence in neural system development and function. They remove the S-acylation of synaptic proteins like SNAP25 (synaptosome associated protein 25) or VAMP2 (vesicle associated membrane protein 2) (Kim et al., 2008) but also interact with signaling proteins like Fyn (Sapir et al., 2019).

PPT1 is also palmitoylated on the Cys6 by DHHC3 and DHHC7. However, contrary to what happens with APT1/2, when the cysteine is mutated and the palmitoylation abolished, the location of the protein does not seem to be affected. Apparently, PPT1 palmitoylation would regulate its enzymatic activity but not its location. The S-acylation inhibits the enzyme in an allosteric fashion (Segal-Salto et al., 2016).

2.1.2.3 ABHD17

Until recently, it was thought that APT1/2 and PPT1/2, were the only enzymes responsible for protein depalmitoylation. Nonetheless, a few years ago, Lin et al. realized that upon inhibition or silencing of APTs, N-Ras can still get deacylated by any of the three members of the ABHD17 (Abhydrolase domain containing protein 17A) family of Ser-hydrolases (ABHD17A, ABHD17B, ABHD17C) (Lin et al., 2015). Another study also identified PSD-95 as a substrate of these enzymes as well (Yokoi et al., 2016).

ABHD17 enzymes also have a cysteine that can be palmitoylated at the N-terminal cysteine-rich cluster (Yokoi et al., 2016). This acylation is necessary for their membrane association at the PM or recycling endosomes (Yokoi et al., 2016), although is not directly implicated in the catalytic activity. The membrane localization is necessary for the activity of the enzymes on their substrates (Lin et al., 2015). Neither the PAT nor the thioesterase responsible for the palmitoylation/depalmitoylation of these enzymes have been described (Lin et al., 2015).

ABHD17 enzymes are not the unique ABHD enzymes with S-deacylase activity. Some years ago, it was shown *in vitro* that ABHD10 and ABHD13 have also a Ser-hydrolase activity with preference for lipid substrates (Martin et al., 2012). More recently, ABHD10 was discovered to be a mitochondria resident protein with depalmitoylase activity against PRDX5 (peroxiredoxin 5) *in vivo*. One of the mechanisms of regulation of PRDX5 activity seems to be the palmitoylation of its catalytic cysteine. Therefore, by deacylating that residue, ABHD10 can control the redox homeostasis of the mitochondria (Cao et al., 2019).

Many studies suggest that the different depalmitoylases show specificity in their substrates. For example, ABHD17 can revert the palmitoylation of PSD-95 or N-Ras but it cannot depalmitoylate Fyn (Yokoi et al., 2016), while APT2, removes the S-acylation of SCRIB (Chen et al., 2016), APT-1 acts on CD36 acylation (Hao et al., 2020) and PPT1 cleaves the palmitoylation of SNAP25 or VAMP2. However, some substrates can be deacylated by more than one enzyme from different families. This is the case of GAP-43 (growth associated protein 43) that can be depalmitoylated by ABDH17 (Yokoi et al., 2016), APT2 (Tomatis et al., 2010) and PPT1 (Koster et al., 2019). The same happens with H-Ras, which can be depalmitoylated by ABDH17 (Yokoi et al., 2016), APT1 or 2 (Kong et al., 2013) and even by PPT1 (*in vitro*) (Camp et al., 1993). Thus, similar to what happens with DHHC-PATs, part of this specificity can be given not just by the structure of the enzyme and the substrate, but also by the expression and subcellular location of the thioesterases and their substrates.

2.1.3 Functions of protein palmitoylation

As many other lipid modifications of proteins, palmitoylation main function is the membrane association of otherwise soluble proteins. Nevertheless, S-palmitoylation of proteins is a reversible PTM that can be tightly regulated by the cell which confers it more relevance due to its implications in cell signaling.

2.1.3.1 Membrane association and protein trafficking

Protein palmitoylation takes place mainly at the different membranes of the cell: PM, Golgi or ER membranes. In order to be palmitoylated, soluble proteins first need to interact with a membrane for a period of time long enough for the acyl-transferase activity to occur. For this interaction to happen, many DHHCs substrates are first modified with other lipids (prenyl or myristoyl groups) that trigger a transient translocation of the proteins to a cellular membrane (Smotrys and Linder, 2004). During these short interactions with the membranes, the substrates contact with the DHHC-PATs, which are integral membrane proteins, and get palmitoylated (Smotrys and Linder

,2004). This would be the case of eNOS which needs to interact with the membrane through a N-myristoylation to further get S-palmitoylated and relocated to caveolae domains at the PM (Prabhakar et al., 2000). H-Ras for its part, needs a farnesylation and the interaction of its polybasic domain with the membrane in order to get S-palmitoylated (Hancock et al., 1990).

Palmitoylation does not just anchor soluble proteins to the cellular membranes, in fact, transmembrane proteins can also get palmitoylated. This PTM also helps in the trafficking of proteins through membranes and determines their particular location within specific organelles (Fukata et al., 2016). Calnexin and TMX (thioredoxin related transmembrane protein 1) transmembrane proteins, preferentially localize at the mitochondrial-associated membrane (MAM) of the ER thanks to their double palmitoylation. When their palmitoylated cysteine residues are mutated and cannot get palmitoylated, these two proteins relocate to other fractions of the ER membrane (Lynes et al., 2012). CD36 needs to be palmitoylated at its C- and N- termini in order to be transferred to the PM where it exerts its functions (Figure 12.4). The non-palmitoylated mutant version of CD36 is unable to traffic towards the PM (Wang et al., 2019d). The relevance of protein palmitoylation for the trafficking of proteins through membranes will be further discussed with Ras family and EGFR examples in the next section of the thesis.

S-palmitoylation of proteins also helps in their location in particular specialized domains of membranes (Fukata et al., 2016). Although it is quite controversial, the lipid raft hypothesis states that within cell membranes, especially at the PM, lipids interact with each other and organize lateral areas of order-preferring lipids, like cholesterol or sphingolipids; or disordered lipids such as PUFAs or short lipids. Those tightly packaged areas full of saturated phospholipids, sphingolipids and cholesterol are the lipid-rafts, also called detergent-resistant membranes (DRM) (Levental et al., 2020). Palmitoylated proteins are predicted to have high affinity for lipid rafts. In fact, lipid raft composition shows an enrichment in extracellular proteins anchored to the membrane with lipids like GPI on the outer part or myristoylated and palmitoylated cytoplasmic proteins on the inner part (Levental et al., 2020; Smotrys and Linder, 2004). Proteins modified with unsaturated FA or prenyl groups tend to be excluded from these organized DRM domains (Levental et al., 2020). Therefore, lipid rafts are fundamental areas of the PM, given that they allow the colocalization of different proteins that can interact with each other. We can find a clear example of the importance of protein location at the lipid rafts in the activation of T cells (Kabouridis, 2006). LAT (Linker for activation of T cells) and Lck tyrosine kinase, are two well-known actors of the TCR (T cell antigen receptor) signaling, necessary for T-cell activation (Janes et al., 1999; Kabouridis, 2006; Tanimura et al., 2003). After TCR activation, LAT adaptor protein (Tanimura et al., 2003) and Lck kinase (Janes et al., 1999) get palmitoylated and recruited to lipid rafts where they

interact with TCR or ZAP-70 and trigger T cell activation signaling. The lipid raft structure is not only useful for the colocalization of the proteins, it also helps immobilizing and stabilizing LAT at that particular location (Tanimura et al., 2003). Inhibition of the palmitoylation of either LAT or Lck, leads to their miss-localization and inactivation of the TCR signaling (Janes et al., 1999; Tanimura et al., 2003).

2.1.3.2 Signaling and regulation of protein function

Protein palmitoylation, as other PTMs like phosphorylation, can be used by the cell to regulate different signaling cascades, for instance by membrane re-location of signaling proteins. The most studied example of signaling cascade regulated by palmitoylation is the Ras cascade. There are three human genes of Ras: H-Ras, N-Ras and K-Ras (K-RasA and K-RasB isoforms); and all of them are palmitoylated except K-RasB (Xiang et al., 2017). Right after synthesis, these three hydrophilic globular proteins undergo several PTMs that lead to their farnesylation and interaction with ER membrane with modest affinity (Xiang et al., 2017). Then, Ras proteins are transferred to the Golgi where H-Ras, N-Ras and K-RasA get palmitoylated by DHHC9 (Swarthout et al., 2005). H-Ras is palmitoylated twice, in two different cysteines, and N-Ras and K-RasA are just palmitoylated once. Upon palmitoylation, the three enzymes travel to the PM where they locate at different micro-domains, get activated and interact with their substrates. Upon GTP binding and activation, H-Ras tends to be localized at lipid rafts while N-Ras is present preferentially in disordered areas of the membrane (Eisenberg et al., 2013), although this effect can be cell-type dependent (Agudo-Ibáñez et al., 2015). Few minutes later, they get depalmitoylated by APT-1 and travel back to the Golgi membrane to be re-acylated and start the cycle again (Xiang et al., 2017). It seems that GTP-bound forms of H-Ras and N-Ras have more affinity for APT1, which can be facilitated by conformational changes induced in the Ras proteins upon GTP binding (Baker et al., 2003) or by the interaction with FKBP12 (FKBP prolyl isomerase 1A) (Ahearn et al., 2011). Thus, the cell can limit Ras signaling controlling its presence in the membrane. Disruption of the S-palmitoylation/depalmitoylation cycle of Ras proteins by either palmitoylation or depalmitoylation inhibition, leads to their miss-localization in endomembranes and signaling alteration (Ahearn et al., 2011; Chandra et al., 2012; Xiang et al., 2017).

Apart from regulating cell signaling, palmitoylation can directly alter the function of certain proteins. PRDX5, PPT1 and TEAD are good examples of proteins whose function is directly regulated by S-acylation. As previously mentioned, PRDX5 is a mitochondrial peroxiredoxin that is inhibited by palmitoylation of its catalytic cysteine (Cao et al., 2019). PPT1, one of the few known depalmitoylases, also gets inhibited by the conformational change induced upon palmitoylation (Segal-Salto et al., 2016). On the contrary, in all members of TEAD TF family, the palmitoylation is necessary for their interaction with YAP and the transcription of YAP/TAZ target genes. The PA moiety is

introduced in a hydrophobic cavity of the protein altering its conformation and favoring the interaction with YAP (Chan et al., 2016).

Palmitoylation-induced conformational alterations in the structure of proteins can also affect other PTMs that might regulate the proteins' function. For instance, EGF (epidermal growth factor) binding to EGFR promotes the dimerization and activation of the receptor, which gets auto-phosphorylated at its C-terminal cytoplasmic tail. This phosphorylation favors the interaction and activation of downstream effectors (Sigismund et al., 2018). A few years ago, Runkle et al. described that the mechanism of control and termination of this signaling is based on EGFR palmitoylation by DHHC20. Upon activation of the receptor, DHHC20 palmitoylates EGFR at two independent cysteines present at the C-terminal domain. The S-acylation of the first cysteine attaches the C-tail to the PM preventing EGFR autophosphorylation and downstream signaling by hiding the tyrosine residue that should be phosphorylated. The second palmitoylation triggers the endocytosis and trafficking of the receptor to the lysosome to be degraded (Runkle et al., 2016). Interestingly, the palmitoylation of a third cysteine is necessary for the dimerization of the receptor and its activation (Bollu et al., 2015; Runkle et al., 2016). These results also show that, despite protein palmitoylation is normally thought to increase protein stability by binding proteins to membranes such as in calnexin (Dallavilla et al., 2016), Fas receptor (Rossin et al., 2015) or PD-L1 (programmed cell death ligand 1) (Yao et al., 2019), it can also facilitate protein internalization and degradation as in EGFR (Runkle et al., 2016) or DHHC6 (Abrami et al., 2017).

2.1.4 Regulation of protein palmitoylation

DHHC-PATs and protein thioesterases activity is regulated in response to external or intracellular signals, which allows the cell to tightly control palmitoylation-dependent signaling. For instance, dynamic palmitoylation of CD36 to promote FA internalization is tightly regulated by kinases controlling the PAT's function (**Figure I2.4**). CD36 needs to be palmitoylated by DHHC4 and DHHC5 in order to travel to the PM and remain there, at least in adipocytes. In basal conditions, APT-1 depalmitoylates CD36 but at the same time DHHC5 S-palmitoylates the receptor reaching a homeostatic equilibrium that maintains CD36 at the PM (**Figure I2.4A**) (Hao et al., 2020; Wang et al., 2019d). When a long-chain FA binds CD36, the scavenger receptor activates Lyn kinase, which in turn phosphorylates DHHC5 at Tyr91 and inactivates the enzyme. Without DHHC5 activity, CD36 is depalmitoylated by APT-1 (**Figure I2.4B**). Depalmitoylated CD36 recruits SYK (spleen tyrosine kinase), which phosphorylates VAV and JNK (C-Jun N-terminal kinase 1 (also known as MAPK8)). VAV is an adapter of DNMT1 (dynamin), which triggers the caveolar endocytosis of CD36 bound to the FA (**Figure I2.4C**) (Hao et al. 2020). After FA withdrawal, CD36 can get re-palmitoylated by DHHC4 at the Golgi and re-transported to the PM. Newly synthesized CD36 is also transported from the ER to the Golgi for DHHC4

palmitoylation (**Figure I2.4D**) (Wang et al., 2019d). In other cases, PTMs on PATs can regulate their function by determining their location instead of their activity (Brigidi et al., 2015).

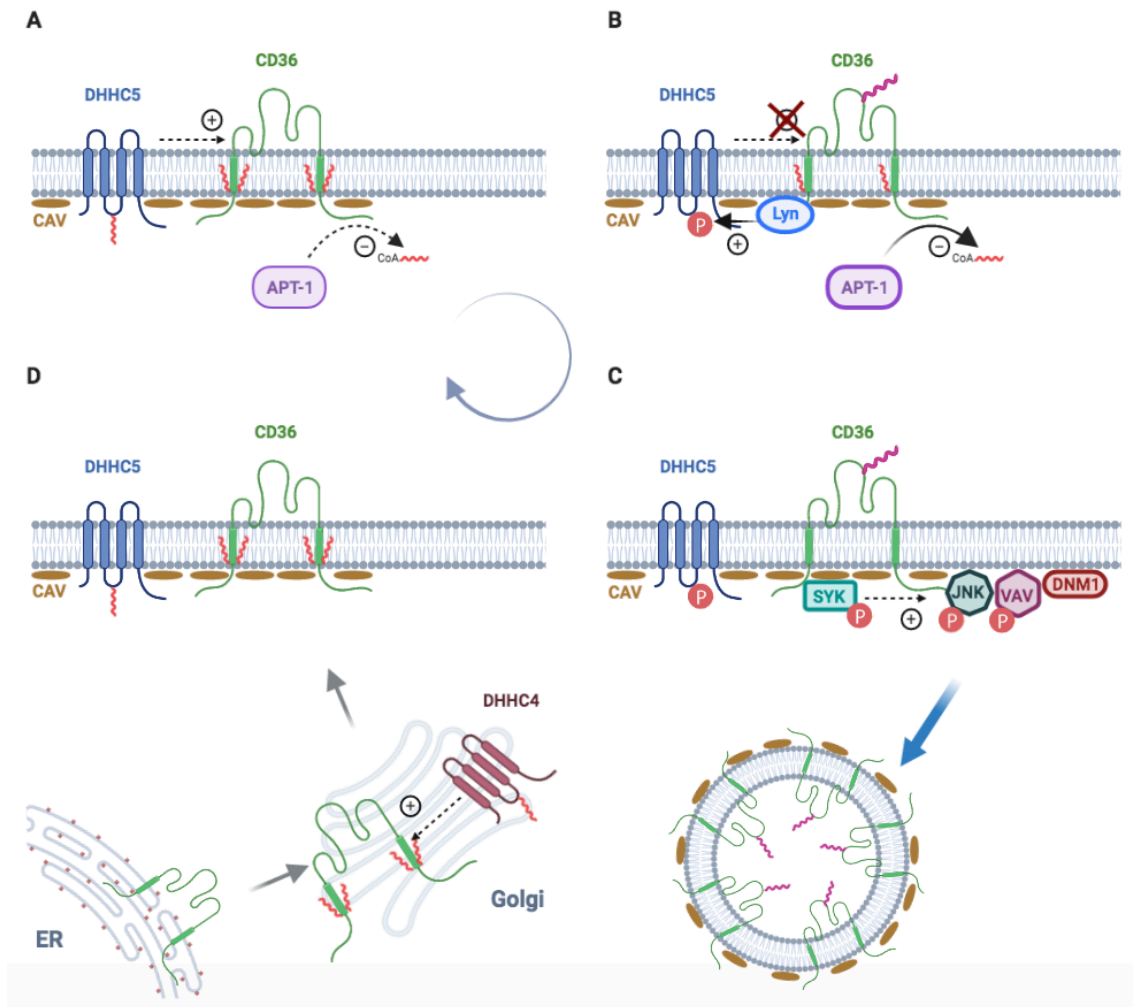


Figure I2.4. CD36 acylation/deacylation cycle. Adapted from the schemes at Wang et al., 2019d and Hao et al., 2020. A) In basal condition, CD36 located at the PM gets palmitoylated by DHH5 and depalmitoylated by APT-1. B) Upon long-chain FA binding Lyn phosphorylates and inhibits DHH5. APT-1 continues depalmitoylating CD36. C) Depalmitoylated CD36 activates SYK, which phosphorylates VAV and JNK and together with DNM1 they trigger the caveolar endocytosis of CD36 bound to the FA. D) CD36 is re-synthesized at the ER and palmitoylated at the Golgi by DHH4 before trafficking to PM. Red zigzagging line represents PA moiety and the pink one any long-chain fatty acid. Created with BioRender.com

Interestingly, PATs can interact with each other generating palmitoylation cascades that allow further dynamic and precise regulation of S-acylation. DHH16 palmitoylates DHH6 in three different Cys at its SH3 domain. The different combinations of those 3

sites of palmitoylation determine the level of DHHC6 activity, but also its degradation rate, probably as a regulatory mechanism. APT2 can depalmitoylate DHHC6 controlling its level of S-acylation, thus generating a palmitoylation/depalmitoylation cascade with DHHC16 (Abrami et al., 2017).

The function of the thioesterases can also be regulated by signaling mechanisms. Wnt5a signaling can control cell polarity through APT1 thioesterase and the depalmitoylation of specific cell adhesion molecules in melanoma cells (Wang, W. et al 2015). Upon Wnt5a binding with its receptor, the inhibitory interaction of APT1 with Dvl2 (dishevelled segment polarity protein 2) is destroyed, enhancing therefore APT1 thioesterase activity. This triggers the specific deacylation of MCAM (melanoma cell adhesion molecule) but not of other proteins like CAV1 (caveolin 1). Depalmitoylated MCAM loses its location at the PM inducing cell invasion (Wang, W. et al 2015).

2.1.5 Protein palmitoylation and cancer

Despite most protein palmitoylation mechanisms have been studied in the context of neural system development and functioning (Cho et al., 2016; Gupta et al., 2001; Kim et al., 2008; Koster et al., 2019; Sapir et al., 2019), palmitoylation dependent processes have also been related to cancer (Ko et al., 2018; Anderson et al., 2016; Chen et al., 2017; Yamamoto et al., 2007; Ducker et al., 2004; Draper et al., 2010; Yuan et al., 2020).

As above mentioned, well-known cancer-related proteins like Ras family of GTPases can be palmitoylated (Xiang et al., 2017). Furthermore, around 25% of 299 validated cancer driver genes can be palmitoylated according to a recent study (Ko et al., 2018), which highlights the importance of this PTM in cancer disease. Inhibition of palmitoylation of oncogenic N-Ras^{G12D} mutant at Cys181 induces miss localization of mutant N-Ras and inhibits downstream signaling, extending the life-expectancy of leukemia bearing animals up to 8 times (Cuiffo, B. et al. 2010).

SCRIB oncogenic signaling cascade is also regulated by palmitoylation. SCRIB is a cell junction localized tumour suppressor protein that has a role in the regulation of cell polarity but also interacts with many different proteins and pathways. Through its PDZ domain, SCRIB interacts with PTEN (phosphatase and tensin homolog) and localizes it to the PM where PTEN dephosphorylates PIP₃ (phosphatidylinositol-3,4,5-triphosphate) and stops Akt signaling (Feigin et al., 2014). SCRIB also interacts with a complex of proteins to activate the Hippo pathway (Mohseni et al., 2014). For its proper localization and function at the cell junctions, SCRIB has to be palmitoylated by DHHC7 at two different cysteines (Chen, B. et al. 2016). When these two acylations are not present, SCRIB miss-localizes to the cytoplasm, which leads to the loss of cell polarity and overactivation of pathways like PI3K (phosphatidylinositol-4,5-biphosphate 3

kinase)/Akt, MAPK or YAP, increasing the malignancy of the cell (Chen et al., 2016; Feigin et al., 2014; Mohseni et al., 2014). The palmitoylation state of SCRIB is particularly relevant in BC where *ZDHHC7* is usually lost (Hungermann et al., 2011) and APT2 (SCRIB's specific thioesterase) tends to be upregulated (Hernandez et al., 2017), underlining the anti-tumoural function of SCRIB palmitoylation.

Another important cancer-related pathway in which palmitoylation plays a relevant role is EGF. EGF pathway overactivation is a common event in many cancers and some of the mutations that enhance the receptor's activity can interfere with its palmitoylation cycle. EGFR palmitoylation is fundamental to prevent its autophosphorylation, provoking its internalization and the termination of the signaling cascade (Runkle et al., 2016). Furthermore, deletion of EGFR exons 25-27, where the palmitoylated residue responsible for the control of the receptor phosphorylation is located (Runkle et al., 2016), has been described in lung cancer and glioblastoma multiforme (Imielinski et al., 2012; Cho et al., 2011). However, a few years ago, Ali et al. demonstrated that cells bearing different mutations in the tyrosine kinase domain of EGFR, but sensitive to kinase inhibitors, can acquire resistance by enhancing the palmitoylation of the receptor. Upon treatment with gefitinib or other tyrosine kinase inhibitors, the cells with acquired resistance enhance FASN activity and with it, the pool of free PA that acylates EGFR. They also showed that these mutants are more prone to be palmitoylated when compared to the WT version of the receptor probably as a consequence of alterations in the structure. On top of that, those palmitoylated mutant-EGFRs are more active and can relocate to the nucleus of the cell (Ali et al., 2018). This may be explained by a previous observation showing that the palmitoylation of EGFR dependent on FASN can enhance the ligand-independent homodimerization and activation of the receptor (Bollu et al., 2015). Thus, to date, the functional role of EGFR palmitoylation remains unclear. Different studies have found opposite functions for the acylation of the receptor (Ali et al., 2018; Bollu et al., 2015; Runkle et al., 2016). Further studies are needed to clarify the reason for these contradictory results although it seems that the reason behind might be the mutational status of EGFR and whether the receptor has undergone changes in its conformation that can affect its interaction with other proteins.

Palmitoylation is even implicated in the functional regulation of p53, guardian of the genome and one of the most important tumor suppressor genes. Despite the extensive study of this protein over the years, its palmitoylation has not been described until 2021. Tang et al. observed that in those tumours where *TP53* was not mutated, *ZDHHC1* was always downregulated through hypermethylation of the promoter. Indeed, they found a correlation between *TP53* mutational status and *ZDHHC1* expression. They saw that p53 palmitoylation in several Cys by DHHC1 is fundamental for the later phosphorylation of p53 and nuclear translocation. p53 S-palmitoylation is fundamental for its function

and the inhibition of tumour growth. Furthermore, in p53 WT cancer cells, the palmitoylated tumour suppressor recruits DNMT3A (DNA methyltransferase 3 alpha) to the *ZDHHC1* promoter for its hypermethylation and signaling in a negative feed-back loop (Tang et al., 2021). These results can explain the requirement of protein palmitoylation for a proper DNA damage response (Cao et al., 2016).

Another evidence of the relevance of protein palmitoylation in cancer is the association that different DHHC-PATs and acyl-thioesterases show with the progression of the disease. Some PATs, like DHHC2 or DHHC13 can act as tumour suppressors. *ZDHHC2* was first named *REAM* (reduced expression associated with metastasis) because it maps a region of chromosome 8 frequently deleted in several cancers such as non-small cell lung cancer (Fujiwara et al., 1994), CRC (Fujiwara et al., 1994), HCC (Emi et al., 1993; Fujiwara et al., 1994) or gastric cancer (Yan et al., 2013). DHHC2 is the PAT responsible for the palmitoylation of the tetraspanins CD9 and CD151, fundamental proteins for cell-cell adhesion and motility (Sharma et al., 2008). DHHC13, in turn, palmitoylates MC1R (melanocortin-1 receptor), which is required for a proper protective response against UV irradiation and oncogenic mutations in MC1R reduce its palmitoylation (Chen et al., 2017). Other PATs, such as DHHC11, DHHC12, DHHC17 and DHHC20, mainly act as oncogenes and are overexpressed or amplified in different tumours (Draper et al., 2010; Ducker et al., 2004; Yamamoto et al., 2007; Yuan et al., 2020). Nevertheless, in most cases, the different PATs can act both as oncogenes or as tumour suppressors depending on the cancer type (Ko et al., 2018). This could be explained by the different substrates that a DHHC has depending on the tissue. Concerning protein thioesterases, ABHD17A was identified as one of the main tumour suppressors in the microenvironment of lung metastasis in mice (Van Der Weyden et al., 2017). Full-body KO mice for ABHD17A have more lung metastases after intravenous injection of melanoma cells, suggesting a possible role of this protein in the immune surveillance against metastatic cells (Van Der Weyden et al., 2017). In contrast, elevated expression of PPT1 in tumours correlates with poor survival in a variety of cancers and its inhibition impairs tumour growth (Rebecca et al., 2019).

2.1.6 Targeting protein palmitoylation

As it has just been described, protein palmitoylation can directly affect the function of many oncogenes, tumour suppressors and cancer-associated signaling pathways. It is also true, that this PTM is fundamental for many vital processes like neural synapses function but certain studies suggest that normal tissues might be less sensitive to the inhibition of PATs than tumour cells (Ko et al., 2018). Certain DHHC-PATs and cofactors are essential for some of the most important oncogenic signaling pathways driving tumour growth and cancer progression, which creates in the tumour cells a non-oncogene addiction to some of those enzymes and sensitizes them to PAT inhibition (Ko

et al., 2018). This is supported by the fact that various mouse models KO for specific *ZDHHC* genes or cofactors of these enzymes, present no developmental alterations while the incidence or aggressiveness of the tumours they develop is reduced (Liu et al., 2016; Marciel et al., 2018).

Specific inhibitors of DHC enzymes are yet to be developed and preclinical studies using broad-spectrum DHCs inhibitors like 2-BP show low specificity and numerous off-target effects, making these drugs unsuitable candidates for therapy. The recent publication of hDHC20 crystal structure (Rana et al., 2018) opens the possibility to the design of target-based drugs. New specific inhibitors can be designed targeting differential domains of the acyl transferases such as the ankyrin-repeat. Nonetheless, in many cases different DHCs have overlapping functions and can palmitoylate the same substrate. The inhibition of a particular PAT can be compensated by the activity of other DHCs. One approach that can solve this issue would be the discovery of compounds that prevent the palmitoylation of a specific substrate by blocking its cysteine residue (Haag et al., 2018). Another possible approach to discover specific inhibitors of DHCs relies on the rational synthesis of competitive inhibitors. These competitive inhibitors would be small peptides containing the amino acid sequence that gets palmitoylated in the protein of interest and that can outcompete the endogenous protein (Yao et al., 2019).

Palmitoylation of certain proteins could be beneficial to fight the progression of specific cancers. In those circumstances, the use of protein thioesterase inhibitors would be beneficial to block tumour progression. Unlike for DHCs, there are specific inhibitors for the main protein depalmitoylases APT1 and APT2 (**Table I2.3**). Inhibition of APT2, the specific depalmitoylase of SCRIB, either with the promiscuous inhibitor palmostatin B (Chen et al., 2016) or with the specific APT2 inhibitor ML349 (Hernandez et al., 2017), enhances SCRIB location at the PM and attenuates MAPK activation and cancer progression (Hernandez et al., 2017). Thus, inhibition of APT2 could represent a potential therapeutic approach to treat cancers in which SCRIB plays an important role, such as BC (Hungermann et al., 2011). Moreover, systemic inhibition of PPT1 could have a beneficial anti-tumour effect through alteration of MDSCs, M2 macrophages and exhausted CD8+ responses (Sharma et al., 2020).

Regulation of protein palmitoylation can be particularly useful in combination with other treatments. As aforementioned, EGFR signaling is controlled by palmitoylation. Upon activation, WT EGFR gets acylated by DHC20, inducing the internalization and degradation of the receptor (Runkle et al., 2016). In triple negative BC cells, broad inhibition of the PATs with 2-BP or KD of *ZDHHC20* increases EGFR presence at the PM and EGF-induced activation of the downstream signaling (Runkle et al., 2016). In triple negative BC cells, broad inhibition of the PATs with 2-BP or KD of *ZDHHC20* increases

EGFR presence at the PM and EGF-induced activation of the downstream signaling (Runkle et al., 2016). Nonetheless, this enhances the dependence of cancer cells on EGF signaling and sensitizes them to EGFR inhibitors such as gefitinib. Combination of gefitinib and 2-BP treatments double the percentage of death cells as compared to gefitinib alone (Runkle et al., 2016). However, EGFR is mutated in many tumours and its palmitoylation no longer stops the signaling cascade. Acylation of mutant-EGFR can even help the tumour cell by stabilizing the receptor in endomembranes, where it remains active (Ali et al., 2018), or by triggering the ligand-independent dimerization of EGFR (Bollu et al., 2015). In these cases, inhibition of FASN, which is activated by mutant EGFR, emerges as a good option to diminishing the availability of PA moieties that can be used to palmitoylate the receptor. FASN inhibition with orlistat, decreased tumour growth in

Inhibitor	Enzyme	References
Hexadecylfluorophosphonate (HDFP)	Non-selective lipase inhibitor	Martin et al., 2012
Methyl arachidonyl fluorophosphonate (MAFP)	Broad spectrum serine hydrolase inhibitor	Zhang et al., 2010
Phenylmethylsulphonyl fluoride (PMSF)	Broad spectrum serine hydrolase inhibitor with low PPT1 inhibition efficiency	Zhang et al., 2010
Palmostatin B	APT1/2, ABHD17A-C	Lin et al., 2015
ML211	APT1/2	Hernandez et al., 2017
ML378	APT1/2	Won et al., 2018
AA401	APT1/2	Hernandez et al., 2017
ML348	APT1	Hernandez et al., 2017
ML349	APT2	Hernandez et al., 2017
Chloroquines (CQ)	Autophagy inhibitors, some inhibit PPT1 specifically	Rebecca et al., 2019

Table I2.3 Described inhibitors of protein thioesterases.

The table shows the main used inhibitors in research, their specificity and references in which they were synthesized or used.

mice bearing gefitinib resistant tumours (Ali et al., 2018). Moreover, the inhibition of EGFR activation with gefitinib can be synergistically enhanced by inhibiting FA and steroid synthesis with cerulenin or by broad inhibition of DHCs with 2-BP (Bollu et al., 2015). Thus, regardless of the mutational status of EGFR, the inhibition of its palmitoylation, either by blocking palmitate synthesis or the transference of the moiety to the protein, can synergize with current therapies using tyrosine kinase inhibitors.

Although protein palmitoylation is an enzymatically regulated process, cellular availability of PA can also have a strong impact on S-acylation. An excess of PA through HFD or PA cell culture treatment can also boost the palmitoylation of certain proteins (Spinelli et al., 2017; Tang et al., 2021). However, if the cells do not have enough PA, they can still synthesize it through FASN upregulation. All the different approaches for the inhibition of FA uptake and synthesis can also affect protein palmitoylation. Further studies are required to elucidate the extent to which protein palmitoylation plays a role in cancer, and whether it can be therapeutically modulated.

3.1 Chromatin & epigenetics

Chromatin is the complex of DNA and histones that can be found in the nucleus of eukaryotic cells. Each one of our diploid cells contains approximately 2 meters of DNA packaged in the form of chromatin within the 10-20 μm diameter space of the nucleus. This feat is achieved through the compaction of DNA in different levels of condensation (Annunziato, 2008).

Nucleosomes are the basic structural and functional units of chromatin (**Figure 13.1**). They are formed by 146-7 base pairs of DNA wrapped around a histone octamer. Histones are a family of small and positively charged proteins that are fundamental for DNA compaction and the regulation of transcription. There are four core histones: H2A, H2B, H3 and H4; and one linker histone: H1 (Annunziato, 2008). The nucleosome core particle is formed by two of each one of the core histones. Electrostatic interactions favor the DNA (negatively charged) folding around the histone octamer (positively charged) leading to the nucleosome formation. The next level of condensation is the chromatosome and it is accomplished through the addition of the linker histone H1 to the internucleosomal space (Annunziato, 2008). Chromatin is further coiled into a higher-order structure known as the “30 nanometer fiber” but to date, there is still a great deal of controversy over the manner in which chromatosomes are folded into that structure (**figure 13.1**) (Chen, P. et al, 2014).

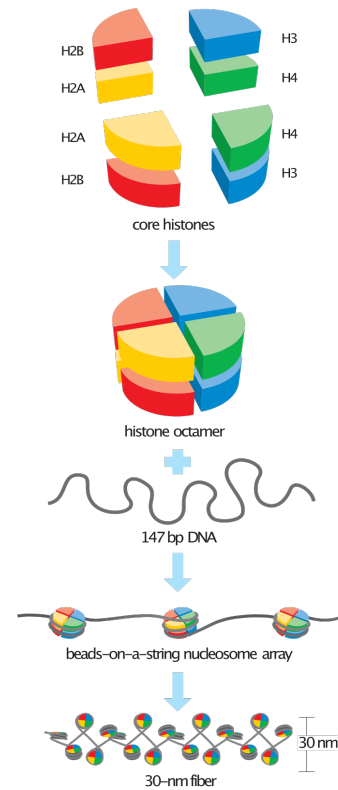


Figure 13.1. Chromatin condensation. Adopted from Morgan, 2006. Representation of the nucleosome formation and chromatin condensation in the 30 nm fiber.

Although all the cells in our body contain virtually the same DNA sequence (except for somatic mutations), a massive phenotypic diversity of cells is generated during development and this is possible thanks to epigenetic mechanisms. The term epigenetics refers to those processes that can alter the activity of genes without changing the DNA sequence and these modifications can potentially be transferred to daughter cells (Weinhold, 2006).

Processes such as RNA transcription or DNA repair and replication require the separation of the two DNA strands to allow the interaction between the DNA molecule

and the different protein complexes in charge of those functions. Epigenetic modifications determine which parts of the genome remain condensed in the 30 nanometer fiber form and which ones can be open to allow transcription or other functions. The main epigenetic modifications determining chromatin accessibility are DNA methylation (Moore et al., 2013) and histone PTMs (Bannister and Kouzarides, 2011).

The crystal structure of the nucleosome was first solved in 1997 and showed that the N-terminal tails of the core histones can protrude from their own nucleosome and contact neighboring nucleosomes (Luger et al., 1997). It is within these highly basic N-terminal tails where most histone PTMs have been described to happen. Indeed, different PTMs in these tails can interact with those of other nucleosomes and alter overall chromatin structure (Bannister and Kouzarides, 2011). These modifications can also alter the accessibility of the chromatin by recruiting remodeling enzymes that re-locate nucleosomes. Certain histone PTMs will be further described in a separated section but first, the relevance of [REDACTED], which can add another layer of complexity to epigenetics, will be discussed.

3.2 [REDACTED]

The nucleosome comprises a hetero-octamer constituted by two H3-H4 dimers forming a tetramer flanked by two H2A-H2B dimers. One of the factors modulating the stability of the nucleosome are the different [REDACTED] [REDACTED] have different isoforms that differ in sequence and regulatory mechanisms. Some of those [REDACTED] and present an expression peak coinciding with S phase of mitosis, while other isoforms [REDACTED] and are expressed throughout the cell cycle, with no particular expression peak.

3.2.1 [REDACTED]

Mammals have different [REDACTED] two of which are [REDACTED] and the rest of which [REDACTED] [REDACTED] In addition to these well-studied variants, there might be two more [REDACTED] [REDACTED], which are especially expressed in some areas of the brain and in malignant tissues; and one [REDACTED] [REDACTED] The expression of [REDACTED] can be regulated in a time- and tissue-dependent manner, making them influential during development and cell differentiation ([REDACTED]). The [REDACTED] [REDACTED] are the most broadly studied ones due to their general expression in all cell types and their implication in the regulation of [REDACTED].

3.2.1.1 Genetic and proteomic characteristics of [REDACTED]

[REDACTED] present a particular genomic organization and transcription regulation that allow their massive production at S-phase but not at any other moment of the cycle. [REDACTED]

[REDACTED]. On top of that, their translation is tightly regulated. [REDACTED]

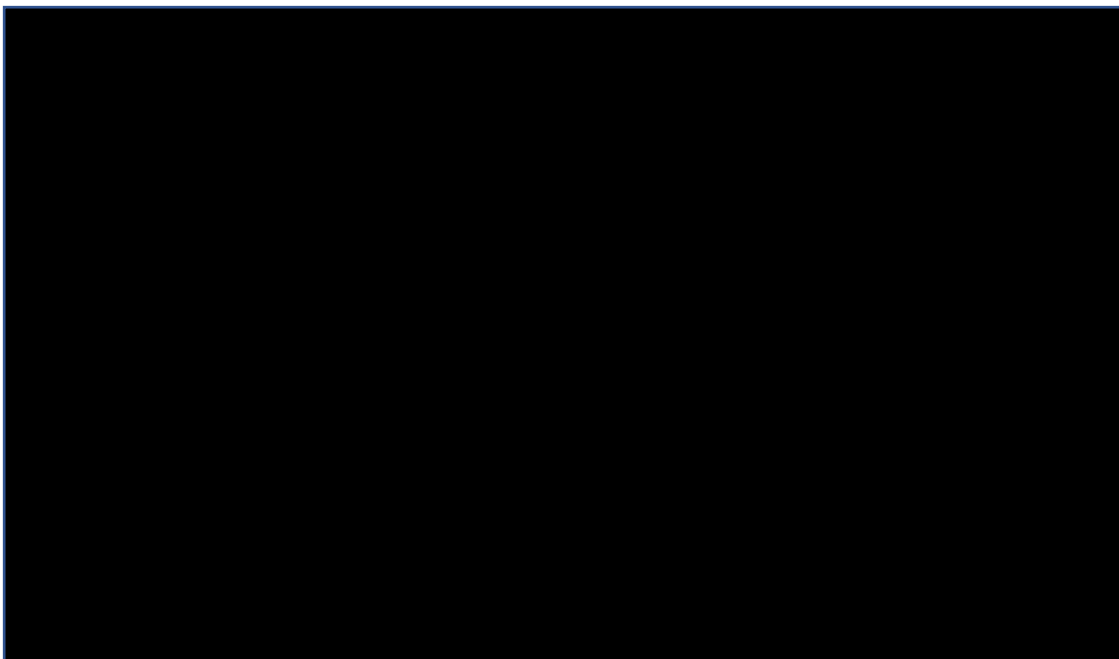


Figure 3.2. Alignment of the amino acid sequences of [REDACTED]. Adopted from [REDACTED]

The amino acids that differ between [REDACTED]. In grey, the differential amino acids between [REDACTED] In yellow, specific amino acids of [REDACTED] and in blue the ones of [REDACTED]

In contrast, the genomic organization and regulation of [REDACTED] is like most other genes: [REDACTED]

For instance, there are two [REDACTED], which encode the same amino acid sequence but differ in the nucleotide sequence and in their regulatory regions [REDACTED] These genes are transcribed throughout the cycle and [REDACTED].

differs only by amino acids from and by from (Figure 13.2). Interestingly, the residues found at those positions vary between species but they always remain different in . Those amino acids in the determine the . They probably provide specificity to the interaction of those with . Indeed, mutation of those residues in allow the in areas of the and are usually located (). Furthermore, those differential residues also have a role in the maintenance of due to their relevance for).

3.2.1.2 Genomic location and function of

only differ at one amino acid and are both ; thus, in many studies, they are grouped as a single . However, are associated to different and , which suggests that they have independent biological functions. While is associated to such as and and located in areas of is enriched in associated to both and) modifications (). In fact, can be out of S-phase, but still in a manner, at sites of DNA repair upon UV-damage ().

Unlike is mainly associated to which is evidenced by its enrichment in associated such as and) It is preferentially located at the . can have a “passive” role that compensates for the eviction of as well as an “active” one that maintains the . Although is mostly located in enrichment has also been observed in , such as of embryonic cells and of somatic cells ().

Deposition of the different is regulated not only by their expression and translation timing but also by the chaperones that interact with them and . The term “ ” comprises the diverse proteins that escort from their synthesis, modification and . They prevent unspecific interactions and aggregates

formation and they also determine the [REDACTED] [REDACTED]. [REDACTED] formation involves the transfer of [REDACTED] by a complex network of [REDACTED] chaperone partners. [REDACTED] [REDACTED] [REDACTED]). Regulation of [REDACTED] [REDACTED] shows higher complexity due to the different [REDACTED] areas where it can be found. Two different chaperone complexes are responsible for [REDACTED] [REDACTED] [REDACTED] complexes. [REDACTED] [REDACTED] [REDACTED]). The homeostasis and regulation of the [REDACTED] play fundamental roles in gametogenesis, development and cell differentiation, and alterations in these are associated to developmental diseases and cancer ([REDACTED] [REDACTED])

3.2.2 [REDACTED] and cancer

Metabolic plasticity, which is necessary for cancer cells to adapt to the particular metabolites and stressors they encounter during cancer progression, requires previous epigenetic plasticity. The epigenetic landscape of a cell determines its identity and phenotype by restricting or promoting the expression of specific genes. Thus, the capacity of a healthy differentiated normal cell to adapt to external signals or environmental changes is limited. In contrast, chromatin in cancer cells tends to be in a more permissive state, they tend to have epigenetic plasticity that enables the rapid activation or repression of different genes upon stimuli ([REDACTED]). Cancer cells acquire that plasticity through different mechanisms. On the one hand, the expression or function of epigenetic writers, erasers and readers can be altered. On the other hand, alterations can directly affect the nucleosomes by [REDACTED] mutations or by modification of [REDACTED] [REDACTED] [REDACTED]

3.2.2.1 [REDACTED] mutations

Classical [REDACTED] mutations are specific missense driver mutations affecting residues within the [REDACTED]. They were first described in rare pediatric tumours (pontine gliomas, glioblastomas, sarcomas, diffuse large B-cell lymphomas and carcinosarcomas) ([REDACTED]) where they happen with high frequency but they have also been observed in common

cancers (melanoma, AML, ovarian cancer, bladder cancer and CRC) with a lower frequency (██████████). Nevertheless, very recent publications have discovered that those mutations can also affect the ██████████ with great impact on tumour progression as well (██████████). In fact, ██████████ is the most mutated ██████████, with ██████████ being the most affected ██████████, and the majority of its mutations affect the ██████████). Mutations within the ██████████, while those in the ██████████ affect the 3D structure of the ██████████.

Interestingly, mutation of just one of the many different genes encoding each ██████████ is enough to generate an impact on the ██████████ of the tumour cell. ██████████ mutants ██████████ present a dominant-negative effect and affect the non-mutated proteins altering all ██████████ dependent processes such as ██████████. For example, mutated ██████████), common in pediatric brain cancers, inhibits the activity of ██████████. ██████████ mutations and the epigenetic rearrangements they generate are associated to undifferentiation of the cancer cells (██████████). Within the ██████████ domain, ██████████ mutation hotspots are ██████████. ██████████ mutations have been described to induce alterations of the cell fate inhibiting cell differentiation as well (██████████).

Strikingly, a very recent study found out that ██████████ can be ██████████

██████████

██████████

██████████

██████████

██████████

██████████

██████████

██████████

3.2.2.2 Alteration of ██████████

Although ██████████ mutations are not really frequent in common adult cancers, tumour cells still acquire epigenetic plasticity through alteration of the ██████████. Incorporation of different ██████████ can directly influence the ██████████ due to their differences in sequence and structure. Moreover, they can alter the ██████████ in an indirect manner. Each ██████████ is associated

to specific [REDACTED] but also due to differences in their sequence of amino acids. In fact, some [REDACTED] recognize not just the [REDACTED] but also the [REDACTED] structure ([REDACTED]).

The [REDACTED] are frequently over expressed or over-represented in the [REDACTED] of cancers ([REDACTED]). Both [REDACTED] are associated to [REDACTED], favoring epigenetic plasticity. [REDACTED] can even impair the binding of linker H1 to the DNA ([REDACTED]). This overexpression can be achieved by [REDACTED] gene amplification ([REDACTED]) or by regulation of its expression and [REDACTED] through alterations in the chaperone machinery ([REDACTED]). EMT inducing signals can lead to a decreased presence of [REDACTED] within the [REDACTED] and, as a consequence, an increase in [REDACTED] downregulation and [REDACTED] overexpression ([REDACTED]). The epigenetic rearrangement induced by [REDACTED] downregulation triggers EMT program expression and boosts the metastatic capacity of the cells ([REDACTED] [REDACTED] amplification and [REDACTED] is also associated to lung cancer cell aggressiveness ([REDACTED]).

Nonetheless, in some tumours [REDACTED] expression or [REDACTED] is decreased and the protein can be seen as a tumour suppressor. In adult glioblastoma, [REDACTED] is involved in tumour cell differentiation and its expression correlates with increased overall survival ([REDACTED]). In [REDACTED] lung cancer, the carcinogen can induce cell transformation by [REDACTED] displacement from [REDACTED], inducing [REDACTED] ([REDACTED]). [REDACTED] alterations are also given by [REDACTED] Loss of function [REDACTED] mutations impede [REDACTED]. This lack of [REDACTED] is compensated by the [REDACTED] ([REDACTED]), which can induce the alternative [REDACTED] pathway, associated to [REDACTED] dysfunction ([REDACTED] [REDACTED]).

3.3 [REDACTED] PTMs

3.3.1 PTMs on the [REDACTED] domain

Although most [REDACTED] PTMs occur on [REDACTED], the core regions of [REDACTED] can also be post-translationally modified with similar impact on [REDACTED]. The globular domain of [REDACTED] comprises three [REDACTED] and two [REDACTED] that are involved in the [REDACTED] and [REDACTED] modifications of the core region, unlike those

on [REDACTED], directly affect the [REDACTED] and therefore, [REDACTED], without [REDACTED]). These core-region specific PTMs of [REDACTED] influence the [REDACTED] architecture through the modulation of [REDACTED] interactions with other [REDACTED].

Many of these modifications occur in areas of [REDACTED]. For instance, this is the case of [REDACTED], which can be either [REDACTED]. [REDACTED] [REDACTED] [REDACTED] [REDACTED] [REDACTED] [REDACTED] [REDACTED] [REDACTED] [REDACTED] [REDACTED]

Other PTMs in the [REDACTED] domain can affect [REDACTED]. For example, [REDACTED], located at the [REDACTED]. [REDACTED] [REDACTED] [REDACTED] [REDACTED] [REDACTED] [REDACTED] [REDACTED] [REDACTED] [REDACTED] [REDACTED]

Finally, [REDACTED] modifications can also interfere in the interactions with the [REDACTED] responsible for their [REDACTED]. [REDACTED] [REDACTED] [REDACTED] [REDACTED] [REDACTED] [REDACTED] [REDACTED] [REDACTED] [REDACTED] [REDACTED]

To sum up, [REDACTED] PTMs within the [REDACTED] domain can affect [REDACTED] and with it, [REDACTED]. [REDACTED] are also affected by these modifications and in many occasions [REDACTED] PTMs colocalize and cooperate. In fact, [REDACTED]. [REDACTED] [REDACTED]

3.3.2 [REDACTED] acylation

[REDACTED] (as any other protein) can be acylated, for instance with the recently discovered short-chain Lys acylations. These modifications are similar to Lys acetylation (Kac), which occurs in the ϵ -amino group of Lys, but they differ in the length, hydrophobicity and charge of the hydrocarbon chains ([REDACTED]). Functionally, Kac neutralizes the positive charge of the Lys amine group decreasing the formation of hydrogen bonds while increasing Van der Waals interactions, similar to the actions of [REDACTED] acylations. Both, [REDACTED] acetylation and acylation, are associated with [REDACTED]. Eight different short-chain acyl groups have been described to modify [REDACTED] Lys and they are classified based on their physicochemical characteristics in: hydrophobic, polar or acidic (Figure I3.3) ([REDACTED]).

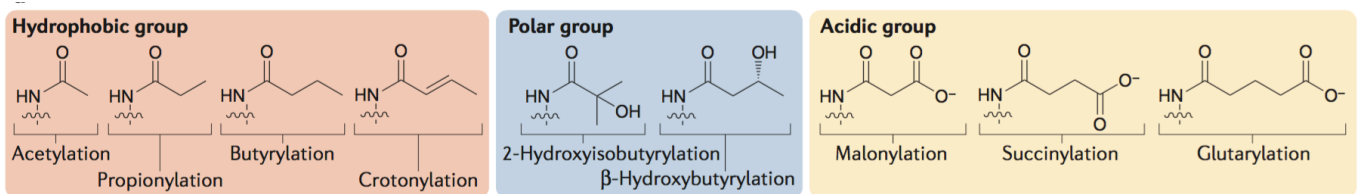


Figure I3.3. Classification of Lys acyl groups. From ([REDACTED])

- The **hydrophobic acyl group** comprises propionyl ([REDACTED]), butyryl ([REDACTED]) and crotonyl ([REDACTED]) moieties, which generate the modifications Kpr, Kbu and Kcr respectively. These acyl groups present a longer hydrocarbon chain that increases the hydrophobicity and bulk of the Lys.
- The **polar acyl group**, includes 2-hydroxyisobutyryl ([REDACTED]) and β -hydroxybutyryl ([REDACTED]) that produce Khib and Kbhb, respectively. These acyl groups contain hydroxyl groups that enable the formation of hydrogen bonds with other residues.
- The **acidic group** contains acyl moieties that alter the charge of the Lys residue from +1 to -1, producing Lys malonylation (Kma) ([REDACTED]), succinylation (Ksucc) ([REDACTED]) and glutarylation (Kglu) ([REDACTED]).

In total, [REDACTED] different [REDACTED] sites bearing these acylations have been discovered. Lysines within the [REDACTED] can be modified by one or different acyl groups ([REDACTED]).

3.3.2.1 [REDACTED] acylation

[REDACTED] acylation is an enzymatic reaction driven by the same enzymes responsible for [REDACTED] acetylation. Specific writers, erasers or readers for [REDACTED] acylation have not been described yet. Within [REDACTED] [REDACTED] being able to catalyze the formation of Kpr and Kbu ([REDACTED] [REDACTED] as well as Kcr, Kbhb, Ksucc and Kglu ([REDACTED])). However, the catalytic rate of [REDACTED] decreases with acyl-chain lengthening. Other [REDACTED] can acylate [REDACTED] *in vitro* but with highly reduced kinetics.

Only [REDACTED] have been studied as [REDACTED] acylation erasers to date, which have [REDACTED] [REDACTED]. Specifically, [REDACTED] has really high desuccinylase, demalonylase and deglutarylase activities but very little [REDACTED] [REDACTED] present broad-range deacylase function [REDACTED] and [REDACTED] prefers Ksucc deacylation, especially upon DNA damage ([REDACTED]).

There are three different families of [REDACTED]: proteins containing a [REDACTED] [REDACTED] [REDACTED] [REDACTED] [REDACTED]

3.3.2.2 Metabolic regulation of [REDACTED] acylation

The differential acylation of [REDACTED] is probably driven by the competition of the various acyl-CoAs for promiscuous [REDACTED]. Thus, the ratio of acetyl/acyl-CoAs determines whether [REDACTED] are acetylated or acylated and directly links the cell metabolism to the regulation of this PTM ([REDACTED]). Most cell lines grow in high glucose media, which leads to the accumulation of cytoplasmic citrate, which is transformed to acetyl-CoA by ACLY (**Figure I1.4**). Under these conditions, the ratio acetyl/acyl-CoA increases and most [REDACTED] are acetylated. Nevertheless, in mice or upon glucose depletion in cell culture, the ratio is not that dramatically shifted towards acetyl-CoA and [REDACTED] acylations can be easily detected ([REDACTED]). Indeed low-nutrient conditions favor non-acetyl acylation of [REDACTED] in [REDACTED] [REDACTED]. Furthermore, treatment with short-chain FAs in cell culture also increases the deposition of those acyl groups on [REDACTED] in a dose-dependent manner ([REDACTED]).

To sum up, epigenetic plasticity is a fundamental trait of malignant tumour cells that is acquired through the regulation of the [REDACTED] [REDACTED]

[REDACTED] The different [REDACTED] present independent biological functions and are associated to distinct [REDACTED]. The focus has been set on the acyl or lipid modifications of [REDACTED] in particular due to the relevance of these metabolites in cancer progression. Changes in the lipid metabolism of cancer cells have been suggested to have an indirect impact on the epigenetic landscape of the cell through the activation of different metabolic pathways ([REDACTED]), [REDACTED] [REDACTED]). Microenvironmental or newly synthesized FAs can [REDACTED]

[REDACTED] The protein acylation field has not evolved as fast as others, probably due to the strong technical challenges that are inherent to working with lipids. More studies are needed to properly characterize the direct role that dietary lipids might play on epigenetic plasticity, especially in cancer progression.

BACKGROUND, HYPOTHESIS AND OBJECTIVES

The influence of lipid metabolism on cancer progression has been broadly studied in the past years. Two recent publications of our laboratory have further enhanced our knowledge on the possible mechanisms by which certain dietary FAs can induce the metastatic capacity of OSCC and melanoma cells (Pascual et al., 2017; Pascual et al., 2021). MICs within PTs express the CD36 scavenger receptor on their PM and present an enhanced lipid metabolism, as compared to the rest of the PT cells. The metastatic capacity of these cells is fully dependent on CD36, and its abrogation by shRNA or by blocking antibodies decreases the metastatic burden of tumours and even leads to remission of already established LN or lung metastases. Lard-enriched HFD feeding of mice can increase the number of MICs within the PT and thus, the metastatic capacity of that tumour in a CD36-dependent manner (Pascual et al., 2017). However, not all the FAs present in our diet work the same: unlike PA, neither OA nor LA cell culture treatment induces CD36 expression or increases the metastatic capacity of the tumour cells when injected in mice. Similarly, feeding of PT-bearing mice with a PA-enriched HFD increases the number and size of the generated metastases, but this does not happen with an OA-enriched HFD (Pascual et al., 2021). Strikingly, dietary PA/CD36 axis can generate an epigenetic memory in cancer cells based on H3K4me3 deposition on promoters of neural genes, that maintains the increased metastatic capacity of the cells for months. Specifically, PA-based activation of CD36 induces EGR2 (early growth response 2) TF, which is responsible, at least in part, for the transcriptional changes that the metastatic cells undergo following PA exposure. These transcriptional changes are then epigenetically established by Set1A (SET domain-containing protein 1) which is an H3K4 methyl transferase. Galanin is among the neural genes induced by EGR2 and epigenetically modified by Set1A; it is a glial-inducing peptide that can be secreted by tumour cells and can promote tumour-associated Schwann cells accumulation within the PT. These tumour-associated Schwann cells present a regenerative phenotype and secrete a specialized ECM, called perineuronal net, that enhances the aggressiveness of tumours (Pascual et al., 2021).

These studies have illuminated part of the mechanism by which dietary PA can boost the metastatic capacity of the cells, but there are still several open questions. Previous studies have mainly focused on the analysis of the changes induced by PA on the epigenome and transcriptome of cancer cells without considering the proteome alterations. Nonetheless, proteins, and not their transcripts, are usually the final effectors responsible for most structures and enzymatic reactions taking place within the cell. In many occasions, transcriptional changes do not fully correlate with proteome alterations (Ghazalpour et al., 2011; Hoogendijk et al., 2019; Wang et al., 2019), and both should be studied to fully understand the phenotypic changes of the cell. Further, the exact functions of a PA molecule upon entering a cell is unknown. We know that CD36+ MICs present an enhanced FAO and that ACSL1 KD decreases the metastatic

capacity of the cells (Pascual et al., 2017); thus, it seems that at least some of the PA entering the cells are oxidized. Nevertheless, ACSL1 catalyzes the conversion of long-chain FAs to their active form acyl-CoA, which can then be used for lipid synthesis and oxidation, but also for protein palmitoylation. It seems logic that cancer cells could use part of the PA entering the cell via CD36 for protein palmitoylation altering signaling pathways. Thus, protein palmitoylation could be responsible to some extent for the phenotypic rewiring observed in previous studies upon PA treatment (Pascual et al., 2017; Pascual et al., 2021).

Objectives

- 1- Analyze the proteome alterations elicited by pro-metastatic PA and anti-metastatic OA both in cell culture and in tumour cells growing in mice.
- 2- Characterize the palmitoylome of metastatic OSCC cells and the changes induced by PA and OA treatments.
- 3- Identify and characterize palmitoylated targets that could explain the pro-metastatic phenotypic changes.

MATERIALS & METHODS

1 Cell culture

All cell lines were cultured in standard conditions in a humidified incubator at 37°C with 5% CO₂. Two human OSCC cell lines were used in this study: SCC-25 (ATCC®, CRL-1628™) and VDH-15. This second cell line was established in our laboratory from the tumour of a Vall d'Hebron hospital's OSCC patient (Pascual G. et al, 2021). Both lines were grown in KSFM (Keratinocyte Serum-Free growth medium) (17-005-034, Gibco) supplemented with 38 µg/ml bovine pituitary extract (BPE) (13028-014, Gibco), 0.218 ng/ml recombinant human EGF (hEGF) (10450-013, Gibco) and 1X penicillin-streptomycin (P/S) (100X, 15140122, Life Technologies). Human melanoma 501Mel (kindly provided by Dr. Claudia Wellbrock, Manchester Cancer Research Centre, The University of Manchester, UK) and HEK293T (human embryonic kidney 293, SV40 large T antigen) (ATCC®, CRL-3216™) cell lines were maintained in high-glucose Dulbecco's Modified Eagle Medium (DMEM) (41965-039, Gibco) containing 10% fetal bovine serum (FBS) (10270106, Life Technologies) and 1X P/S. SCC-25, VDH-15 and 501Mel cell lines were infected with MSCV-IRES-Luciferase-GFP (green fluorescent protein) (pLuc-GFP) retrovirus, kindly provided by Dr. Johannes Zuber (Research Institute of Molecular Pathology (IMP), Vienna Biocenter, Austria).

1.1 Stable isotope labelling by amino acids in cell culture (SILAC)

Stable isotope labelling by amino acids in cell culture (SILAC) methodology is a time- and cost-efficient method that allows to directly quantify proteome changes between conditions in the same sample by mass spectrometry (MS), therefore reducing the intrinsic experimental variability. In this method, cells are first metabolically labelled by culturing them in media supplemented with different stable isotope containing amino acids (normally with ¹³C and/or ¹⁵N atoms) which are incorporated into their proteins. Cells are grown for enough cell divisions to make sure all proteins are fully labelled (normally ≥ 5 doublings). Then, distinct labelled cells are subjected to different experimental conditions (normally up to 3) and extracted protein or cells from the different conditions are equally combined in a 1:1 ratio. Thus, the same peptides coming from different conditions elute together but the stable-isotope containing amino acids produce a mass shift in the m/z ratio of each peptide derived MS spectra analyzed, allowing the discrimination of the peptides coming from each condition and their relative quantification (Ong et al., 2002) (**Figure M&M1A**).

SILAC media was used for those experiments in which protein extracts from cell culture were analyzed by liquid chromatography-mass spectrometry (LC-MS). Three different SILAC flavors containing arginine (Arg) and lysine (Lys) amino acids labelled with ¹³C and ¹⁵N isotopes were used (**Table M&M1**). L-Arg and L-Lys depleted KSFM (ME110229L3,

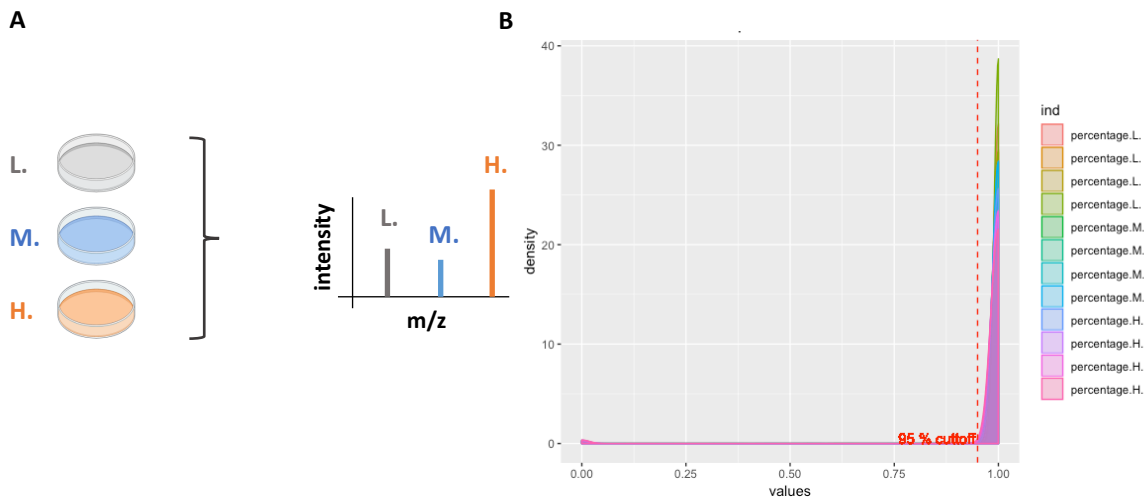


Figure M&M1. SILAC proteomics.

A) Graphical scheme of a SILAC experiment. The different conditions are labelled in culture with diverse stable isotope amino acids and proteomic samples are then analyzed together by MS. 3 different SILAC peaks are detected for each peptide allowing for the comparison of the relative amount (intensity) of the peptide in each condition. 3 SILAC conditions are used in our experiments: light (L.), Arg0 and Lys0; medium (M.), Arg6, Lys4; and heavy (H.), Arg10, Lys8. Created with BioRender.com **B)** Density plot showing the distribution of the % of light-, medium- and heavy-labelled Lys incorporation within protein peptides. In all cases the labelling efficiency was over 95%

Gibco) was supplemented with “heavy” (H.) amino acids, L-arginine- $^{13}\text{C}_6,^{15}\text{N}_4$ hydrochloride (Arg10) and L-lysine $^{13}\text{C}_6,^{15}\text{N}_2$ hydrochloride (Lys8); “medium” (M.) amino acids, L-arginine $^{13}\text{C}_6$ hydrochloride (Arg6) and L-lysine-4,4,5,5- d_4 hydrochloride (Lys4); or “light” (L.) amino acids, L-arginine hydrochloride (Arg0) and Lysine hydrochloride (Lys0) (**Table M&M1**).

In all the conditions the final concentration of Arg in the medium was 2 mM and the concentration of Lys 0.7 mM. These mediums were supplemented as normal KSFM with 38 $\mu\text{g}/\text{ml}$ BPE, 0.218 ng/ml hEGF and 1X P/S. Cells were grown in SILAC media for a minimum of 6 passages and the incorporation of the isotope labelled amino acids into proteins was analyzed prior to any large-scale experiment. The labelling efficiency was above 95% in all conditions (**Figure M&M1B**).

Amino acid	Isotope	Formula	Reference
Arginine, Arg	Arg0-HCl, light (L.)	L-Arg $^{13}\text{C}_0,^{15}\text{N}_0$	A6969, Silantes
	Arg6-HCl, medium (M.)	L-Arg $^{13}\text{C}_6,^{15}\text{N}_0$	201204102, Silantes
	Arg10-HCl, heavy (H.)	L-Arg $^{13}\text{C}_6,^{15}\text{N}_4$	201604102, Silantes
Lysine, Lys	Lys0-HCl, light (L.)	L-Lys $^{13}\text{C}_0,^{15}\text{N}_0$	L8662, Silantes
	Lys4-HCl, medium (M.)	L-Lys $^{13}\text{C}_4,^{15}\text{N}_0$	211104113, Silantes
	Lys8-HCl, heavy (H.)	L-Lys $^{13}\text{C}_6,^{15}\text{N}_2$	211604102, Silantes

Table M&M1. Isotopes used for SILAC experiments.

1.2 FA stimulation

Prior to any experiment, cells were trypsinized with 0.05% trypsin (25300-054, Gibco), digestion was stopped with 10% FBS containing phosphate-buffered saline (PBS) and then they were centrifuged at 350g for 5 minutes at room temperature (RT). The pellet was resuspended in KSFM and the number of living cells was counted with a Neubauer chamber after 1:1 dilution in 0.4% Trypan blue stain (15250-061, Gibco). SCC-25 cells were plated at a density of 8,000 living cells per square centimeter and VDH15 at 6,000 due to their increased proliferative capacity. Cells were always plated 24 hours before the beginning of the treatment and, once added, the treatment was not removed for the duration of the stimulation (6 hours – 4 days). After treatment, cells were trypsinized and analyzed by flow cytometry or pelleted, frozen in liquid nitrogen and stored at -80°C for later processing.

1.3 Retroviral particle generation and infection [REDACTED] overexpression

Retroviral particles were generated in HEK293T cells by transient co-transfection of the cells with the retroviral [REDACTED] plasmid of interest, the envelope plasmid pCMV-VSVG and the packaging plasmid pBS-CMV-gagpol in a 2:1:1.5 ratio. Both envelope and packaging plasmids were purchased from AddGene. This transfection was performed using jetPRIME transfection reagent (114-01, Polyplus) and following manufacturer's instructions. After transfection HEK293T cells were incubated with KSFM for viral particles generation. Retrovirus-containing supernatant was collected 24 hours after transfection and filtered through a 0.45 µm filter.

SCC-25 cells were plated as previously described at 8,000 cells/cm² 24 hours prior to retroviral infection. Cells were incubated for 24 hours with the filtered-virus-containing supernatant after addition of 1 µg/ml polybrene to increase infection efficiency. Infected cells were selected with 25 µg/ml hygromycin B (ant-hg, InvivoGen) until negative control was dead.

1.4 Cell viability

Cell viability was measured using CellTiter-blue (G8080, Promega) as specified by the manufacturer. Briefly, after treatment cells were washed with PBS and incubated with 20% CellTiter-Blue reagent in culture medium for 4 hours at 37°C. After treatment fluorescence was measured at 560/590nm.

2 Treatments preparation

Cells were treated with PA, OA, 17-ODYA (17-octadecynoic acid) or their vehicle, bovine serum albumin (BSA). Commercial FAs were saponified for proper dissolution in aqueous culture media. PA and OA were prepared at 5 mM stock concentration and diluted as required for experimental use. For the preparation of 45 ml of 5 mM stock solutions, 65 mg of sodium palmitate (P9767, Sigma-Aldrich) or 68.5 mg of sodium oleate (O7501, Sigma-Aldrich) were dissolved in 5 ml of 0.1 M NaOH with an incubation of 15 minutes or until clear at 70°C. Then, the solution with the FA was added drop by drop onto 40 ml of 12.5% FA-free-BSA (A7030, Sigma-Aldrich) in NaCl 0.9% previously warmed at 45°C and stirring. The mixture was left 15 more minutes in agitation for proper conjugation and then it was filtered through a 0.22 µm filter for sterilization, aliquoted and stored at -20°C. The control BSA solution was prepared following the same protocol without the addition of any FA to the NaOH solution.

17-ODYA (sc-200488A, Santa Cruz) stock preparation was similar to that of the other FAs but required ethanol addition for the full solubilization of the analog. 17-ODYA was resuspended in 100% ethanol at 50 mM and warmed at 70°C. That ethanol solution was diluted to 70% ethanol with 70°C pre-warmed 258 mM NaOH generating a mix of 34.9 mM 17-ODYA in 77.5 mM NaOH and 70% ethanol. This mix was then added dropwise onto the 12.5% BSA in 0.9% NaCl solution warmed at 45°C. The final 17-ODYA stock solution contained 5 mM 17-ODYA and 10% ethanol.

2-Bromopalmitate (2-BP) (238422, Sigma-Aldrich) stock solution was prepared in DMSO (dimethyl sulfoxide) at 5 mM.

3 [REDACTED] overexpression construct design

[REDACTED] cDNA sequence was obtained from NCBI CCDS database [REDACTED]. That cDNA was fused to FLAG and HA tags at the 3' terminal end and to a Kozak sequence at the 5' end. FLAG tag was separated from the [REDACTED] protein sequence by three alanine and two glycine residues, and HA tag was separated from the FLAG by one serine, two alanine and two glycine residues. In the [REDACTED] mutant version of the construct, the codon codifying for [REDACTED] was interchanged by the [REDACTED]. The construct was designed with SnapGene® software. DNA synthesis and cloning into pMSCV-hygromycin plasmid (Addgene, OneKendall, Cambridge, MA, USA) was performed by GENEWIZ (Azenta Life Sciences).

4 Animal studies

NOD Scid gamma (NOD.Cg-Prkdcscid Il2rgtm1Wjl/SzJ) mice housed in standard 12h light/12h dark cycles and specific-pathogen-free (SPF) conditions were used for this study. Mice were purchased from Charles Rivers and bred in-house. The Ethical Committee for Animal Experimentation of the Government of Cataluña evaluated and approved all the procedures.

4.1 PT generation and follow up

For PT generation, mice were anesthetized with 75 mg/kg ketamine and 1 mg/kg medetomidine intraperitoneal injection. 40,000 tumour cells resuspended in a volume of 30 μ l of KSFM were injected orthotopically, intra-tongue, with a 30G syringe. Once the procedure was done, mice were awakened with a 1 mg/kg atipemazol intraperitoneal injection and 0.1 mg/ml buprenorphine was subcutaneously injected for analgesia. The tumour size was measured immediately after injection by luminescence and followed weekly with Xenogen IVIS Imaging System-100 (Caliper Life Sciences).

For the visualization of the tumour cells, mice were anesthetized with continuous administration of isoflurane gas and 50 μ l of 5 mg/ml D-luciferin (115144-35-9, GoldBio) diluted in PBS were injected by retro-orbital injection. All the images were then analyzed with Living Image software version 4.5 (v.4.4; Caliper Life Sciences). The same measurement region of interest (ROI) was drawn on all the tumours of a specific timepoint. The background signal of each image was subtracted from the total photon flux coming from each tumour during the analysis.

4.2 Metastasis quantification

PTs were covered with a black strip in the late timepoints of the experiments in order to properly visualize and quantify the signal coming from the cervical LN metastases. In some experiments, mice were imaged post-mortem to increase the sensitivity and precision in the detection of the metastases. Briefly, they were anesthetized with isoflurane, injected with luciferin and euthanized by continuous CO₂ administration. Upon sacrifice, PTs were removed and neck skin dissected for LN exposition prior to image acquisition.

4.3 Dietary intervention

To address the changes in the proteome of the tumour cells induced by different diets, mice were fed with a modified Western HFD either with palm oil (TD.160620, ENVIGO) or olive oil (TD.09820, ENVIGO). In both HFDs lipids accounted for the 42% of the calories

(table M&M2). The standard chow diet used for maintenance of the mice was used as control diet (A40, SAFE).

Palm and olive oil diets differed in the origin of the lipids (Table M&M3) and in the presence of 50 g/Kg maltodextrin in the olive oil diet, used to favor solidification of the diet pellets. Those 50 g of carbohydrates were compensated in the palm diet with corn starch.

	% Kcal from proteins	% Kcal from carbohydrates	% Kcal from lipids
Palm oil (TD.160620)	15.2%	42.8%	42%
Olive oil (TD.09820)	15.2%	42.9%	41.9%
Maintenance chow diet (A40)	18.2%	73.1%	8.6%

Table M&M2. Protein, carbohydrate and lipid composition of each experimental diet.

When the average PT signal of all the animals in the experiment was over 5×10^7 total photon flux, around week 4, mice were semi-randomized and changed to their specific diet. For the semi-randomization, the tumour size, the sex of the animal and the number of metastases were taken into consideration. After 10 days of fatty diet feeding mice were euthanized by continuous CO₂ administration and PTs were collected.

	Palm oil (g/Kg)	Olive oil (g/Kg)	% of fat is PA	% of fat is OA	Reference
Palm oil (TD.160620)	210 g	-	44%	40%	Mancini et al., 2015
Olive oil (TD.09820)	-	210 g	7.5 - 20%	55 - 83%	Boskou et al., 2006
Maintenance chow diet (A40)	-	-	18.6%	16.5%	

Table M&M3. Origin of the fat and percentage of PA and OA contained in each diet.

The exact percentage of PA and OA within palm and olive oil enriched HFDs was not specified by the manufacturer. These percentages were calculated based on the average PA and OA composition of palm and olive oils according to the referenced papers.

5 Single cell preparation from tumours

Tumours were collected and pooled by diet and sex in groups of 4 to 6 for further processing. Samples were chopped and digested in 10 ml of digestion buffer containing 2.5 mg/ml collagenase A (C0130, Sigma-Aldrich) and 0.75 mg/ml EDTA-free trypsin (15090-046, Gibco) in calcium-free Eagle's Minimum Essential Medium (EMEM) (BE06-174G, Lonza), for 90 minutes at 37°C in a horizontal shaker. After digestion, samples were centrifuged at 350g for 10 minutes and the supernatant was further centrifuged at 400g for 5 more minutes. Pellets were resuspended in 2 ml of 37°C pre-warmed 0.25% trypsin-EDTA (25200-056, Gibco) containing 0.1 mg/ml DNase (DN25, Sigma-Aldrich) and pipetted up and down for one minute. This digestion was stopped by addition of 10 ml calcium-free EMEM with 10% calcium-chelated-FBS and 1% glutamax (35050-038, Gibco). After another centrifugation at 400g and 4°C for 10 minutes, samples were resuspended in 5 ml of ice-cold PBS, filtered sequentially through 100 µm and 40 µm cell strainers and transferred to FACS tubes for staining, analysis and sorting.

6 Fluorescence activated cell sorting (FACS)

Flow cytometry was used to test the cell culture treatment efficacy by CD36 induction analysis and to sort human tumour cells from mice experiments. Single cell suspensions were resuspended to 1×10^7 cells/ml in staining solution containing direct APC-conjugated anti-CD36 antibody, in the case of the cell culture experiments, or a staining master mix containing biotin-conjugated anti-mouse H-2Kd (Mo MHC Class I) and biotin-conjugated anti-mouse CD45 (lineage markers), if the samples were coming from mice, in 2% calcium-chelated FBS in PBS. Upon 30 minutes incubation on ice, cells were washed with PBS and the samples from the animal experiments were resuspended in a second staining master mix with 1:200 BV605 streptavidin (563260, BD Horizon), incubated on ice for 30 more minutes and washed with PBS again. Before flow cytometry analysis all samples were resuspended in 2 µg/ml DAPI (32670, Sigma-Aldrich) in PBS to exclude dead cells. Samples for cell culture treatments were analyzed using Gallios (Beckman Coulter) instrument and a BD FACSAria™ Fusion flow cytometer (BD Biosciences) was used for the analysis and sorting of tumour cells coming from mice experiments. Cellular debris and cell doublets were excluded on the basis of cells forward and side scatter (FSC and SSC) parameters by FSC-A/SSC-A and FSC-W/FSC-A respectively and dead cells were omitted by DAPI+ staining. Data was processed using FlowJo™ 10 software (version 10.4.2). Details on the antibodies on **table M&M4**.

70,000-120,000 tumour cells, negative for the mouse lineage markers-BV605 and positive for GFP, were sorted per replicate from the tumours in mice. Upon sorting

tuomour cells were pelleted by centrifugation at 400g and 4°C for 15 minutes, frozen in liquid nitrogen and lyophilized.

7 Immunofluorescence staining

██████████ bearing SCC-25 cells plated on autoclaved coverslips (ECN 631-1577, VWR) and treated for 4 days with 50 μM OA, 300 μM PA or BSA, were fixed with 4% PFA (paraformaldehyde) and 4% sucrose in PBS for 15 minutes at RT. Upon fixation cells were permeabilized with 0.25% Triton X-100 (T8787, Sigma-Aldrich) in PBS for 5 minutes at RT, blocked with 10% BSA in PBS for 30 minutes at 37°C and stained with primary antibody anti-FLAG diluted in 3% BSA in PBS for 2 hours at 37°C. Cells were washed 3 times with PBS before incubation with anti-mouse Alexa 568 in 3% BSA for 45 minutes at 37°C. Then, after three more washes with PBS and one with dH₂O, coverslips were mounted on microscope slides (J1800AMNZ, Thermo Scientific) with DAPI containing mounting medium (H1200, Vector) (antibodies on **table M&M4**).

Fluorescent pictures were acquired using a Leica SPE confocal microscope (63x/1.40 oil objective, 1024x1024 pixel resolution) and processed using Fiji 1.49b software (ImageJ) (Schindelin et al., 2012).

8 Protein and peptide sample preparation

8.1 Protein extraction

For **whole proteome** analysis, cells from the three different treatments and SILAC flavors were mixed in a 1:1:1 ratio and resuspended in a urea lysis buffer (50 mM Tris-HCl pH8.2, 8 M urea (BP169-212, Fisher BioReagents), 75 mM NaCl, 1X cOmplete, EDTA-free protease inhibitor cocktail (PI) (05056489001, Roche)). Then, they were sonicated during 4 cycles of 10 seconds ON/1 minute OFF at 40% amplitude in a Vibra-Cell VCX750 ultrasonic processor and debris were pelleted by centrifugation at 16,000g for 10 minutes at 4°C.

Lyophilized **cells sorted from tumours** growing in mice were incubated in lysis buffer (50 mM Tris-HCl pH8.2, 2 M urea, 5 U/μl benzonase (E1014, Sigma-Aldrich) and 1X PI) for 5 minutes at RT shaking and sonicated during 20 cycles (15 seconds ON/ 30 seconds OFF) in a Bioruptor Pico (Diagenode).

For the **palmitoylome studies**, the SILAC mixes were prepared at the protein level. Pelleted cells were resuspended in lysis buffer (50 mM HEPES pH7.9, 150 mM NaCl, 1 mM PMSF (P7626, Sigma-Aldrich), 1X PI) and sonicated in a Bioruptor Pico (Diagenode)

during 20 cycles of 15 seconds ON/30 seconds OFF. Then, samples were ultracentrifuged at 100,000g for 50 minutes at 4°C for the membrane compartment enrichment and pellets were resuspended in the previous lysis buffer with 0.25% SDS and further sonicated in a Vibra-Cell VCX750 during 10 seconds for proper resuspension. After protein measurement with Pierce BCA Protein Assay kit (23223, Thermo Scientific) following manufacturer's instructions, SILAC mixes were prepared in a 1:1:1 ratio and the final amount of protein within each mix was 2 mg. In those experiments in which palmitoylated proteins were pulldown for western blot analysis, protein was extracted following this protocol but with the addition of 0.1% SDS to the lysis buffer.

Nuclear protein extracts were used for the immunoprecipitation of [REDACTED] To obtain the nuclear extracts, treated cells were incubated 10 minutes on ice with in swelling buffer containing 10 mM KCL, 1.5 mM MgCl₂, 0.1% NP-40 (18896, Sigma-Aldrich), 25 mM HEPES pH7.9, 1X PI and 1 mM PMSF. Then, a Dounce homogenizer with a tight pestle was used to lyse the cells and isolate the nuclei (50 strokes). Nuclei were pelleted with 5 minutes 3,000g centrifugation at 4°C and incubated in RIPA buffer: 50 mM Tris-HCL pH7.4, 150 mM NaCl, 2 mM EDTA (E9884, Sigma-Aldrich), 0.5% sodium deoxycholate, 0.1% SDS, 1% NP-40, 1X PI, 1 mM PMSF. For proper nuclei lysis, samples were passed 15 times through a 26G syringe while the 15 minutes incubation in RIPA on ice. Nuclear extracts were cleared by a 15 minutes centrifugation at 14,000g and 4°C and protein concentration was measured using Pierce BCA Protein Assay kit (23223, Thermo Scientific).

For the **cellular fractionation**, around 10 million [REDACTED] bearing SCC-25 cells were resuspended in ice-cold buffer A (10 mM HEPES pH7.9, 10 mM KCL, 1.5 mM MgCl₂, 0.34 M sucrose, 10% glycerol, 1mM DL-Dithiothreitol (DTT) (D9779, Sigma-Aldrich), 1XPI). After homogeneization, Triton X-100 was added to a final concentration of 0.1% and samples were incubated for 30 minutes on ice. Upon centrifugation at 1,300g for 5 minutes at 4°C, supernatant was collected and further centrifuged at 18,000g for 15 minutes at 4°C; the supernatant of the second centrifugation was saved as the **cytosolic fraction**. The pellet of the first centrifugation was washed with buffer A, resuspended in buffer B (3 mM EDTA, 2 mM EGTA (E3889, Sigma-Aldrich), 1 mM DTT, 1X PI) and incubated 30 minutes on ice for nuclear lysis. After a 5 minutes centrifugation at 1,700g at 4°C, supernatant was saved as the **nuclear soluble fraction** and pellet was washed with buffer B and further resuspended in urea lysis buffer with benzonase (4 M urea, 25 mM Tris-HCL pH8.2, 40 mM NaCl, 1 mM CaCl₂ and 2.5 U/μl benzonase). Upon 10 minutes incubation at 37°C shaking, EGTA was added to 1mM final concentration and samples were centrifuged at 1,700g for 5 minutes at 4°C. The supernatant contained the **chromatin soluble fraction** and the pellet (resuspended in urea lysis buffer) the **chromatin insoluble** one.

For the analysis of [REDACTED] protein abundance by Western blot, pelleted cells were resuspended in RIPA with 1X PI, incubated on ice for 15 minutes and sonicated in a Bioruptor Pico (Diagenode) (two rounds of 10 cycles 15 seconds ON/30 seconds OFF). Protein solution was cleared by 15 minutes centrifugation at maximum speed at 4°C.

8.2 Click-chemistry

For **palmitoylome studies** click chemistry was performed right after SILAC protein mix preparation at 2 mg/ml protein concentration. The following reagents were added sequentially to the protein mix: 500 µM biotin-azide PEG3 (762024, Sigma-Aldrich) (stock at 100 mM in DMSO), 2 mM TCEP (tris(2-carboxyethyl)phosphine) (stock solution freshly prepared before each use at 50 mM in PBS) (C4706, Sigma-Aldrich), 2 mM TBTA (Tris[(1-benzyl-1H-1,2,3-triazol-4-yl)methyl]amine) (678937, Sigma-Aldrich) and 2 mM CuCO₄ (451657, Sigma-Aldrich) (stock solution freshly prepared before each use at 50 mM in ddH₂O). Samples were incubated for 1.5 hours rocking at RT in the dark. Then, after stopping the click chemistry reaction, protein was precipitated by a chloroform-methanol precipitation to remove the reaction reagents.

For the **gel-based visualization** of palmitoylated proteins the click chemistry was performed with TAMRA (5-Carboxytetramethylrhodamine)-azide (760757, Sigma-Aldrich) (instead of biotin-azide) at 200 µM final concentration and in the dark.

In the **immunoprecipitation experiment** click chemistry was performed on the proteins enriched with the sepharose beads with biotin-azide in a final liquid volume of 50 µl (not considering the solid volume of the beads). The concentration of the click chemistry reagents was identical to the one used for the palmitoylome experiments and the reaction was performed for 1 hour at RT with gentle shaking for beads resuspension. Upon finalization of the click chemistry the beads of each sample were split in two and 0.7 M NH₂OH was added to one of the halves prior to the incubation with Laemmli buffer.

Click chemistry reaction was always stopped by addition of EDTA to a final concentration of 10 mM.

8.3 Chloroform-methanol precipitation of proteins

For protein precipitation, four volumes of methanol, one of chloroform and three of ddH₂O were added to the samples and upon mixing they were centrifuged at 14,000g for 5 minutes at 4°C. After centrifugation, the upper aqueous phase was removed and four more volumes of methanol were added carefully to avoid protein disc disruption.

Upon a second centrifugation at maximum speed (>18,000g) for 10 minutes at 4°C, the supernatant was removed and the protein pellets were air-dried.

8.4 Enrichment of palmitoylated proteins

Pelleted proteins for the palmitoylome analysis were resuspended in urea buffer (6 M urea, 1% SDS, 5 mM EDTA) and 50 µg of protein was separated from each mix as input. After alkylation and reduction of the proteins, samples were diluted with PBS to a final concentration of 1 mg/ml of protein in 1.6 M urea and 0.2% SDS and incubated with streptavidin beads (LSKMAGT, Millipore PureProteome) (25 µg of protein per µl of beads) for 1.5 hours rotating at RT. Prior to the incubation with the samples, streptavidin beads were equilibrated through three washes with 1.6 M urea and 0.2% SDS. After incubation with the samples, beads were washed three times with 1.6 M urea and 0.2% SDS buffer and another three times with 1.6 M urea. Finally, beads were resuspended in 1.6 M urea for on-beads tryptic digestion.

8.5 Protein alkylation and reduction

Prior to tryptic digestion (proteome studies) or streptavidin beads pulldown (palmitoylome studies), protein samples to be analyzed by mass spectrometry were reduced and alkylated. For the **proteome** studies, samples were incubated with 5 mM DTT for 30 minutes shaking at 55°C. Then, after cool down, protein samples were alkylated with a 30 minutes incubation with 15 mM iodoacetamide (I1149, Sigma-Aldrich) at RT shaking in the dark. After alkylation, more DTT was added to the samples, to a final concentration of 10 mM, and samples were incubated at RT for 15 minutes shaking.

In the case of the **palmitoylome** experiments, the DTT was replaced by TCEP (C4706, Sigma-Aldrich). TCEP was added to the protein samples to a final concentration of 5 mM and they were incubated for 30 minutes at 37°C. After alkylation with 15 mM iodoacetamide for 30 minutes in the dark at RT, more TCEP was added to a final concentration of 10 mM and samples were incubated for 15 minutes at RT.

8.6 Tryptic digestion of protein

For **whole proteome** analysis protein samples were diluted to 2 M urea and 1 µg/ml protein concentration and digested with 1:100 w/w trypsin (V5111, Promega) and 2 mM CaCl₂ overnight (ON) at 37°C shaking. Digestion was stopped by trifluoroacetic acid (TFA) addition until pH < 2 and samples were cleared by centrifugation at 16,000g for 10 minutes at 4°C.

For the **palmitoylome** analysis protein digestion was performed on beads upon enrichment of palmitoylated proteins. Streptavidin beads were resuspended in digestion buffer containing 50 mM Tris-HCL pH8.2, 1.6 M urea, 2 mM CaCl₂ and 1:100 v/v trypsin (V5111, Promega) and were incubated ON shaking at 37°C. Digestion was stopped by TFA addition.

8.7 Peptides desalting

8.7.1 Sep-Pak columns

Peptide samples with over 50 µg material that were to be analyzed by LC-MS, were desalted with Sep-Pak C18 (WAT054955, Waters) columns. Cartridges were equilibrated through sequential washes with 3 volumes 100% acetonitrile (ACN), 1 volume 70% ACN/0.25% acetic acid (AA), 1 volume 40% ACN/0.5% AA and 3 volumes of 0.1% TFA. After equilibration, peptide samples in 0.5% TFA were added to the column, collected upon filtration and re-filtered to maximize protein collection by the cartridge. Then, C18 cartridges were washed with 3 volumes 0.1% TFA and 0.5 volumes 0.5% AA. Finally, peptides were eluted with 0.75 volumes 40% ACN/0.5% AA followed by 0.5 volumes 70% ACN/0.25% AA. The different solvents passed through the column by gravity flow. After desalting the solvent of the eluted peptides was evaporated with a SpeedVac vacuum concentrator and drought peptides were stored at -80°C until mass spectrometry analysis.

8.7.2 StageTip

Peptide samples below 50 µg were desalted with 4 layers of C18 polymer (WAT054955, Waters) in StageTips. The polymer was equilibrated prior to sample addition with 2 volumes 100% methanol, 1 volume of 100% ACN, 1 volume of 70% ACN/0.25% AA and 2 volumes 0.1% TFA. Peptide samples in 1% TFA were then loaded on the StageTip twice and washed with 2 volumes 0.1% TFA and 1 volume 0.5% AA. Elution was performed in 4% formic acid/3% ACN. Peptides were drought with SpeedVac and stored at 80°C until mass spectrometry analysis. One-minute centrifugations at 200g were performed to favor solvents flow through the StageTip.

8.8 Deep reverse-phase basic fractionation of the proteome

The deep reverse-phase basic fractionation of the proteome was performed after peptide desalting. Four layers of SDB cartridge discs (2240, 3M) were placed in each StageTip for the fractionation of 60 µg peptides. The equilibration of the SDB cartridges was performed by sequential filtering of 2 volumes 100% methanol, 1 volume of 100% ACN, 1 volume of 70% ACN/0.25% AA, 1 volume 80% ACN/0.1% ammonium hydroxide, 1 volume 40% ACN/0.5%AA and 2 volumes 0.1% TFA. Peptides, resuspended in 0.1%

TFA, were loaded twice in each StageTip to ensure their retention in the SDB cartridge and then, samples were washed with 3 volumes of 0.1% TFA. The basic fractionation of the proteome was done by sequential elutions in different tubes with 1 volume of diluents with increasing concentrations of ACN (6%, 12%, 18%, 80%) in 0.1% ammonium hydroxide. All samples were then acidified with 1/3 volume 10% TFA in 70% ACN, dried with SpeedVac and stored at -80°C until MS analysis.

9 Liquid chromatography-mass spectrometry (LC-MS) analysis

All mass spectrometry analyses were performed by our collaborators Dr. David Gomez and Mr. Kieran Wynne at the University College Dublin. Proteomics experiments with cell culture using SILAC were analyzed on a Q-Exactive (ThermoFischer Scientific) mass-spectrometer while the proteomic analyses of tumour samples coming from mice using label-free quantification (LFQ) were performed on a TiMS-TOF Pro (Bruker Daltonics) mass-spectrometer.

9.1 In culture SILAC-based proteomic analysis (Thermo Scientific Q Exactive)

9.1.1 LC-MS/MS method

The samples were run on a Thermo Scientific Q Exactive mass spectrometer connected to a Dionex Ultimate 3000 (RSLCnano) chromatography system. Tryptic peptides were resuspended in 0.1% formic acid. Each sample was loaded onto a fused silica emitter (75 µm ID, pulled using a laser puller (Sutter Instruments P2000)), packed with ReproCil Pur C18 (1.9 µm) reverse phase media and was separated by an increasing ACN gradient over 120 minutes at a flow rate of 200 nL/min. The mass spectrometer was operated in positive ion mode with a capillary temperature of 320 °C, and with a potential of 2300V applied to the frit. All data was acquired with the mass spectrometer operating in automatic data dependent switching mode. A high resolution (70,000) MS scan (350-1600 m/z) was performed using the Q Exactive to select the 12 most intense ions prior to MS/MS analysis using HCD.

9.1.2 MS data analysis

The raw data was searched against the Homo sapiens subset of the Uniprot Swissprot database (reviewed) using the search engine Maxquant (release 1.6.17.0) for peptides cleaved with trypsin. Each peptide used for protein identification met specific Maxquant parameters, i.e., only peptide scores that corresponded to a false discovery rate (FDR) of 0.01 were accepted from the Maxquant database search. The “match between runs”

option was enabled with a time window of 0.7 min to match identifications between replicates. The “requant” option of MaxQuant was enabled for the quantification of SILAC pairs.

9.2 In vivo LFQ-based proteomic analysis (Bruker timsTOF Pro)

9.2.1 LC-MS/MS method

Samples were run on a Bruker timsTOF Pro mass spectrometer connected to a Bruker nanoElute nano-LC or to an Evosep One liquid chromatography system. Tryptic peptides were resuspended in 0.1% formic acid and each sample was loaded onto an Aurora UHPLC column (25 cm x 75 µm ID, C18, 1.6 µm) (Ionopticks) or onto an Evosep tip. The samples analyzed with Aurora UHPLC columns were separated with an increasing ACN gradient over 60 minutes or 90 minutes at a flow rate of 250 nl/min.

Alternatively, samples were run on a Bruker timsTOF Pro mass spectrometer connected to an Evosep One liquid chromatography system. Tryptic peptides were resuspended in 0.1% formic acid and each sample was loaded on to an Evosep tip. The Evosep tips were placed in position on the Evosep One, in a 96-tip box. The autosampler was configured to pick up each tip, elute and separate the peptides using a set chromatography method (30 samples a day).

In both cases, the chromatography buffers utilized were buffer A (99.9% H₂O, 0.1% formic acid) and buffer B (99.9% ACN, 0.1% formic acid). All buffers used were LC-MS grade.

The mass spectrometer was operated in positive ion mode with a capillary voltage of 1500 V, dry gas flow of 3 l/min and a dry temperature of 180 °C. All data was acquired with the instrument operating in trapped ion mobility spectrometry (TIMS) mode. Trapped ions were selected for ms/ms using parallel accumulation serial fragmentation (PASEF). A scan range of (100-1700 m/z) was performed at a rate of 5 - 10 PASEF MS/MS frames to 1 MS scan with a cycle time between 1.03 - 1.89s.

9.2.2 MS data analysis

The raw data was searched against the Homo sapiens subset of the Uniprot Swissprot database (reviewed) using the search engine Maxquant (release 1.6.17.0) using specific parameters for trapped ion mobility spectra data dependent acquisition (TIMS DDA). Each peptide used for protein identification met specific Maxquant parameters, i.e., only peptide scores that corresponded to an FDR of 0.01 were accepted from the Maxquant

database search. The normalised protein intensity of each identified protein was used for label free quantitation (LFQ).

10 Immunoprecipitation

650 µg of nuclear protein extract in 800 µl RIPA was incubated ON at 4°C and rotating with 4µg anti-██████████ or mock rabbit IgG (see **table M&M4** for further details on the antibodies). Protein A sepharose beads (17528001, Cytiva) were used to capture IgGs. Upon equilibration through three washes with RIPA and blocking with 0.1% BSA in RIPA for 20 minutes at 4°C rotating, 40 µl beads were added to the nuclear protein extract and incubated for 2 hours at 4°C rotating. Beads were pelleted by 3 minutes centrifugation at 1,000g and washed two times with mild-RIPA buffer (50 mM Tris-HCL buffer pH7.4, 150 mM NaCl, 2 mM EDTA, 0.1% NP-40), another two times with mild-HEPES buffer (50 mM HEPES pH7.9, 150 mM NaCl, 0.1% SDS) and two more times with PBS for unspecific protein binding removal prior to click chemistry on beads.

11 In gel fluorescence detection and Western Blot

11.1 SDS-polyacrylamide gel electrophoresis (SDS-PAGE)

Protein samples were boiled at 95°C for 5 minutes in 1X Laemmli buffer (1610747, BIO-RAD) and 2.5% β-mercaptoethanol and loaded in 15% SDS-PAGE gels or 4-15% Mini-PROTEAN® TGX precast gels (4561085, BIO-RAD). Running buffer was prepared by dilution of 10X Tris/Glycine/SDS buffer (1610772, BIO-RAD) with dH₂O and gels were run at 200V for in gel fluorescence detection and at 100V for western blot.

11.2 In-gel fluorescence detection

For the detection of TAMRA fluorophore, after running, gels were washed twice with dH₂O and imaged with LI-COR Odyssey® Fc at 600nm. Then, they were incubated ON at RT with InstantBlue™ Coomassie (ab119211, Abcam) for loading control. Images of this Coomassie blue staining were acquired with Syngene™ GBox Chemi.

11.3 Western blot

In the case of the Western blots (WB), once the dye front was out of the gel, proteins were transferred to 0.45 µm PVDF (IPVH00010, Immobilon-P) membranes previously activated with 30 seconds methanol incubation. Transfer buffer was prepared as specified by the product: 10X Tris/Glycine buffer (1610771, BIO-RAD) was diluted in 20% methanol and dH₂O. Transferences were done at continuous voltage of 100V for 90 minutes. After transference, membranes were washed with dH₂O and stained with 0.5% Ponceau (P3504, Sigma-Aldrich) in 5% AA for loading control. Then they were further

washed with dH₂O and blocked for 1 hour at RT with 5% BSA in Tris-buffered saline (28358, Thermo Scientific) with 0.001% Tween-20 (P1379, Sigma-Aldrich) (TBST), for biotin detection, or 5% milk in TBST for protein detection.

The different primary antibodies utilized for western blot and their dilutions are specified in **table M&M4**. They were all diluted in 3% BSA and incubated ON at 4°C rotating. After primary antibody incubation membranes were washed 3 times for 5 minutes with TBST and incubated for 1 hour at RT with the correspondent secondary-HRP (Horseradish peroxidase) antibody diluted in 3% BSA in TBST rotating. Streptavidin-HRP (S5512, Sigma-Aldrich) was also diluted at 1:200 in 3% BSA in TBST and incubated with the membrane for 1 hour at RT. After washing, membranes were incubated for 5 minutes with SuperSignal™ West Pico PLUS Chemiluminiscent substrate (34577, Thermo Scientific) and HRP signal was detected with LI-COR Odyssey® Fc.

All LI-COR Odyssey® Fc images were analyzed and processed with Image Studio™ Lite quantification software.

11.3.1 HRP inactivation

Some membranes were incubated with more than one primary antibody. If both primary antibodies were from different animal origin, after the first protein detection the membrane was incubated for 30 minutes at 37°C in 10% AA for denaturalization of the HRP. Then, after thorough washing with dH₂O and TBST, membranes were blocked again prior to primary tumour incubation.

11.3.2 Harsh stripping

When the primary antibodies had the same origin and the same secondary antibody was to be used, a harsh stripping of the membrane was performed. The membrane was incubated for 45 minutes shaking at 50°C in 2% SDS diluted in 62.5 mM Tris-HCL pH6.8 and with 0.008% β-mercaptoethanol. Again, membrane was then profusely washed with dH₂O and TBST and blocked for the second protein detection.

12 Real-time quantitative PCR (RT-qPCR)

RNA was isolated using RNeasy Mini Kit (74104, Quiagen) followed by cDNA synthesis using the High capacity cDNA reverse transcription kit (4368814, Applied Biosystems), in both cases according to manufacturer's instructions. TaqMan Master Mix (4369016, Applied Biosystems) and the following TaqMan probes were used for the RT-qPCR analysis according the manufacturer's instructions:

- *PPIA*: Hs.PT.39a.22214851 (Integrated DNA Technologies, IDT)
- *CD36*: Hs01567185_m1 (Thermo Scientific)
- [REDACTED] (Integrated DNA Technologies, IDT)

A LightCycler® 480 instrument (Roche) was used for the analysis. The reference gene *PPIA* (peptidylprolyl isomerase A) was used for normalization and data was analyzed using the $\Delta\Delta C_t$ method.

13 Statistical analyses

Statistical significance was analyzed utilizing Prism 8 (Graphpad) using two-tailed t-test for RT-qPCR analysis and Fisher's exact test for the analysis of the metastasis incidence. Sample sizes are indicated in the figure legends. Data are generally shown as the mean \pm standard deviation (SD).

Proteomic datasets were normality tested by using Kolmogorov-Smirnov test. Statistical comparisons were performed by t-test or nonparametric Mann-Whitney test depending on whether the data was normally distributed or not, respectively. Significant differences were established at the level of p-value < 0.05 in both cases. Boxplots represents 25 and 75 percentiles and whiskers 10 and 90 percentiles unless otherwise stated.

PCAs, correlation plots, hierarchical clustering for heatmaps and 1D / 2D annotation enrichment analysis were performed in Perseus (Cox and Mann, 2012).

14 Antibodies

Antibody/Streptavidin	Company	Reference	Dilution	Technique
anti-BRG1	Abcam	ab110641	1:5,000	WB
anti-CAV1	Santa Cruz biotech.	sc-53564	1:500	WB
anti-CD9	Santa Cruz biotech.	sc-13118	1:200	WB
anti-DSP	Santa Cruz biotech.	sc-390975	1:500	WB
anti-FLAG	Sigma	F1804	1:500	Immunofluor.
anti-HA	Abcam	Ab9110	1:4,000	WB
anti-██████████	Abcam	██████████	1:2,000	WB
anti-██████████	Abcam	██████████	1:162 (w/w)	IP
anti-██████████	Abcam	██████████	1:1,000	WB
anti-██████████	Sigma-Aldrich	██████████	1:100	WB
anti-LPCAT1	Sigma-Aldrich	HPA012501	1:500	WB
anti-mouse Alexa Fluor 568	Invitrogen	A10037	1:500	Immunofluor.
anti-NAT10	Santa Cruz biotech.	sc-271770	1:500	WB
anti-rabbit IgG	Abcam	ab46540	1:162 (w/w)	IP
APC-conjugated anti-CD36	BD Pharmingen	550956	1:100	FACS
biotin-conjugated anti-mouse CD45	Invitrogen	13-0451-85	1:100	FACS
biotin-conjugated anti-mouse H-2Kd	Invitrogen	13-5957-82	1:100	FACS
HRP anti-mouse IgG	DAKO	P0447	1:1,500	WB
HRP anti-rabbit IgG	Invitrogen	31466	1:5,000	WB

Table M&M4. Antibodies used.

References and dilutions of the antibodies used for each technique. Dilutions are given in volume, unless otherwise specified. w = weight; WB = western blot; IP = immunoprecipitation; FACS = fluorescence-activated cell sorting; Immunofluor. = immunofluorescence staining.

RESULTS

1 Changes in the proteome induced by dietary PA and OA in OSCC

1.1 Changes in the proteome of OSCC cells induced by cell culture treatment with PA and OA

1.1.1 Proteomic changes induced in SCC-25

Our laboratory has previously demonstrated that some FAs present in our diet, like PA, boost CD36 scavenger receptor expression and the metastatic capacity of tumour cells, while others, like OA, decrease CD36 expression and may even reduce the aggressiveness of the cancer cells (Pascual et al., 2021). To gain new insights about the mechanisms behind the opposite phenotypic response of tumour cells to OA and PA, we decided to analyze the changes induced by these two FAs in the proteome of OSCC cells.

We first analyzed the changes in the proteome of OSCC cells elicited by the two distinct FAs in cell culture using the SILAC quantitative proteomics method, in which isotope-labeled amino acids are incorporated into proteins during translation *in vivo* (see *Materials and Methods* section for further details). We grew SCC-25 cells (a commercial human OSCC cell line) in different SILAC media (L, M, and H) and stimulated them for four days with 50 μ M OA, 300 μ M PA or the FA vehicle (BSA) (herein named as control, CT). FA concentrations used in the treatments of our cell culture experiments were in the lower range of the physiological concentrations in plasma, as previously used (Pascual et al., 2021), since high concentrations of these FAs can affect cell viability. In humans, the plasma concentration of PA can range between 0.3 and 4.1 mM, while that of OA is always lower, with an average range of 0.03 to 3.2 mM (Abdelmagid et al., 2015). Likewise, in mice OA levels are lower than the PA ones (Broadfield et al., 2021).

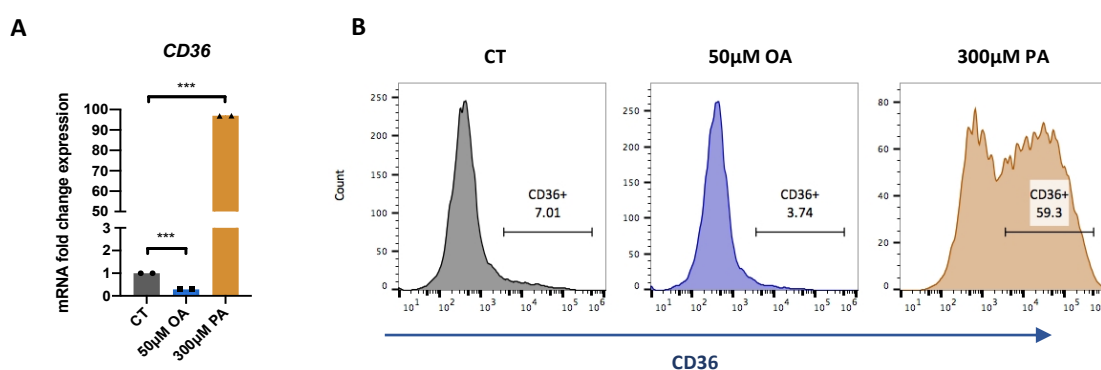


Figure R1.1. CD36 changes induced by PA and OA in SCC-25

A) Relative mRNA expression of *CD36* upon 50 μ M OA and 300 μ M PA four days treatment in SCC-25, by RT-qPCR. *** p-value < 0.001 **B)** Representative histograms of the FACS analysis of CD36 membrane expression in SCC-25 upon four days 50 μ M OA, 300 μ M PA or control (CT) treatments. Analyzed by FACS.

We first checked the effectiveness of the treatment by measuring the *CD36* transcript levels by RT-qPCR, and protein expression in membrane by FACS. Indeed, PA treatment enhanced both the *CD36* mRNA expression and protein levels in membrane, while OA treatment reduced them (**Figure R1.1**). We then collected cells from each condition in four biological replicates ($n = 4$), prepared whole cell lysates and mixed the proteins in a 1:1:1 SILAC ratio. After tryptic digestion, we performed a deep reverse-phase basic fractionation of the peptides prior to LC-MS analysis, to increase the proteome coverage.

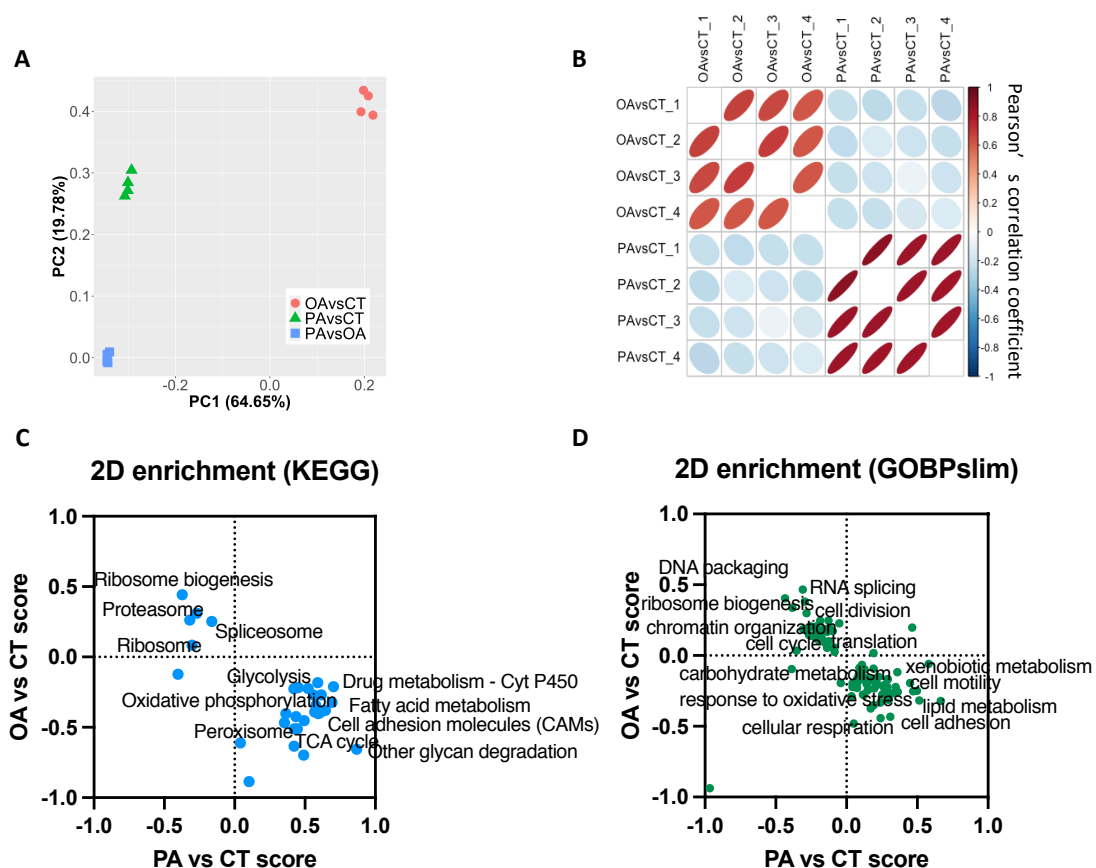


Figure R1.2. PA and OA treatments induce an opposite proteomic response in SCC-25.

A) Principal component analysis (PCA) plot of the \log_2 SILAC ratios indicating protein abundance differences induced by 50 μM OA or 300 μM PA treatments in SCC-25. Each treatment was analyzed in 4 biological replicates ($n = 4$). **B)** Correlation matrix depicting the Pearson's correlation coefficients between protein expression changes in the different experimental replicates. **C)** 2D annotation enrichment analysis of the proteomic changes induced by OA and PA treatments using KEGG (Kyoto encyclopedia of genes and genomes) annotation database (FDR q -value < 0.05). **D)** 2D annotation enrichment analysis of the proteomic changes induced by OA and PA treatments using the GOBP slim (gene ontology biological process slim) annotation database (FDR q -value < 0.05).

We quantified a total of 3941 proteins with high reproducibility as evidence by the principal component analysis (PCA) of the SILAC ratios for the proteins detected in all replicates, where all comparisons clustered apart (**Figure R1.2A**). Strikingly, the matrix of Pearson's correlation coefficients among biological replicates showed that PA and OA treatments exerted opposite responses at the proteome level as compared to the control group (**Figure R1.2B**). We then performed a 2D annotation enrichment analysis, which compares the proteomic changes in the context of categorical annotation of the proteins, and observed the same opposite trend among the biological terms significantly changed upon PA or OA treatment. Among the categories upregulated by PA (and downregulated by OA) were lipid metabolism and various other metabolic pathways (e.g., glycolysis, TCA cycle, OXPHOS), together with terms related to oxidative stress and drug resistance (e.g., cytochrome P450, xenobiotic metabolism, response to oxidative stress) and categories related to metastasis like cell motility or cell adhesion (**Figure R1.2C, D**). On the other hand, the biological processes downregulated by PA (and upregulated by OA) were mainly involved in cell cycle processes (e.g., DNA packaging, cell division), ribosome biogenesis, RNA splicing and protein turnover (**Figure R1.2C and D**).

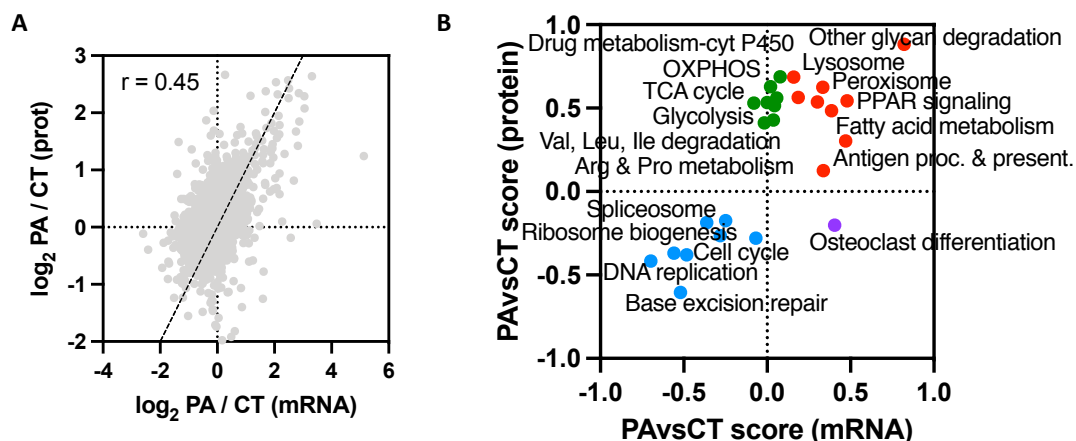


Figure R1.3. Proteome and transcriptome changes correlate in PA treated cells

A) Correlation plot of the differentially expressed proteins and transcripts upon four days 300 μ M PA treatment in SCC-25. Fold change expression is represented in \log_2 scale. Dashed line indicates the identity function ($x=y$) and Pearson's correlation coefficient (r) is indicated. prot=protein **B)** 2D annotation enrichment analysis of the transcriptomic and proteomic changes induced by PA treatment using KEGG annotation database (FDR q -value < 0.05).

To test whether the observed proteome changes induced by PA were transcriptionally regulated, we compared the proteomic changes induced by PA in our experiment with previous transcriptomic data from the laboratory under the same experimental conditions (Pascual et al., 2021). Interestingly, we found a significant correlation ($r = 0.45$, ANOVA test significance < 0.0001) between the proteomic and transcriptomic (mRNA) changes induced by a four-day PA treatment of SCC-25 cells (**Figure R1.3A**), in

line with previous studies comparing proteomic and transcriptomic responses in human cells (Jovanovic et al., 2015; Lindhout et al., 2020). 2D annotation enrichment analysis between mRNA and protein changes showed that most categories directly correlated, suggesting that proteomic responses to PA, such as the enhancement of lipid metabolism and the downregulation of cell cycle-related processes, were largely regulated at the transcription level (**Figure R1.3B**). Interestingly, we found that several metabolic categories (mostly mitochondrial, such as TCA cycle and OXPHOS, but also glycolysis) as well as those related to drug resistance, were upregulated at the proteome but not at the transcriptome level, suggesting transcription-independent regulatory mechanisms for those processes (**Figure R1.3B**).

1.1.2 Comparison of the response induced by PA and OA in two different OSCC cell lines: SCC-25 and VDH-15

We next tested whether the distinct proteomic changes upon PA or OA treatment was observed for other OSCC cells closer to a clinical situation. For this, we performed the same SILAC experiment using the VDH-15 cell line, which was previously established in our laboratory from a patient with OSCC from the Vall d'Hebron hospital (Pascual G. et al, 2021). Indeed, treating VDH-15 cells with the same protocol as used for the SCC-25 cell line (i.e., 50 μ M OA and 300 μ M PA, for four days) led to an increase or a decrease of CD36 membrane expression after PA or OA treatment, respectively (**Figure R1.4A**). The proteomic analysis from four independent biological replicates ($n = 4$) (chemically fractionated as before to increase proteome coverage) gave a total of 3719 proteins that quantified with good reproducibility from VDH-15 cells (**Figure R1.4B**). Correlation analysis showed again an inverse relationship between OA and PA treatments response. Direct comparison of the proteomic changes between PA and OA treatments in both OSCC cell lines resulted in a similar proteomic response, both at the individual protein level (Pearson's correlation coefficient = 0.55, ANOVA test significance < 0.0001) (**Figure R1.4C**) and at the level of biological processes (**Figure R1.4D**). Of note, PA induced the same changes in VDH-15 cells as in SCC-25: increased expression of genes involved in metabolic pathways (e.g., lipid metabolism, TCA cycle, OXPHOS), cell adhesion and categories related to immunity or drug resistance, and decreased expression of genes involved in cell proliferation, protein synthesis and degradation pathways and mRNA splicing processes (**Figure R1.4D**).

These experiments extended our understanding of the mechanisms of action of different FA in cancer, showing that PA or OA treatment in cell culture reshapes the proteome of OSCC cells in opposite directions, which correlates with their influence on CD36 expression and the metastatic potential observed in previous studies from the laboratory (Pascual G. et al, 2021) (**Figure I1.5**).

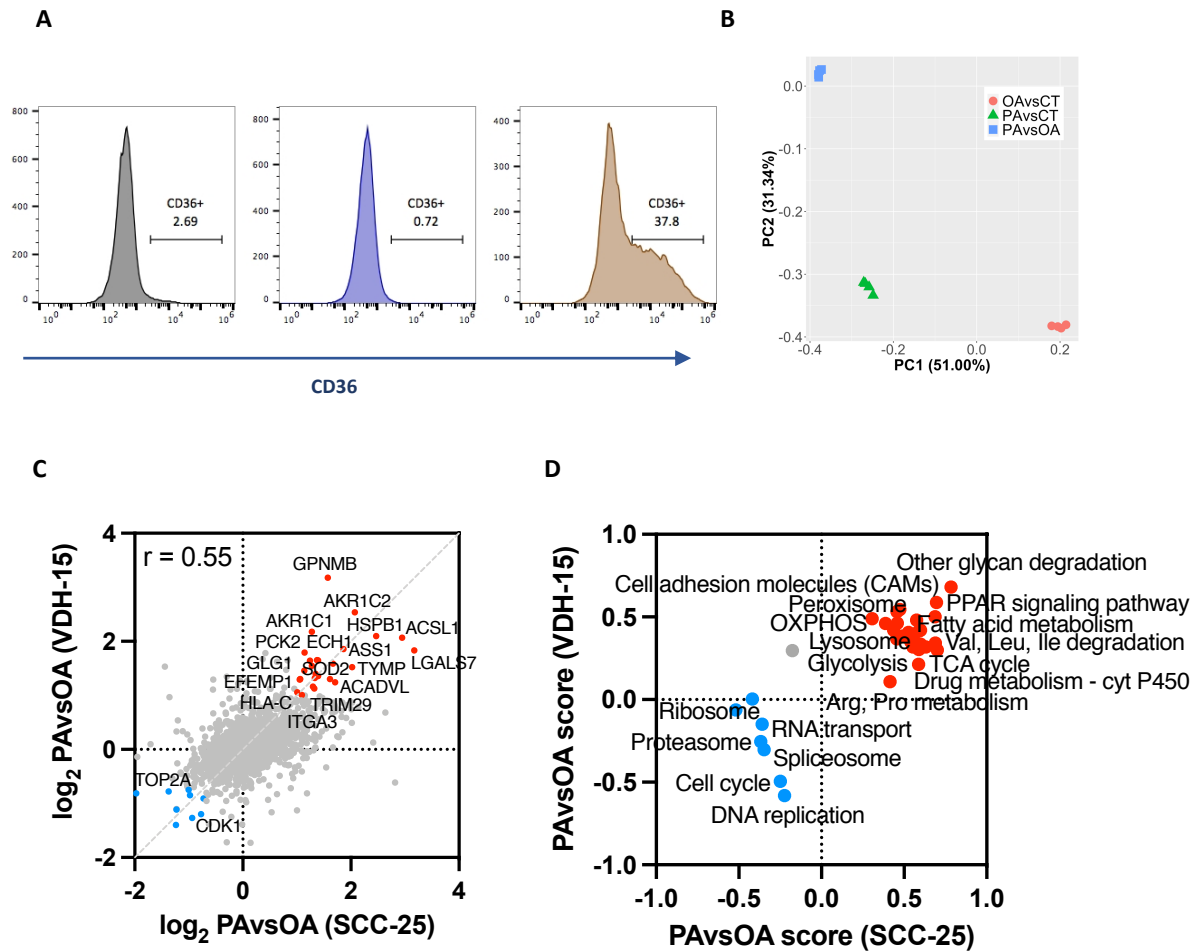


Figure R1.4. Similar results are obtained with a second OSCC cell line: VDH-15

A) Representative histograms of the FACS analysis of CD36 presence in the PM of VDH-15 cells upon four days of 50 μ M OA or 300 μ M PA treatment. **B)** PCA plot of \log_2 SILAC ratios showing the proteomic changes induced by 50 μ M OA or 300 μ M PA treatments in VDH-15. $n = 4$ **C)** Correlation of the proteomic changes induced by PA and OA treatments in SCC-25 versus VDH-15 cell lines. Fold change expression is represented in \log_2 scale. Dashed line indicates the identity function ($x = y$) and Pearson's correlation coefficient (r) is indicated. Upregulated (fold change > 2) and downregulated (fold change < 1.66) proteins are colored in red and blue respectively. Some names representative of specific pathways are indicated. **D)** 2D annotation enrichment analysis of the GOBP categories of the proteins altered by PA treatment compared to OA in SCC-25 and VDH-15 cell lines (FDR q -value < 0.05).

1.2 Changes in the proteome of SCC-25 induced by PA- and OA-enriched diets in mice

To study the relevance of these proteomic alterations observed in cell culture in a more physiological context, we analyzed the changes in the proteome of OSCC cells orthotopically grown in mice fed HFDs enriched with either PA or OA. Previous studies from our laboratory showed that feeding tumour-bearing animals with a HFD rich in PA

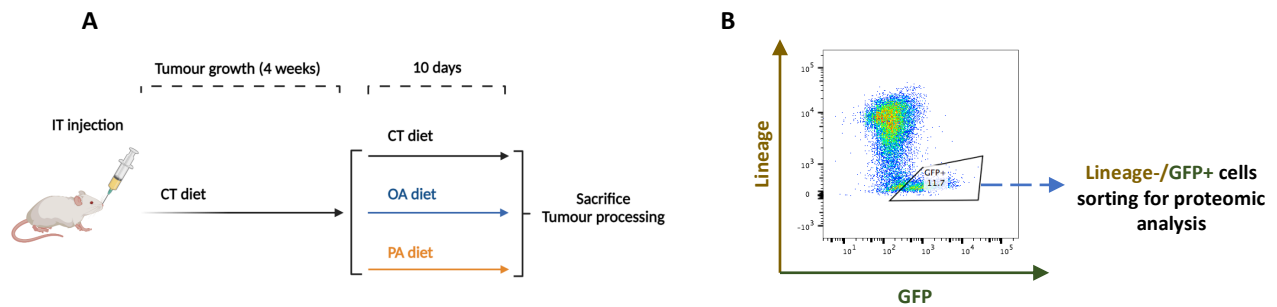


Figure R1.5. Mouse OSCC dietary model scheme and sorting strategy.

A) Graphical depiction of the mouse experiment performed to analyze the changes in the proteome induced by different fatty diets. SCC-25 cells were orthotopically injected, IT, in NSG mice fed with CT diet. After 4 weeks tumour bearing mice were randomized in three groups and two of those groups were changed to OA-enriched (OA-diet) or PA-enriched (PA-diet) HFDs. After ten days of fatty diet feeding, mice were sacrificed and tumours were processed to single cell suspension for FACS sorting. **B)** Representative FACS plot of the cells sorted for proteome analysis. Only mouse lineage (H-2Kd, CD45)-/GFP+ cells were sorted for protein extraction.

can boost the metastatic capacity of the tumour cells in secondary recipients that are only ever fed a (non-HFD) control diet; in contrast, this effect is not observed from primary animals fed an OA-enriched HFD. This enhanced aggressiveness induced by the PA diet is epigenetically codified in the cell (Pascual G. et al, 2021). We used a similar experimental design to analyze the proteomic alterations induced by diet; briefly, pLuc-GFP-expressing SCC-25 cells were orthotopically injected, intra-tongue (IT) into NOD SCID gamma (NSG) mice fed a control diet (**Figure R1.5A**). Tumour growth was monitored weekly by bioluminescence and, when the average bioluminescence signal of the PTs was above 5×10^7 total photon flux (approximately 4 weeks after injection), mice were divided in three dietary groups. The tumour size, number of developed metastases and sex of animals were considered for the semi-randomization of the mice. One group was kept on the same control diet, while the other two were switched to an OA- or PA-enriched HFD (see *Materials and Methods* for further details on the diet compositions) (**Figure R1.5A**). After ten days under each dietary condition, mice were sacrificed, PTs were pooled based on mouse sex and processed to single-cell suspensions for FACS sorting. The bioluminescence threshold used to determine the moment of the dietary change (i.e., 5×10^7 total photon flux) was established considering previous animal experiments performed with the same cell line. Based on the PT growth dynamics of SCC-25, the harvesting time was a few days before the tumour size reached the humane endpoint (when animals stop eating).

Human cells were sorted based on GFP-positive labelling and mouse lineage-negative expression and further processed for proteomic analysis by label-free protein quantification (**Figure R1.5B**). A minimum number of cells (around 100,000) was required for optimal low-input sample processing and protein quantification, which

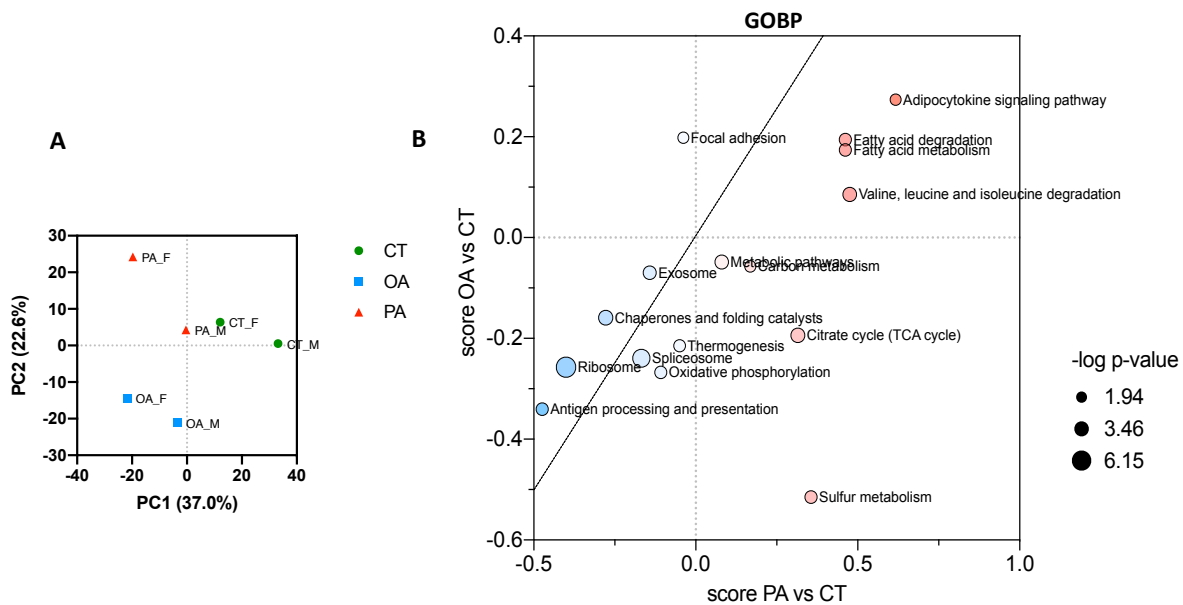


Figure R1.6. PA- and OA-enriched HFDs do not induce opposite responses.

A) PCA plot of the different proteome samples obtained from tumour cells sorted from mice fed a control (CT), OA-enriched (OA) or PA-enriched (PA) HFDs. $n = 2$. F stands for female and M for male. **B)** 2D annotation enrichment analysis of KEGG terms on the proteomic changes induced by OA and PA enriched diets. In red, categories upregulated by PA diet; in blue, downregulated categories. (FDR q -value < 0.2 ; p -value < 0.01). The size of the circle determines the significance of that category (p -value). Dashed line indicates identity function ($x = y$).

restricted the analysis to two biological replicates per group ($n = 2$). A total number of 4,307 proteins were quantified and the PCA analysis showed that the samples of each diet clustered apart, although the difference was not as striking as in the cell culture treatment experiment. This reduced distinction was due in part to the variability between sexes (**Figure R1.6A**) and to the less pure lipid component of the diets (as opposed to treatments in culture), which is in fact a mix of FAs. Specifically, the PA-enriched diet fat was palm oil, which however contains 40% OA; likewise, the OA-enriched diet fat was olive oil, which contains 7.5% to 20% PA. In fact, the main PCA component differentiated animals on a HFD from the CT diet group (**Figure R1.6A**) and the 2D annotation enrichment analysis showed that OA- and PA-enriched HFDs induced a similar proteomic response in the tumour cells (**Figure R1.6B**)

Tumour cells exposed to either diet upregulated certain metabolic categories, such as FA metabolism and degradation of valine, leucine and isoleucine, while they downregulated others related to the protein turnover (e.g., ribosome, chaperones and folding catalysis), splicing, exosome and the antigen presentation (**Figure R1.6B**). However, the effect on the upregulation of FA metabolic processes (FA metabolism, FA degradation, adipocytokine signaling) was stronger in the PA-enriched diet group than in the OA-enriched one (**Figure R1.6B**). The only two categories with an opposite

response were the TCA cycle and sulfur metabolism, both of which were induced by the PA-enriched diet and downregulated by the OA-enriched one (**Figure R1.6B**).

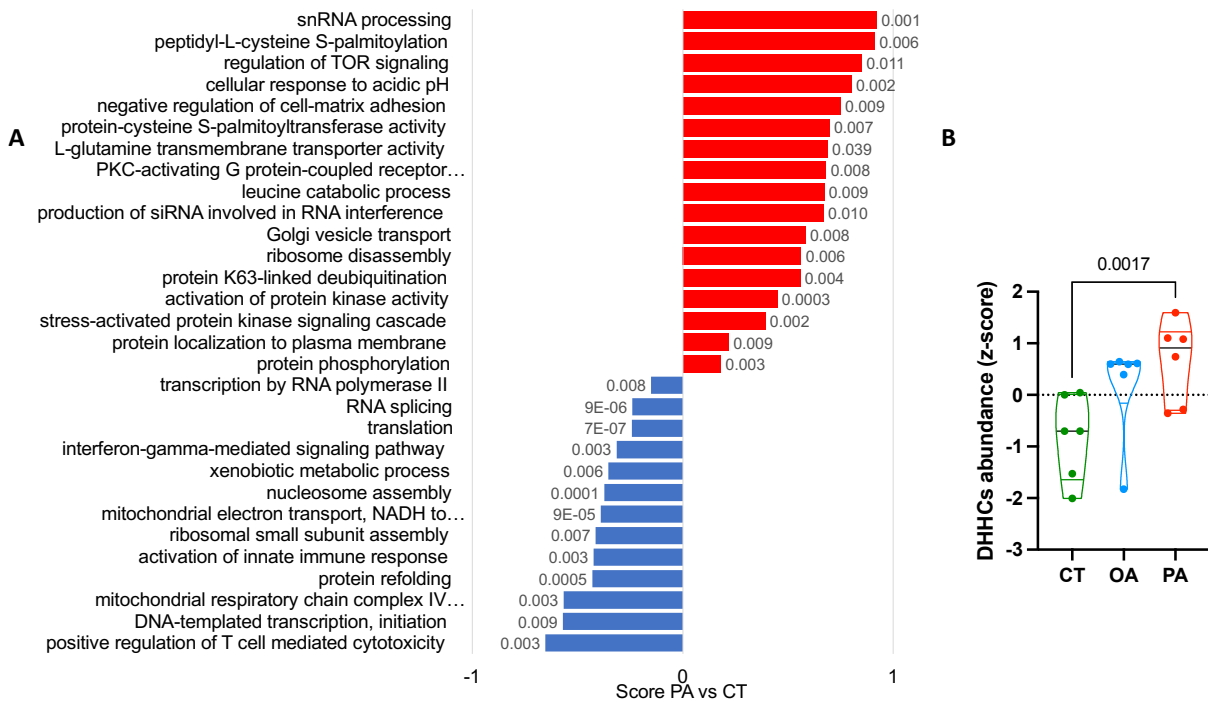


Figure R1.7. Protein palmitoylation and DHC-PATs are upregulated in SCC-25 upon PA-enriched diet mice feeding.

A) Bar plot showing representative GO categories significantly changing (1D annotation enrichment analysis, p -value < 0.05) based on the proteomic changes induced by PA-enriched HFD in SCC-25. In red and with a positive score, the categories upregulated. In blue and with a negative score the downregulated ones. P-values of each category are indicated at the end of each bar. **B)** Violin plot of z-score normalized abundance values of the different DHC-PATs identified in the tumor proteomes coming from each dietary group. CT stands for proteins in the control group; OA are proteins in the OA-enriched HFD fed group; PA represents proteins in the PA-enriched HFD group (p -value = 0.0017).

Direct analysis of the proteomic changes upon PA-enriched diet showed two categories involved in protein palmitoylation among the most upregulated: L-cysteine S-palmitoylation (DHC3, DHC4, DHC20) and protein cysteine S-palmitoyl transferase activity (DHC3, DHC4, DHC20, YKT6, GLUL (glutamine synthetase)) (**Figure R1.7A**). Global protein expression changes of the palmitoyl transferase family (DHC-PATs) corroborated that tumours in mice fed with a PA-enriched diet had higher expression of DHCs (**Figure R1.7B**). To further explore the effects of PA on this family of proteins, we analyzed the transcriptomic data from previous studies (Pascual et al., 2017 and Pascual et al., 2021) and found that a four-day PA treatment in cell culture upregulated most *ZDHC* genes expression in SCC-25 cells: specifically, *ZDHC1*, -3, -5, -7, -13, -14, -20 and -24 were significantly upregulated (p -value < 0.05), while only *ZDHC6* and -16 were significantly downregulated (p -value < 0.01) (**Figure R1.8A**). Interestingly, the expression of most *ZDHC*s genes also seemed to be upregulated in LN metastases compared to PT

with no previous treatment. In particular, expression levels of *ZDHHC8*, -11, -14 and -18 (q-value ≤ 0.1) and *ZDHHC2* and -23 (p-value < 0.05) were significantly upregulated (Figure R1.8B).

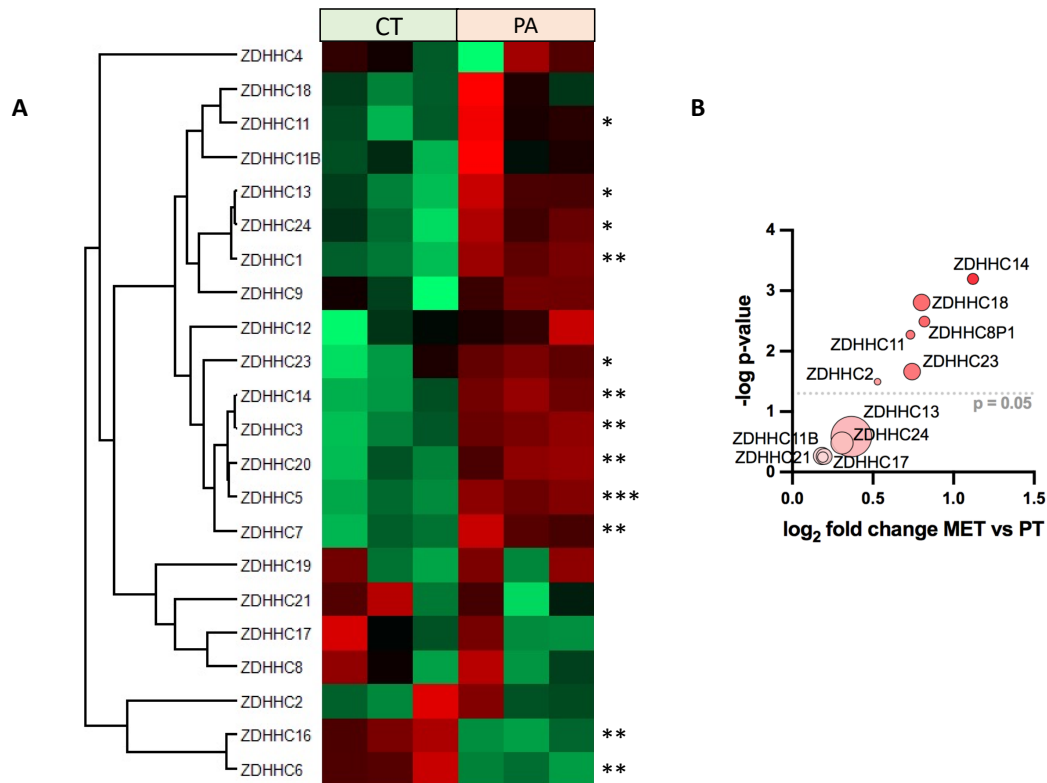


Figure R1.8. *ZDHHCs* gene expression is upregulated by PA cell culture treatment and in the LN metastases in mice.

A) Heat map of differential transcriptomic expression of the *ZDHHC* genes upon 4 days of 300 μM PA treatment of SCC-25 in cell culture ($n = 3$; p-values: * < 0.05 ; ** < 0.01 ; *** < 0.001). **B)** Scatter plot showing differences in *ZDHHCs* expression between SCC-25 cells coming from lymph node metastases (MET) and primary tumor (PT) lesions, dashed line represents statistical p-value = 0.05. Fold change expression is represented in log₂ scale.

In sum, these results show that the PA-enriched diet enhanced the lipid metabolism and protein palmitoylation in tumour cells. Also, previous transcriptomic results showed that protein palmitoylation could have a role in the spontaneous LN metastases of OSCC as well as in the metastatic phenotype induced by PA. Since alterations in protein palmitoylation can have a strong impact on the biology and signaling of tumour cells, we next studied the palmitoylome of OSCC cells and its possible implications in metastasis.

2 Palmitoylome studies

To study the palmitoylome of OSCC cells, we used a metabolic labelling strategy based on the addition of the PA analogue 17-ODYA in the culture media (**Figure R2.1A**). 17-ODYA can be metabolically incorporated into proteins using the cellular palmitoylation/depalmitoylation machinery but, unlike PA, it has an alkyne group on the omega end that can react with an azide group in a Huisgen's cycloaddition reaction, also known as click chemistry ([Martin et al., 2012](#)) (**Figure R2.1B**). Upon treatment with the analog, 17-ODYA-tagged (i.e., palmitoylated proteins) can be isolated and coupled to azide-reporter tags, such as biotin-azide or TAMRA-azide using click-chemistry (**Figure R2.1B**). Coupling of 17-ODYA-acylated proteins with fluorescent azide-tags such as TAMRA allows for their gel-based visualization, while the biotin-azide tag enables their visualization by Western blot or the enrichment of acylated proteins with streptavidin beads pulldown for downstream LC-MS analysis ([Martin et al., 2012](#)). This methodology, unlike others based on ex-vivo chemical labelling like acyl-biotin exchange (ABE) ([Drisdell](#)

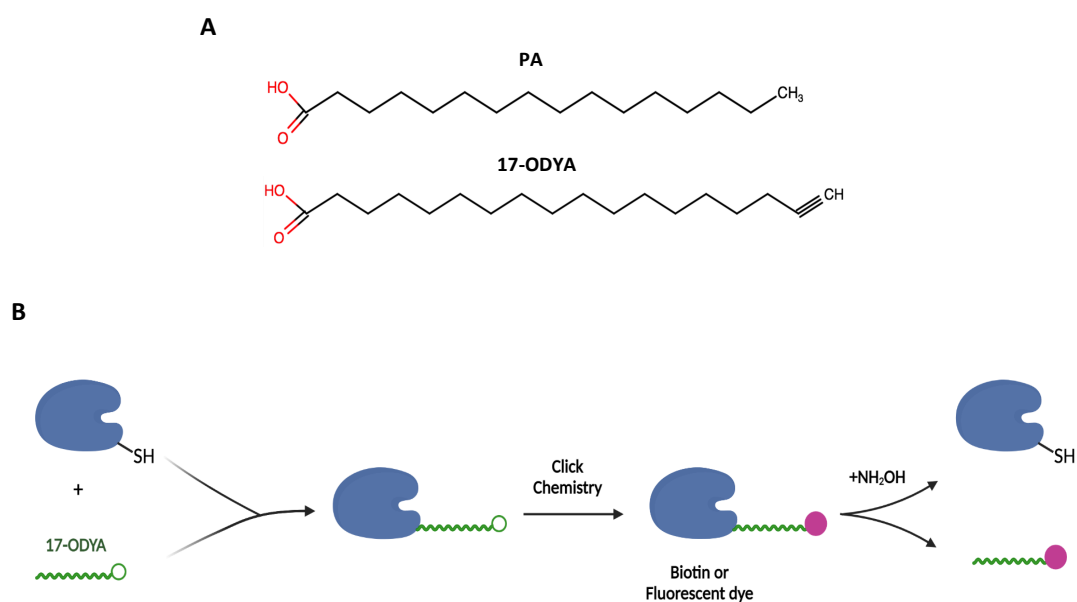


Figure R2.1. 17-ODYA and the metabolic labelling of palmitoylated proteins.

A) Chemical structure of PA and the PA analog 17-ODYA. Oxygen (O) atoms and their covalent bonds are colored in red. H represents hydrogen and C carbon. Chemical structures were drawn using BioEddie tool from Chem Axon. **B)** Graphical description of the metabolic labelling of an S-palmitoylated protein with 17-ODYA. Proteins that can be palmitoylated are enzymatically acylated with 17-ODYA within the cell. After extraction, proteins are submitted to click chemistry and biotin or a fluorescent dye (TAMRA) are attached to the 17-ODYA moiety. Upon hydroxylamine (NH₂OH) treatment, only the thioester bonds between the S-palmitoylated proteins and 17-ODYA are broken and the signal of those proteins is lost. O- and N-palmitoylated proteins remain acylated upon NH₂OH treatment. Created with BioRender.com

and Green, 2004; Wan et al., 2007), is not restricted to S-palmitoylation but rather allows the whole palmitoylome (including N- and O- palmitoylation) to be studied (see also *Discussion* section for differences between these two methods).

2.1 Phenotypic characterization of 17-ODYA in OSCC

2.1.1 Incorporation of 17-ODYA into proteins

Palmitoylation events can exhibit markedly different turnover rates in cells (Martin et al., 2012). Thus, we decided to characterize the incorporation of 17-ODYA into proteins of SCC-25 cells to optimize the treatment concentrations and timings for maximizing the labelling of palmitoylated proteins. First, we observed that the incorporation of 17-ODYA into proteins was dose- and time- dependent (**Figure R2.2**). We treated SCC-25 cells with different concentrations of 17-ODYA (0.4 - 50 μ M) for 1 hour and, after click chemistry with TAMRA fluorophore, SDS-PAGE and in-gel fluorescent scanning at 600 nm, we observed specific fluorescent bands with an intensity that positively correlated with an increasing 17-ODYA dose (red arrows in **Figure R2.2A**). In parallel, we treated the cells with 10 μ M 17-ODYA for different periods of time (15 minutes to 2 hours); similarly, we observed a time-dependent incorporation of the PA analog into proteins (**Figure R2.2B**). In both experiments, most of this specific signal was lost upon treatment with 0.7 M NH_2OH (hydroxylamine). NH_2OH breaks the thioester linkage between palmitoylated Cys and the PA moiety in S-palmitoylated proteins but does not affect the amide nor the oxyester chemical bonds of N- or O-palmitoylated proteins (**Figure R2.1B**). This result showed that most palmitoylated proteins were S-palmitoylated, as previously observed by others (Martin and Cravatt, 2009) (**Figure R2.2**).

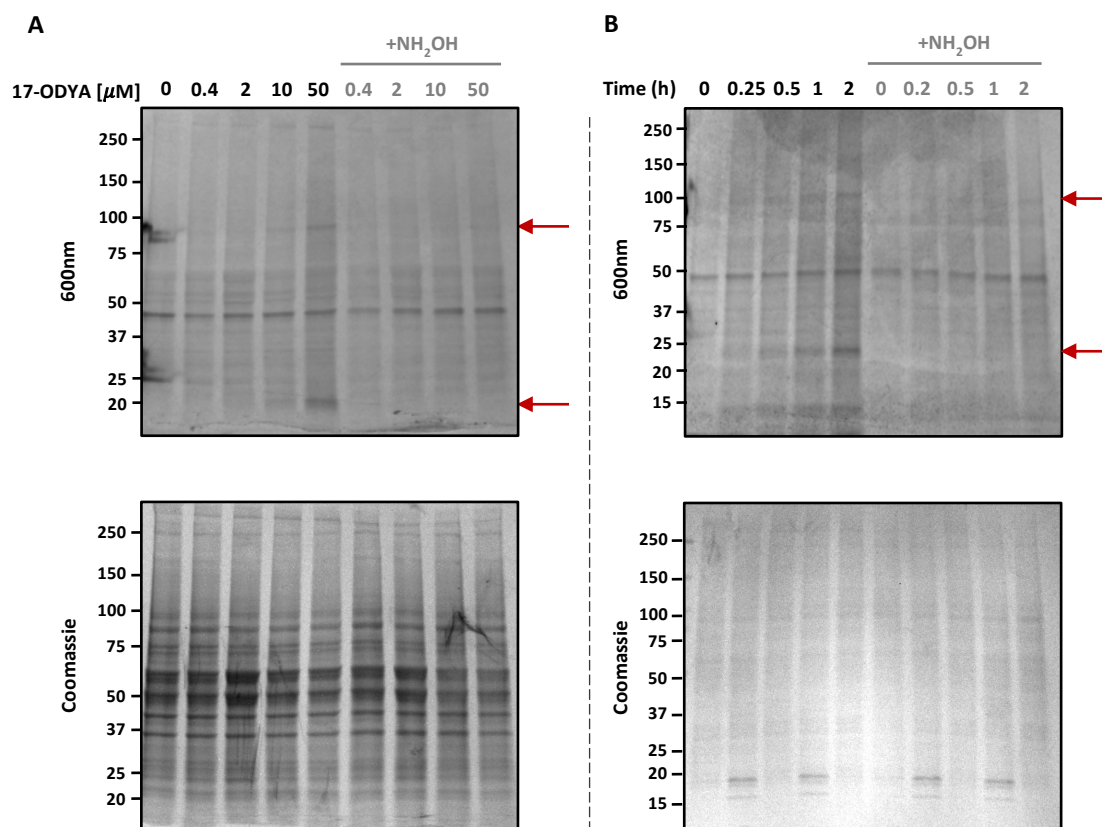


Figure R2.2. 17-ODYA is incorporated into proteins in a dose and time dependent manner. Upper panels in **A)** and **B)** are fluorescent images of gels taken at 600nm for TAMRA detection. SCC-25 cells were treated with 17-ODYA at different concentrations for 1 hour **A)**, or with the same 17-ODYA concentration (10 μM) for different times **B)**. After treatment protein was extracted and click chemistry was performed with TAMRA. Half of the protein of each sample was treated with 0.7 M NH₂OH for the detection of S-palmitoylated proteins. The red arrows mark clear specific S-palmitoylated protein bands. Lower panels show the Coomassie staining of the gels in **A)** and **B)** for protein loading control. Numbers on the left mark different molecular weights.

To confirm that 17-ODYA was metabolically incorporated into the proteins (and not just chemically bound to them), we inhibited the enzymatic machinery responsible for its incorporation. Given that most of the specific signal detected in-gel came from S-palmitoylated proteins, we used 2-BP to inhibit all DHHC-PATs. SCC-25 cells were treated with 10 μM 17-ODYA and increasing doses of 2-BP (3-300 μM) for 2 hours. Indeed, the same bands that disappeared after NH₂OH treatment were not present in the 300 μM 2-BP condition, confirming that DHHC-PATs were responsible for the S-palmitoylation of proteins with 17-ODYA (**Figure R2.3A**). Finally, we tested whether 17-ODYA modified the same proteins as PA in a competition assay. We treated SCC-25 cells with a constant dose of 10 μM of 17-ODYA and increasing doses of PA (3-300 μM) for 2 hours. Of note, PA treatment outcompeted 17-ODYA protein S-palmitoylation, shown by the specific fluorescent signal loss with increasing doses of PA (**Figure R2.3B**).

Thus, we concluded that 17-ODYA was enzymatically incorporated into proteins in OSCC cells (at least in the case of S-palmitoylated proteins, which made the majority of these proteins), in a dose- and time-dependent manner and that it modified the same proteins affected by PA.

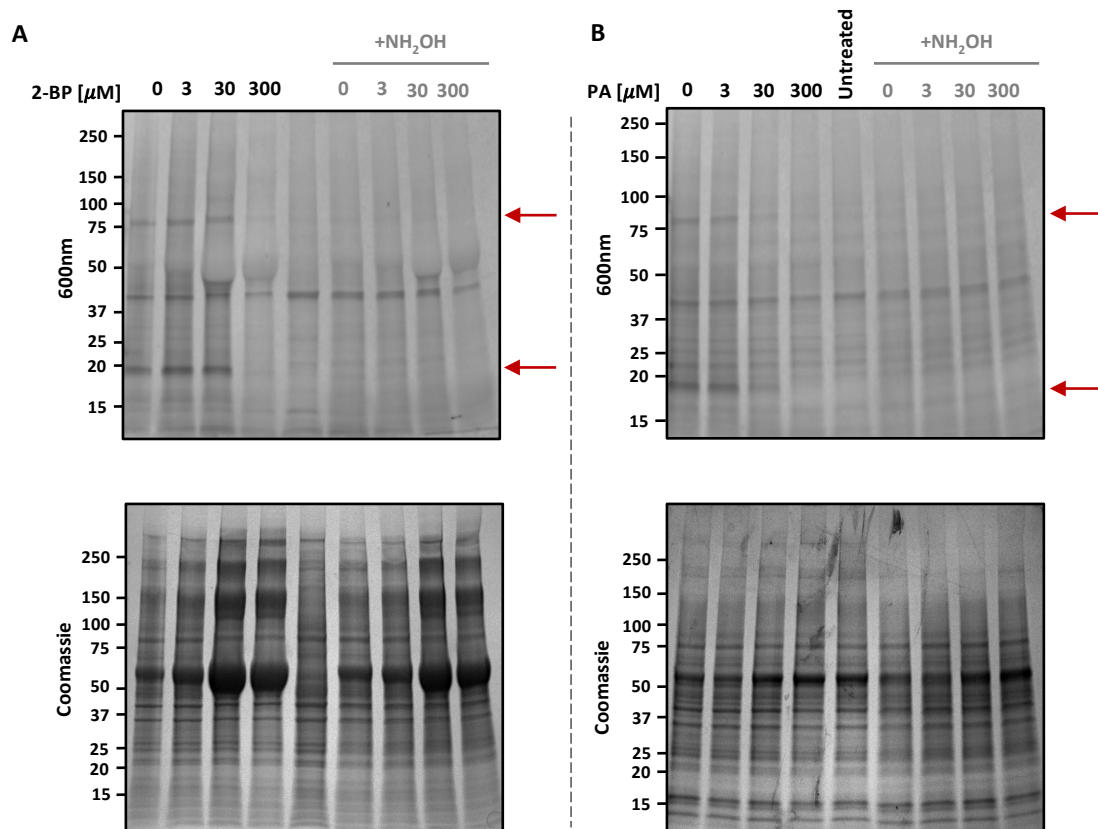


Figure R2.3. 17-ODYA is incorporated into proteins by the same enzymatic machinery than PA and can compete with it.

Upper panels in **A** and **B** show fluorescent images of gels at 600 nm for TAMRA detection. **A**) SCC-25 cells were treated with 10 μM 17-ODYA and different doses of the DHHC-PAT inhibitor 2-BP. **B**) Competitive experiment. SCC-25 cells were treated with 17-ODYA and increasing doses of PA. In both cases **A**) and **B**) half of the sample was treated with 0.7 M NH₂OH for the specific detection of S-palmitoylated proteins. The red arrows mark clear specific bands of S-palmitoylated proteins. The lower panels in A and B show the Coomassie staining of the gels as protein loading control. The numbers on the left the different molecular weights.

2.1.2 Metastatic phenotype induced by 17-ODYA treatment

Once we knew 17-ODYA could be used by the cell to palmitoylate proteins in the same way that PA, we wondered whether the analog could have the same impact on the metastatic phenotype of the cells. Previous studies of our laboratory showed that a four-day treatment of OSCC cells in culture with PA enhances their CD36 membrane

expression, boosts their metastatic potential and increases the incidence of metastasis when those cells are orthotopically injected in mice (Pascual G. et al, 2017; Pascual G. et al, 2021). We decided to assess if 17-ODYA treatment could induce the same phenotypic changes.

First, we tested the toxicity of long-term treatments with 17-ODYA. We observed that the viability of SCC-25 cells decreased (by 92%) at 75 μ M 17-ODYA treatment (**Figure R2.4A**), a lower concentration than in PA treatment. Despite their similarity, PA and 17-ODYA can produce a different molecular response. Indeed, 17-ODYA is considered an inhibitor of cytochrome P450 (Zou, A. P. et al, 1994), which may increase its toxicity as compared to PA. We chose a 50 μ M dose for the next experiments as a compromise between cell viability and a dose high enough to induce a phenotypic change.

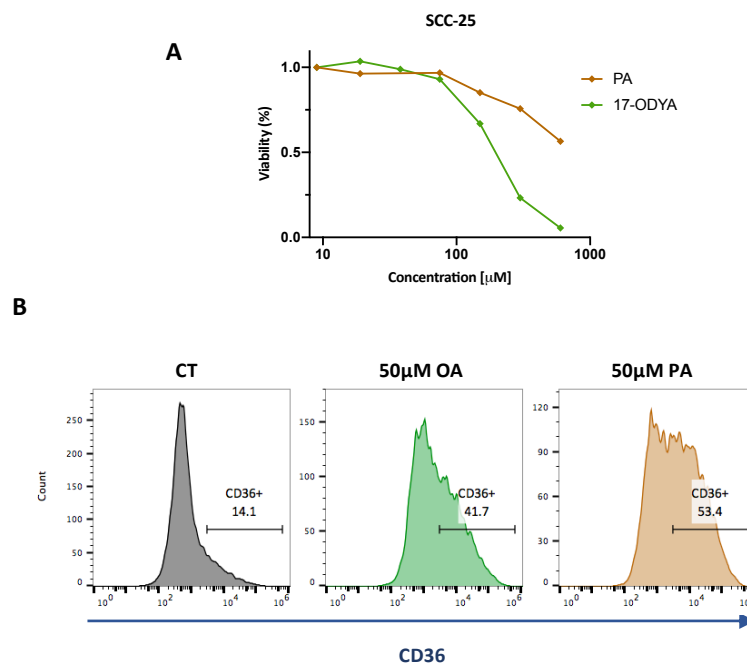


Figure R2.4. 17-ODYA toxicity and CD36 induction capacity.

A) Viability curve of SCC-25 cell line upon PA and 17-ODYA treatment. Cells were treated for 2 days with increasing doses of PA or 17-ODYA. **B)** Representative histograms of the FACS analysis of CD36 presence in the PM of SCC-25 cells upon 4 days of treatment with 50 μ M 17-ODYA, 50 μ M PA or CT.

We then tested the metastatic capacity of OSCC cells treated with 17-ODYA in two independent experiments. In both experiments, pLuc-GFP-expressing SCC-25 cells were treated for four days with either 50 μ M PA or 50 μ M 17-ODYA before being orthotopically injected IT in NSG mice. Prior to IT injection, we observed by FACS that 17-ODYA and PA treatments induced CD36 membrane expression to similar extents (**Figure R2.4B**). We monitored PT growth weekly by bioluminescence and determined that there was no difference in the tumour growth rate between groups (**Figure R2.5A and C**). At the end

of each experiment, we analyzed the incidence of developed LN metastases per group. We observed that both 17-ODYA and PA treatments tended to increase the incidence of metastases in each experiment (**Figure R2.5 B and D**). This difference was significant for 17-ODYA (p-value < 0.05) when combining the results of both experiments. In the first experiment, the metastases were quantified while the animals were still alive, as previously done (Pascual et al., 2017; Pascual et al., 2021), but in the second one, mice were sacrificed for PT removal and neck dissection prior to bioluminescence detection. This is the reason for the difference in the frequency of metastases observed between both experiments (see *Materials and Methods* for further clarification of the metastasis quantification). In conclusion, we observed that 17-ODYA and PA induced a similar metastatic phenotype in SCC-25 cells, with no differences in the PT growth.

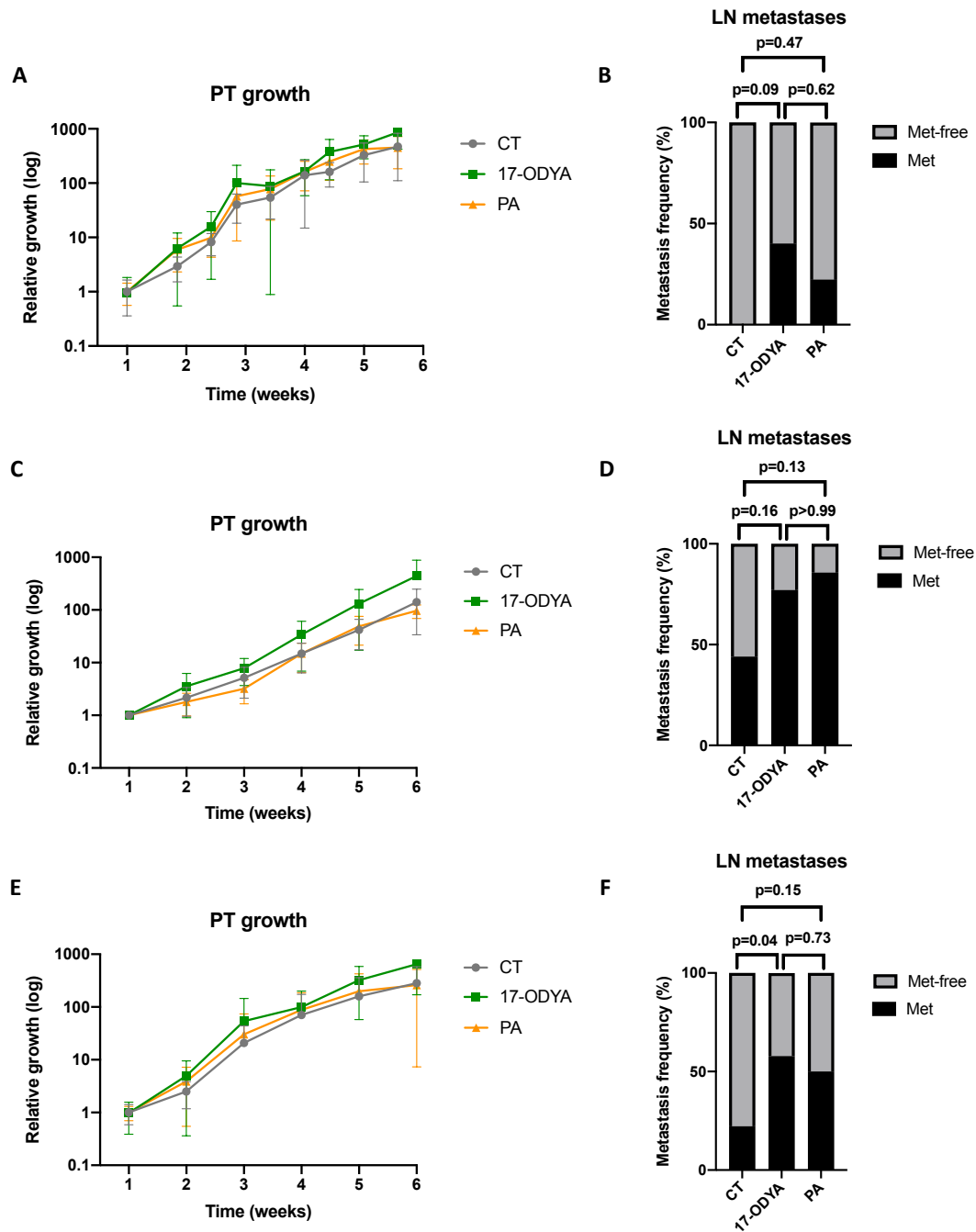


Figure R2.5. PA and 17-ODYA induce tumour cell aggressiveness to similar extent.

A) Bioluminescent PT growth quantification of mice inoculated with pLucGFP expressing SCC-25 cells previously treated for four days with 50 μ M 17-ODYA, 50 μ M PA or CT. $n = 10$ **B)** Frequency of developed LN metastases from animals in **A**. **C)** Bioluminescent PT growth quantification of mice in an independent experiment performed using the same conditions as in **A**. $n = 9$ **D)** Frequency of developed LN metastases from animals in **C**. **D)** PT growth curve of the combination of the independent experiments in **A** and **C**. **E)** Frequency of developed LN metastases from animals in both experiments. In **A**, **C** and **E** The total photon flux signal of each tumour at the different monitoring timepoints is normalized by the bioluminescent signal of that particular tumour at week 1 post-injection. Data is given as the mean \pm SD. The frequency of metastases in **B**, **D** and **F** is expressed as the percentage of total animals included in the study that developed a metastasis. Two-tailed Fisher's exact test was used for the statistical analysis. $p = p$ -value.

2.1.3 Proteomic changes induced by 17-ODYA

To better characterize the pro-metastatic molecular responses induced by 17-ODYA and PA, and to test if they were similar, we compared the proteome alterations generated by both treatments using SILAC in four independent replicates ($n = 4$) (**Figure R2.6A**). A four-day treatment with 50 μM dose of 17-ODYA or PA produced a similar response, as evidenced by the significant correlation ($r = 0.56$; ANOVA test significance < 0.0001) observed between the protein expression changes induced by both treatments with

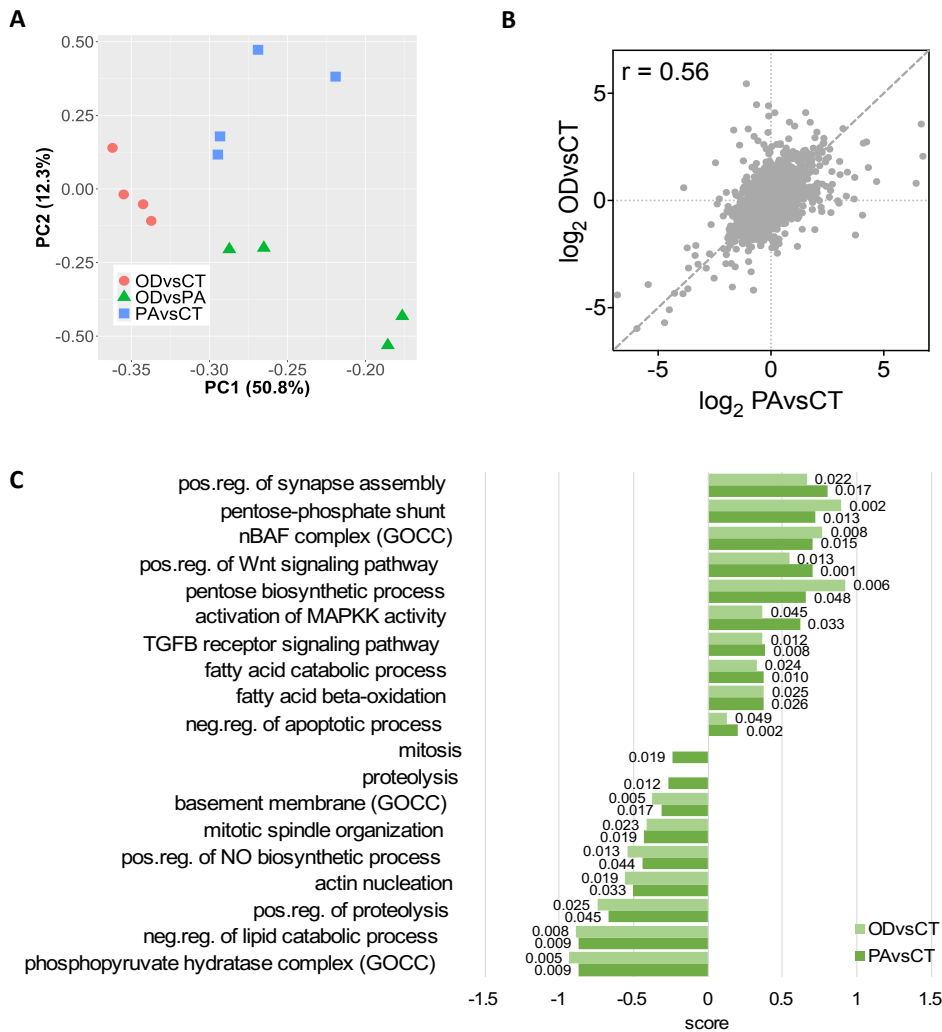


Figure R2.6. PA and 17-ODYA generate similar proteomic response.

A) PCA plot of the \log_2 SILAC ratios indicating the proteomic changes induced by four days 50 μM PA or 50 μM 17-ODYA treatments in SCC-25. $n = 4$. **B)** Correlation plot of the changes in the proteome of SCC-25 induced PA or 17-ODYA (OD) treatments in **A**. Dashed line indicates the identity function ($x = y$) and Pearson's correlation coefficient (r) is indicated. **C)** Bar plot showing representative GO categories significantly changing upon a 1D annotation enrichment analysis (p -value < 0.05) on the proteomic changes induced by PA or 17-ODYA (OD) treatments in SCC-25 in **A**. In light green, categories up- or downregulated by 17-ODYA (OD) treatment and in dark green the ones altered by PA. The categories upregulated have a positive score and the downregulated ones a negative score. p-values of each category are indicated at the end of each bar.

respect to control (**Figure R2.6B**). Both treatments upregulated the Wnt, TGF β (transforming growth factor beta) and MAPK pathways, FA catabolism, FAO and the pentose-phosphate pathway (**Figure R2.6C**); similarly, they both downregulated the proteolysis, NO biosynthesis and actin nucleation categories among others (**Figure R2.6C**). The main differences between treatments are observed in the mitosis and proteolysis GOBP categories, which are both downregulated only by PA. Nevertheless, as both treatments downregulated the mitotic spindle organization and the positive regulation of proteolysis, they probably both affected the cell cycle and protein degradation biological processes through different proteomic alterations (**Figure 2.6C**).

These results showed that 17-ODYA modified the proteome to a similar extent as PA, suggesting a comparable phenotypic switch in OSCC cells towards a more aggressive phenotype by inducing CD36 PM expression and LN metastasis.

2.2 Palmitoylome of metastatic SCC-25

As both PA and its analog 17-ODYA increased the metastatic potential of SCC-25 cells and can be used indistinctly by the cell to palmitoylate proteins, we next analyzed the palmitoylome of OSCC cells after a four-day treatment with 17-ODYA, to identify palmitoylated proteins that could have a role in metastasis. First, we compared the palmitoylome profiles, by in-gel fluorescence detection, of SCC-25 cells treated with 50 μ M 17-ODYA for up to four days to test whether longer labelling periods can alter the set of labelled proteins due to the metabolization of the analog. Of note, we did not find differences in protein labelling after the long-term treatment (**Figure R2.7**). In fact, many

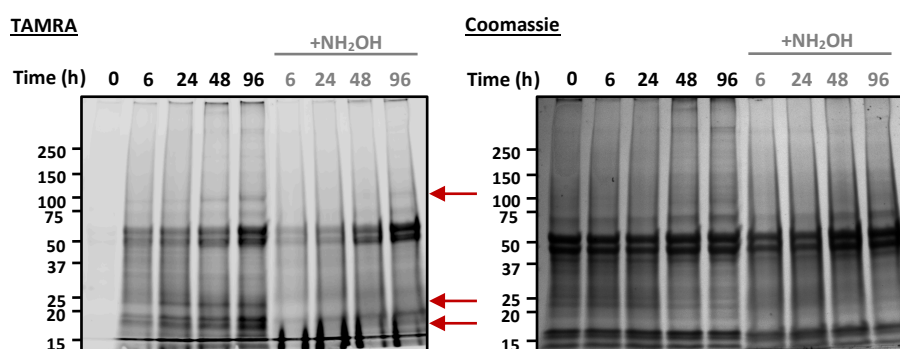


Figure R2.7. Four days 17-ODYA treatment palmitoylates the same proteins with higher intensity.

SCC-25 cells were treated with 50 μ M 17-ODYA for different periods of time. Protein was extracted and click chemistry was performed with TAMRA. Half of each sample was treated with NH₂OH for the specific detection of S-palmitoylated proteins. The picture on the left shows a fluorescent image taken at 600 nm for TAMRA detection. The red arrows indicate clear bands of S-palmitoylated proteins. Image on the right shows the Coomassie staining of the gel for protein loading control. h = hour.

S-palmitoylated protein bands (i.e., detected with TAMRA and that disappeared upon NH_2OH treatment) showed a markedly higher intensity after 4 days of treatment, suggesting a slow palmitoylation turnover.

To analyze the palmitoylome of metastatic SCC-25 cells, we combined the 17-ODYA treatment with SILAC proteomics (**Figure R2.8A**). Briefly, differently SILAC-labelled SCC-25 cells were treated for four days with 50 μM 17-ODYA, PA or control (BSA) in four independent replicates ($n = 4$), and protein from each condition was collected and mixed in a 1:1:1 ratio for further processing (**Figure R2.8A**). Then, we performed click chemistry on the SILAC protein mix with biotin-azide to conjugate a biotin molecule to those proteins modified with 17-ODYA (i.e., palmitoylated). Finally, we enriched for the palmitoylated proteins with a streptavidin bead pulldown and analyzed them by LC-MS (**Figure R2.8A**). Proteins from the CT or PA conditions should not react or bind to biotin-azide during the click chemistry, thus they were used as negative controls of enrichment, to detect unspecific binding as well as endogenously biotinylated proteins. The median enrichment ratio comparing protein enrichment abundances between CT and PA conditions in \log_2 scale was around 0, while practically all protein enrichment ratios between 17-ODYA (OD) and both controls gave positive values with a median \log_2 ratio around 1.5 (i.e., 3-fold change (fc)) (**Figure R2.8C**). This result indicated that we specifically enriched for palmitoylated proteins coming from the 17-ODYA treatment condition.

Out of the 1,200 proteins quantified in this experiment, only 327 proteins with a positive and statistically significant enrichment (p -value < 0.05 and FDR q -value < 0.05) as compared to PA condition were considered as palmitoylated. We used the PA condition as a reference as the proteome changes elicited by PA and 17-ODYA were equivalent. Almost all proteins (90%) that we considered to be palmitoylated in SCC-25 cells with a certain level of confidence (p -value < 0.05 ; indicated in red in **Figure R2.8D**) are included in SwissPalm repository for palmitoylated proteins (Blanc et al., 2015), which corroborates the robustness of our approach to identify palmitoylated proteins. We identified well-known palmitoylated proteins among the most enriched ones, such as: caveolin 1 (CAV1), IFITM1 (interferon induced transmembrane protein 1), CD44, CD9, ITGA6 (integrin subunit alpha 6) and ITGB4 (integrin subunit beta 4) (**Figure R2.8D**). Some of these proteins were further validated (see section 2.3 *Validation of palmitoylated proteins*).

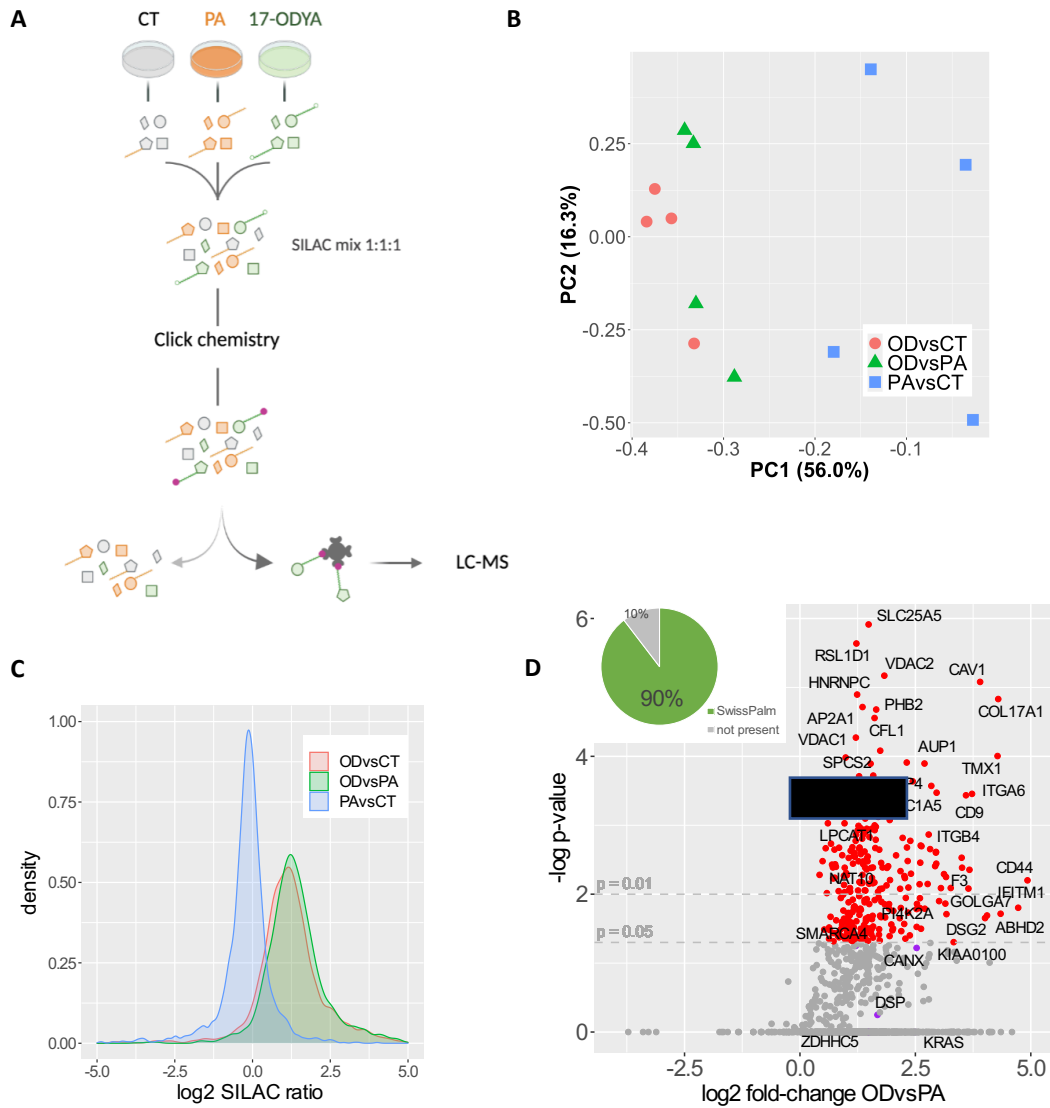


Figure R2.8. Enrichment of palmitoylated proteins in metastatic SCC-25.

A) Scheme of the steps followed for the enrichment of the palmitoylated proteins. SCC-25 cells were treated with 50 μ M PA, cells in medium (M.) SILAC media (orange); 17-ODYA, to cells in heavy (H.) media (green); or BSA (CT), cells in light (L.) media (grey); for four days. Protein from the 3 conditions was collected and mixed 1:1:1. Click chemistry was performed with biotin-azide (pink dots) and palmitoylated proteins were enriched with streptavidin beads for LC-MS analysis. Only proteins acylated with 17-ODYA can be specifically enriched. Created with BioRender.com **B)** PCA plot of log₂ SILAC ratios indicating protein abundance differences between conditions in the enriched samples ($n = 4$). **C)** Global density plot of log₂ SILAC ratios between conditions indicating the relative enrichment of proteins of each treatment. Ratios from all mixes are included in the distributions ($n = 4$). Red and green curves display the positive enrichment of proteins from 17-ODYA treatment with respect to CT and PA samples. The blue curve shows no enrichment of proteins from PA and CT treatments. **D)** Volcano plot of all the palmitoylated proteins (regardless of their quality of detection) specifically enriched after four days of 17-ODYA treatment *versus* PA. In red all the proteins significantly enriched p-value < 0.05. In purple proteins of interest not significantly enriched. Proteins of interest are named. Fold-change enrichment is expressed in log₂ scale. The plot also shows a pie chart with the percentage of significantly enriched proteins (p-value < 0.05) present in SwissPalm (Blanc et al., 2015).

Next, we performed a 1D annotation enrichment analysis on the palmitoylome of SCC-25 cells and found a significant enrichment in categories associated with membranes, as expected considering that the main function of protein lipidation is anchoring proteins to membranes. The most enriched GO terms relating to cellular components (GOCC) were membrane, membranous organelles (such as ER, Golgi and vesicles), and membrane-associated structures (such as hemidesmosomes, cell junctions and synapses) (**Figure R2.9A**). Regarding the GO categories involved in biological processes (GOBP slim), we found mostly enriched membrane-associated functions, such as cell adhesion, vesicle transport and motility (**Figure R2.9B**). Interestingly, we found “palmitate” or “transmembrane” among the significantly enriched keywords, as well as other membrane-related terms, underscoring that we successfully enriched for palmitoylated proteins (**Figure R2.9C**).

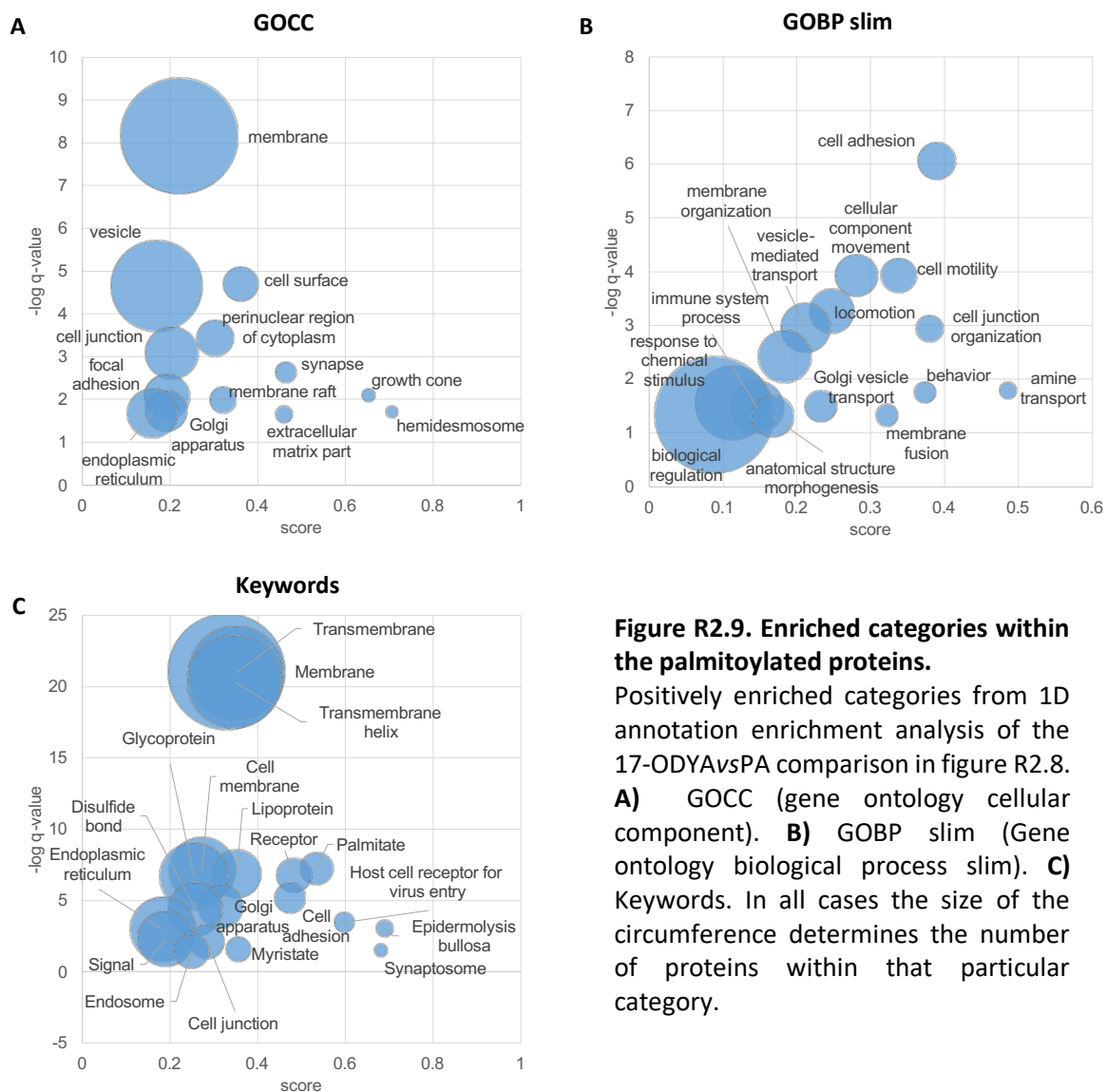


Figure R2.9. Enriched categories within the palmitoylated proteins.

Positively enriched categories from 1D annotation enrichment analysis of the 17-ODYAvsPA comparison in figure R2.8. **A**) GOCC (gene ontology cellular component). **B**) GOBP slim (Gene ontology biological process slim). **C**) Keywords. In all cases the size of the circumference determines the number of proteins within that particular category.

In conclusion, we identified a specific set of palmitoylated proteins in OSCC cells with increased metastatic capacity. These proteins were mostly associated to membrane functions, which could be implicated in the metastatic phenotype, such as cell adhesion and motility.

2.3 Validation of palmitoylated proteins

We followed the protocol depicted in **Figure R2.10A** to validate some of the proteins found to be palmitoylated in our previous large-scale experiment using mass-spectrometry. Briefly, SCC-25 cells were treated with 50 μ M 17-ODYA for four days and after protein extraction, each sample was split into two (with keeping 5 μ g of protein from each half kept as input). Both protein samples were incubated with the click

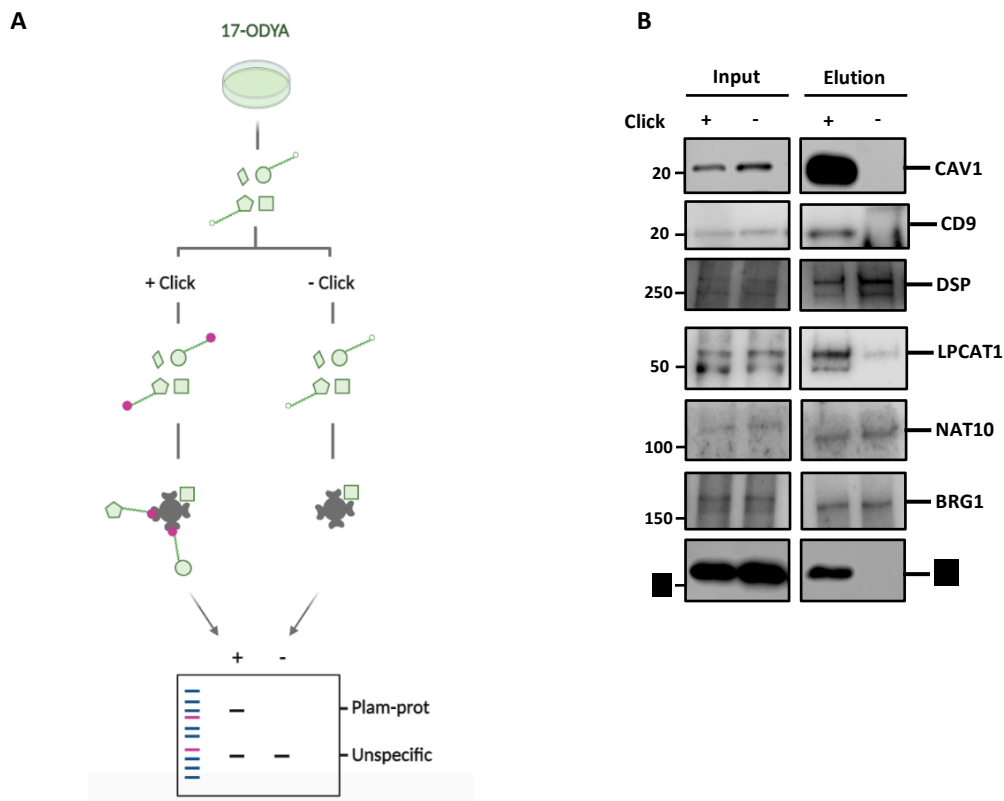


Figure R2.10. Western blot validation of palmitoylated proteins.

A) Depiction of the steps followed for the validation of the palmitoylated candidates. SCC-25 cells were treated for four days with 50 μ M 17-ODYA. Protein was extracted and divided in two samples. Both samples were submitted to click chemistry but in one of the samples biotin-azide was not added to the reaction. Palmitoylated proteins were enriched with streptavidin beads pulldown, eluted and run in an SDS-PAGE WB for their detection. Those proteins detected in both conditions are unspecifically enriched by streptavidin beads. Only those proteins specifically enriched in the condition with biotin-azide can be considered palmitoylated proteins. Created with BioRender.com **B)** Immunoblot images of the proteins tested for validation. Input samples (5 μ g) were separated before click chemistry. Numbers on the left mark the closest molecular weight size marker. CAV1 = caveolin-1; DSP = desmoplakin; LPCAT1 = lysophosphatidylcholine acyltransferase 1; Nat10 = N-acetyltransferase 10; BRG1 = SMARCA4; [REDACTED].

chemistry reagents but biotin-azide was only added to one of them, while the other one remained as a negative control. Then, palmitoylated proteins were enriched by pulldown with streptavidin beads and analyzed by western blot. Only proteins specifically enriched upon click chemistry with biotin-azide were considered as validated palmitoylated proteins (**Figure R2.10A**).

First, we proved that our validation method worked by detecting CAV1 and CD9 (**Figure R2.10B**), two of the most studied and validated palmitoylated proteins. We then focused on proteins that, due to their location or function, could well be palmitoylated. DSP (desmoplakin) is a critical component of the desmosome structure in epithelial cells. Although some components of desmosomes, such as desmoglein-2 or plakophilin-3, had been previously validated as palmitoylated proteins ([Woodley and Collins, 2019](#)), we did not validate DSP palmitoylation (**Figure R2.10B**) and concluded that the enrichment of this protein prior to LC-MS analysis was probably unspecific. On the other hand, we validated the palmitoylation of LPCAT1 (**Figure R2.10B**), which is an acyl transferase implicated in phospholipid metabolism that has also been described as the enzyme responsible for histone H4 palmitoylation. According to SwissPalm database ([Blanc et al., 2015](#)), this protein had been described in other palmitoylome studies but had never been validated before.

We next tested the palmitoylation of key regulatory proteins, as any PTM regulating the activity of these proteins would have a strong impact on the cell biology and could explain the vast molecular rewiring and the pro-metastatic phenotype observed upon PA treatment. We tested: i) SMARCA4 (SWI/SNF related, matrix associated, actin dependent regulator of chromatin, subfamily A member 4) (also known as BRG1 [Brahma related gene-1]), as a promising candidate, as it is a member of the SWI/SNF family of proteins and is required for the ATP-dependent chromatin remodeling and transcriptional activation of previously repressed genes ([Mittal and Roberts, 2020](#)); and ii) NAT10 (N-acetyltransferase 10), which is an RNA cytidine acetyltransferase that modifies mRNAs, tRNAs and ribosomal RNAs and thereby increases their stability ([Arango et al., 2018](#)). Further, it could also have a role in protein acetylation ([Liu et al., 2016b](#)). Both BRG1 and NAT10 are included in SwissPalm database, as they had been previously described in other large-scale palmitoylome studies ([Blanc et al., 2015](#)). However, we were not able to validate the palmitoylation of either BRG1 or NAT10 (**Figure R2.10B**). Finally, we tested whether [REDACTED] was palmitoylated in SCC-25 as it could [REDACTED]

[REDACTED] ([Blanc et al., 2015](#)) [REDACTED]

2.4 Changes in protein palmitoylation induced by PA and OA treatments

We next addressed if any of the proteins that we identified to be palmitoylated in a pro-metastatic cell were specifically palmitoylated in that particular phenotype, in other words, if any proteins showed changes in their palmitoylation state upon PA (pro-metastatic) and/or OA (anti-metastatic) treatments. To address this question, we followed a strategy inspired by other lipidomic studies (Niphakis et al., 2015), based on the competition between 17-ODYA and PA for the modification of a particular protein combined with SILAC proteomics (Figure R2.11A). We first treated SCC-25 cells for four days with 50 μM OA, 300 μM PA or control (BSA) to achieve the different metastatic phenotypes. We washed out the treatments and then incubated all conditions with 100

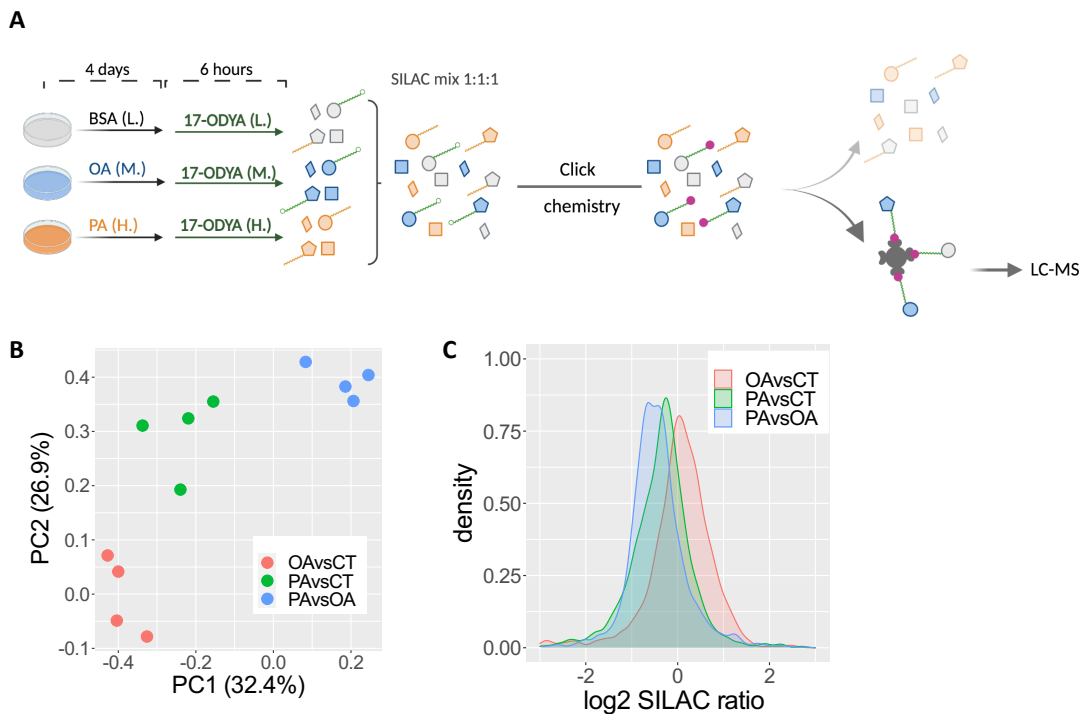


Figure R2.11. Analysis of the palmitoylome of SCC-25 upon PA and OA treatments.

A) Graphical scheme of the protocol followed for the analysis of the changes in the palmitoylome induced by OA and PA treatments. SCC-25 cells were treated for four days with BSA (CT) in light (L.) SILAC media; 50 μM OA, cells in medium (M.) media; or 300 μM PA, in heavy (H.) media. Then, treatments were removed and all the conditions were treated with 100 μM 17-ODYA in their correspondent SILAC media for 6 hours. Protein was collected from four biological replicates ($n = 4$), SILAC mixes 1:1:1 were prepared and click chemistry performed with biotin-azide. Palmitoylated proteins were enriched by pulldown with streptavidin beads and analyzed by LC-MS. Created with BioRender.com **B)** PCA plot of \log_2 SILAC ratios indicating protein abundance differences between conditions in the enriched samples ($n = 4$). **C)** Global density plot of \log_2 SILAC ratios between conditions indicating the relative enrichment of proteins of each treatment. Ratios from all mixes are included in the distributions ($n = 4$). The red curve displays the positive enrichment of proteins from OA treatment with respect to CT; the green one the negative enrichment of proteins from PA with respect to CT and the blue curve shows the negative enrichment of proteins from PA with respect to OA.

μM 17-ODYA for 6 hours (**Figure R2.11A**), a period long enough to label most palmitoylated proteins without altering the phenotype and proteome of the cell too much. For the analysis, we extracted the proteins, mixed them in a 1:1:1 SILAC ratio, and performed click chemistry with biotin-azide and pulldown enrichment of palmitoylated proteins with streptavidin beads. Palmitoylated proteins were analyzed by mass spectrometry (**Figure R2.11A**). With this experimental setup, we expected to saturate the palmitoylation sites of proteins after four-day PA treatment but not after the other treatments. We presumed a negative read-out whereby proteins that were already palmitoylated before the short-term (6-hour) 17-ODYA treatment, had less incorporation of the analog and were less abundant in the MS analysis. Higher enrichment of a particular protein in the control condition than in the PA treatment would probably indicate that that protein was more palmitoylated in the PA condition after four days treatment, thus less 17-ODYA was bound to it. Of course, this method has its limitations (further analyzed in the *Discussion* section), as proteins with very fast palmitoylation turnover may show similar 17-ODYA incorporation in all conditions after the 6-hour treatment, blurring previous differences, while proteins with very slow palmitoylation turnover may not be captured by the relatively short analog treatment.

We quantified 732 proteins with good reproducibility according to the PCA analysis (**Figure R2.11B**). As expected, PA was the condition with the lowest incorporation of 17-ODYA and therefore the lowest abundance in the pulldown samples (i.e., lower SILAC ratio) (**Figure R2.11C**). In contrast, proteins from cells treated with OA had a slight increase in 17-ODYA incorporation as compared to the control group (**Figure R2.11C**). These results indicated that proteins from cells treated with PA for four days are globally more palmitoylated than in the other conditions prior to the 17-ODYA treatment ($p\text{-value} < 0.0001$), whereas OA treatment seemed to reduce protein palmitoylation as compared to control ($p\text{-value} = 0.013$) (**Figure R2.11C**). This agrees with the observed enhancement of the protein palmitoylation machinery (DHHC-PATs) that we observed after a four-day PA treatment.

Most of the proteins quantified in this experiment (569; 78%), were in the set of proteins identified in our previous long-term (four-day) 17-ODYA experiment (**Figure R2.12A**), and were thus considered as high-confidence palmitoylated proteins. Interestingly, the vast majority of these 569 proteins, had a negative enrichment in the PA *versus* OA treatments comparison (i.e., SILAC ratio), indicating higher level of palmitoylation after four-day PA treatment (**Figure R1.12B**). To our surprise, a 1D annotation enrichment

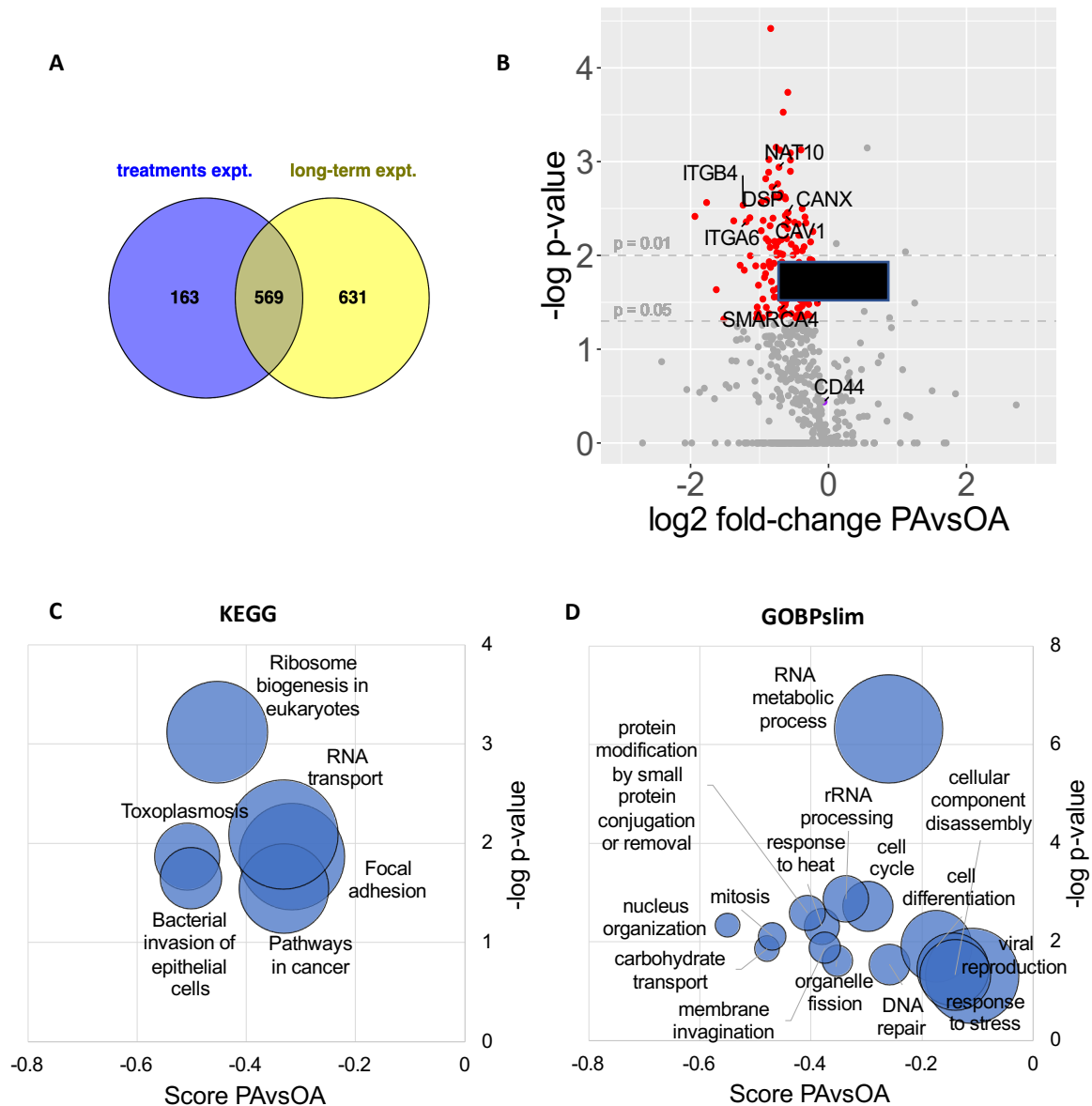


Figure R2.12. Proteins more palmitoylated upon PA treatment.

A) Venn diagram of the proteins identified in the two large-scale palmitoylome studies. In the “treatments expt.” (blue) SCC-25 cells were treated with 50 μM OA, 300 μM PA or BSA (CT) for four days and then they were incubated with 100 μM 17-ODYA for 6 hours. Protein was extracted, click chemistry performed with biotin-azide and palmitoylated proteins were enriched by pulldown with streptavidin beads. 732 proteins were identified by LC-MS. In the “long-term expt.”, (yellow), SCC-25 cells were treated with 50 μM 17-ODYA for four days. Upon click chemistry and enrichment with streptavidin beads 1,200 proteins were identified by LC-MS. **B)** Volcano plot of the 569 palmitoylated proteins identified in both large-scale palmitoylome studies in **A**. The plot shows the enrichment SILAC ratio of these proteins upon 50 μM OA or 300 μM PA treatments in the “treatments expt.”. Fold-change enrichment is expressed in \log_2 scale. In red all the proteins significantly more enriched in upon OA treatment (p -value < 0.05). **C)** and **D)** show the positively enriched categories from 1D annotation enrichment analysis of the 569 palmitoylated proteins identified in both large-scale experiments in **A**. **C)** KEGG (Kyoto encyclopedia of genes and genomes). **D)** GOBPslim (Gene ontology biological process slim). In **C)** and **D)** the size of the circumference determines the number of proteins within that particular category.

analysis on the high confidence palmitoylated proteins showed that they were enriched

in categories related to membranes (membrane invagination, focal adhesion) but also in transcription and translation (mRNA metabolism, RNA transport, ribosome biogenesis), as well as cell cycle and nuclear organization processes (**Figure R2.12C and D**).

The categories related to transcription and translation included proteins involved in mRNA stability (e.g., ELAVL1 [ELAV like RNA binding protein 1]) and translation initiation (e.g., EIF4A3 [eukaryotic translation initiation factor 4A3]), as well as different ribosomal protein components of the 40S subunit, such as RSP14 (ribosomal protein S 14A) and the 60S subunit, such as RPL10A (ribosomal protein L10A). Palmitoylation of RPL10A was already validated and is involved in the lipid raft localization of the protein (Yang et al., 2010). Considering that the main function of these proteins is performed in the cytoplasm, and that the PA moiety probably binds them to the cell membranes, protein palmitoylation could be involved in inhibition of protein synthesis. This result could further support the decrease in protein translation observed in the proteome of OSCC cells upon PA treatment and might be involved in the cell cycle arrest.

Interestingly, [REDACTED] appeared as one of the high confidence palmitoylated proteins that was significantly (p-value < 0.05) more palmitoylated upon PA treatment (**Figure R2.12B**). [REDACTED]

[REDACTED] palmitoylation increased in the pro-metastatic phenotype of OSCC cells, we hypothesized that it could be implicated in [REDACTED] necessary for metastatic induction and further characterize [REDACTED] palmitoylation.

3 Characterization of [REDACTED] palmitoylation

3.1 Validation of the palmitoylation of [REDACTED]

Given the profound implications that [REDACTED] palmitoylation could have on the biology of cancer cells, we decided to further characterize this modification. First, we used an orthogonal method to validate that [REDACTED] was palmitoylated. For this, we treated SCC-25 cells overnight with 50 μ M 17-ODYA or PA, extracted the nuclear protein fraction and immunoprecipitated [REDACTED] in both conditions. We then performed click chemistry on the immunoprecipitated protein to add a biotin-tag to those [REDACTED] molecules that had incorporated 17-ODYA during the overnight treatment. Next, we split the sample in two and treated one half with NH_2OH (which would remove the

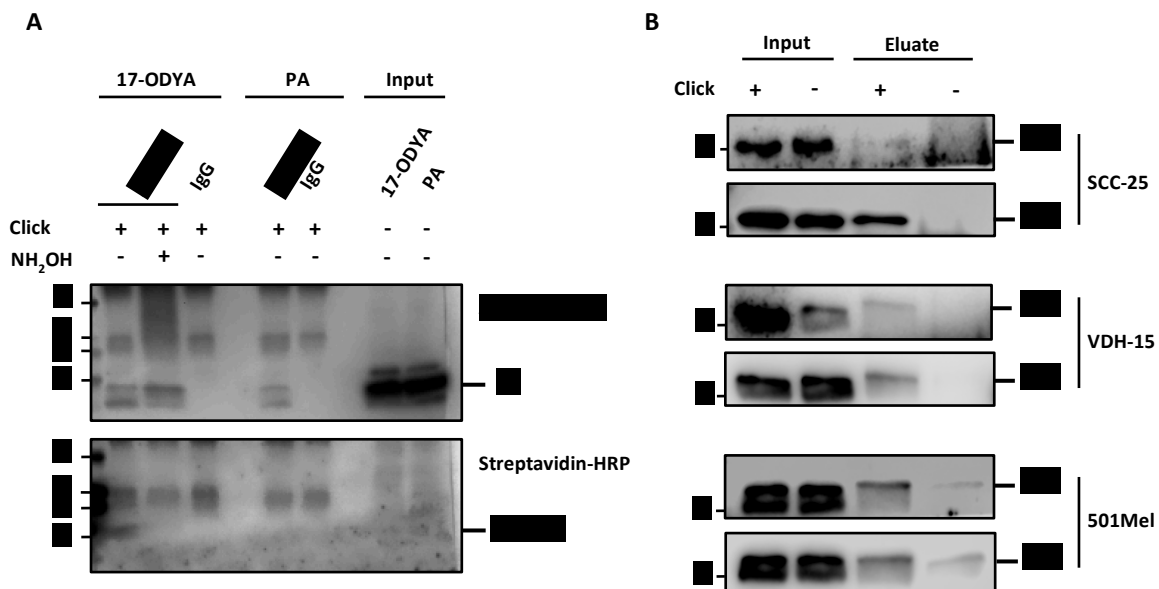


Figure R3.1. Validation of [REDACTED] palmitoylation.

A) Immunoblot images of the IP of [REDACTED]. SCC-25 cells were treated overnight with 50 μ M 17-ODYA or 50 μ M PA. Protein was collected, inputs separated (5 μ g) and each sample was split in two for immunoprecipitation with anti-[REDACTED] (anti-[REDACTED]) antibody or unspecific IgG mock antibody. Click chemistry with biotin-azide was performed on the immunoprecipitated proteins. After click part of the 17-ODYA anti-[REDACTED] sample was treated with NH_2OH for the specific removal of S-palmitoylation signal. **B)** Immunoblot images of the validation of [REDACTED] and [REDACTED] palmitoylation with specific antibodies. SCC-25 and 501Me1 cells were treated for four days and VDH15 cells were treated overnight all of them with 50 μ M 17-ODYA. Samples were processed following the protocol described in figure R2.10A. Numbers on the left mark the closest molecular weight size marker.

palmitic analog moiety if [REDACTED] was S-palmitoylated by selectively cleaving the thioester bond). Finally, we blotted the immunoprecipitated samples against biotin using streptavidin-HRP to find palmitoylated proteins. Of note, a biotin band of the same mass of [REDACTED] only appeared in the lane of the 17-ODYA treated sample, indicating that

██████████ was indeed palmitoylated (**Figure R3.1A**). Furthermore, incubation with NH_2OH completely abolished the biotin signal, thereby confirming that ██████████ was S-palmitoylated (**Figure R3.1A**).

We next addressed whether this palmitoylation event is common for all or only some of the different ██████████. This is particularly important given that each ██████████ has a particular regulation and localization in specific ██████████, which leads to different functions. Looking at the proteomics data, we were not able to distinguish between ██████████, since their amino acid sequence is highly conserved and the peptides identified in the MS were common for all ██████████. Therefore, we used specific antibodies to discriminate between the palmitoylation of the different ██████████ following the protocol described in **Figure R2.10A**. We intended to focus our attention on the most broadly expressed ██████████: the ██████████ however, there is no commercial antibody specific for ██████████ detection, so we could only test ██████████ palmitoylation.

We found that ██████████ was palmitoylated in SCC-25 but ██████████ was not, or at least had a much lower palmitoylation stoichiometry (**Figure R3.1B**). We repeated the experiment with two other cell lines: VDH-15 (a non-commercial OSCC cell line established in our laboratory) and 501Mel (a melanoma cell line). The VDH-15 cell line had a higher sensitivity to 17-ODYA and could not be treated for four days, so we performed an overnight treatment with 50 μM 17-ODYA. We corroborated that ██████████ was palmitoylated and that ██████████ palmitoylation showed a much lower stoichiometry (**Figure R3.1B**). We were able to confirm ██████████ palmitoylation in other tumour types using 501Mel cells, which were treated for four days with 50 μM 17-ODYA. Unexpectedly, both ██████████ variants were enriched to a similar extent in these cells (**Figure R3.1B**).

Overall, we showed with an orthogonal method that ██████████ was S-palmitoylated and that the ██████████ was palmitoylated in all cell lines tested, while palmitoylation of the ██████████ might be tumour-type dependent.

3.2 Identification of the S-palmitoylated Cys residue

Next, we addressed which residue of the ██████████ palmitoylated; as ██████████ was S-palmitoylated, the palmitoylated residue had to be a Cys. Since ██████████ ██████████ we overexpressed a mutant version of the protein lacking that Cys residue to test the ability of the cell to palmitoylate the mutant protein.

Before generating the [REDACTED] overexpression (OE) construct, we checked in previous RNA sequencing data from the laboratory (published in Pascual et al., 2017) which of the [REDACTED] genes in humans was most highly expressed in SCC-25 cells, since depending on the tissue or cell line, [REDACTED] genes can be equally transcribed or one can present higher expression ([REDACTED]). [REDACTED] genes encode the same amino acid sequence but vary in their nucleotide sequence and regulatory regions (Bramlage et al [REDACTED] [REDACTED] gene is preferentially expressed over [REDACTED] in SCC-25; thus, we used [REDACTED] nucleotide sequence for the generation of the overexpression construct (Figure R3.2A). We synthesized two different constructs: i) the WT version of the gene ([REDACTED]) and ii) a mutant version in which we replaced [REDACTED] with an [REDACTED]) (Figure R3.2B). In both constructs, two different tags (FLAG and HA) were added at the C-terminal side of the protein (Figure R3.2B), following a previously reported strategy in which they demonstrated that a C-terminal HA-tagged [REDACTED] is functional ([REDACTED]).

The [REDACTED] constructs were synthesized in the retroviral pMSCV plasmid under a strong ubiquitous promoter and stable SCC-25 cells lines expressing these constructs were generated through retroviral infection. However, the constructs were not strongly expressed by the cells. By RT-qPCR, we could see that the gene [REDACTED] was similarly expressed in non-infected (WT) SCC-25 and [REDACTED] or [REDACTED] bearing cell lines (Figure R3.2C); by Western blot we observed that the exogenously expressed [REDACTED] was barely detected compared to the endogenous [REDACTED] (Figure R3.2D). The addition of FLAG and HA tags increased the molecular weight of the overexpressed [REDACTED] proteins ([REDACTED]), what allowed us to distinguish them from the endogenous protein ([REDACTED]) (Figure R3.2D). Although the amount of exogenous [REDACTED] was negligible compared to total endogenous [REDACTED] protein, we observed that the exogenous [REDACTED] was expressed at similar levels to endogenous [REDACTED] (Figure R3.2E). This result is in line with previous studies that showed that, [REDACTED]

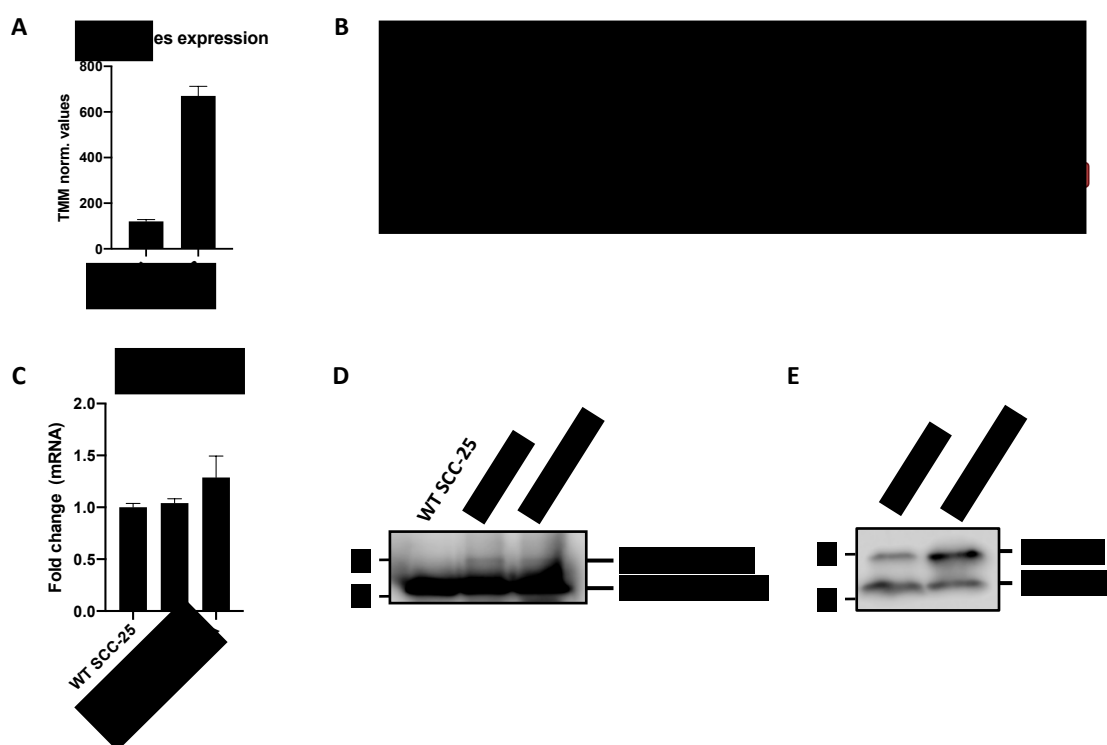


Figure R3.2. Expression of exogenous

A) Bar plot showing the mRNA expression levels of the [redacted] in SCC-25. TMM normalized values extracted from an RNA sequencing experiment published in Pascual et al., 2017. Data given as the mean and SD. **B)** Illustration of the construct used for the overexpression (OE) of [redacted] gene. The sequence of the gene was maintained in the wild type (WT) version of the construct and [redacted] was mutated to an [redacted] in the mutant version. In both cases FLAG and HA tags were added at the C-terminal of the protein. Created with BioRender.com **C)** Relative [redacted] expression in non-infected SCC-25 cells (WT SCC-25) or SCC-25 cells bearing the OE WT construct ([redacted]) or the OE mutant construct ([redacted]), by RT-qPCR. Data given as the mean and the SD. **D)** [redacted] immunoblot image of WT SCC-25 cells, [redacted] and [redacted] cells. The over expressed exogenous (exo.) [redacted] was heavier than the endogenous (endo.) [redacted] **E)** [redacted] immunoblot of [redacted] and [redacted] bearing cells. Numbers on the left in **D** and **E** mark the closest molecular weight size marker.

To determine whether [redacted] was the palmitoylated residue, we treated [redacted] and [redacted] cell lines with 50 μ M 17-ODYA for four days. Then, we performed the click chemistry with biotin-azide, enriched via streptavidin beads and tested the enrichment of each [redacted] protein by Western blot against HA tag (**Figure R3.3A**). We observed a much higher enrichment of the [redacted] protein than of the [redacted] in the streptavidin beads eluant fraction, indicating that the PA analog 17-ODYA was preferentially bound at [redacted] in [redacted], thus proving that [redacted] was S-palmitoylated (**Figure R3.3A**). However, we still detected a faint band in the [redacted] eluant lane, indicating that the analog was being specifically incorporated into the mutant [redacted] protein but in a different position and at a much lower stoichiometry. To elucidate whether the enrichment of mutant [redacted] was due to a secondary acylation on the protein

result of the metabolism of 17-ODYA during the long-term incubation, we tested a shorter treatment. We incubated the cells overnight (around 16 hours) with 17-ODYA and performed the same experiment. After this short treatment, we had again a higher enrichment of [REDACTED] in the streptavidin beads eluant fraction, but we could still detect a faint band corresponding to the [REDACTED] protein (**Figure R3.3B**). We concluded that [REDACTED] was S-palmitoylated at [REDACTED], given that mutation of that residue decreased the enrichment of the protein upon click chemistry. Nevertheless, 17-ODYA could also be used for other acylations on [REDACTED] independent of [REDACTED] that have a fast turnover of less than 16 hours, similar to [REDACTED] palmitoylation.

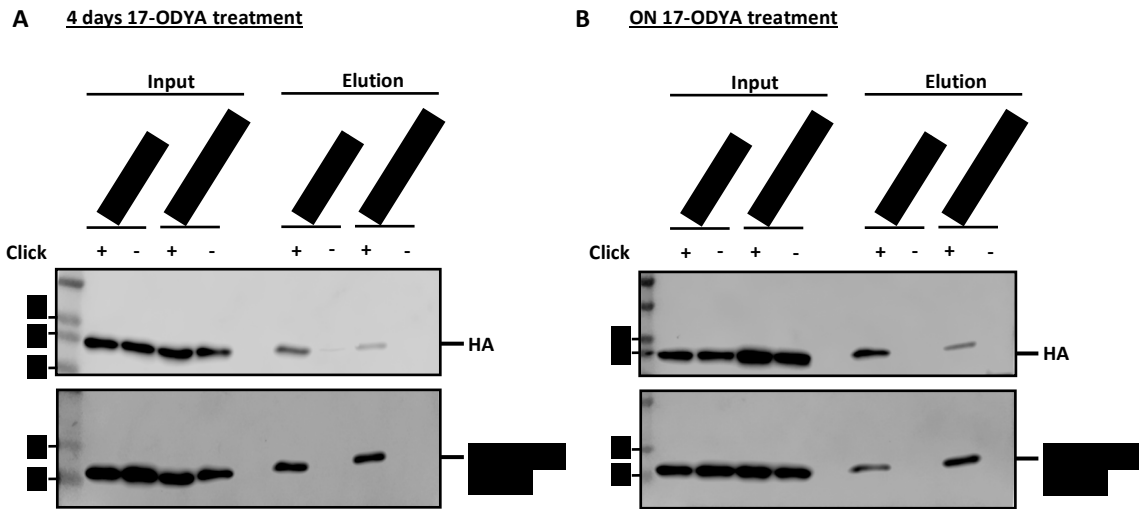


Figure R3.3. [REDACTED] is the palmitoylated residue in [REDACTED]. SCC-25 [REDACTED] and [REDACTED] cells were incubated with 50 μ M 17-ODYA for four days **A**) or overnight (16 hours) **B**). Then, samples were processed as described in figure R2.10A and palmitoylated proteins were enriched. Upper immunoblot images in **A**) and **B**) compare the differential enrichment upon click chemistry of overexpressed [REDACTED] and [REDACTED] with an anti-HA tag antibody. Lower images in **A**) and **B**) show the endogenous (endo.) [REDACTED] pool as a loading control of the amount of protein pulldown with the streptavidin beads. The exogenous [REDACTED] is undetectable at that exposition time due to its low expression compared to the global amount of [REDACTED]. Numbers on the left in all immunoblots mark the closest molecular weight size marker.

3.3 Function of [REDACTED] palmitoylation at [REDACTED]

3.3.1 [REDACTED] is not implicated in its [REDACTED]

The [REDACTED] residue (that we identified as the main palmitoylation site) is located within the [REDACTED], at the globular part of the protein ([REDACTED] (**Figure R3.2B**). PTMs in the [REDACTED], and can be involved in the [REDACTED] recognition for [REDACTED]

([REDACTED]). To test the relevance of [REDACTED] [REDACTED], we overexpressed [REDACTED], performed a cellular fractionation and analyzed the localization of overexpressed [REDACTED] in the different cellular fractions (cytoplasm, nuclear soluble, chromatin soluble and chromatin insoluble) by immunoblotting using the HA tag. Interestingly, we observed that, regardless of the mutational status of the protein, the exogenous [REDACTED] was almost exclusively enriched in the [REDACTED] fractions (which contain

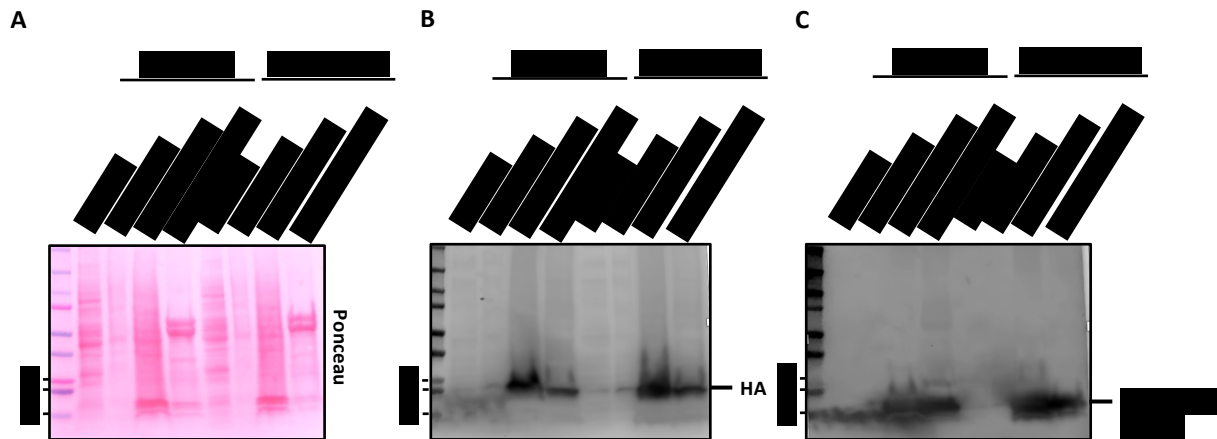


Figure R3.4. [REDACTED] does not interfere with and it is not necessary for [REDACTED]

A cellular fractionation was performed upon lysis of SCC-25 [REDACTED] and [REDACTED] cell lines. The content of the different fractions was ran in an SDS-PAGE followed by Western blot for further analysis. The four fractions are: cytosolic; nuclear soluble (sol.), proteins within the nuclear envelope but not bound to the chromatin; chromatin soluble (sol.), proteins loosely bound to chromatin; and chromatin insoluble (insol.), proteins tightly bound to the chromatin. **A)** Scan of the ponceau staining of the Western blot membrane as a loading control. **B)** Immunoblot of the detection of exogenous [REDACTED] through HA tag. **C)** Immunoblot of [REDACTED]-[REDACTED]. The detected band is the endogenous (endo.) [REDACTED]. Exogenous [REDACTED] can be barely detected with that exposition time. Numbers on the left mark the closest molecular weight size marker of interest in each image.

proteins [REDACTED], respectively) (**Figure R3.4B**). A very small percentage of [REDACTED] were detected in the [REDACTED] fraction (which contains [REDACTED]) (**Figure R3.4B**). Endogenous [REDACTED] was also enriched in [REDACTED] fractions (**Figure R3.4C**). Thus, despite the lack of genomic regulatory elements and the presence of HA and FLAG tags, exogenous [REDACTED] was physiologically used by the cell and [REDACTED], which validated the use of this tool for studying the biology of the [REDACTED]. Importantly, both [REDACTED] were equally [REDACTED]; thus, [REDACTED] and any possible PTMs affecting this residue, such as palmitoylation, should not affect [REDACTED].

3.3.2 [REDACTED] in not implicated in the [REDACTED] localization of [REDACTED]

Next, we wondered whether the palmitoylation of [REDACTED] could be involved in the [REDACTED] tethering of [REDACTED], since protein palmitoylation is usually implicated in the association of proteins to membranes. Even though the [REDACTED]
[REDACTED]
[REDACTED] We speculated that [REDACTED] palmitoylation could have a role in the formation of that interaction. To test this hypothesis, we assessed the location of [REDACTED] by immunofluorescence staining.

In basal conditions, both [REDACTED] were localized [REDACTED]
[REDACTED] (Figure R3.5). To assess whether we were missing any difference due to low palmitoylation stoichiometry, we challenged the cells by a four-day treatment of 50 μ M OA or 300 μ M PA, to produce a low or high protein palmitoylation state, respectively. Notably, we did not observe any alteration in the cellular localization in either condition for the WT or the [REDACTED] mutant [REDACTED] (Figure R3.5). These results indicated that the palmitoylation of [REDACTED] is not involved in the [REDACTED] localization of [REDACTED]

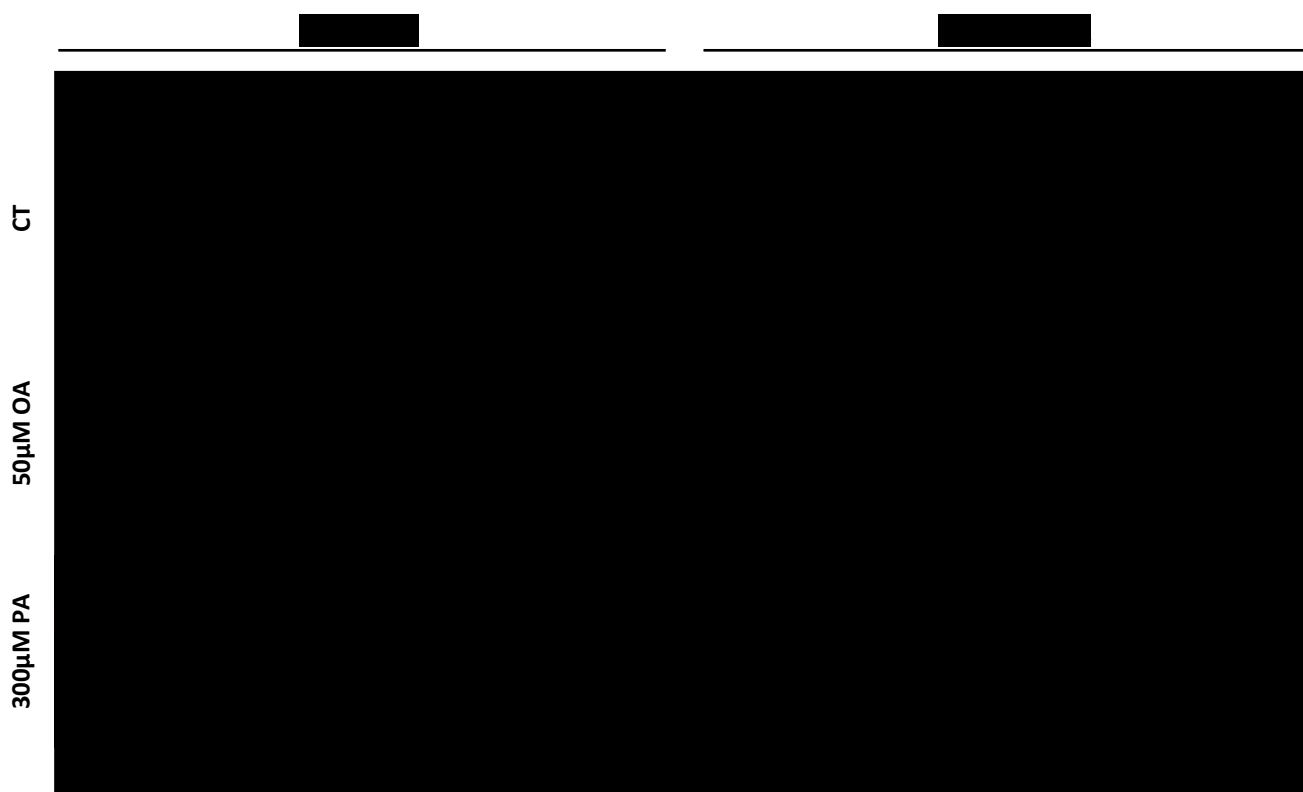


Figure R3.5. [REDACTED] is not implicated in [REDACTED] and [REDACTED] localization.

Representative immunofluorescence images of [REDACTED] and [REDACTED] bearing SCC-25 cells treated with 50 μ M OA or 300 μ M PA for four days. FLAG tag is shown in red for exogenous [REDACTED] detection. DAPI is shown in blue for DNA detection. Merged images are composed by FLAG (red) and DAPI (blue) staining. A unique confocal stack is shown in each image for proper detection of [REDACTED] localization [REDACTED]. White scale bar on merged images represents 10 μ m.

DISCUSSION

1 Changes in the proteome induced by dietary PA and OA in OSCC

1.1 Dietary PA vs OA in healthy and cancer cells

PA and OA are the most abundant dietary and plasmatic FAs (Palomer et al., 2018); both serve as energy reservoirs as well as being fundamental structural components of cell membranes and participate in signaling processes. However, the molecular differences between saturated PA and monounsaturated OA (**Figure 11.4**) confer them specific biological functions that in some occasions can even be opposite (Palomer et al., 2018). In fact, the proteomic characterization of PA and OA treatments on the OSCC cell lines showed a strikingly opposite effect, which correlated well with the metastatic capacity shown by PA, but not OA, in previous studies performed in our laboratory (Pascual et al., 2021). Indeed, the opposite effects of PA and OA have also been deeply documented for type 2 diabetes mellitus (T2DM). In this context, a diet rich in SFAs (such as PA) potentiates insulin resistance, while increasing the MUFA intake improves insulin sensitivity (Vessby et al., 2001). Some of the cellular responses observed in our study are comparable to those previously analyzed in healthy cells, although there are clear molecular differences as well, as discussed below.

In this study, we observed an upregulation of FAO, the TCA cycle and OXPHOS of cells in culture upon PA treatment. Interestingly, the treatment with PA induced glycolysis and carbohydrate metabolism as well. A recent publication suggests that the lipotoxicity induced by PA and the excess of ROS generated in the mitochondria could signal and induce glycolysis activation (Kakimoto et al., 2021). The intracellular accumulation of an excess of PA can exceed the mitochondrial oxidation and induce conversion of the FA into deleterious complex lipids, such as diacylglycerols (DAGs) or ceramides (Palomer et al., 2018). Ceramides can affect mitochondrial function, which combined with the oversupply of FAs into the mitochondria can lead to incomplete FAO and increased ROS generation (Chaurasia and Summers, 2015). Indeed, PA treatment probably induced a redox imbalance in OSCC cells, as seen by the upregulation of the response to oxidative stress category, composed by different ROS detoxifying enzymes, such as SOD2 (superoxide dismutase 2) and PRDX2 (peroxiredoxin 2).

The proteomic response induced by OA was less predictable. In sharp contrast to PA, OA treatment decreased FAO, TCA cycle and OXPHOS as compared to controls in our experiment. This result is in apparent contrast to previous studies performed with healthy cells or even some cancer cells, which showed that OA promotes FAO even to a higher extent than PA (Henique et al., 2010; Palomer et al., 2018). Regarding redox homeostasis, the response to oxidative stress in our study is downregulated upon OA

treatment as compared to control, which is consistent with the lower expression of mitochondrial OXPHOS enzymes and could also be related to the promotion of LD formation and detoxification of basal ROS (Corbet et al., 2020). Unlike PA, the excess of intracellular OA in healthy cells is usually incorporated into TAG and accumulated in LDs (Listenberger et al., 2003), avoiding the conversion into complex lipids that could affect the mitochondrial function. This difference in the direction that the excess of each FA takes is based on the downregulation by PA of DGAT2, an enzyme responsible of the synthesis of TAG from DAG, and the upregulation of DEGS1 (dihydroceramide desaturase 1), which is involved in the synthesis of ceramides (Henique et al., 2010). In fact, in our experiment, DEGS1 was upregulated by PA treatment and downregulated by OA.

Other biological processes enhanced by PA treatment were related to immunity, such as specific subunits of the immunoproteasome, including PSME1, PSME2 (proteasome activator subunit 1 and 2), PSMB8 (proteasome subunit beta type 8), and several proteins involved in the MHCI (class I major histocompatibility complex), including HLA-A and HLA-C (class I histocompatibility antigen, A and C alpha chain) and B2M (beta-2-microglobulin). T2DM studies have shown that the accumulation DAGs and ceramides upon PA treatment attenuate insulin signaling and stimulate the inflammasome (Chaurasia and Summers, 2015; Wen et al., 2011). Nevertheless, did not see an upregulation in IL-1 β (interleukin 1 beta) or inflammasome-related proteins such as PYCARD (PYD And CARD Domain Containing), or any proteins of the NLRP (NOD-like receptor protein) family, although we did observe IFI16 (interferon gamma induced protein 16) induction (Latz et al., 2013). In fact, what PA stimulation induced in OSCC cell lines was a type I IFN (interferon) signaling and the antiviral response, as evidenced by the upregulation of: i) several members of the oligoadenylate synthetase family (OAS1, OAS2, OAS3); ii) interferon gamma-induced proteins (IFI16, IFI30, IFI35) or interferon-induced protein with tetratricopeptide repeats (IFIT1, IFIT2, IFIT3) families, whose production is stimulated by interferon; and iii) MHCI. Several studies suggest that PA could act as a TLR2/4 (toll-like receptor 2/4) ligand activating different proinflammatory pathways (Nicholas et al., 2017; Tse et al., 2015), although the antiviral response induced by PA might not be effective (Tse et al., 2015).

In contrast to PA, we observed that OA stimulation downregulated the IFN mediated immune response. This result is in line with a recent study that showed that MUFAs are involved in the negative control of type I IFN response via STING (stimulator of interferon genes) inactivation in Th1 cells (Kanno et al., 2021). Indeed, T2DM studies have shown that SFA-enriched HFDs induce systemic inflammation and insulin resistance through inflammasome activation in adipose tissue and IL-1 β secretion (Finucane et al., 2015; Wen et al., 2011), while a MUFA-enriched HFD decreases inflammasome activation and IL-1 β secretion even in obese mice (Finucane et al., 2015; Wen et al., 2011).

The final set of GO categories upregulated by PA treatment in our study were related to cell motility and cell adhesion, which could be associated to the induction of the metastatic phenotype previously observed (Pascual et al., 2021). PA treatment upregulated numerous proteins, including: i) different members of the galectin family (LGAL1, LGAL3, LGAL7); ii) actin-related protein 2/3 complex (ARPC1A/B, ARPC2, ARPC4) family of proteins; iii) integrins (ITGB1, ITGB4, ITGB6); iv) members of the desmosome, such as DSP, PKP1, PKP3 (plakophilin-1 and 3) and DSC3 (desmocollin-3); and v) MMP14 (matrix metalloproteinase 14). PA uptake has also been described to increase the motility and metastatic capacity of ovarian cancer cells (Yu et al., 2020), PDAC cells (Binker-Cosen et al. 2017) and gastric cancer cells (Pan et al., 2019). On the other hand, OA treatment downregulated all these categories and proteins that were upregulated by PA (mentioned above); likewise, OA treatment downregulated the metastatic capacity of OSCC cells (Pascual et al., 2021). However, the influence of OA on tumour aggressiveness remains controversial. Several studies show that OA acts as an anti-cancer agent, preventing tumour progression by being more toxic to tumour cells than to healthy cells. In an HCC model, OA treatment can reduce autophagy and induce tumour cell death without affecting the viability of healthy hepatocytes (Giulitti et al., 2021). Indeed, OA-embedded nanoliposomes show specific toxicity to breast and lung cancer cells, but not to healthy cells; thus, they could be used as anticancer therapy (Jung et al., 2016). Moreover, in BC, OA suppresses Her-2/*neu* (*erbB-2*) expression and synergizes with already existing therapies such as trastuzumab to enhance tumour growth inhibition (Menendez et al., 2005). Nevertheless, other studies suggest that OA boosts the metastatic capacity of tumour cells by increasing MMPs secretion and cell invasion (Shen et al., 2020; Soto-Guzman et al., 2010), or by protecting them from ferroptosis upon extravasation into blood circulation (Ubellacker et al., 2020).

Regarding the biological processes downregulated by PA, we observed a clear reduction in protein translation. Many different cytoplasmic and mitochondrial ribosomal proteins, as well as proteins involved in translation initiation or the tRNA biology appeared to be downregulated. This decrease in the protein synthesis could be a consequence of a possible ER stress induced by the lipid dysregulation, as some studies on the effect of PA treatment on healthy cells suggest (Peng et al., 2011). However, after PA treatment, we did not detect the canonical markers of ER stress or the unfolded protein response (e.g., PERK [protein kinase R-like endoplasmic reticulum kinase]; ATF6 [activating transcription factor 6] or ERN1 [Endoplasmic Reticulum to Nucleus Signaling 1]); or their downstream effectors (e.g., HSPA5 [Heat Shock Protein Family A Member 5] or ERP72 [endoplasmic reticulum resident protein 72]) (Kennedy et al., 2015). Although we detected a slight upregulation of other proteins related to ER stress, such as ERP29 and ERP44, we believe that the reduction in protein synthesis could be associated to other pathways, such as a decreased cell proliferation or biological

processes still to be defined. Indeed, cell cycle was the other main category downregulated by PA. A previous investigation of our laboratory already showed that PA treatment results in a slow-down of the cell cycle and a G1-phase arrest (Pascual et al., 2021). Nevertheless, upon PA withdrawal, tumour cells resumed their proliferation and no differences in PT growth were observed upon injection in mice (Pascual et al., 2021). Initial studies identified the MICs as slow-cycling CD44^{bright} CD36⁺ cells with an enhanced lipid metabolism (Pascual et al., 2017). Thus, PA treatment can induce a MIC-like phenotype by enhancing CD36 and FAO, slowing down the cell cycle and boosting the metastatic capacity of the cells. Conversely, cell cycle and protein synthesis were the main biological categories upregulated by OA treatment. Other studies have also seen an increase in the tumour cell proliferation upon OA treatment in BC (Hardy et al., 2000), HCC (Seo et al., 2020), prostate cancer (Liotti et al., 2018) and cervical cancer (Yang et al., 2018). Although this induction in proliferation has also been observed upon PA stimulation in CRC (Fatima et al., 2019) and ovarian cancer (Yu et al., 2020).

1.2 Cell culture vs animal studies

The opposite responses induced by PA or OA treatment in cell culture was not observed in mice fed with PA- or OA-enriched diets. As detailed in *Materials and Methods*, the fat of these HFDs comes from olive oil or palm oil, and both oils comprise a mix of FAs. Palm oil contains 44% of PA but also 40% of OA (Mancini et al., 2015). The composition of olive oil is more variable and depends on the culture conditions and the process of oil extraction. The range of OA within olive oil is 55%-83%, and the amount of PA 7.5%-20% (Boskou et al., 2006). Given that both diets contain both PA and OA, we did not expect a difference as striking as the one observed for cell treatment with the pure PA or OA.

The results we obtained after PA- and OA-enriched dietary feeding of mice suggested that PA exerted a stronger influence on tumour cells than OA. In other words, even under conditions with a high OA/PA ratio (OA-enriched diet), the proteomic response was more similar to the one induced by PA in cell culture, rather to the one induced by OA. This suggests that the amount of PA provided in the OA-enriched diet is enough to trigger a metabolic response that cannot be neutralized by OA. Indeed, based on previous studies, we knew that the beneficial effect of OA treatment in cell culture does not counteract the enhanced metastatic potential of OSCC cells previously treated with PA (Pascual et al., 2021). Nevertheless, while the response induced by OA-enriched diet in tumour cells growing in mice was in the same direction as the response to PA-enriched diet, it was not enough to induce the metastatic capacity of the tumour cells (Pascual et al., 2021), suggesting that there is a threshold in the PA/OA ratio availability for triggering the metastatic response.

The only two GO categories that had an opposite direction in the response to PA and OA were TCA cycle and sulfur metabolism: both were upregulated by the PA-enriched diet and downregulated by the OA diet. Little is known about the interaction of a HFD with the sulfur metabolism, but the downregulation of the TCA cycle in the tumour cells growing in mice fed an OA-enriched diet agreed with the response observed in cell culture upon OA stimulation. The results obtained in this study upon OA treatment or OA-enriched HFD feeding were unanticipated. They suggest that the biological reaction to OA in OSCC cells is not comparable to the one induced in healthy cells, based on T2DM studies. This difference, also observed by others (Giulitti et al., 2021; Jung et al., 2016), opens the door to the use of OA as an anti-tumour therapy, at least in certain tumour types.

The dietary intervention in mice and posterior proteome analysis has several limitations that need to be addressed in the future. For instance, it was performed with a low number of biological replicates ($n = 2$) due to the high basal protein requirements for the analysis; thus, this experiment should be repeated to fully confirm the alterations induced by both diets. Additionally, although we can deduce the concentration of both FAs in the diet, we did not directly measure the changes in the plasma concentration of PA and OA induced by each diet. Thus, we do not know how the animals metabolized these diets, nor the amount of each FA that arrived to the cancer cells through circulation.

1.3 Dietary interventions in cancer

To date, different nutritional interventions are being explored to improve treatment efficacy or reduce morbidity of cancer patients (Lévesque et al., 2019). Many of these interventions are related to fasting or calorie intake reduction, with the hope that this depletes the amount of carbohydrates and fats available for the tumour, and limits tumour growth while enhancing therapy efficacy (Groot et al., 2020). This caloric restriction or the intake of caloric restriction mimetics can also induce autophagy in the tumour cells, boosting their immunogenicity and can even protect non-tumoural cells from therapy side effects (Klement and Champ, 2014; Pietrocola et al., 2016).

Other clinical trials explore the benefits of lowering the intake of a particular nutrient category, such as fat. There are various ongoing clinical trials testing the effects of a low-fat diet in cancer progression with or without further treatment (published at ClinicalTrials.gov). Some finished studies show that the reduction of the percentage of calories coming from fat can be beneficial for cancer patients. A low-fat diet can decrease tumour cell proliferation in prostate cancer (Aronson et al., 2010) or improve the relapse-free survival and even the overall survival in BC (Chlebowski et al., 2006; Chlebowski et al., 2018). However, this dietary intervention might have no impact on BC

incidence, supporting the idea of the implication of the lipid metabolism especially in later stages of tumour progression ([Martin et al., 2011](#)).

Nevertheless, based on other's and our results, it might be worth considering controlling the SFA/MUFA ratio in cancer patients diet rather than lowering the total amount of fat consumption. Dietary OA could have a beneficial, anti-tumour, effect itself and on top of that, counteract the detrimental, pro-tumor, effects of PA. More studies are required to fully characterize and understand the influence of each dietary FA on tumour cells and cancer progression.

2 Palmitoylome studies

Traditional methods of studying protein palmitoylation rely on the metabolic incorporation of radiolabelled FAs into proteins, followed by immunoprecipitation (IP) and detection of the target palmitoylated protein. Those methods lacked sensitivity and did not allow large-scale analysis of the palmitoylome. The apparition of non-radioactive click-chemistry-based chemical probes for the detection of palmitoylated proteins boosted the field of protein acylation and the identification of new palmitoylated proteins. Different chain-length alkynyl-FAs have been designed (C10, C11, C13, C14, C16, C18) to study protein acylation. Alk-C13 (12-tridecynoic acid) and Alk-C14 (13-tetradecynoic acid) label sites of protein myristoylation, while Alk-C16 (15-hexadecynoic acid) and Alk-C18 (17-octadecynoic acid, 17-ODYA) label palmitoylated proteins (Hannoush and Arenas-Ramirez, 2009). Alk-C16 (also known as Alk-14) and 17-ODYA can generate slightly different results () but both are alternatively used. Of the two, 17-ODYA is the main FA analog utilized for the study of protein palmitoylation (Cao et al., 2019; Lin and Conibear, 2015; Martin and Cravatt, 2009; Martin et al., 2012; Segal-Salto et al., 2016). In our experiments, we have validated 17-ODYA as an alkynyl-FA capable of modifying the same proteins acylated by PA in OSCC cells, in a dose and time dependent manner and through the same cellular enzymatic machinery.

Importantly, we have generated the first list of palmitoylated proteins in OSCC cells, which is quite reliable as evidenced by the enrichment in membrane-related categories and lipid modification terms (lipidation, palmitate) as well as by the presence of canonical palmitoylated proteins (caveolin, calnexin, cofilin, flotillin, CD molecules). We validated some of the palmitoylated proteins in this list (e.g., CAV1, CD9, LPCAT1) but not others (e.g., NAT10, BRG1), which could be consequence of false discovery events from the mass-spectrometry analysis. Different studies using alkynyl- FAs to enrich palmitoylated proteins use diverse criteria to determine which proteins are considered to be palmitoylated and which ones are considered as unspecific enrichment from streptavidin beads. For example, the pioneering work of Martin and Cravatt in 2009 identified a total of 125 high-confidence predicted proteins with a fc enrichment of ≥ 5 for 17-ODYA treated *versus* control, and 200 medium-confidence palmitoylated proteins with a fc enrichment of ≥ 2 (Martin and Cravatt, 2009). Nevertheless, in 2012, the same group used a less stringent analysis and accepted an enrichment of 50% (fc ≥ 1.5), identifying 400 proteins (Martin et al., 2012). In our study we used a rather permissive criteria (enrichment fc ≥ 1.5 and p-value < 0.05), to detect a wider spectrum of palmitoylated proteins (327 proteins), from those with a high stoichiometry of palmitoylation to those with a low one. This criterion of analysis probably led to more false positive results (NAT10, BRG1) but also allowed us to detect proteins with a lower enrichment score like histone H3, compared with well-known palmitoylated proteins

such as CAV1 with higher palmitoylation stoichiometry. In any case, the targets of our interest were always validated by Western blot to discard false positives.

The main drawback of the use of alkynyl-FA for the study of the basal palmitoylome of a particular cell line is precisely that the cells must be incubated with a modified FA, which could alter their metabolism and phenotype, as we have observed. Most palmitoylome studies utilizing alkynyl-FA probes treat the cells with the analog for periods of time ranging from 2 to 15 hours (overnight) (Zhang et al., 2010; Martin and Cravatt, 2009). These short treatments aim to label as many proteins as possible while minimizing the response that the incubation with an alkynyl-FA could induce on the cell. According to pulse-chase experiments using FA analogs, the half-life of protein palmitoylation is in the order of minutes to hours (Zhang et al., 2010). However, these pulse-chase experiments are also performed with short treatments (2 to 15 hours), thus stably palmitoylated proteins can never be labelled with these protocols (Yang et al., 2020). If the palmitate half-life on a particular protein is of five hours yet the cells are only treated for two hours with the alkynyl-FA, only a very low amount of the protein would be labelled limiting its enrichment signal respect to control; thus, it would probably be discarded during analysis. Despite the existence of fast turnover palmitoylation events, a large-scale experiment on palmitoylation turnover showed that palmitoylation is a rather stable PTM in many proteins (Martin et al., 2012). Therefore, we decided to use a long-term labelling (4 days) to include very stable palmitoylated proteins and to capture the palmitoylome in a pro-metastatic cellular state

In our experiments, we observed that 17-ODYA binds to proteins in a time-dependent manner. The longer the treatment, the higher the intensity we detected by in-gel fluorescent scanning (Figures R2.2B and R2.7). Furthermore, after four days of treatment, we detected bands that could not be detected with shorter treatments, although the intensity of others decreases (Figure R2.7). To our knowledge, this is the first time in which a large-scale palmitoylome study has been performed with such long treatment. Of note, as different biochemical processes could affect the result, it should be interpreted with caution. For instance, the four-day 17-ODYA treatment altered the phenotype of the cell and induced several proteome alterations. Therefore, we are unable to know whether those new bands observed are stably palmitoylated proteins that can only be labelled upon very long treatments or proteins upregulated and palmitoylated upon FA exposure. Similarly, the proteins of the bands that are lost upon long treatment can be downregulated or no longer palmitoylated. Another difficulty for the interpretation of long-term alkynyl-FA treatment results is that we do not know how the FA analog has been metabolized by the cell. 17-ODYA can enter in any FA metabolic pathway of the cell (Thiele et al., 2012). It could be completely consumed by the cell in the β -oxidation (Thiele et al., 2012) or shortened to 13-tridecynoic acid or 15-pentadecynoic acid, which can then be incorporated to N-myristoylation sites (Won et

al., 2018). Also, longer incubation times lead to incorporation of the alkynyl-FA into phospholipids or LDs, which is a considerable drawback for pulse-chase experiments but might not be that relevant for our experiments (Thiele et al., 2012). Thus, we can conclude that, in our long-term 17-ODYA treatment experiment, we could identify a set of acylated proteins in an OSCC cell with a metastatic phenotype. We cannot be sure about the length of the FA modifying each protein, but this is a common unanswered question in palmitoylome studies, since any alkynyl-FA can be metabolized within minutes.

Among the palmitoylated proteins in the pro-metastatic OSCC cell, we validated CAV1, CD9 and LPCAT1 palmitoylation. CAV1 is the main structural component of caveolae, which are microdomains within the PM with diverse functions such as exo- and endocytosis or regulation of different signaling pathways. CAV1 palmitoylation is not required for its PM localization (Eisinger et al., 2018) but is fundamental for the proper functioning of the protein, maybe by alteration of its localization within the PM (Koh et al., 2021). Further, CAV1 palmitoylation is necessary for very diverse functions, such as synaptic vesicle exocytosis (Koh et al., 2021) and the regulation of steroid hormone receptor (Eisinger et al., 2018) or Src kinase (Lee et al., 2001) signaling pathways. On the other hand, CD9 palmitoylation prevents its lysosomal degradation and affects the interaction of CD9 with other tetraspanins (Sharma et al., 2008), although there is certain controversy on the later function. Some studies have observed that CD9 palmitoylation can potentiate its homodimerization (Yang et al., 2006) while others indicate that it could favor CD9 interaction with CD151 (Sharma et al., 2008) or EWI-F (Glu-Trp-Ile (EWI) motif-containing protein) (Neviani et al., 2020). In any case, CD9 has been associated to CSCs and tumour progression, and palmitoylation can increase its stability (Wang et al., 2019b). Finally, we have been able to validate the palmitoylation of LPCAT1 for the first time. As previously described, this enzyme is responsible for histone H4 O-palmitoylation and is also involved in the transference of acyl-CoA moieties to phospholipids within membranes. Its palmitoylation could be an intermediate state in the process of PA transference to the H4 or phospholipids. The palmitoylation of other proteins detected after a four-day 17-ODYA stimulation but not validated in our study such as ITGA6 and ITGB4, has also been described to affect their stability and function and could have a role in metastasis (Sharma et al., 2012).

In our second large-scale experiment with 17-ODYA, we compared differences in the palmitoylome of cells treated for four days with PA or OA. We observed that the four-day PA treatment increased the palmitoylation state of most proteins. This result is in line with other studies, which showed that providing PA to cells also increases the palmitoylation of some proteins (Tang et al., 2021). Of note, analyzing with alkynyl-FAs the changes in palmitoylation induced by treatments with different FAs is not straight forward, and neither it is the interpretation of the results. We used a long-term (four

days) treatment of the cells with PA and OA followed by a short pulse (6 hours) incubation with 17-ODYA to reduce the phenotypic alteration induced by the incubation with the analog (**Figure R2.10A**). It is important to note that right before the incubation with the analog, the metabolism of the cells in the three experimental groups was most likely completely different, as they had been incubated for four days with different treatments. Thus, if PA treatment induced an increased rate of palmitoylation but OA or the control treatments did not, 17-ODYA was probably incorporated into proteins faster in this condition. However, this was not the case, as the PA treated samples showed the lowest enrichment, which suggested that protein palmitoylation is a rather stable PTM. Nevertheless, the excess of PA from the four-day treatment was probably stored in phospholipids or LDs and could still compete with 17-ODYA after treatment washout. Thus, these results should be carefully interpreted and further validated with orthologous methods, such as chemical labelling.

2.1 Variability within palmitoylome studies

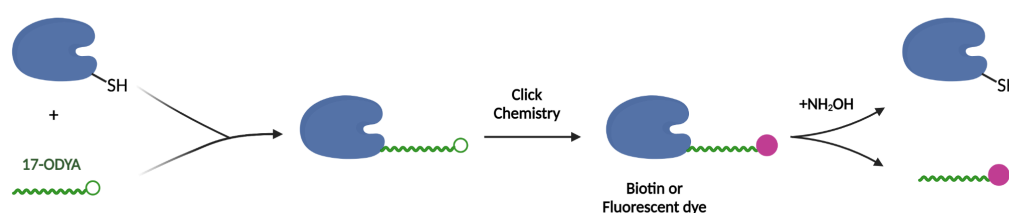
Comparisons of palmitoylome studies from different groups normally show low overlap in terms of palmitoylated proteins identified, even when the same alkynyl-FA probe is used. For instance, the comparison of two studies using the same cell line, same probe (17-ODYA) and same time of labelling (8 hours) showed an overlap of just 17%-28% of proteins identified using IPI numbers or gene symbols ([Martin and Cravatt, 2009](#); ██████████ ██████████). Of course, if any variations existed in the cell line, the time or dose of treatment or the alkynyl-FA used, the disparities are even higher. The two main differences between our palmitoylome studies and others using alkynyl-FAs were the duration of treatment and the analysis.

Not surprisingly, the overlap of the results obtained with other techniques used for large-scale palmitoylome studies, such as the chemical labelling, is even lower than when comparing two metabolic labelling experiments. In fact, a comparison of 18 different palmitoylome studies using one or the other method showed that 61.7% of the palmitoylated proteins identified at high confidence in each study were not replicated in any other study ([Edmonds et al., 2017](#)).

2.1.1 Metabolic labelling vs chemical labelling

Similar to alkynylated-FAs and the metabolic labelling approach, the chemical labelling or ABE method was developed to overcome the limitations of previous radioactive assays (Drisdell and Green, 2004). ABE protocol is based on the three *in vitro* chemical steps described in **Figure D2.1B**. First, free thiols within proteins are blocked with NEM (N-ethylmaleimide) and then proteins are incubated with NH_2OH . This incubation breaks the thioester bonds between S-palmitoylated proteins and the PA moieties and generates new, unblocked, free thiols. Those free thiols can then virtually react with any sulfhydryl reactive reagent. In the case of ABE, the compound used to label those free thiols is biotin-HPDP (N-[6-(Biotinamido)hexyl]-3'-(2'-pyridyldithio)propionamide)

A Metabolic labelling



B Chemical labelling

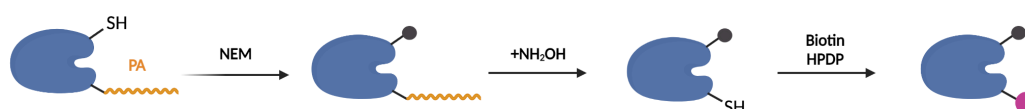


Figure D2.1 Metabolic labelling vs chemical labelling.

Graphical schemes of the two main methods used for large-scale studies of the cell palmitoylome. **A**) Description of the metabolic labelling of an S-palmitoylated protein with 17-ODYA. 17-ODYA is enzymatically incorporated into palmitoylated proteins inside the cells and upon extraction, proteins are submitted to click chemistry and biotin or a fluorescent dye are attached to the 17-ODYA moiety. Upon hydroxylamine (NH_2OH) treatment, only the thioester bonds between the S-palmitoylated proteins and 17-ODYA are broken and the signal of those proteins is lost. O- and N-palmitoylated proteins remain acylated upon NH_2OH treatment with this method. **B**) In the chemical labelling, upon protein extraction sulfhydryl groups within proteins are blocked with NEM (N-ethylmaleimide). Then, NH_2OH incubation breaks the thioester bonds between S-palmitoylated proteins and the PA moieties and the newly generated sulfhydryl groups are labelled with biotin-HPDP. Only S-palmitoylated proteins can be detected with this method. Created with BioRender.com

(Drisdell and Green, 2004; Wan et al., 2007). Biotin labelled proteins can then be visualized in a WB or enriched with streptavidin beads and analyzed by LC-MS. The main advantage of this method with respect to the metabolic labelling is that there is no need to incubate cells with any FA, thus palmitoylation can be analyzed in native cells and tissues. As previously discussed, treatment with alkynyl-FAs can change the phenotype

and metabolism of the cell and only those proteins palmitoylated during the metabolic labelling pulse will be detected. Furthermore, the addition of the clickable FA in the metabolic labelling experiments can increase the acyl-CoA pool of the cell and promote non-enzymatic palmitoylation of accessible Cys residues (Won et al., 2018).

On the other hand, ABE assay also presents several limitations. First of all, the method is only useful for the detection of S-palmitoylated proteins, while N- and O-palmitoylation remains invisible with this protocol. Also, the method relies especially on two chemical reactions that should be carried out with high efficiency to avoid false positive results. All pre-existing sulfhydryl groups have to be perfectly blocked and the NH_2OH treatment has to be strong enough to break all thioester bonds yet avoid protein degradation. Another source of false positives in this method are those proteins that use the thioester linkage to bind non-acyl groups. In an ABE study in *Saccharomyces cerevisiae*, 1/3 of the proteins with higher confidence were later discarded as false positives with orthogonal validations, proving the main limitation of the method (Roth et al., 2006). Moreover, this assay can identify the palmitoylome of a cell in a particular moment but cannot be used to study palmitoylation dynamics. Finally, in the metabolic labelling the chain-length of the alkynyl-FA used is known and depending on the analog used, the result can vary. Some proteins are preferentially acylated with longer moieties than others. In the case of ABE, it is impossible to know which is the FA modifying each protein.

Palmitoylome studies and their analyses are complex and still have not been unified. Slight differences in the protocol can generate diverse results. Each technique has advantages and disadvantages that should be analyzed prior to any experimental design and in consideration of the scientific question to be addressed. We decided to use the metabolic labelling with 17-ODYA because we were interested in analyzing the palmitoylome of the metastatic cell. In our study, the phenotypic changes induced by the long-treatment with the FA analog were beneficial and sought. Then, to investigate which of those palmitoylated proteins were specific of the metastatic phenotype, we continued using the metabolic labelling for the seek of comparison between both experiments. These experiments, as any other palmitoylome assays, present certain limitations that have been discussed and should be considered prior to the interpretation of the results. In any case, we have been able to identify a set of proteins differentially palmitoylated upon OA and PA treatments and the palmitoylation of the main target of interest was validated by orthogonal methods.

3 [REDACTED] palmitoylation

3.1 Palmitoylation of the [REDACTED]

This is not the first study in which [REDACTED] is described to be palmitoylated. [REDACTED] a large-scale analysis of protein acylation using [REDACTED] and different-length FA reporters (myristic, palmitic and stearic analogs) enriched and detect (by LC-MS) the [REDACTED] using palmitic and, to a lower extent, stearic acid analogs [REDACTED]. The palmitoylation of the [REDACTED] was validated with the transient overexpression of the proteins and [REDACTED] was identified as the acylated residue with [REDACTED] mutant [REDACTED].

In our study, we have shown that the palmitoylation of endogenous [REDACTED] and [REDACTED] has a variable stoichiometry depending on the cell line. In the OSCC cell lines SCC-25 and VDH-15, [REDACTED] was clearly more palmitoylated than [REDACTED] (Figure R3.1B). We also know that after four days of PA treatment, [REDACTED] was more palmitoylated in SCC-25 cells, but we have not tested yet whether all [REDACTED] are more palmitoylated or if that increase in palmitoylation only occurred in [REDACTED]. In the 501Mel cell line, both [REDACTED] seem to be equally palmitoylated, and the stoichiometry of palmitoylated [REDACTED] appears to be lower than in SCC-25 (Figure R3.1B). The melanoma cell line received the same four-day treatment as SCC-25 cells, thus the differential palmitoylation of [REDACTED] might be tumour-type dependent. Nevertheless, it is important to consider that 501Mel cell line grows in a medium supplemented with 10% FBS, which also contains PA and other FAs that could compete to some extent with the 17-ODYA treatment or alter the activity of the palmitoylation/depalmitoylation machinery (Else, 2020).

[REDACTED] and co-authors found the [REDACTED] [REDACTED] equally palmitoylated in their MS data and in their validations, unlike what we observed in OSCC cells [REDACTED]. This disparity could be explained by the fact that they used [REDACTED] cells, which would suggest a cell-type dependent palmitoylation stoichiometry of [REDACTED], as we observed for melanoma, or by differences due to the growing conditions, as [REDACTED] cells are also grown in FBS-containing media. Further studies are required to determine the palmitoylation status of [REDACTED] and the influence that a PA rich environment could have on the S-acylation of each [REDACTED].

3.2 S-palmitoylation of [REDACTED]

Cysteines are one of the most rarely found amino acids in proteins (1.9% of the amino acids in proteins), which suggests that they might have specialized functions within

proteins that contain them (██████████). We have proven that ██████████ is palmitoylated using stable SCC-25 cell lines expressing ██████████ constructs. The main drawbacks of exogenous protein expression experiments are that usually the physiological enzyme/substrate stoichiometry is disrupted and that the exogenously expressed protein can be mislocalized, which can generate misleading results (Hou et al., 2009). Nonetheless, different controls have shown that both exogenous versions of ██████████ were expressed at similar levels to the endogenous ██████████ and were also ██████████. Thus, the cells used the exogenous proteins in a physiological manner, conferring more reliability to the results obtained using these cell lines. As mentioned in the *Results* section, ██████████ enrichment after 17-ODYA treatment was higher than that of ██████████ at different incubation times (four days and overnight treatment, **Figure R3.3**), indicating that ██████████ is specifically S-palmitoylated at ██████████.

However, ██████████ was also enriched upon click chemistry, although at a much lower level, pointing to a secondary acylation of ██████████ in a different residue. This may reflect a compensatory mechanism induced upon ██████████ mutation, since endogenous ██████████ seems to be exclusively S-palmitoylated according to the complete loss of metabolic labelling when treated with NH₂OH (**Figure R3.1A**). This secondary acylation was not previously observed by ██████████ when mutating ██████████ in ██████████; however, they used a transient overexpression (18 hours) and cells shortly overexpressing the mutant version might not have adapted to compensate for the lack of Cys at position ██████████ (██████████). SCC-25 cells use exogenous ██████████ and ██████████, regardless of their mutational status; thus, if ██████████ palmitoylation is required to regulate the ██████████ of the cell but ██████████ is no longer there, cells might compensate somehow with other acylations. Alternative ██████████, ██████████, ██████████ (██████████). The occurrence of this compensatory mechanism would support the relevance of ██████████ palmitoylation for the cell.

Although a compensatory acylation seems the most likely explanation for the enrichment of ██████████, we cannot fully discard that 17-ODYA is used by the cell for other physiological acylations in the endogenous or WT version of ██████████. In other words, the PA analog could be metabolized by the cell and used for other protein acylations such as the ██████████. Nevertheless, we were not able to detect those acylations upon NH₂OH treatment (see **Figure R3.1A**). Further, the enrichment of ██████████ is very low compared to ██████████; thus, if it happened, these acylations are probably minimally labelled with 17-ODYA as compared to the S-palmitoylation of ██████████.

3.3 Functions of [REDACTED] and possible roles of its palmitoylation

3.3.1 Structural functions of [REDACTED]

[REDACTED] is an evolutionary conserved residue present in almost every [REDACTED], namely, in [REDACTED] is the only cysteine present except [REDACTED], which present a second Cys in their residue [REDACTED] (Figure I3.2) ([REDACTED]). [REDACTED] is located at the end of the [REDACTED] ([REDACTED]) and forms hydrogen bonds with [REDACTED], within [REDACTED], and [REDACTED] (Figure D3.1) that could help stabilizing the tertiary structure of the protein.

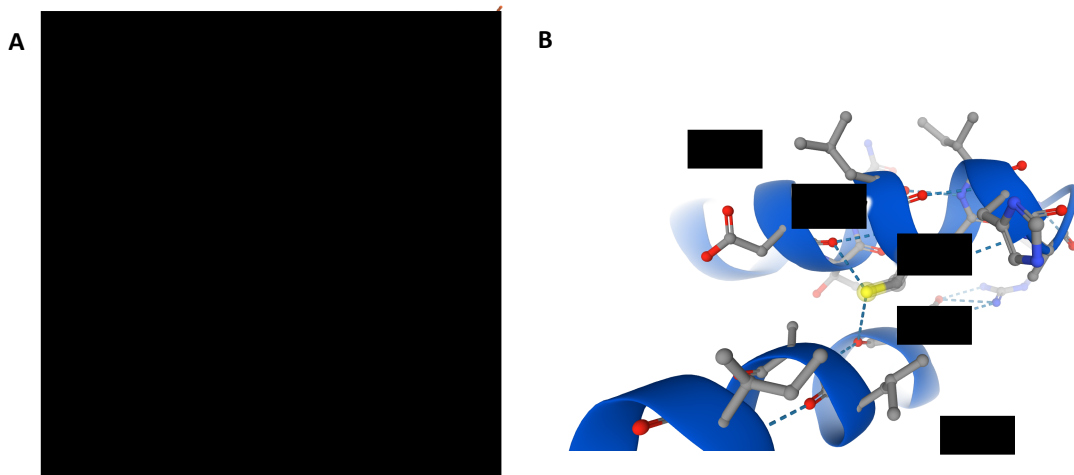


Figure D3.1. [REDACTED] structure

Ribbon diagrams of [REDACTED] protein structure prediction generated with AlphaFold software (Jumper et al., 2021). The different structural domains have been named based on [REDACTED]. description ([REDACTED] and its surrounding residues have been highlighted with ball-and-stick model. Grey balls represent carbons; yellow, sulfur; red, oxygen; and blue, nitrogen. Dotted lines represent hydrogen bonds **A)** Illustration of the whole protein. **B)** Detail of [REDACTED] area and interactions with [REDACTED] in [REDACTED] and [REDACTED] in [REDACTED] through hydrogen bonds, represented by blue dotted lines.

Within the [REDACTED], both [REDACTED] residues lie buried in the centre of the [REDACTED] ([REDACTED] (Figure D3.2A) ([REDACTED]). Located at the interface between [REDACTED], [REDACTED] residues are fundamental for [REDACTED] interactions and [REDACTED] formation. In fact, replacement of [REDACTED] with a [REDACTED] alters the charges within the [REDACTED] and impedes [REDACTED] formation without altering [REDACTED] ([REDACTED]). [REDACTED] sulfhydryl groups from [REDACTED] with a separation of [REDACTED] depending on the oxidized level of the [REDACTED] (Figure D3.2B) ([REDACTED]).

[REDACTED]). This distance is too large for a disulfide formation without [REDACTED]
[REDACTED]. Indeed, the [REDACTED]
formation might be incompatible with the [REDACTED]),
although some authors argue that it could happen in areas of [REDACTED]
([REDACTED])

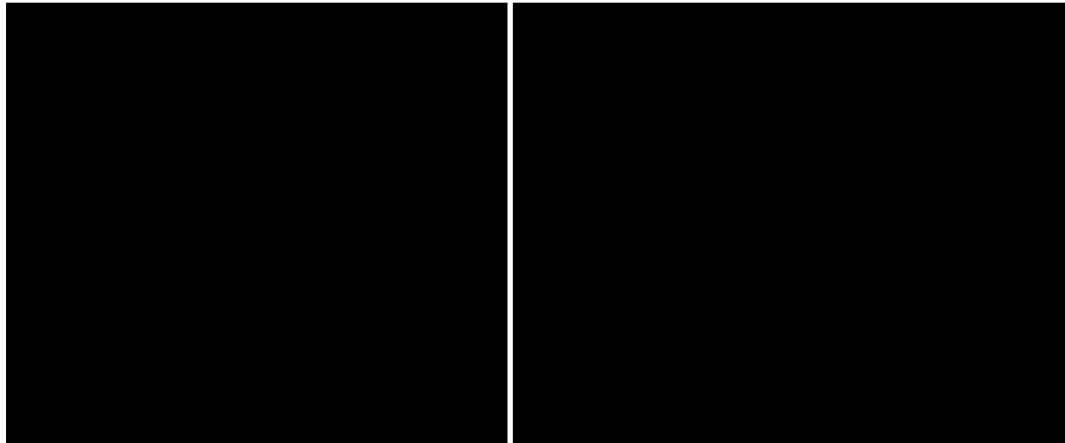


Figure D3.2. [REDACTED] within the [REDACTED].

Cartoon representation of the crystal structure of a human [REDACTED] visualized with PyMol (2.3.4). [REDACTED]. Salmon pink and green structures represent [REDACTED]; white and light blue are [REDACTED]; dark blue and pink are [REDACTED]; and orange and yellow represent [REDACTED]. Surrounding the [REDACTED], the [REDACTED] is represented in orange with the [REDACTED]. **A)** Structure of the whole [REDACTED]. The area where [REDACTED] from [REDACTED] are located is highlighted with a white square. **B)** Detail of the area highlighted in **A**. [REDACTED] in both [REDACTED] are represented with balls-and-sticks and pointed with red arrows. The yellow stick represents the sulfhydryl group.

[REDACTED] are completely protected in native [REDACTED] ([REDACTED]). Access to these residues would require an alteration in the conformation of [REDACTED] side chain, which is sterically possible and could happen *in vivo* ([REDACTED]). In fact, it was shown that [REDACTED] or areas of [REDACTED] [REDACTED] are preferentially labelled with sulfhydryl reagents, suggesting that in these areas, the [REDACTED] changes its conformation and exposes [REDACTED]. Further, these areas of [REDACTED] are where fibroblasts tend to accumulate mercury, probably via [REDACTED] ([REDACTED]). These studies align with our findings showing that [REDACTED] is the [REDACTED] that is preferentially palmitoylated. Similar to other [REDACTED] described in the *Introduction*, modifications of the exposed [REDACTED] regardless of their size, allow the [REDACTED] but [REDACTED] [REDACTED], all of which could further favour the [REDACTED].

In addition, we have observed that the [REDACTED] mutant is normally incorporated [REDACTED], meaning that this residue is most likely not important for the [REDACTED], and that palmitoylation may not be necessary for [REDACTED]. Furthermore, based on the localization of [REDACTED] and [REDACTED] within the [REDACTED] it seems that [REDACTED] palmitoylation does not favor [REDACTED] tethering to the [REDACTED].

Considering our results and previous data on the consequences of [REDACTED] modification, we speculate that [REDACTED] S-palmitoylation could induce [REDACTED] and [REDACTED]. In this sense, [REDACTED] palmitoylation would have similar function to other [REDACTED] that are also associated to [REDACTED] or to [REDACTED], which is also associated to the [REDACTED]. In the case of [REDACTED] cell culture treatment with those specific FA moieties increases their deposition at [REDACTED] in a dose-dependent manner ([REDACTED]). The same seems to happen with [REDACTED] palmitoylation, as we have observed an increment of [REDACTED] S-palmitoylation when cells are treated with PA.

Interestingly, mutations within [REDACTED] residues can abrogate the need for the SWI/SNF remodeling complex for regulating gene expression in yeast ([REDACTED]). Indeed, in human cancers, some of those residues such as [REDACTED] are commonly mutated. Based on cBioPortal modeling method annotation, they might be three-dimensional hotspot mutations ([REDACTED]). These studies confirm the relevance of that particular area of the [REDACTED] for maintaining the [REDACTED] and also indicate that tumour cells tend to prefer [REDACTED] that favor [REDACTED]. In fact, [REDACTED], the main [REDACTED], is commonly amplified in several tumours ([REDACTED]).

3.3.2 Implication of [REDACTED] in the [REDACTED]

The unique chemistry of the thiol group is what confers especial functions to cysteines within proteins. Thiol groups are particularly reactive to electrophiles and oxidants and have high affinity for metals. Further, cysteines hold reduction potential and can donate electrons to different molecules and then, in most cases, become regenerated by other cellular reductants, such as NADH or NADPH (nicotinamide adenine dinucleotide phosphate) (Poole, 2015). The relevance that cysteines have on cellular redox homeostasis is well exemplified by GSH. GSH is the most abundant low molecular weight thiol compound synthesized in cells. This tripeptide (L- γ -glutamyl-L-cysteinyl-glycine) plays critical roles in maintaining redox homeostasis and in protecting cells from oxidative damage and xenobiotic electrophiles. Through the active thiol group of its

cysteine, it acts as antioxidant directly interacting with reactive oxygen and nitrogen species (ROS and RNS) or as a cofactor of different enzymes (Lushchak, 2012).

Redox homeostasis is fundamental for the correct functioning of the cell metabolism and can also be implicated in processes occurring within the nucleus. In fact, we can find different important TFs regulated by redox-sensing mechanisms. For example, both p53 and NF- κ B (nuclear factor kappa B) require reduction of their DNA-interacting Cys residues for proper DNA binding and transcription (Hainaut and Mann, 2001; Matthews et al., 1992). Others, like HoxB5 TF, can only bind DNA upon oxidation of their Cys residues (Galang and Hauser, 1993). In fact, different [REDACTED] are affected by oxidative stress ([REDACTED]). For many years, different studies have tried to elucidate the capacity of [REDACTED] cysteines to sense redox changes within the nucleus ([REDACTED]). Strikingly, a recent study shows that [REDACTED] could not only sense but also play an active role in redox homeostasis acting as a [REDACTED]. [REDACTED] observed that [REDACTED] and [REDACTED], which are localized within the [REDACTED], are arranged in a conformation typical of [REDACTED]; indeed, the [REDACTED] can bind and [REDACTED]). Both residues are necessary for the [REDACTED] and [REDACTED], but [REDACTED] is not the electron donor. In fact, the electron donor used by [REDACTED] *in vivo* is still unknown although [REDACTED] is used by the [REDACTED] *in vitro* for the [REDACTED]. Interestingly, this study also showed that the [REDACTED] generated by [REDACTED] is relevant for processes happening within the [REDACTED] activation and can also affect enzymes within other compartments of the cell such as [REDACTED] or ubiquitous [REDACTED].

On the other hand, [REDACTED] can also be modified by [REDACTED] on [REDACTED]. This [REDACTED] of [REDACTED] seems to especially affect [REDACTED] and, as expected based on previous literature, the modification of [REDACTED] decreases the [REDACTED]). This [REDACTED] PTM is proliferation-dependent, given that proliferative cells present higher levels of [REDACTED]. This could be explained by the variations in [REDACTED] concentration and location occurred during the cell cycle. During S/G2/M phases of the cell cycle, [REDACTED] is mainly localized at the nucleus of the cells but upon confluency, it is redistributed throughout the cell ([REDACTED]). Thus, nuclear [REDACTED] could provide the appropriate [REDACTED] environment for DNA replication. Moreover, oxidation of the cytoplasm accompanied by certain increase in the ROS levels are required for EGFR cascade activation and this would be achieved by [REDACTED] relocation to the nucleus ([REDACTED]).

The connection between the [REDACTED] and [REDACTED] is unknown. [REDACTED] plays a well-documented role in the metabolism of [REDACTED]. It is involved in [REDACTED] mobilization for the formation of mature proteins but also in the [REDACTED] of the [REDACTED]. In fact, [REDACTED] complex is used for [REDACTED] incorporation into SOD1 ([REDACTED]). Thus, it can be argued that [REDACTED] could be used by the [REDACTED] as the electron donor for [REDACTED]. Upon reduction, oxidized [REDACTED] could react with [REDACTED] and generate the [REDACTED]. Nevertheless, [REDACTED] and [REDACTED] have been shown to have a distinct role in [REDACTED] metabolism ([REDACTED]), although it is important to consider that this study was performed in *Saccharomyces cerevisiae*, while the study described in the previous paragraph was done with mouse and human fibroblasts and human cancer cell lines ([REDACTED]).

S-palmitoylation of [REDACTED] could interfere with both processes. It could probably hamper the [REDACTED], which would alter the function of [REDACTED] enzymes and consequently the detoxifying capacity of the cell via SOD1 and the energy production ability via OXPHOS. Nevertheless, S-palmitoylation could also probably prevent or displace [REDACTED] from [REDACTED], which might liberate [REDACTED] that could be used in other compartments of the cell for redox homeostasis. Liberated [REDACTED] could be used for [REDACTED] metabolism, and this would mitigate the need for the [REDACTED] activity of the [REDACTED].

Overall, [REDACTED] seems to be a particularly relevant residue within the [REDACTED]. Any modification affecting this residue could have an impact in the cell [REDACTED], as any other [REDACTED], but in this case, it would also alter the [REDACTED] structure and even the redox homeostasis in the [REDACTED]. Thus, it is especially worrying to assume that such an important residue can be modified by a dietary FA so closely associated to metastasis. Further studies are required to characterize in detail the functions and consequences of [REDACTED] S-palmitoylation in different tumour types. The next step is to identify the enzyme is responsible for [REDACTED] palmitoylation, which could set the stage for finding potential inhibitors that could prevent it if needed.

CONCLUSIONS

- PA and OA treatments induce opposite proteomic responses in OSCC cultured cells. These responses are characterized by the upregulation via PA (and downregulation via OA) of the lipid metabolism, oxidative stress, drug resistance and cell motility processes and the downregulation via PA (and upregulation via OA) of the cell cycle, mRNA processing and protein turnover.
- Most proteomic changes induced by PA are regulated at the transcription level, with the exception of some metabolic pathways such as the TCA cycle, OXPHOS or glycolysis.
- PA- and OA-enriched HFDs, unlike cell culture treatments, do not induce an opposite proteomic response in OSCC cells orthotopically injected in mice. Both fatty diets upregulate the FA metabolism and downregulate protein synthesis, mRNA splicing and antigen presentation processes, although the responses are stronger for the PA-enriched diet.
- The protein palmitoylation machinery (i.e., the DHHC protein acyl transferase family of proteins) is upregulated in SCC-25 cells growing in mice fed a PA-enriched HFD. The gene expression of most DHHCs is also upregulated upon PA treatment in cell culture and in the LN metastasis lesions in mice.
- The PA analog 17-ODYA increases the metastatic potential of SCC-25 to a similar extent than PA and induces a similar proteomic response. Both moieties (PA and 17-ODYA) can be used indistinctly by the cell to palmitoylate proteins.
- The palmitoylome of pro-metastatic SCC-25 cells is enriched in proteins related to membrane functions, such as cell adhesion or motility, which could be implicated in the metastatic phenotype (e.g., CD44, CD9).
- PA treatment enhances global protein palmitoylation while OA treatment reduces it. Proteins that are more palmitoylated upon PA treatment are enriched in membrane categories such as focal adhesion, as well as in processes related to RNA processing, and protein translation.
- [REDACTED] is palmitoylated in OSCC cells, and its palmitoylation increases upon PA treatment.
- [REDACTED] is preferentially palmitoylated over the [REDACTED] in OSCC cells, whereas melanoma cells show similar palmitoylation stoichiometry in both [REDACTED], suggesting a tumour-type dependent stoichiometry.
- [REDACTED] is S-palmitoylated at the [REDACTED] residue.

- [REDACTED] and its distinct PTMs (including palmitoylation) are not implicated in the [REDACTED] or in the [REDACTED] localization of the [REDACTED].

REFERENCES

- Abdelmagid, S. A., Clarke, S. E., Nielsen, D. E., Badawi, A., El-Sohehy, A., Mutch, D. M., & Ma, D. W. L. (2015). Comprehensive profiling of plasma fatty acid concentrations in young healthy canadian adults. *PLoS ONE*, *10*(2), 1–16. <https://doi.org/10.1371/journal.pone.0116195>
- Abrami, L., Dallavilla, T., Sandoz, P. A., Demir, M., Kunz, B., Savoglidis, G., Hatzimanikatis, V., & van Der Goot, F. G. (2017). Identification and dynamics of the human ZDHHC16-ZDHHC6 palmitoylation cascade. *ELife*, *6*. <https://doi.org/10.7554/eLife.27826>
- Adibekian, A., Martin, B. R., Chang, J. W., Hsu, K. L., Tsuboi, K., Bachovchin, D. A., Speers, A. E., Brown, S. J., Spicer, T., Fernandez-Vega, V., Ferguson, J., Hodder, P. S., Rosen, H., & Cravatt, B. F. (2012). Confirming target engagement for reversible inhibitors in vivo by kinetically tuned activity-based probes. *Journal of the American Chemical Society*, *134*(25), 10345–10348. <https://doi.org/10.1021/ja303400u>
- Agostini, M., Almeida, L. Y., Bastos, D. C., Ortega, R. M., Moreira, F. S., Seguin, F., Zecchin, K. G., Raposo, H. F., Oliveira, H. C. F., Amoêdo, N. D., Salo, T., Coletta, R. D., & Graner, E. (2014). The fatty acid synthase inhibitor orlistat reduces the growth and metastasis of orthotopic tongue oral squamous cell carcinomas. *Molecular Cancer Therapeutics*, *13*(3), 585–595. <https://doi.org/10.1158/1535-7163.MCT-12-1136>
- Agudo-Ibáñez, L., Herrero, A., Barbacid, M., & Crespo, P. (2015). H-Ras Distribution and Signaling in Plasma Membrane Microdomains Are Regulated by Acylation and Deacylation Events. *Molecular and Cellular Biology*, *35*(11), 1898–1914. <https://doi.org/10.1128/mcb.01398-14>
- Ahearn, I. M., Tsai, F. D., Court, H., Zhou, M., Jennings, B. C., Ahmed, M., Fehrenbacher, N., Linder, M. E., & Philips, M. R. (2011). FKBP12 Binds to Acylated H-Ras and Promotes Depalmitoylation. *Molecular Cell*, *41*(2), 173–185. <https://doi.org/10.1161/CIRCULATIONAHA.110.956839>
- Akimzhanov, A. M., Boehning, D., & Snyder, S. H. (2015). Rapid and transient palmitoylation of the tyrosine kinase Lck mediates Fas signaling. *Proceedings of the National Academy of Sciences of the United States of America*, *112*(38), 11876–11880. <https://doi.org/10.1073/pnas.1509929112>
- Akram, M. (2014). Citric Acid Cycle and Role of its Intermediates in Metabolism. *Cell Biochemistry and Biophysics*, *68*(3), 475–478. <https://doi.org/10.1007/s12013-013-9750-1>
- Ali, A., Levantini, E., Teo, J. T., Goggi, J., Clohessy, J. G., Wu, C. S., Chen, L., Yang, H., Krishnan, I., Kocher, O., Zhang, J., Soo, R. A., Bhakoo, K., Chin, T. M., & Tenen, D. G. (2018). Fatty acid synthase mediates EGFR palmitoylation in EGFR mutated non-small cell lung cancer. *EMBO Molecular Medicine*, *10*(3), 1–19. <https://doi.org/10.15252/emmm.201708313>
- Alicea, G. M., Rebecca, V. W., Goldman, A. R., Fane, M. E., Douglass, S. M., Behera, R., Webster, M. R., Iii, C. H. K., Brett, L., Caino, M. C., Kossenkov, A. V., Tang, H., Frederick, D. T., Flaherty, K. T., Xu, X., Liu, Q., Gabrilovich, D. I., Herlyn, M., Ian, A., ... Weeraratna, A. T. (2020). Changes in Aged Fibroblast Lipid Metabolism Induce Age- dependent Melanoma Cell Resistance to Targeted Therapy Via the Fatty Acid Transporter FATP2. *Cancer Discovery*, *10*(9), 1282–1295. <https://doi.org/10.1158/2159-8290.CD-20-0329>. Changes
- Al-Khami, A. A., Zheng, L., Del Valle, L., Hossain, F., Wyczechowska, D., Zabaleta, J., Sanchez, M. D., Dean, M. J., Rodriguez, P. C., & Ochoa, A. C. (2017). Exogenous lipid uptake induces metabolic and functional reprogramming of tumor-associated myeloid-derived suppressor cells. *Onc Immunology*, *6*(10). <https://doi.org/10.1080/2162402X.2017.1344804>
- Aloia, A., Müllhaupt, D., Chabbert, C. D., Eberhart, T., Vukolic, A., Eichhoff, O., Irmisch, A., Alexander, L. T., Scibona, E., Frederick, D. T., Miao, B., Tian, T., Cheng, C., Kwong, L. N., Wei, Z., Sullivan, R. J., Boland, G. M., Flaherty, K. T., Zamboni, N., ... Kovacs, W. J. (2019). A fatty acid oxidation-dependent metabolic shift regulates the adaptation of BRAF-mutated melanoma to MAPK inhibitors. *Clinical Cancer Research*, *25*(22), 6852–6867. <https://doi.org/10.1158/1078-0432.CCR-19-0253>
- Anderson, A. M., & Ragan, M. A. (2016). Palmitoylation: A protein s-acylation with implications for breast cancer. *Npj Breast Cancer*, *2*(1), 1–10. <https://doi.org/10.1038/npjbcancer.2016.28>
- Arango, D., Sturgill, D., Alhusaini, N., Dillman, A. A., Sweet, T. J., Hanson, G., Hosogane, M., Sinclair, W. R., Nanan, K. K., Mandler, M. D., Fox, S. D., Zengeya, T. T., Andresson, T., Meier, J. L., Collier, J., & Oberdoerffer, S. (2018). Acetylation of Cytidine in mRNA Promotes Translation Efficiency. *Cell*, *175*(7), 1872–1886. <https://doi.org/10.1016/j.cell.2018.10.030>
- Aronson, W. J., Barnard, J. R., Freedland, S. J., Henning, S., Elashoff, D., Jardack, P. M., Cohen, P., Heber, D., & Kobayashi, N. (2010). Growth Inhibitory Effect of Low Fat Diet on Prostate Cancer Cells: Results of a Prospective, Randomized Dietary Intervention Trial in Men With Prostate Cancer. *Journal of Urology*, *183*(1), 345–350. <https://doi.org/10.1016/j.juro.2009.08.104>

[REDACTED]

Auciello, F. R., Bulusu, V., Oon, C., Tait-Mulder, J., Berry, M., Bhattacharyya, S., Tumanov, S., Allen-Petersen, B. L., Link, J., Kendersky, N. D., Vringer, E., Schug, M., Novo, D., Hwang, R. F., Evans, R. M., Nixon, C., Dorrell, C., Morton, J. P., Norman, J. C., ... Sherman, M. H. (2019). A stromal lysolipid-autotaxin signaling axis promotes pancreatic tumor progression. *Cancer Discovery*, 9(5), 617–627. <https://doi.org/10.1158/2159-8290.CD-18-1212>

[REDACTED]

Baker, T. L., Zheng, H., Walker, J., Coloff, J. L., & Buss, J. E. (2003). Distinct rates of palmitate turnover on membrane-bound cellular and oncogenic H-Ras. *Journal of Biological Chemistry*, 278(21), 19292–19300. <https://doi.org/10.1074/jbc.M206956200>

[REDACTED]

Baumgart, F., Corral-Escariz, M., Pérez-Gil, J., & Rodríguez-Crespo, I. (2010). Palmitoylation of R-Ras by human DHHC19, a palmitoyl transferase with a CaaX box. *Biochimica et Biophysica Acta - Biomembranes*, 1798(3), 592–604. <https://doi.org/10.1016/j.bbamem.2010.01.002>

Bergers, G., & Fendt, S. M. (2021). The metabolism of cancer cells during metastasis. *Nature Reviews Cancer*, 21(3), 162–180. <https://doi.org/10.1038/s41568-020-00320-2>

Bi, J., Ichu, T. A., Zanca, C., Yang, H., Zhang, W., Gu, Y., Chowdhry, S., Reed, A., Ikegami, S., Turner, K. M., Zhang, W., Villa, G. R., Wu, S., Quehenberger, O., Yong, W. H., Kornblum, H. I., Rich, J. N., Cloughesy, T. F., Cavenee, W. K., ... Mischel, P. S. (2019). Oncogene Amplification in Growth Factor Signaling Pathways Renders Cancers Dependent on Membrane Lipid Remodeling. *Cell Metabolism*, 30, 525–538. <https://doi.org/10.1016/j.cmet.2019.06.014>

Binker-Cosen, M. J., Richards, D., Oliver, B., Gaisano, H. Y., Binker, M. G., & Cosen-Binker, L. I. (2017). Palmitic acid increases invasiveness of pancreatic cancer cells AsPC-1 through TLR4/ROS/NF- κ B/MMP-9 signaling pathway. *Biochemical and Biophysical Research Communications*, 484(1), 152–158. <https://doi.org/10.1016/j.bbrc.2017.01.051>

Blanc M, Fabrice P.A. David, Laurence Abrami, Daniel Migliozi, Florence Armand, Jérôme Burgi and F. Gisou van der Goot, SwissPalm: Protein Palmitoylation database. *F1000Res*. 4, 261 (2015). pmid: 26339475

Blomme, A., Ford, C. A., Mui, E., Patel, R., Ntala, C., Jamieson, L. E., Planque, M., Mcgregor, G. H., Peixoto, P., Hervouet, E., Nixon, C., Salji, M., Gaughan, L., Markert, E., Repiscak, P., Sumpton, D., Blanco, G. R., Lilla, S., Kamphorst, J. J., ... Leung, H. Y. (2020). 2,4-dienoyl-CoA reductase regulates lipid homeostasis in treatment-resistant prostate cancer. *Nature Communications*, 11(2508), 1–17.

Bollu, L. R., Katreddy, R. R., Blessing, A. M., Pham, N., Zheng, B., Wu, X., & Weihua, Z. (2015). Intracellular activation of EGFR by fatty acid synthase dependent palmitoylation. *Oncotarget*, 6(33), 34992–35003. <https://doi.org/10.18632/oncotarget.5252>

Bort, A., Sánchez, B. G., de Miguel, I., Mateos-Gómez, P. A., & Diaz-Laviada, I. (2020). Dysregulated lipid metabolism in hepatocellular carcinoma cancer stem cells. *Molecular Biology Reports*.

Brabletz, T., Kalluri, R., Nieto, M. A., & Weinberg, R. A. (2018). EMT in cancer. *Nature Reviews Cancer*, 18(2), 128–134. <https://doi.org/10.1038/nrc.2017.118>

[REDACTED]

- Brigidi, G. S., Santyr, B., Shimell, J., Jovellar, B., & Bamji, S. X. (2015). Activity-regulated trafficking of the palmitoyl-acyl transferase DHHC5. *Nature Communications*, 6. <https://doi.org/10.1038/ncomms9200>
- Brigidi, G. S., Sun, Y., Beccano-Kelly, D., Pitman, K., Mobasser, M., Borgland, S. L., Milnerwood, A. J., & Bamji, S. X. (2014). Palmitoylation of δ -catenin by DHHC5 mediates activity-induced synapse plasticity. *Nature Neuroscience*, 17(4), 522–532. <https://doi.org/10.1038/nn.3657>
- Broadfield, L. A., Duarte, J. A. G., Schmieder, R., Broekaert, D., Veys, K., Planque, M., Vriens, K., Karasawa, Y., Napolitano, F., Fujita, S., Fujii, M., Eto, M., Holvoet, B., Vangoitsenhoven, R., Fernandez-Garcia, J., Van Elsen, J., Dehairs, J., Zeng, J., Dooley, J., ... Fendt, S. M. (2021a). Fat induces glucose metabolism in nontransformed liver cells and promotes liver tumorigenesis. *Cancer Research*, 81(8), 1988–2001. <https://doi.org/10.1158/0008-5472.CAN-20-1954>
- Broadfield, L. A., Pane, A. A., Talebi, A., Swinnen, J. V., & Fendt, S. M. (2021b). Lipid metabolism in cancer: New perspectives and emerging mechanisms. *Developmental Cell*, 56(10), 1363–1393. <https://doi.org/10.1016/j.devcel.2021.04.013>

- Bueno, M. J., Jimenez-Renard, V., Samino, S., Capellades, J., Junza, A., López-Rodríguez, M. L., Garcia-Carceles, J., Lopez-Fabuel, I., Bolaños, J. P., Chandel, N. S., Yanes, O., Colomer, R., & Quintela-Fandino, M. (2019). Essentiality of fatty acid synthase in the 2D to anchorage-independent growth transition in transforming cells. *Nature Communications*, 10(1), 1–18. <https://doi.org/10.1038/s41467-019-13028-1>

- Camp, L. A., & Hofmann, S. L. (1993). Purification and properties of a palmitoyl-protein thioesterase that cleaves palmitate from H-Ras. *Journal of Biological Chemistry*, 268(30), 22566–22574. [https://doi.org/10.1016/S0021-9258\(18\)41567-0](https://doi.org/10.1016/S0021-9258(18)41567-0)
- Caneba, C. A., Bellance, N., Yang, L., Pabst, L., & Nagrath, D. (2012). Pyruvate uptake is increased in highly invasive ovarian cancer cells under anoikis conditions for anaplerosis, mitochondrial function, and migration. *American Journal of Physiology - Endocrinology and Metabolism*, 303(8), 1036–1052. <https://doi.org/10.1152/ajpendo.00151.2012>
- Cao, N., Li, J. K., Rao, Y. Q., Liu, H., Wu, J., Li, B., Zhao, P., Zeng, L., & Li, J. (2016). A potential role for protein palmitoylation and zDHHC16 in DNA damage response. *BMC Molecular Biology*, 17(12). <https://doi.org/10.1186/s12867-016-0065-9>
- Cao, Y., Qiu, T., Kathayat, R. S., Azizi, S.-A., Thorne, A. K., Ahn, D., Fukata, Y., Fukata, M., Rice, P. A., & Dickinson, B. C. (2019). ABHD10 is an S-depalmitoylase affecting redox homeostasis through peroxiredoxin-5. *Nature Chemical Biology*, 15(12), 1232–1240. <https://doi.org/10.1016/j.physbeh.2017.03.040>
- Cao, W., Ramakrishnan, R., Tuyrin, V. A., Veglia, F., Condamine, T., Amoscato, A., Mohammadyani, D., Johnson, J. J., Zhang, L. M., Klein-Seetharaman, J., Celis, E., Kagan, V. E., & Gabrilovich, D. I. (2014). Oxidized lipids block antigen cross-presentation by dendritic cells in cancer1 Oxidized lipids and DCs in cancer. *Journal of Immunology*, 192(6), 1920–1931. <https://doi.org/10.4049/jimmunol.1302801>
- Chan, P., Han, X., Zheng, B., Deran, M., Yu, J., Jarugumilli, G. K., Deng, H., Pan, D., Luo, X., & Wu, X. (2016). Autopalmitoylation of TEAD proteins regulates transcriptional output of the Hippo pathway. *Nature Chemical Biology*, 12(4), 282–289. <https://doi.org/10.1038/nchembio.2036>
- Chandra, A., Grecco, H. E., Pisupati, V., Perera, D., Cassidy, L., Skoulidis, F., Ismail, S. A., Hedberg, C., Hanzal-Bayer, M., Venkitaraman, A. R., Wittinghofer, A., & Bastiaens, P. I. H. (2012). The GDI-like solubilizing factor PDE δ sustains the spatial organization and signalling of Ras family proteins. *Nature Cell Biology*, 14(2), 148–158. <https://doi.org/10.1038/ncb2394>
- Chang, C. H., Qiu, J., O'Sullivan, D., Buck, M. D., Noguchi, T., Curtis, J. D., Chen, Q., Gindin, M., Gubin, M. M., Van Der Windt, G. J. W., Tonc, E., Schreiber, R. D., Pearce, E. J., & Pearce, E. L. (2015). Metabolic Competition in the Tumor Microenvironment Is a Driver of Cancer Progression. *Cell*, 162(6), 1229–1241. <https://doi.org/10.1016/j.cell.2015.08.016>

Charych, E. I., Jiang, L. X., Lo, F., Sullivan, K., & Brandon, N. J. (2010). Interplay of palmitoylation and phosphorylation in the trafficking and localization of phosphodiesterase 10A: Implications for the treatment of schizophrenia. *Journal of Neuroscience*, *30*(27), 9027–9037. <https://doi.org/10.1523/JNEUROSCI.1635-10.2010>

Chaurasia, B., & Summers, S. A. (2015). Ceramides – Lipotoxic Inducers of Metabolic Disorders. *Trends in Endocrinology and Metabolism*, *26*(10), 538–550.

Chen, B., Zheng, B., DeRan, M., Jarugumilli, G. K., Fu, J., Brooks, Y. S., & Wu, X. (2016). ZDHHC7-Mediated S-Palmitoylation of Scribble Regulates Cell Polarity. *Nature Chemical Biology*, *12*(9), 686–693. <https://doi.org/10.1038/nchembio.2119>

Chen, S., Zhu, B., Yin, C., Liu, W., Han, C., Chen, B., Liu, T., Li, X., Chen, X., Li, C., Hu, L., Zhou, J., Xu, Z. X., Gao, X., Wu, X., Goding, C. R., & Cui, R. (2017). Palmitoylation-dependent activation of MC1R prevents melanomagenesis. *Nature*, *549*(7672), 399–403. <https://doi.org/10.1038/nature23887>

Chlebowski, R. T., Aragaki, A. K., Anderson, G. L., Simon, M. S., Manson, J. E., Neuhaus, M. L., Pan, K., Stefanic, M. L., Rohan, T. E., Lane, D., Qi, L., Snetselaar, L., & Prentice, R. L. (2018). Association of Low-Fat Dietary Pattern with Breast Cancer Overall Survival: A Secondary Analysis of the Women’s Health Initiative Randomized Clinical Trial. *JAMA Oncology*, *4*(10), 1–10. <https://doi.org/10.1001/jamaoncol.2018.1212>

Chlebowski, R. T., Blackburn, G. L., Thomson, C. A., Nixon, D. W., Shapiro, A., Hoy, M. K., Goodman, M. T., Giuliano, A. E., Karanja, N., McAndrew, P., Hudis, C., Butler, J., Merkel, D., Kristal, A., Caan, B., Michaelson, R., Vinciguerra, V., Del Prete, S., Winkler, M., ... Elshoff, R. M. (2006). Dietary fat reduction and breast cancer outcome: Interim efficacy results from the women’s intervention nutrition study. *Journal of the National Cancer Institute*, *98*(24), 1767–1776. <https://doi.org/10.1093/jnci/djj494>

Cho, E., & Park, M. (2016). Palmitoylation in Alzheimer’s disease and other neurodegenerative diseases. *Pharmacological Research*, *111*, 133–151. <https://doi.org/10.1016/j.phrs.2016.06.008>

Cho, J., Pastorino, S., Zeng, Q., Xu, X., Johnson, W., Vandenberg, S., Verhaak, R., Cherniack, A. D., Watanabe, H., Dutt, A., Kwon, J., Chao, Y. S., Onofrio, R. C., Chiang, D., Yuza, Y., Kesari, S., & Meyerson, M. (2011). Glioblastoma-derived epidermal growth factor receptor carboxyl-terminal deletion mutants are transforming and are sensitive to EGFR-directed therapies. *Cancer Research*, *71*(24), 7587–7596. <https://doi.org/10.1158/0008-5472.CAN-11-0821>

Chou, C. W., Lin, C. H., Hsiao, T. H., Lo, C. C., Hsieh, C. Y., Huang, C. C., & Sher, Y. P. (2019). Therapeutic effects of statins against lung adenocarcinoma via p53 mutant-mediated apoptosis. *Scientific Reports*, *9*(1), 1–12. <https://doi.org/10.1038/s41598-019-56532-6>

Clements, V. K., Long, T., Long, R., Figley, C., Smith, D. M. C., & Ostrand-Rosenberg, S. (2018). High fat diet and leptin promote tumor progression by inducing myeloid-derived suppressor cells. *Journal of Leukocyte Biology*, *103*(3), 395–407. <https://doi.org/10.1002/JLB.4HI0517-210R>

Cong, J. (2020). Metabolism of Natural Killer Cells and Other Innate Lymphoid Cells. *Frontiers in Immunology*, *11*(August), 1–12. <https://doi.org/10.3389/fimmu.2020.01989>

Corbet, C., Bastien, E., Santiago de Jesus, J. P., Dierge, E., Martherus, R., Vander Linden, C., Doix, B., Degavre, C., Guilbaud, C., Petit, L., Michiels, C., Dessy, C., Larondelle, Y., & Feron, O. (2020). TGFβ2-induced formation of lipid droplets supports acidosis-driven EMT and the metastatic spreading of cancer cells. *Nature Communications*, *11*(1), 1–15. <https://doi.org/10.1038/s41467-019-14262-3>

Cox, J., & Mann, M. (2012). 1D and 2D annotation enrichment: a statistical method integrating quantitative proteomics with complementary high-throughput data. *BMC Bioinformatics*, *13* (Suppl(S12)). <https://doi.org/10.1186/1471-2105-13-S16-S12>

- Cubillos-Ruiz, J. R., Silberman, P. C., Rutkowski, M. R., Chopra, S., Perales-Puchalt, A., Song, M., Zhang, S., Bettigole, S. E., Gupta, D., Holcomb, K., Ellenson, L. H., Caputo, T., Lee, A. H., Conejo-Garcia, J. R., & Glimcher, L. H. (2015). ER Stress Sensor XBP1 Controls Anti-tumor Immunity by Disrupting Dendritic Cell Homeostasis. *Cell*, *161*(7), 1527–1538. <https://doi.org/10.1016/j.cell.2015.05.025>
- Cuiffo, B., & Ren, R. (2010). Palmitoylation of oncogenic NRAS is essential for leukemogenesis. *Blood*, *115*(17), 3598–3605. <https://doi.org/10.1182/blood-2009-03-213876>
- Da Poian, A. T., & Castanho, M. A. R. B. (2016). Integrative Human Biochemistry. In *Biochemist* (Vol. 38, Issue 4). Springer. <https://doi.org/10.1042/bio03804072>

- Dallavilla, T., Abrami, L., Sandoz, P. A., Savoglidis, G., Hatzimanikatis, V., & van der Goot, F. G. (2016). Model-Driven Understanding of Palmitoylation Dynamics: Regulated Acylation of the Endoplasmic Reticulum Chaperone Calnexin. *PLoS Computational Biology*, *12*(2). <https://doi.org/10.1371/journal.pcbi.1004774>
- DeBerardinis, R. J., Lum, J. J., Hatzivassiliou, G., & Thompson, C. B. (2008). The Biology of Cancer: Metabolic Reprogramming Fuels Cell Growth and Proliferation. *Cell Metabolism*, *7*(1), 11–20. <https://doi.org/10.1016/j.cmet.2007.10.002>
- Di Bello, E., Zwergel, C., Mai, A., & Valente, S. (2020). The Innovative Potential of Statins in Cancer: New Targets for New Therapies. *Frontiers in Chemistry*, *8*(June), 1–9. <https://doi.org/10.3389/fchem.2020.00516>
- Draper, J. M., & Smith, C. D. (2010). DHHC20: a human palmitoyl acyltransferase that causes cellular transformation. *Molecular Membrane Biology*, *27*(2–3), 123–136. <https://doi.org/10.3109/09687681003616854>
- Drisdell, R. C., & Green, W. N. (2004). Labeling and quantifying sites of protein palmitoylation. *BioTechniques*, *36*, 276–285.
- Drury, J., Rychahou, P. G., He, D., Jafari, N., Wang, C., Lee, E. Y., Weiss, H. L., Evers, B. M., & Zaytseva, Y. Y. (2020). Inhibition of Fatty Acid Synthase Upregulates Expression of CD36 to Sustain Proliferation of Colorectal Cancer Cells. *Frontiers in Oncology*, *10*(July). <https://doi.org/10.3389/fonc.2020.01185>
- Ducker, C. E., Stettler, E. M., French, K. J., Upson, J. J., & Smith, C. D. (2004). Huntingtin interacting protein 14 is an oncogenic human protein: Palmitoyl acyltransferase. *Oncogene*, *23*(57), 9230–9237. <https://doi.org/10.1038/sj.onc.1208171>
- Edmonds, M. J., Geary, B., Doherty, M. K., & Morgan, A. (2017). Analysis of the brain palmitoyl-proteome using both acyl-biotin exchange and acyl-resin-assisted capture methods. *Scientific Reports*, *7*(1), 1–13. <https://doi.org/10.1038/s41598-017-03562-7>
- Eisenberg, S., Laude, A. J., Beckett, A. J., Mageean, C. J., Aran, V., Hernandez-Valladares, M., Henis, Y. I., & Prior, I. A. (2013). The role of palmitoylation in regulating Ras localization and function. *Biochemical Society Transactions*, *41*(1), 79–83. <https://doi.org/10.1042/BST20120268>
- Eisinger, K. R. T., Woolfrey, K. M., Swanson, S. P., Schnell, S. A., Meitzen, J., Dell'Acqua, M., & Mermelstein, P. G. (2018). Palmitoylation of caveolin-1 is regulated by the same DHHC acyltransferases that modify steroid hormone receptors. *Journal of Biological Chemistry*, *293*(41), 15901–15911. <https://doi.org/10.1074/jbc.RA118.004167>
- Elia, I., Doglioni, G., & Fendt, S. M. (2018). Metabolic Hallmarks of Metastasis Formation. *Trends in Cell Biology*, *28*(8), 673–684. <https://doi.org/10.1016/j.tcb.2018.04.002>
- Else, P. L. (2020). The highly unnatural fatty acid profile of cells in culture. *Progress in Lipid Research*, *77*(April). <https://doi.org/10.1016/j.plipres.2019.101017>
- Emi, M., Fujiwara, Y., Ohata, H., Tsuda, H., Hirohashi, S., Koike, M., Miyaki, M., Monden, M. and Nakamura, Y. (1993). Allelic loss at chromosome band 8p21.3-p22 is associated with progression of hepatocellular carcinoma. *Genes Chromosomes Cancer*, *7*: 152-157. <https://doi.org/10.1002/gcc.2870070307>
- Ewertz, M., Jensen, M. B., Gunnarsdóttir, K. Á., Højris, I., Jakobsen, E. H., Nielsen, D., Stenbygaard, L. E., Tange, U. B., & Cold, S. (2011). Effect of obesity on prognosis after early-stage breast cancer. *Journal of Clinical Oncology*, *29*(1), 25–31. <https://doi.org/10.1200/JCO.2010.29.7614>
- Fahy, E., Subramaniam, S., Brown, H. A., Glass, C. K., Merrill, A. H., Murphy, R. C., Raetz, C. R. H., Russell, D. W., Seyama, Y., Shaw, W., Shimizu, T., Spener, F., Van Meer, G., VanNieuwenhze, M. S., White, S.

- H., Witztum, J. L., & Dennis, E. A. (2005). A comprehensive classification system for lipids. *Journal of Lipid Research*, 46(5), 839–861. <https://doi.org/10.1194/jlr.E400004-JLR200>
- Fairbank, M., Huang, K., El-Husseini, A., & Nabi, I. R. (2012). RING finger palmitoylation of the endoplasmic reticulum Gp78 E3 ubiquitin ligase. *FEBS Letters*, 586(16), 2488–2493. <https://doi.org/10.1016/j.febslet.2012.06.011>
- Fares, J., Fares, M. Y., Khachfe, H. H., Salhab, H. A., & Fares, Y. (2020). Molecular principles of metastasis: a hallmark of cancer revisited. *Signal Transduction and Targeted Therapy*, 5(1). <https://doi.org/10.1038/s41392-020-0134-x>
- Farge, T., Saland, E., Toni, F. De, Aroua, N., Fraisse, M., Scotland, S., Larrue, C., Boutzen, H., Cassant-sourdy, S., Broin, N., Iacovoni, J., Linares, L. K., Montersino, C., Castellano, R., Griessinger, E., Collete, Y., Duchamp, O., Barreira, Y., Hirsch, P., ... Sarry, J.-E. (2017). Chemotherapy Resistant Human Acute Myeloid Leukemia Cells are Not Enriched for Leukemic Stem Cells but Require Oxidative Metabolism. *Cancer Discovery*, 7(7), 716–735. <https://doi.org/10.1158/2159-8290.CD-16-0441>. Chemotherapy
- Farooq, I., & Bugshan, A. (2020). Oral squamous cell carcinoma: Metastasis, potentially associated malignant disorders, etiology and recent advancements in diagnosis. *F1000Research*, 9, 1–10. <https://doi.org/10.12688/f1000research.22941.1>
- Fatima, S., Hu, X., Huang, C., Zhang, W., Cai, J., Huang, M., Gong, R. H., Chen, M., Ho, A. H. M., Su, T., Wong, H. L. X., Bian, Z., & Kwan, H. Y. (2019). High-fat diet feeding and palmitic acid increase CRC growth in β 2AR-dependent manner. *Cell Death and Disease*, 10(711). <https://doi.org/10.1038/s41419-019-1958-6>
- Feigin, M. E., Akshinthala, S. D., Araki, K., Rosenberg, A. Z., Muthuswamy, L. B., Martin, B., Lehmann, B. D., Berman, H. K., Pietenpol, J. A., Cardiff, R. D., & Muthuswamy, S. K. (2014). Mislocalization of the cell polarity protein Scribble promotes mammary tumorigenesis and is associated with basal breast cancer. *Cancer Research*, 74(11), 3180–3194. <https://doi.org/10.1158/0008-5472.CAN-13-3415>. Mislocalization
- Feldman, J. L., Baeza, J., & Denu, J. M. (2013). Activation of the protein deacetylase SIRT6 by long-chain fatty acids and widespread deacylation by Mammalian Sirtuins. *Journal of Biological Chemistry*, 288(43), 31350–31356. <https://doi.org/10.1074/jbc.C113.511261>
- Fernández-Hernando, C., Fukata, M., Bernatchez, P. N., Fukata, Y., Lin, M. I., Bredt, D. S., & Sessa, W. C. (2006). Identification of Golgi-localized acyl transferases that palmitoylate and regulate endothelial nitric oxide synthase. *Journal of Cell Biology*, 174(3), 369–377. <https://doi.org/10.1083/jcb.200601051>
- [REDACTED]
- Feng, J., Dai, W., Mao, Y., Wu, L., Li, J., Chen, K., Yu, Q., Kong, R., Li, S., Zhang, J., Ji, J., Wu, J., Mo, W., Xu, X., & Guo, C. (2020). Simvastatin re-sensitizes hepatocellular carcinoma cells to sorafenib by inhibiting HIF-1 α /PPAR- γ /PKM2-mediated glycolysis. *Journal of Experimental and Clinical Cancer Research*, 39(1), 1–18. <https://doi.org/10.1186/s13046-020-1528-x>
- Feng, W. W., Wilkins, O., Bang, S., Ung, M., Li, J., An, J., Genio, C., Canfield, K., DiRenzo, J., Wells, W., Gaur, A., Robey, R. B., Guo, J. Y., Powles, R. L., Sotiriou, C., Puzstai, L., Febbraio, M., Cheng, C., Kinlaw, W. B., & Kurokawa, M. (2019). CD36-Mediated Metabolic Rewiring of Breast Cancer Cells Promotes Resistance to HER2- Targeted Therapies. *Cell Reports*, 29, 3405–3420.
- Ferraro, G. B., Ali, A., Luengo, A., Kodack, D. P., Deik, A., Abbott, K. L., Bezwada, D., Blanc, L., Prideaux, B., Jin, X., Possada, J. M., Chen, J., Chin, C. R., Amoozgar, Z., Ferreira, R., Chen, I. X., Naxerova, K., Ng, C., Westermarck, A. M., ... Vander Heiden, M. G. (2021). Fatty acid synthesis is required for breast cancer brain metastasis. *Nature Cancer*, 2(4), 414–428. <https://doi.org/10.1038/s43018-021-00183-y>
- Finucane, O. M., Lyons, C. L., Murphy, A. M., Reynolds, C. M., Klinger, R., Healy, N. P., Cooke, A. A., Coll, R. C., Mcallan, L., Nilaweera, K. N., Reilly, M. E. O., Tierney, A. C., Morine, M. J., Alcalá-díaz, J. F., Lopez-miranda, J., Connor, D. P. O., Neill, L. A. O., McGillicuddy, F. C., & Roche, H. M. (2015). Monounsaturated Fatty Acid – Enriched High-Fat Diets Impede Adipose NLRP3 Inflammasome – Mediated IL-1 b Secretion and Insulin Resistance Despite Obesity. *Diabetes*, 64, 2116–2128. <https://doi.org/10.2337/db14-1098>
- [REDACTED]
- Flavin, R., Peluso, S., Nguyen, P. L., & Loda, M. (2010). Fatty acid synthase as a potential therapeutic target in cancer. *Future Oncology*, 6(4), 551–562. <https://doi.org/10.2217/fon.10.11>. Fatty

Fontana, E., Eason, K., Cervantes, A., Salazar, R., & Sadanandam, A. (2019). Context matters - Consensus molecular subtypes of colorectal cancer as biomarkers for clinical trials. *Annals of Oncology*, 30(4), 520–527. <https://doi.org/10.1093/annonc/mdz052>

Fredericks, G. J., Hoffmann, F. K. W., Rose, A. H., Osterheld, H. J., Hess, F. M., Mercier, F., & Hoffmann, P. R. (2014). Stable expression and function of the inositol 1,4,5-triphosphate receptor requires palmitoylation by a DHHC6/selenoprotein K complex. *Proceedings of the National Academy of Sciences of the United States of America*, 111(46), 16478–16483. <https://doi.org/10.1073/pnas.1417176111>

Fujiwara, Y., Ohata, H., Emi, M., Okui, K., Koyama, K., Tsuchiya, E., Nakajima, T., Monden, M., Mori, T., Kurimasa, A., Oshimura, M. and Nakamura, Y. (1994), A 3-Mb physical map of the chromosome region 8p21.3-p22, including a 600-kb region commonly deleted in human hepatocellular carcinoma, colorectal cancer, and non-small cell lung cancer. *Genes Chromosom. Cancer*, 10: 7-14. <https://doi.org/10.1002/gcc.2870100103>

Fukata, M., Fukata, Y., Adesnik, H., Nicoll, R. A., & Brecht, D. S. (2004). Identification of PSD-95 palmitoylating enzymes. *Neuron*, 44(6), 987–996. <https://doi.org/10.1016/j.neuron.2004.12.005>

Fukata, Y., Murakami, T., Yokoi, N., & Fukata, M. (2016). Local Palmitoylation Cycles and Specialized Membrane Domain Organization. *Current Topics in Membranes*, 77, 97–141. <https://doi.org/10.1016/bs.ctm.2015.10.003>

Gao, F., Liu, C., Guo, J., Sun, W., Xian, L., Bai, D., Liu, H., Cheng, Y., Li, B., Cui, J., Zhang, C., & Cai, J. (2015). Radiation-driven lipid accumulation and dendritic cell dysfunction in cancer. *Scientific Reports*, 5(9613), 1–8. <https://doi.org/10.1038/srep09613>

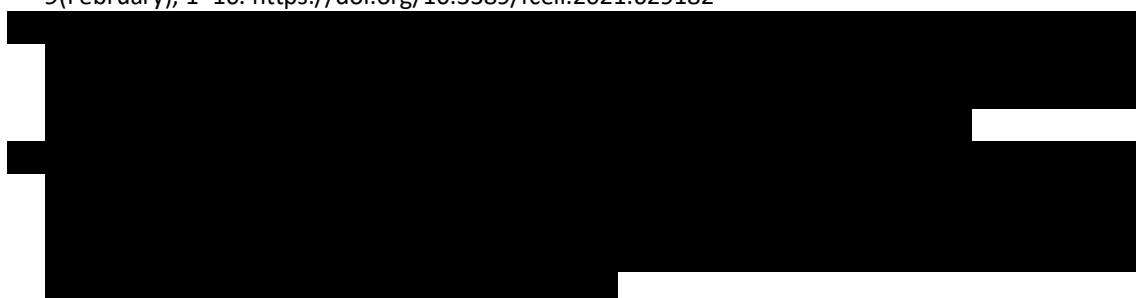
Garcia-Bermudez, J., Baudrier, L., Bayraktar, E. C., Shen, Y., La, K., Guarecuco, R., Yucel, B., Fiore, D., Tavora, B., Freinkman, E., Chan, S. H., Lewis, C., Min, W., Inghirami, G., Sabatini, D. M., & Birsoy, K. (2019). Squalene accumulation in cholesterol auxotrophic lymphomas prevents oxidative cell death. *Nature*, 567(118–122). <http://dx.doi.org/10.1038/s41586-019-0945-5>

Ganesh, K., Basnet, H., Kaygusuz, Y., Laughney, A. M., He, L., Sharma, R., O'Rourke, K. P., Reuter, V. P., Huang, Y. H., Turkecul, M., Er, E. E., Masilionis, I., Manova-Todorova, K., Weiser, M. R., Saltz, L. B., Garcia-Aguilar, J., Koche, R., Lowe, S. W., Pe'er, D., ... Massagué, J. (2020). L1CAM defines the regenerative origin of metastasis-initiating cells in colorectal cancer. *Nature Cancer*, 1(1), 28–45. <https://doi.org/10.1038/s43018-019-0006-x>

Ganesh, K., & Massagué, J. (2021). Targeting metastatic cancer. *Nature Medicine*, 27, 34–44. <https://doi.org/10.1126/scisignal.abi4338>

Ghazalpour, A., Bennett, B., Petyuk, V. A., Orozco, L., Hagopian, R., Mungrue, I. N., Farber, C. R., Sinsheimer, J., Kang, H. M., Furlotte, N., Park, C. C., Wen, P. Z., Brewer, H., Weitz, K., Camp, D. G., Pan,

- C., Yordanova, R., Neuhaus, I., Tilford, C., ... Lusic, A. J. (2011). Comparative analysis of proteome and transcriptome variation in mouse. *PLoS Genetics*, 7(6). <https://doi.org/10.1371/journal.pgen.1001393>
- Giannoni, E., Buricchi, F., Grimaldi, G., Parri, M., Cialdai, F., Taddei, M. L., Raugei, G., Ramponi, G., & Chiarugi, P. (2008). Redox regulation of anoikis: Reactive oxygen species as essential mediators of cell survival. *Cell Death and Differentiation*, 15(5), 867–878. <https://doi.org/10.1038/cdd.2008.3>
- Gilmore, A. P. (2005). Anoikis. *Cell Death and Differentiation*, 12, 1473–1477. <https://doi.org/10.1038/sj.cdd.4401723>
- Gimple, R. C., Kidwell, R. L., Kim, L. J. Y., Sun, T., Gromovsky, A. D., Wu, Q., Wolf, M., Lv, D., Bhargava, S., Jiang, L., Prager, B. C., Wang, X., Ye, Q., Zhu, Z., Zhang, G., Dong, Z., Zhao, L., Lee, D., Bi, J., ... Rich, J. N. (2019). Glioma stem cell-specific superenhancer promotes polyunsaturated fatty-acid synthesis to support EGFR signaling. *Cancer Discovery*, 9(9), 1248–1267. <https://doi.org/10.1158/2159-8290.CD-19-0061>
- Giulitti, F., Petrunaro, S., Mandatori, S., Tomaipitnca, L., de Franchis, V., D'Amore, A., Filippini, A., Gaudio, E., Ziparo, E., & Giampietri, C. (2021). Anti-tumor Effect of Oleic Acid in Hepatocellular Carcinoma Cell Lines via Autophagy Reduction. *Frontiers in Cell and Developmental Biology*, 9(February), 1–16. <https://doi.org/10.3389/fcell.2021.629182>



- Gong, J., Lin, Y., Zhang, H., Liu, C., Cheng, Z., Yang, X., Zhang, J., Xiao, Y., Sang, N., Qian, X., Wang, L., Cen, X., Du, X., & Zhao, Y. (2020). Reprogramming of lipid metabolism in cancer-associated fibroblasts potentiates migration of colorectal cancer cells. *Cell Death and Disease*, 11(4). <https://doi.org/10.1038/s41419-020-2434-z>
- González Montoro, A., Quiroga, R., Maccioni, H. J. F., & Valdéz Taubas, J. (2009). A novel motif at the C-terminus of palmitoyltransferases is essential for Swf1 and Pfa3 function in vivo. *Biochemical Journal*, 419(2), 301–308. <https://doi.org/10.1042/BJ20080921>
- Gorleku, O. A., Barns, A. M., Prescott, G. R., Greaves, J., & Chamberlain, L. H. (2011). Endoplasmic reticulum localization of DHHC palmitoyltransferases mediated by lysine-based sorting signals. *Journal of Biological Chemistry*, 286(45), 39573–39584. <https://doi.org/10.1074/jbc.M111.272369>
- Gottlieb, C. D., Zhang, S., & Linder, M. E. (2015). The cysteine-rich domain of the DHHC3 palmitoyltransferase is palmitoylated and contains tightly bound zinc. *Journal of Biological Chemistry*, 290(49), 29259–29269. <https://doi.org/10.1074/jbc.M115.691147>
- Greaves, J., & Chamberlain, L. H. (2011). DHHC palmitoyl transferases: Substrate interactions and (patho)physiology. *Trends in Biochemical Sciences*, 36(5), 245–253. <https://doi.org/10.1016/j.tibs.2011.01.003>
- Greaves, J., Gorleku, O. A., Salaun, C., & Chamberlain, L. H. (2010). Palmitoylation of the SNAP25 protein family: Specificity and regulation by DHHC palmitoyl transferases. *Journal of Biological Chemistry*, 285(32), 24629–24638. <https://doi.org/10.1074/jbc.M110.119289>
- Greaves, J., Munro, K. R., Davidson, S. C., Riviere, M., Wojno, J., Smith, T. K., Tomkinson, N. C. O., & Chamberlain, L. H. (2017). Molecular basis of fatty acid selectivity in the zDHHC family of S-acyltransferases revealed by click chemistry. *Proceedings of the National Academy of Sciences of the United States of America*, 114(8), E1365–E1374. <https://doi.org/10.1073/pnas.1612254114>
- Groot, S., Lugtenberg, R. T., Cohen, D., Welters, M. J. P., Ehsan, I., Vreeswijk, M. P. G., Smit, V. T. H. B. M., de Graaf, H., Heijns, J. B., Portielje, J. E. A., van de Wouw, A. J., Imholz, A. L. T., Kessels, L. W., Vrijaldenhoven, S., Baars, A., Kranenbarg, E. M. K., Carpentier, M. D. de, Putter, H., van der Hoeven, J. J. M., ... Kroep, J. R. (2020). Fasting mimicking diet as an adjunct to neoadjuvant chemotherapy for breast cancer in the multicentre randomized phase 2 DIRECT trial. *Nature Communications*, 11(1), 1–9. <https://doi.org/10.1038/s41467-020-16138-3>
- Guerrero-Ros, I., Clement, C. C., Reynolds, C. A., Patel, B., Santambrogio, L., Cuervo, A. M., & Macian, F. (2020). The negative effect of lipid challenge on autophagy inhibits T cell responses. *Autophagy*, 16(2), 223–238. <https://doi.org/10.1080/15548627.2019.1606635>

- Guo, W., Abudumijiti, H., Xu, L., & Hasim, A. (2019). CD147 promotes cervical cancer migration and invasion by up-regulating fatty acid synthase expression. *International Journal of Clinical and Experimental Pathology*, *12*(12), 4280–4288. <http://www.ncbi.nlm.nih.gov/pubmed/31933828><http://www.pubmedcentral.nih.gov/articlerender.fcgi?artid=PMC6949868>
- Gupta, G. P., & Massagué, J. (2006). Cancer Metastasis: Building a Framework. *Cell*, *127*(4), 679–695. <https://doi.org/10.1016/j.cell.2006.11.001>
- Gupta, P., Soyombo, A. A., Atashband, A., Wisniewski, K. E., Shelton, J. M., Richardson, J. A., Hammer, R. E., & Hofmann, S. L. (2001). Disruption of PPT1 or PPT2 causes neuronal ceroid lipofuscinosis in knockout mice. *Proceedings of the National Academy of Sciences of the United States of America*, *98*(24), 13566–13571. <https://doi.org/10.1073/pnas.251485198>
- Haag, S. M., Gulen, M. F., Reymond, L., Gibelin, A., Abrami, L., Decout, A., Heymann, M., Goot, F. G. Van Der, Turcatti, G., Behrendt, R., & Ablasser, A. (2018). Targeting STING with covalent small-molecule inhibitors. *Nature*, *559*(7713), 269–273. <https://doi.org/10.1038/s41586-018-0287-8>
- Hale, M., Itani, F., Buchta, C. M., Wald, G., Bing, M., & Norian, L. A. (2015). Obesity triggers enhanced MDSC accumulation in murine renal tumors via elevated local production of CCL2. *PLoS ONE*, *10*(3), 1–15. <https://doi.org/10.1371/journal.pone.0118784>
- Han, J., Qu, H., Han, M., Ding, Y., Xie, M., Hu, J., Chen, Y., & Dong, H. (2020). MSC-induced lncRNA AGAP2-AS1 promotes stemness and trastuzumab resistance through regulating CPT1 expression and fatty acid oxidation in breast cancer. *Oncogene*.
- Hanahan, D., & Weinberg, R. A. (2000). The hallmarks of cancer. *Cell*, *100*(1), 57–70. [https://doi.org/10.1016/S0092-8674\(00\)81683-9](https://doi.org/10.1016/S0092-8674(00)81683-9)
- Hanahan, D., & Weinberg, R. A. (2011). Hallmarks of cancer: The next generation. *Cell*, *144*(5), 646–674. <https://doi.org/10.1016/j.cell.2011.02.013>
- Hancock JF, Paterson H, Marshall CJ. A polybasic domain or palmitoylation is required in addition to the CAAX motif to localize p21ras to the plasma membrane. *Cell*. 1990 Oct 5;63(1):133-9. doi: 10.1016/0092-8674(90)90294-o. PMID: 2208277.
- Hannoush, R. N., & Arenas-Ramirez, N. (2009). Imaging the Lipidome: w-Alkynyl Fatty Acids for Detection and Cellular Visualization of Lipid-Modified Proteins. *ACS Chemical Biology*, *4*(7), 581–587.
- Hannun, Y. A., & Obeid, L. M. (2018). Sphingolipids and their metabolism in physiology and disease. *Nature Reviews Molecular Cell Biology*, *19*(3), 175–191. <https://doi.org/10.1038/nrm.2017.107>
- Hao, J. W., Wang, J., Guo, H., Zhao, Y. Y., Sun, H. H., Li, Y. F., Lai, X. Y., Zhao, N., Wang, X., Xie, C., Hong, L., Huang, X., Wang, H. R., Li, C. Bin, Liang, B., Chen, S., & Zhao, T. J. (2020). CD36 facilitates fatty acid uptake by dynamic palmitoylation-regulated endocytosis. *Nature Communications*, *11*(1), 1–16. <https://doi.org/10.1038/s41467-020-18565-8>
- Hardy, S., Langelier, Y., & Prentki, M. (2000). Oleate activates phosphatidylinositol 3-kinase and promotes proliferation and reduces apoptosis of MDA-MB-231 breast cancer cells, whereas palmitate has opposite effects. *Cancer Research*, *60*(22), 6353–6358.
- Henique, C., Mansouri, A., Fumey, G., Lenoir, V., Girard, J., Bouillaud, F., Prip-Buus, C., & Cohen, I. (2010). Increased mitochondrial fatty acid oxidation is sufficient to protect skeletal muscle cells from palmitate-induced apoptosis. *Journal of Biological Chemistry*, *285*(47), 36818–36827. <https://doi.org/10.1074/jbc.M110.170431>
- Hernandez, J. L., Davda, D., Cheung See Kit, M., Majmudar, J. D., Won, S. J., Gang, M., Pasupuleti, S. C., Choi, A. I., Bartkowiak, Ca. M., & Martin, B. R. (2017). APT2 inhibition restores Scribble localization and S- palmitoylation in Snail-transformed cells. *Cell Chemical Biology*, *24*(1), 87–97. <https://doi.org/10.1016/j.chembiol.2016.12.007>
- Hirano, T., Kishi, M., Sugimoto, H., Taguchi, R., Obinata, H., Ohshima, N., Tatei, K., & Izumi, T. (2009). Thioesterase activity and subcellular localization of acylprotein thioesterase 1/lysophospholipase 1.

- Biochimica et Biophysica Acta - Molecular and Cell Biology of Lipids*, 1791(8), 797–805. <https://doi.org/10.1016/j.bbalip.2009.05.001>
- Hishikawa, D., Hashidate, T., Shimizu, T., & Shindou, H. (2014). Diversity and function of membrane glycerophospholipids generated by the remodeling pathway in mammalian cells. *Journal of Lipid Research*, 55(5), 799–807. <https://doi.org/10.1194/jlr.R046094>
- Hoogendijk, A. J., Pourfarzad, F., Aarts, C. E. M., Tool, A. T. J., Hiemstra, I. H., Grassi, L., Frontini, M., Meijer, A. B., van den Biggelaar, M., & Kuijpers, T. W. (2019). Dynamic Transcriptome-Proteome Correlation Networks Reveal Human Myeloid Differentiation and Neutrophil-Specific Programming. *Cell Reports*, 29(8), 2505–2519. <https://doi.org/10.1016/j.celrep.2019.10.082>
- Hossain, F., Al-Khami, A. A., Wyczechowska, D., Hernandez, C., Zheng, L., Reiss, K., Del Valle, L., Trillo-Tinoco, J., Maj, T., Zou, W., Rodriguez, P. C., & Ochoa, A. C. (2015). Inhibition of Fatty Acid Oxidation Modulates Immunosuppressive Functions of Myeloid-Derived Suppressor Cells and Enhances Cancer Therapies. *Cancer Immunology Research*, 3(11), 1236–1247. <https://doi.org/10.1158/2326-6066.CIR-15-0036>
- Hou, H., John Peter, A. T., Meiringer, C., Subramanian, K., & Ungermann, C. (2009). Analysis of DHHC acyltransferases implies overlapping substrate specificity and a two-step reaction mechanism. *Traffic*, 10(8), 1061–1073. <https://doi.org/10.1111/j.1600-0854.2009.00925.x>
- Houten, S. M., & Wanders, R. J. A. (2010). A general introduction to the biochemistry of mitochondrial fatty acid β -oxidation. *Journal of Inherited Metabolic Disease*, 33(5), 469–477. <https://doi.org/10.1007/s10545-010-9061-2>
- Howie, D., Bokum, A. Ten, Necula, A. S., Cobbold, S. P., & Waldmann, H. (2018). The role of lipid metabolism in T lymphocyte differentiation and survival. *Frontiers in Immunology*, 8(JAN). <https://doi.org/10.3389/fimmu.2017.01949>
- Huang, K., Sanders, S., Singaraja, R., Orban, P., Cijssouw, T., Arstikaitis, P., Yanai, A., Hayden, M. R., & El-Husseini, A. (2009). Neuronal palmitoyl acyl transferases exhibit distinct substrate specificity. *The FASEB Journal*, 23(8), 2605–2615. <https://doi.org/10.1096/fj.08-127399>
- Huang, K., Yanai, A., Kang, R., Arstikaitis, P., Singaraja, R. R., Metzler, M., Mullard, A., Haigh, B., Gauthier-Campbell, C., Gutekunst, C. A., Hayden, M. R., & El-Husseini, A. (2004). Huntingtin-interacting protein HIP14 is a palmitoyl transferase involved in palmitoylation and trafficking of multiple neuronal proteins. *Neuron*, 44(6), 977–986. <https://doi.org/10.1016/j.neuron.2004.11.027>
- Hungermann, D., Schmidt, H., Natrajan, R., Tidow, N., Poos, K., Reis-Filho, J. S., Brandt, B., Buerger, H., & Korsching, E. (2011). Influence of whole arm loss of chromosome 16q on gene expression patterns in oestrogen receptor-positive, invasive breast cancer. *Journal of Pathology*, 224(4), 517–528. <https://doi.org/10.1002/path.2938>
- Imielinski, M., Berger, A. H., Hammerman, P. S., Hernandez, B., Pugh, T. J., Hodis, E., Cho, J., Suh, J., Capelletti, M., Sivachenko, A., Sougnez, C., Auclair, D., Lawrence, M. S., Stojanov, P., Cibulskis, K., Choi, K., De Waal, L., Sharifnia, T., Brooks, A., ... Meyerson, M. (2012). Mapping the hallmarks of lung adenocarcinoma with massively parallel sequencing. *Cell*, 150(6), 1107–1120. <https://doi.org/10.1016/j.cell.2012.08.029>
- Injarabian, L., Devin, A., Ransac, S., & Marteyn, B. S. (2020). Neutrophil metabolic shift during their lifecycle: Impact on their survival and activation. *International Journal of Molecular Sciences*, 21(287), 1–23. <https://doi.org/10.3390/ijms21010287>
- Janda, C. Y., Waghay, D., Levin, A. M., Thomas, C., & Garcia, K. C. (2012). Structural basis of Wnt recognition by frizzled. *Science*, 336(6090), 59–64. <https://doi.org/10.1126/science.1222879>
- Janes, P. W., Ley, S. C., & Magee, A. I. (1999). Aggregation of lipid rafts accompanies signaling via the T cell antigen receptor. *Journal of Cell Biology*, 147(2), 447–461. <https://doi.org/10.1083/jcb.147.2.447>
- Jayawardhana, A. M. D. S., Stilgenbauer, M., Datta, P., Qiu, Z., McKenzie, S., Wang, H., Bowers, D., Kurokawa, M., & Zheng, Y. R. (2020). Fatty acid-like Pt(IV) prodrugs overcome cisplatin resistance in ovarian cancer by harnessing CD36. *Chemical Communications*, 56(73), 10706–10709. <https://doi.org/10.1039/d0cc02174a>
- Jennings, B. C., & Linder, M. E. (2012). DHHC protein S-acyltransferases use similar ping-pong kinetic mechanisms but display different Acyl-CoA specificities. *Journal of Biological Chemistry*, 287(10), 7236–7245. <https://doi.org/10.1074/jbc.M111.337246>
- Jiang, H., Khan, S., Wang, Y., Charron, G., He, B., Sebastian, C., Du, J., Kim, R., Ge, E., Mostoslavsky, R., Hang, H. C., Hao, Q., & Lin, H. (2013). SIRT6 regulates TNF- α secretion through hydrolysis of long-chain fatty acyl lysine. *Nature*, 496(7443), 110–113. <https://doi.org/10.1038/nature12038>

- Jiang, X., Stockwell, B. R., & Conrad, M. (2021). Ferroptosis: mechanisms, biology and role in disease. *Nature Reviews Molecular Cell Biology*, 22(4), 266–282. <https://doi.org/10.1038/s41580-020-00324-8>
- Jin, X., Demere, Z., Nair, K., Ali, A., Ferraro, G. B., Natoli, T., Deik, A., Petronio, L., Tang, A. A., Zhu, C., Wang, L., Rosenberg, D., Mangena, V., Roth, J., Chung, K., Jain, R. K., Clish, C. B., Vander Heiden, M. G., & Golub, T. R. (2020). A metastasis map of human cancer cell lines. *Nature*, 588(7837), 331–336. <https://doi.org/10.1038/s41586-020-2969-2>
- Johnson, D. E., Burtness, B., Leemans, C. R., Wai, V., Lui, Y., Bauman, J. E., & Grandis, J. R. (2020). Head and neck squamous cell carcinoma Daniel. *Nature Reviews*, 6(92).
- Jovanovic, M., Rooney, M. S., Mertins, P., Przybylski, D., Satija, R., Rodriguez, E. H., Fields, A. P., Raychowdhury, R., Mumbach, M. R., Eisenhaure, T., Gennert, D., Lu, D., Delorey, T., Weissman, J. S., Carr, S. A., Hacohen, N., & Regev, A. (2015). Dynamic profiling of the protein life cycle in response to pathogens. *Science*, 347(6226), 1–16. <https://doi.org/10.1126/science.1259038>
- Jung, S., Lee, S., Lee, H., Yoon, J., & Lee, E. K. (2016). Oleic acid-embedded nanoliposome as a selective tumoricidal agent. *Colloids and Surfaces B: Biointerfaces*, 146, 585–589. <https://doi.org/10.1016/j.colsurfb.2016.06.058>
- Kabouridis, P. S. (2006). Lipid rafts in T cell receptor signalling. *Molecular Membrane Biology*, 23(1), 49–57. <https://doi.org/10.1080/09687860500453673>
- Kado, T., Nawaz, A., Takikawa, A., Usui, I., & Tobe, K. (2019). Linkage of CD8+ T cell exhaustion with high-fat diet-induced tumourigenesis. *Scientific Reports*, 9(1), 1–8. <https://doi.org/10.1038/s41598-019-48678-0>
- Kakimoto, P. A., Serna, J. D. C., de Miranda Ramos, V., Zorzano, A., & Kowaltowski, A. J. (2021). Increased glycolysis is an early consequence of palmitate lipotoxicity mediated by redox signaling. *Redox Biology*, 45. <https://doi.org/10.1016/j.redox.2021.102026>
- Kakugawa, S., Langton, P. F., Zebisch, M., Howell, S., Liu, Y., Feizi, T., Bineva, G., Reilly, N. O., Snijders, A. P., Jones, Y., & Vincent, J. (2015). Notum deacylates Wnts to suppress signalling activity Europe PMC Funders Author Manuscripts. *Nature*, 519(7542), 187–192. <https://doi.org/10.1038/nature14259>
- Kanno, T., Nakajima, T., Yokoyama, S., Asou, H. K., Sasamoto, S., Kamii, Y., Hayashizaki, K., Ouchi, Y., Onodera, T., Takahashi, Y., Ikeda, K., Hasegawa, Y., Kinjo, Y., Ohara, O., Nakayama, T., & Endo, Y. (2021). SCD2-mediated monounsaturated fatty acid metabolism regulates cGAS-STING-dependent type I IFN responses in CD4+ T cells. *Communications Biology*, 4(1), 1–14. <https://doi.org/10.1038/s42003-021-02310-y>
- Kaplan, M. J., & Radic, M. (2012). Neutrophil Extracellular Traps: Double-Edged Swords of Innate Immunity. *The Journal of Immunology*, 189(6), 2689–2695. <https://doi.org/10.4049/jimmunol.1201719>
- Kathayat, R. S., Cao, Y., Elvira, P. D., Sandoz, P. A., Zaballa, M. E., Springer, M. Z., Drake, L. E., Macleod, K. F., Van Der Goot, F. G., & Dickinson, B. C. (2018). Active and dynamic mitochondrial S-depalmitoylation revealed by targeted fluorescent probes. *Nature Communications*, 9(1). <https://doi.org/10.1038/s41467-017-02655-1>
- Kebede, A. F., Nieborak, A., Shahidian, L. Z., Le Gras, S., Richter, F., Gómez, D. A., Baltissen, M. P., Meszaros, G., De Fatima Magliarelli, H., Taudt, A., Margueron, R., Colomé-Tatché, M., Ricci, R., Daujat, S., Vermeulen, M., Mittler, G., & Schneider, R. (2017). Histone propionylation is a mark of active chromatin. *Nature Structural and Molecular Biology*, 24(12), 1048–1056. <https://doi.org/10.1038/nsmb.3490>
- Kennedy, D., Samali, A., & Jäger, R. (2015). Methods for Studying ER Stress and UPR Markers in Human Cells. In *Stress responses* (pp. 3–18). <https://doi.org/10.1201/9781420051414.ch3>

- Kim, S., Dye, L., & Mukherjee, A. B. (2008). Palmitoyl protein thioesterase-1 deficiency impairs synaptic vesicle recycling at nerve terminals, contributing to neuropathology in humans and mice. *Journal of Clinical Investigations*, *118*(9), 3075–3086. <https://doi.org/10.1172/JCI33482>
- Kim, Y. G., Eun, J. S., Seo, J., Lee, K. J., Lee, H. S., Hwang, I., Whiteway, M., Sacher, M., & Oh, B. H. (2005). Crystal structure of bet3 reveals a novel mechanism for Golgi localization of tethering factor TRAPP. *Nature Structural and Molecular Biology*, *12*(1), 38–45. <https://doi.org/10.1038/nsmb871>
- Kim, H. M., Lee, Y. K., Kim, E. S., & Koo, J. S. (2020). Energy transfer from adipocytes to cancer cells in breast cancer. *Neoplasia*, *67*(5), 992–1001. <https://doi.org/10.4149/>

- Klement, R. J., & Champ, C. E. (2014). Calories, carbohydrates, and cancer therapy with radiation: Exploiting the five R's through dietary manipulation. *Cancer and Metastasis Reviews*, *33*(1). <https://doi.org/10.1007/s10555-014-9495-3>
- Ko, P., & Dixon, S. J. (2018). Protein palmitoylation and cancer. *EMBO Reports*, 1–14.
- Koh, S., Lee, W., Park, S. M., & Kim, S. H. (2021). Caveolin-1 deficiency impairs synaptic transmission in hippocampal neurons. *Molecular Brain*, *14*(1), 1–10. <https://doi.org/10.1186/s13041-021-00764-z>
- Koike, Y., Yozaki, M., Utani, A., & Murota, H. (2020). Fibroblast growth factor 2 accelerates the epithelial–mesenchymal transition in keratinocytes during wound healing process. *Scientific Reports*, *10*(1), 1–13. <https://doi.org/10.1038/s41598-020-75584-7>
- Kong, E., Peng, S., Chandra, G., Sarkar, C., Zhang, Z., Bagh, M. B., & Mukherjee, A. B. (2013). Dynamic palmitoylation links cytosol-membrane shuttling of acyl-protein thioesterase-1 and acyl-protein thioesterase-2 with that of proto-oncogene H-Ras product and growth-associated protein-43. *Journal of Biological Chemistry*, *288*(13), 9112–9125. <https://doi.org/10.1074/jbc.M112.421073>
- Korycka, J., Łach, A., Heger, E., Bogusławska, D. M., Wolny, M., Toporkiewicz, M., Augoff, K., Korzeniewski, J., & Sikorski, A. F. (2012). Human DHHC proteins: A spotlight on the hidden player of palmitoylation. *European Journal of Cell Biology*, *91*(2), 107–117. <https://doi.org/10.1016/j.ejcb.2011.09.013>
- Koster, K. P., & Yoshii, A. (2019). Depalmitoylation by palmitoyl-protein thioesterase 1 in neuronal health and degeneration. *Frontiers in Synaptic Neuroscience*, *11*(AUG), 1–10. <https://doi.org/10.3389/fnsyn.2019.00025>
- Koudhi, S., Elgaai, A. B., & Chouaib, S. (2017). Impact of metabolism on T-cell differentiation and function and cross talk with tumor microenvironment. *Frontiers in Immunology*, *8*, 1–13. <https://doi.org/10.3389/fimmu.2017.00270>

- Kuczynski, E. A., Vermeulen, P. B., Pezzella, F., Kerbel, R. S., & Reynolds, A. R. (2019). Vessel co-option in cancer. *Nature Reviews Clinical Oncology*, *16*, 469–493.
- Kümmel, D., Heinemann, U., & Veit, M. (2006). Unique self-palmitoylation activity of the transport protein particle component Bet3: A mechanism required for protein stability. *Proceedings of the National Academy of Sciences of the United States of America*, *103*(34), 12701–12706. <https://doi.org/10.1073/pnas.0603513103>
- Ladanyi, A., Mukherjee, A., Kenny, H. A., Johnson, A., Mitra, A. K., Sundaresan, S., Nieman, K. M., Pascual, G., Benitah, S. A., Montag, A., Yamada, S. D., Abumrad, N. A., & Lengyel, E. (2018). Adipocyte-induced CD36 expression drives ovarian cancer progression and metastasis. *Oncogene*, *37*(17), 2285–2301. <https://doi.org/10.1038/s41388-017-0093-z>
- Lakkaraju, A. K. K., Abrami, L., Lemmin, T., Blaskovic, S., Kunz, B., Kihara, A., Dal Peraro, M., & Van Der Goot, F. G. (2012). Palmitoylated calnexin is a key component of the ribosome-translocon complex. *EMBO Journal*, *31*(7), 1823–1835. <https://doi.org/10.1038/emboj.2012.15>
- Lambert, A. W., Pattabiraman, D. R., & Weinberg, R. A. (2017). Emerging Biological Principles of Metastasis. *Cell*, *168*(4), 670–691. <https://doi.org/10.1016/j.cell.2016.11.037>
- Landberg, N., Palffy, S. Von, Askmyr, M., Lilljebjörn, H., Sandén, C., Rissler, M., Mustjoki, S., Hjorth-hansen, H., Richter, J., Ågerstam, H., Järås, M., & Fioretos, T. (2018). CD36 defines primitive chronic myeloid targeting vulnerable to antibody-based therapeutic leukemia cells less responsive to imatinib but

- vulnerable to antibody-based therapeutic targeting. *Hematologica*, 103(3), 447–455. <https://doi.org/10.3324/haematol.2017.169946>
- Latz, E., Xiao, S. T., & Stutz, A. (2013). Activation and regulation of the inflammasomes. *Nature Reviews Immunology*, 13(6), 1–7. <https://doi.org/10.1038/nri3452>
- Lauby-Secretan, B., Ph, D., Scoccianti, C., Ph, D., Loomis, D., & Ph, D. (2016). Body Fatness and Cancer — Viewpoint of the IARC Working Group. *New England Journal of Medicine*, 375(8), 794–798.
- Lee, C., Jeong, S., Jang, C., Bae, H., Kim, Y. H., Park, I., Kim, S. K., & Koh, G. Y. (2019). Tumor metastasis to lymph nodes requires YAP-dependent metabolic adaptation. *Science*, 363(6427), 644–649. <https://doi.org/10.1126/science.aav0173>
- Lee, H., Woodman, S. E., Engelman, J. A., Volonte, D., Galbiati, F., Kaufman, H. L., Lublin, D. M., & Lisanti, M. P. (2001). Palmitoylation of Caveolin-1 at a Single Site (Cys-156) Controls its Coupling to the c-Src Tyrosine Kinase. *Journal of Biological Chemistry*, 276(37), 35150–35158. <https://doi.org/10.1074/jbc.M104530200>
- Levental, I., Levental, K. R., & Heberle, F. A. (2020). Lipid Rafts: Controversies Resolved, Mysteries Remain. *Trends in Cell Biology*, 30(5), 341–353. <https://doi.org/10.1016/j.tcb.2020.01.009>
- Lévesque, S., Pol, J. G., Ferrere, G., Galluzzi, L., Zitvogel, L., & Kroemer, G. (2019). Trial watch: dietary interventions for cancer therapy. *Oncotarget*, 10(8), 1591878. <https://doi.org/10.1080/2162402X.2019.1591878>
- Li, S., Wu, T., Lu, Y. X., Wang, J. X., Yu, F. H., Yang, M. Z., Huang, Y. J., Li, Z. J., Wang, S. L., Huang, L., Lu, L., & Tian, T. (2020). Obesity promotes gastric cancer metastasis via diacylglycerol acyltransferase 2-dependent lipid droplets accumulation and redox homeostasis. *Redox Biology*, 36(May). <https://doi.org/10.1016/j.redox.2020.101596>
- Liberti, M. V., & Locasale, J. W. (2016). The Warburg Effect: How Does it Benefit Cancer Cells? *Trends in Biochemical Sciences*, 41(3), 211–218. <https://doi.org/10.1016/j.tibs.2015.12.001>
- Lim, S. A., Wei, J., Nguyen, T. L. M., Shi, H., Su, W., Palacios, G., Dhungana, Y., Chapman, N. M., Long, L., Saravia, J., Vogel, P., & Chi, H. (2021). Lipid signalling enforces functional specialization of Treg cells in tumours. *Nature*, 591(7849), 306–311. <https://doi.org/10.1038/s41586-021-03235-6>
- Lin, D. T. S., & Conibear, E. (2015). ABHD17 proteins are novel protein depalmitoylases that regulate N-Ras palmitate turnover and subcellular localization. *ELife*, 4(DECEMBER2015), 1–14. <https://doi.org/10.7554/eLife.11306>
- Lindhout, F. W., Kooistra, R., Portegies, S., Herstel, L. J., Stucchi, R., Snoek, B. L., Altelaar, A. M., Macgillavry, H. D., Wierenga, C. J., & Hoogenraad, C. C. (2020). Quantitative mapping of transcriptome and proteome dynamics during polarization of human ipsc-derived neurons. *ELife*, 9, 1–25. <https://doi.org/10.7554/ELIFE.58124>
- Liotti, A., Cosimato, V., Mirra, P., Cali, G., Conza, D., Secondo, A., Luongo, G., Terracciano, D., Formisano, P., Beguinot, F., Insabato, L., & Ulianich, L. (2018). Oleic acid promotes prostate cancer malignant phenotype via the G protein-coupled receptor FFA1/GPR40. *Journal of Cellular Physiology*, 233(9), 7367–7378. <https://doi.org/10.1002/jcp.26572>
- Listenberger, L. L., Han, X., Lewis, S. E., Cases, S., Farese, R. V., Ory, D. S., & Schaffer, J. E. (2003). Triglyceride accumulation protects against fatty acid-induced lipotoxicity. *Proceedings of the National Academy of Sciences of the United States of America*, 100(6), 3077–3082. <https://doi.org/10.1073/pnas.0630588100>
- Liu, X., Hartman, C. L., Li, L., Albert, C. J., Si, F., Gao, A., Huang, L., Zhao, Y., Lin, W., Hsueh, E. C., Shen, L., Shao, Q., Hoft, D. F., Ford, D. A., & Peng, G. (2021). Reprogramming lipid metabolism prevents effector

- Markovic, J., Borrás, C., Ortega, Á., Sastre, J., Viña, J., & Pallardó, F. V. (2007). Glutathione is recruited into the nucleus in early phases of cell proliferation. *Journal of Biological Chemistry*, *282*(28), 20416–20424. <https://doi.org/10.1074/jbc.M609582200>
- Marro, M., Nieva, C., De Juan, A., & Sierra, A. (2018). Unravelling the Metabolic Progression of Breast Cancer Cells to Bone Metastasis by Coupling Raman Spectroscopy and a Novel Use of Mcr-Als Algorithm. *Analytical Chemistry*, *90*(9), 5594–5602. <https://doi.org/10.1021/acs.analchem.7b04527>
- Martin, B. R., & Cravatt, B. F. (2009). Large-scale profiling of protein palmitoylation in mammalian cells. *Nature Methods*, *6*(2), 135–138. <https://doi.org/10.1038/nmeth.1293>
- Martin, L. J., Li, Q., Melnichouk, O., Greenberg, C., Minkin, S., Hislop, G., & Boyd, N. F. (2011). A randomized trial of dietary intervention for breast cancer prevention. *Cancer Research*, *71*(1), 123–133. <https://doi.org/10.1158/0008-5472.CAN-10-1436>
- Martin, B. R., Wang, C., Adibekian, A., Tully, S. E., & Benjamin, F. (2012). Global profiling of dynamic protein palmitoylation. *Nature Methods*, *9*(1), 84–89. <https://doi.org/10.1038/nmeth.1769>
- Martin-Perez, M., Urdiroz-Urricelqui, U., Bigas, C., & Benitah, S. A. (2021). Lipid metabolism in metastasis and therapy. *Current Opinion in Systems Biology*, *28*(100401). <https://doi.org/10.1016/j.coisb.2021.100401>
- [REDACTED]
- Massagué, J., & Ganesh, K. (2021). Metastasis-initiating cells and ecosystems. *Cancer Discovery*, *11*(4), 971–994. <https://doi.org/10.1158/2159-8290.CD-21-0010>
- [REDACTED]
- Mattiuzzi, C., & Lippi, G. (2019). Current cancer epidemiology. *Journal of Epidemiology and Global Health*, *9*(4), 217–222. <https://doi.org/10.2991/jegh.k.191008.001>
- Mcdowell, S. A. C., Luo, R. B. E., Arabzadeh, A., Doré, S., Bennett, N. C., Breton, V., Karimi, E., Rezanejad, M., Yang, R. R., Lach, K. D., Issac, M. S. M., Samborska, B., Perus, L. J. M., Moldoveanu, D., Wei, Y., Fiset, B., Rayes, R. F., Watson, I. R., Kazak, L., ... Quail, D. F. (2021). Neutrophil oxidative stress mediates obesity-associated vascular dysfunction and metastatic transmigration. *Nature Cancer*, *2*(May), 545–562. <http://dx.doi.org/10.1038/s43018-021-00194-9>
- Mehla, K., & Singh, P. K. (2019). Metabolic Regulation of Macrophage Polarization in Cancer. *Trends in Cancer*, *5*(12), 822–834. <https://doi.org/10.1016/j.trecan.2019.10.007>
- Menendez, J. A., Vellon, L., Colomer, R., & Lupu, R. (2005). Oleic acid, the main monounsaturated fatty acid of olive oil, suppresses Her-2/neu (erb B-2) expression and synergistically enhances the growth inhibitory effects of trastuzumab (Herceptin™) in breast cancer cells with Her-2/neu oncogene amplification. *Annals of Oncology*, *16*(3), 359–371. <https://doi.org/10.1093/annonc/mdi090>
- Merlo, L. M. F., Pepper, J. W., Reid, B. J., & Maley, C. C. (2006). Cancer as an evolutionary and ecological process. *Nature Reviews Cancer*, *6*(12), 924–935. <https://doi.org/10.1038/nrc2013>
- Mill, P., Lee, A. W. S., Fukata, Y., Tsutsumi, R., Fukata, M., Keighren, M., Porter, R. M., McKie, L., Smyth, I., & Jackson, I. J. (2009). Palmitoylation regulates epidermal homeostasis and hair follicle differentiation. *PLoS Genetics*, *5*(11). <https://doi.org/10.1371/journal.pgen.1000748>
- Mittal, P., & Roberts, C. W. M. (2020). The SWI/SNF complex in cancer — biology, biomarkers and therapy. *Nature Reviews Clinical Oncology*, *17*(7), 435–448. <https://doi.org/10.1038/s41571-020-0357-3>
- Mohseni, M., Sun, J., Lau, A., Curtis, S., Goldsmith, J., Fox, V. L., Wei, C., Frazier, M., Samson, O., Wong, K. K., Kim, C., & Camargo, F. D. (2014). A genetic screen identifies an LKB1-MARK signalling axis controlling the Hippo-YAP pathway. *Nature Cell Biology*, *16*(1), 108–117. <https://doi.org/10.1038/ncb2884>
- [REDACTED]
- [REDACTED]
- Morrison, E., Wegner, T., Zucchetti, A. E., Álvaro-benito, M., Zheng, A., Kliche, S., Krause, E., Brügger, B., Hivroz, C., & Freund, C. (2020). Dynamic palmitoylation events following T-cell receptor signaling. *Communications Biology*, 1–9.

Mukai J, Dhillia A, Drew LJ, Stark KL, Cao L, MacDermott AB, Karayiorgou M, Gogos JA (2008). Palmitoylation-dependent neurodevelopmental deficits in a mouse model of 22q11 microdeletion. *Nat Neurosci* 11, 1302–1310.

Nardi, F., Fitchev, P., Franco, O. E., Ivanisevic, J., Scheibler, A., Hayward, S. W., Brendler, C. B., Welte, M. A., & Crawford, S. E. (2018). PEDF regulates plasticity of a novel lipid-MTOC axis in prostate cancer-associated fibroblasts. *Journal of Cell Science*, 131(13), 1–15. <https://doi.org/10.1242/jcs.213579>

Nath, A., Li, I., Roberts, L. R., & Chan, C. (2015). Elevated free fatty acid uptake via CD36 promotes epithelial-mesenchymal transition in hepatocellular carcinoma. *Scientific Reports*, 5(September), 1–19. <https://doi.org/10.1038/srep14752>

Neviani, V., van Deventer, S., Wörner, T. P., Xenaki, K. T., van de Waterbeemd, M., Rodenburg, R. N. P., Wortel, I. M. N., Kuiper, J. K., Huisman, S., Granneman, J., van Bergen en Henegouwen, P. M. P., Heck, A. J. R., van Spriel, A. B., & Gros, P. (2020). Site-specific functionality and tryptophan mimicry of lipidation in tetraspanin CD9. *FEBS Journal*, 287(24), 5323–5344. <https://doi.org/10.1111/febs.15295>

Niavarani, S. R., Lawson, C., Bakos, O., Boudaud, M., Batenchuk, C., Rouleau, S., & Tai, L. H. (2019). Lipid accumulation impairs natural killer cell cytotoxicity and tumor control in the postoperative period. *BMC Cancer*, 19(823). <https://doi.org/10.1186/s12885-019-6045-y>

Nicholas, D. A., Zhang, K., Hung, C., Glasgow, S., Aruni, A. W., Unternaehrer, J., Payne, K. J., Langridge, W. H. R., & De Leon, M. (2017). Palmitic acid is a toll-like receptor 4 ligand that induces human dendritic cell secretion of IL-1 β . *PLoS ONE*, 12(5), 1–24. <https://doi.org/10.1371/journal.pone.0176793>

Nieman, K. M., Kenny, H. A., Penicka, C. V., Ladanyi, A., Buell-Gutbrod, R., Zillhardt, M. R., Romero, I. L., Carey, M. S., Mills, G. B., Hotamisligil, G. S., Yamada, S. D., Peter, M. E., Gwin, K., & Lengyel, E. (2011). Adipocytes promote ovarian cancer metastasis and provide energy for rapid tumor growth. *Nature Medicine*, 17(11), 1498–1503. <https://doi.org/10.1038/nm.2492>

Niphakis, M. J., Lum, K. M., Cognetta, A. B., Correia, B. E., Ichu, T. A., Olucha, J., Brown, S. J., Kundu, S., Piscitelli, F., Rosen, H., & Cravatt, B. F. (2015). A Global Map of Lipid-Binding Proteins and Their Ligandability in Cells. *Cell*, 161(7), 1668–1680. <https://doi.org/10.1016/j.cell.2015.05.045>

OECD. (2017). Obesity Update 2017. *Diabetologie*, 13(5), 331–341. www.oecd.org/health/obesity-update.htm

Ohno, Y., Kashio, A., Ogata, R., Ishitomi, A., Yamazaki, Y., & Kihara, A. (2012). Analysis of substrate specificity of human DHHC protein acyltransferases using a yeast expression system. *Molecular Biology of the Cell*, 23(23), 4543–4551. <https://doi.org/10.1091/mbc.E12-05-0336>

Oku, S., Takahashi, N., Fukata, Y., & Fukata, M. (2013). In Silico screening for palmitoyl substrates reveals a role for DHHC1/3/10 (zDHHC1/3/11)-mediated neurochondrin palmitoylation in its targeting to Rab5-positive endosomes. *Journal of Biological Chemistry*, 288(27), 19816–19826. <https://doi.org/10.1074/jbc.M112.431676>

Olzmann, J. A., & Carvalho, P. (2019). Dynamics and functions of lipid droplets. *Nature Reviews Molecular Cell Biology*, 20(March), 137–155.

Palomer, X., Pizarro-Delgado, J., Barroso, E., & Vázquez-Carrera, M. (2018). Palmitic and Oleic Acid: The Yin and Yang of Fatty Acids in Type 2 Diabetes Mellitus. *Trends in Endocrinology and Metabolism*, 29(3), 178–190. <https://doi.org/10.1016/j.tem.2017.11.009>

Pan, J., Fan, Z., Wang, Z., Dai, Q., Xiang, Z., Yuan, F., Yan, M., Zhu, Z., Liu, B., & Li, C. (2019). CD36 mediates palmitate acid-induced metastasis of gastric cancer via AKT/GSK-3 β / β -catenin pathway. *Journal of Experimental and Clinical Cancer Research*, 38(52), 1–15. <https://doi.org/10.1186/s13046-019-1049-7>

Paňková, K., Rösel, D., Novotný, M., & Brábek, J. (2010). The molecular mechanisms of transition between mesenchymal and amoeboid invasiveness in tumor cells. *Cellular and Molecular Life Sciences*, 67(1), 63–71. <https://doi.org/10.1007/s00018-009-0132-1>

Papaevangelou, E., Almeida, G. S., Box, C., DeSouza, N. M., & Chung, Y. L. (2018). The effect of FASN inhibition on the growth and metabolism of a cisplatin-resistant ovarian carcinoma model. *International Journal of Cancer*. <https://doi.org/10.1002/ijc.31392>

Pascual, G., Avgustinova, A., Mejetta, S., Martín, M., Castellanos, A., Attolini, C. S. O., Berenguer, A., Prats, N., Toll, A., Hueto, J. A., Bescós, C., Di Croce, L., & Benitah, S. A. (2017). Targeting metastasis-initiating

- cells through the fatty acid receptor CD36. *Nature*, 541(7635), 41–45. <https://doi.org/10.1038/nature20791>
- Pascual, G., Domínguez, D., Elosúa-Bayes, M., Beckedorff, F., Laudanna, C., Bigas, C., Douillet, D., Greco, C., Symeonidi, A., Hernández, I., Gil, S. R., Prats, N., Bescós, C., Shiekhattar, R., Amit, M., Heyn, H., Shilatifard, A., & Benitah, S. A. (2021). Dietary palmitic acid promotes a prometastatic memory via Schwann cells. *Nature*, 599(7885), 485–490. <https://doi.org/10.1038/s41586-021-04075-0>
- Patsoukis, N., Bardhan, K., Chatterjee, P., Sari, D., Liu, B., Bell, L. N., Karoly, E. D., Freeman, G. J., Petkova, V., Seth, P., Li, L., & Boussiotis, V. A. (2015). PD-1 alters T-cell metabolic reprogramming by inhibiting glycolysis and promoting lipolysis and fatty acid oxidation. *Nature Communications*, 6. <https://doi.org/10.1038/ncomms7692>
- Peng, G., Li, L., Liu, Y., Pu, J., Zhang, S., Yu, J., Zhao, J., & Liu, P. (2011). Oleate blocks palmitate-induced abnormal lipid distribution, endoplasmic reticulum expansion and stress, and insulin resistance in skeletal muscle. *Endocrinology*, 152(6), 2206–2218. <https://doi.org/10.1210/en.2010-1369>
- Pepinsky, R. B., Zeng, C., Went, D., Rayhorn, P., Baker, D. P., Williams, K. P., Bixler, S. A., Ambrose, C. M., Garber, E. A., Miatkowski, K., Taylor, F. R., Wang, E. A., & Galdes, A. (1998). Identification of a palmitic acid-modified form of human Sonic hedgehog. *Journal of Biological Chemistry*, 273(22)
- Pietrocola, F., Pol, J., Vacchelli, E., Rao, S., Enot, D. P., Baracco, E. E., Levesque, S., Castoldi, F., Jacquelot, N., Takahiro, Y., Senovilla, L., Marino, G., Aranda, F., Durand, S., Sica, V., Chery, A., Lachkar, S., Sigl, V., Bloy, N., ... Kroemer, G. (2016). Caloric restriction mimetics enhance anticancer immunosurveillance. *Cancer Cell*, 30(1), 147–160. <https://doi.org/10.1016/j.ccell.2016.05.016>. Caloric
- Pinkham, K., Park, D. J., Hashemiaghdam, A., Kirov, A. B., Adam, I., Rosiak, K., da Hora, C. C., Teng, J., Cheah, P. S., Carvalho, L., Ganguli-Indra, G., Kelly, A., Indra, A. K., & Badr, C. E. (2019). Stearoyl CoA Desaturase Is Essential for Regulation of Endoplasmic Reticulum Homeostasis and Tumor Growth in Glioblastoma Cancer Stem Cells. *Stem Cell Reports*, 12, 712–727. <http://dx.doi.org/10.1016/j.stemcr.2015.11.006>
- Poirier, Y., Antonenkov, V. D., Glumoff, T., & Hiltunen, J. K. (2006). Peroxisomal β -oxidation-A metabolic pathway with multiple functions. *Biochimica et Biophysica Acta - Molecular Cell Research*, 1763(12), 1413–1426. <https://doi.org/10.1016/j.bbamcr.2006.08.034>
- [REDACTED]
- Ponimaskin, E., Dityateva, G., Ruonala, M. O., Fukata, M., Fukata, Y., Kobe, F., Wouters, F. S., Delling, M., Brecht, D. S., Schachner, M., & Dityatev, A. (2008). Fibroblast growth factor-regulated palmitoylation of the neural cell adhesion molecule determines neuronal morphogenesis. *Journal of Neuroscience*, 28(36), 8897–8907. <https://doi.org/10.1523/JNEUROSCI.2171-08.2008>
- [REDACTED]
- Prabhakar, P., Cheng, V., & Michel, T. (2000). A chimeric transmembrane domain directs endothelial nitric-oxide synthase palmitoylation and targeting to plasmalemmal caveolae. *Journal of Biological Chemistry*, 275(25), 19416–19421. <https://doi.org/10.1074/jbc.M001952200>
- Prat, A., Pineda, E., Adamo, B., Galván, P., Fernández, A., Gaba, L., Díez, M., Viladot, M., Arance, A., & Muñoz, M. (2015). Clinical implications of the intrinsic molecular subtypes of breast cancer. *Breast*, 24, S26–S35. <https://doi.org/10.1016/j.breast.2015.07.008>
- Priestley, P., Baber, J., Lolkema, M. P., Steeghs, N., de Bruijn, E., Shale, C., Duyvesteyn, K., Haidari, S., van Hoeck, A., Onstenk, W., Roepman, P., Voda, M., Bloemendal, H. J., Tjan-Heijnen, V. C. G., van Herpen, C. M. L., Labots, M., Witteveen, P. O., Smit, E. F., Sleijfer, S., ... Cuppen, E. (2019). Pan-cancer whole-genome analyses of metastatic solid tumours. *Nature*, 575(7781), 210–216. <https://doi.org/10.1038/s41586-019-1689-y>
- Putilina, T., Wong, P., & Gentleman, S. (1999). The DHHC domain: A new highly conserved cysteine-rich motif. *Molecular and Cellular Biochemistry*, 195(1–2), 219–226. <https://doi.org/10.1023/A:1006932522197>
- Qiao, S., Koh, S. B., Vivekanandan, V., Salunke, D., Patra, K. C., Zaganjor, E., Ross, K., Mizukami, Y., Jeanfavre, S., Chen, A., Mino-Kenudson, M., Ramaswamy, S., Clish, C., Haigis, M., Bardeesy, N., & Ellisen, L. W. (2020). REDD1 loss reprograms lipid metabolism to drive progression of RAS mutant tumors. *Genes and Development*, 34(11–12), 751–766. <https://doi.org/10.1101/gad.335166.119>
- Quail, D. F., Olson, O. C., Bhardwaj, P., Walsh, L. A., Akkari, L., Quick, M. L., Chen, I. C., Wendel, N., Ben-Chetrit, N., Walker, J., Holt, P. R., Dannenberg, A. J., & Joyce, J. A. (2017). Obesity alters the lung

- myeloid cell landscape to enhance breast cancer metastasis through IL5 and GM-CSF. *Nature Cell Biology*, 19(8), 974–987. <https://doi.org/10.1038/ncb3578>
- Rambow, F., Rogiers, A., Marin-bejar, O., Aerts, S., Lund, A. W., Rambow, F., Rogiers, A., Marin-bejar, O., Aibar, S., Femel, J., Dewaele, M., Karras, P., Brown, D., Chang, Y. H., Maria, D.-R., Adriaens, C., Radaelli, E., Wolter, P., Bechter, O., ... Marine, J.-C. (2018). Toward Minimal Residual Disease-Directed Therapy in Melanoma Toward Minimal Residual Disease-Directed Therapy in Melanoma. *Cell*, 174, 843–855.
- Ran, H., Zhu, Y., Deng, R., Zhang, Q., Liu, X., Feng, M., Zhong, J., Lin, S., Tong, X., & Su, Q. (2018). Stearoyl-CoA desaturase-1 promotes colorectal cancer metastasis in response to glucose by suppressing PTEN. *Journal of Experimental and Clinical Cancer Research*, 37(54), 1–15. <https://doi.org/10.1186/s13046-018-0711-9>
- Rana, M. S., Kumar, P., Lee, C., Verardi, R., Kanagalaghatta, R., Banerjee, A., & Branch, N. (2018). Fatty acyl recognition and transfer by an integral membrane S- acyltransferase. *Science*, 359(6372). <https://doi.org/10.1126/science.aao6326>
- Rebecca, V. W., Nicastrì, M. C., Fennelly, C., Chude, C. I., Barber-Rotenberg, J. S., Ronghe, A., McAfee, Q., McLaughlin, N. P., Zhang, G., Goldman, A. R., Ojha, R., Piao, S., Noguera-Ortega, E., Martorella, A., Alicea, G. M., Lee, J. J., Schuchter, L. M., Xu, X., Herlyn, M., ... Amaravadi, R. K. (2019). PPT1 promotes tumor growth and is the molecular target of chloroquine derivatives in cancer. *Cancer Discovery*, 9(2), 220–229. <https://doi.org/10.1158/2159-8290.cd-18-0706>
- Reiter, J. G., Makohon-Moore, A. P., Gerold, J. M., Heyde, A., Attiyeh, M. A., Kohutek, Z. A., Tokheim, C. J., Brown, A., DeBlasio, R. M., Niyazov, J., Zucker, A., Karchin, R., Kinzler, K. W., Iacobuzio-Donahue, C. A., Vogelstein, B., & Nowak, M. A. (2018). Minimal functional driver gene heterogeneity among untreated metastases. *Science*, 361(6406), 1033–1037. <https://doi.org/10.1126/science.aat7171>
- Resh MD. (2013). Covalent Lipid Modifications of Proteins Marilyn. *Curr Biol*, 23(1), 431–435. <https://doi.org/10.1016/j.cub.2013.04.024>
- Resh, M. D. (2016). Fatty Acylation of Proteins: The Long and the Short of it. *Progress in Lipid Research*, 63, 120–131. <https://doi.org/10.1016/j.plipres.2016.05.002>
- Ribatti, D., Tamma, R., & Annese, T. (2020). Epithelial-Mesenchymal Transition in Cancer: A Historical Overview. *Translational Oncology*, 13(6). <https://doi.org/10.1016/j.tranon.2020.100773>
- Rocks, O., Gerauer, M., Vartak, N., Koch, S., Huang, Z. P., Pechlivanis, M., Kuhlmann, J., Brunsveld, L., Chandra, A., Ellinger, B., Waldmann, H., & Bastiaens, P. I. H. (2010). The palmitoylation machinery is a spatially organizing system for peripheral membrane proteins. *Cell*, 141(3), 458–471. <https://doi.org/10.1016/j.cell.2010.04.007>
- Rossin, A., Durivault, J., Chakhtoura-Feghali, T., Lounnas, N., Gagnoux-Palacios, L., & Hueber, A. O. (2015). Fas palmitoylation by the palmitoyl acyltransferase DHHC7 regulates Fas stability. *Cell Death and Differentiation*, 22(4), 643–653. <https://doi.org/10.1038/cdd.2014.153>
- Roth, A. F., Feng, Y., Chen, L., & Davis, N. G. (2002). The yeast DHHC cysteine-rich domain protein Akr1p is a palmitoyl transferase. *Journal of Cell Biology*, 159(1), 23–28. <https://doi.org/10.1083/jcb.200206120>
- Roth, A. F., Wan, J., Bailey, A. O., Sun, B., Kuchar, J. A., Green, W. N., Phinney, B. S., Yates, J. R., & Davis, N. G. (2006). Global Analysis of Protein Palmitoylation in Yeast. *Cell*, 125(5), 1003–1013. <https://doi.org/10.1016/j.cell.2006.03.042>
- Rozeveld, C. N., Johnson, K. M., Zhang, L., & Razidlo, G. L. (2020). KRAS controls pancreatic cancer cell lipid metabolism and invasive potential through the lipase HSL. *Cancer Research*, 80(22), 4932–4945. <https://doi.org/10.1158/0008-5472.CAN-20-1255>
- Rudin, C. M., Poirier, J. T., Byers, L. A., Dive, C., Dowlati, A., George, J., Heymach, J. V., Johnson, J. E., Lehman, J. M., MacPherson, D., Massion, P. P., Minna, J. D., Oliver, T. G., Quaranta, V., Sage, J., Thomas, R. K., Vakoc, C. R., & Gazdar, A. F. (2019). Molecular subtypes of small cell lung cancer: a synthesis of human and mouse model data. *Nature Reviews Cancer*, 19(5), 289–297. <https://doi.org/10.1038/s41568-019-0164-2>
- Runkle, K. B., Kharbanda, A. K., Stypulkowski, E., Cao, X.-J., Wang, W., Garcia, B. A., & Witze, E. S. (2016). Inhibition of DHHC20 mediated EGFR palmitoylation creates a dependence on EGFR signaling. *Molecular Cell*, 62(3), 385–396. <https://doi.org/10.1016/j.molcel.2016.04.003>

- Sapir, T., Segal, M., Grigoryan, G., Hansson, K. M., James, P., Segal, M., & Reiner, O. (2019). The interactome of palmitoyl-protein thioesterase 1 (PPT1) affects neuronal morphology and function. *Frontiers in Cellular Neuroscience*, *13*(March). <https://doi.org/10.3389/fncel.2019.00092>
- Satou, M., & Sugimoto, H. (2012). The study of ghrelin deacylation enzymes. *Methods in Enzymology*, *514*, 165–179. <https://doi.org/10.1016/b978-0-12-381272-8.00011-8>
- Sawyer, B. T., Qamar, L., Yamamoto, T. M., McMellen, A., Watson, Z. L., Richer, J. K., Behbakht, K., Schlaepfer, I. R., & Bitler, B. G. (2020). Targeting fatty acid oxidation to promote anoikis and inhibit ovarian cancer progression. *Molecular Cancer Research*, *18*(7), 1088–1098. <https://doi.org/10.1158/1541-7786.MCR-19-1057>

- Segal-Salto, M., Sapir, T., & Reiner, O. (2016). Reversible cysteine acylation regulates the activity of human palmitoyl-protein thioesterase 1 (PPT1). *PLoS ONE*, *11*(1), 1–18. <https://doi.org/10.1371/journal.pone.0146466>
- Seguin, F., Carvalho, M. A., Bastos, D. C., Agostini, M., Zecchin, K. G., Alvarez-Flores, M. P., Chudzinski-Tavassi, A. M., Coletta, R. D., & Graner, E. (2012). The fatty acid synthase inhibitor orlistat reduces experimental metastases and angiogenesis in B16-F10 melanomas. *British Journal of Cancer*, *107*(6), 977–987. <https://doi.org/10.1038/bjc.2012.355>
- Seidel, J. A., Otsuka, A., & Kabashima, K. (2018). Anti-PD-1 and anti-CTLA-4 therapies in cancer: Mechanisms of action, efficacy, and limitations. *Frontiers in Oncology*, *8*(MAR). <https://doi.org/10.3389/fonc.2018.00086>
- Senyilmaz, D., Virtue, S., Xu, X., Tan, C. Y., Griffin, J. L., Miller, A. K., Vidal-Puig, A., & Teleman, A. A. (2015). Regulation of mitochondrial morphology and function by stearoylation of TFR1. *Nature*, *525*(7567), 124–128. <https://doi.org/10.1038/nature14601>
- Seo, J., Jeong, D. W., Park, J. W., Lee, K. W., Fukuda, J., & Chun, Y. S. (2020). Fatty-acid-induced FABP5/HIF-1 reprograms lipid metabolism and enhances the proliferation of liver cancer cells. *Communications Biology*, *3*(638), 1–14. <https://doi.org/10.1038/s42003-020-01367-5>
- Sharma, G., Ojha, R., Noguera-Ortega, E., Rebecca, V. W., Attanasio, J., Liu, S., Piao, S., Lee, J. J., Nicastri, M. C., Harper, S. L., Ronghe, A., Jain, V., Winkler, J. D., Speicher, D. W., Mastio, J., Gimotty, P. A., Xu, X., John Wherry, E., Gabilovich, D. I., & Amaravadi, R. K. (2020). PPT1 inhibition enhances the antitumor activity of anti-PD-1 antibody in melanoma. *JCI Insight*, *5*(17), 1–16. <https://doi.org/10.1172/jci.insight.133225>
- Sharma, C., Rabinovitz, I., & Hemler, M. E. (2012). Palmitoylation by DHHC3 is critical for the function, expression, and stability of integrin $\alpha 6\beta 4$. *Cellular and Molecular Life Sciences*, *69*(13), 2233–2244. <https://doi.org/10.1007/s00018-012-0924-6>
- Sharma, C., Yang, X. H., & Hemler, M. E. (2008). DHHC2 Affects Palmitoylation, Stability, and Functions of Tetraspanins CD9 and CD151. *Molecular Biology of the Cell*, *19*(August), 3415–3425. <https://doi.org/10.1091/mbc.E07>
- Shen, C. J., Chang, K. Y., Lin, B. W., Lin, W. T., Su, C. M., Tsai, J. P., Liao, Y. H., Hung, L. Y., Chang, W. C., & Chen, B. K. (2020). Oleic acid-induced NOX4 is dependent on ANGPTL4 expression to promote human colorectal cancer metastasis. *Theranostics*, *10*(16), 7083–7099. <https://doi.org/10.7150/thno.44744>
- Shen, L. F., Chen, Y. J., Liu, K. M., Haddad, A. N. S., Song, I. W., Roan, H. Y., Chen, L. Y., Yen, J. J. Y., Chen, Y. J., Wu, J. Y., & Chen, Y. T. (2017). Role of S-Palmitoylation by ZDHHC13 in Mitochondrial function and Metabolism in Liver. *Scientific Reports*, *7*(1), 1–14. <https://doi.org/10.1038/s41598-017-02159-4>
- Siegel, R. L., Miller, K. D., & Jemal, A. (2020). Cancer statistics, 2020. *CA: A Cancer Journal for Clinicians*, *70*(1), 7–30. <https://doi.org/10.3322/caac.21590>
- Sigismund, S., Avanzato, D., & Lanzetti, L. (2018). Emerging functions of the EGFR in cancer. *Molecular Oncology*, *12*(1), 3–20. <https://doi.org/10.1002/1878-0261.12155>

- Singaraja, R. R., Kang, M. H., Vaid, K., Sanders, S. S., Vilas, G. L., Arstikaitis, P., Coutinho, J., Drisdell, R. C., El Din El-Husseini, A., Green, W. N., Berthiaume, L., & Hayden, M. R. (2009). Palmitoylation of ATP-

- binding cassette transporter A1 is essential for its trafficking and function. *Circulation Research*, 105(2), 138–147. <https://doi.org/10.1161/CIRCRESAHA.108.193011>
- Smotrys, J. E., & Linder, M. E. (2004). PALMITOYLATION OF INTRACELLULAR SIGNALING PROTEINS : Regulation and Function. *Annu. Rev. Biochem.* <https://doi.org/10.1146/annurev.biochem.73.011303.073954>
- Smotrys, J. E., Schoenfish, M. J., Stutz, M. A., & Linder, M. E. (2005). The vacuolar DHHC-CRD protein Pfa3p is a protein acyltransferase for Vac8p. *Journal of Cell Biology*, 170(7), 1091–1099. <https://doi.org/10.1083/jcb.200507048>
- Snaebjornsson, M. T., Janaki-Raman, S., & Schulze, A. (2020). Greasing the Wheels of the Cancer Machine: The Role of Lipid Metabolism in Cancer. *Cell Metabolism*, 31(1), 62–76. <https://doi.org/10.1016/j.cmet.2019.11.010>
- Soto-Guzman, A., Navarro-Tito, N., Castro-Sanchez, L., Martinez-Orozco, R., & Salazar, E. P. (2010). Oleic acid promotes MMP-9 secretion and invasion in breast cancer cells. *Clinical and Experimental Metastasis*, 27(7), 505–515. <https://doi.org/10.1007/s10585-010-9340-1>
- Spinelli, M., Fusco, S., Mainardi, M., Scala, F., Natale, F., Lapenta, R., Mattera, A., Rinaudo, M., Li Puma, D. D., Ripoli, C., Grassi, A., D'Ascenzo, M., & Grassi, C. (2017). Brain insulin resistance impairs hippocampal synaptic plasticity and memory by increasing GluA1 palmitoylation through FoxO3a. *Nature Communications*, 8(2009). <https://doi.org/10.1038/s41467-017-02221-9>
- Staalduinen, J. Van, Baker, D., Peter Ten, D., & Dam, H. van. (2018). Epithelial – mesenchymal-transition-inducing transcription factors : new targets for tackling chemoresistance in cancer ? *Oncogene*.
- Stein, A. P., Saha, S., Kraninger, J. L., Swick, A. D., Yu, M., Lambertg, P. F., & Kimple, R. (2016). Prevalence of human papillomavirus in oropharyngeal cancer: a systematic review. *Cancer Journal*, 21(3), 138–146. <https://doi.org/10.1097/PPO.000000000000115>.Prevalence
- Stevenson, F. T., Burstent, S. L., Fanton, C., Locksley, R. M., & Lovett, D. H. (1993). The 31-kDa precursor of interleukin 1a is myristoylated on specific lysines within the 16-kDa N-terminal propiece. *Proc. Natl. Acad. Sci. USA*, 90(August), 7245–7249.
- Stevenson, F. T., Bursten, S. L., Locksley, R. M., & Lovett, D. H. (1992). Myristyl acylation of the tumor necrosis factor α precursor on specific lysine residues. *Journal of Experimental Medicine*, 176(4), 1053–1062. <https://doi.org/10.1084/jem.176.4.1053>
- Stix, R., Lee, C. J., Faraldo-Gómez, J. D., & Banerjee, A. (2020). Structure and Mechanism of DHHC Protein Acyltransferases. *Journal of Molecular Biology*, 432(18), 4983–4998. <https://doi.org/10.1016/j.jmb.2020.05.023>
- Su, P., Wang, Q., Bi, E., Ma, X., Liu, L., Yang, M., Qian, J., & Yi, Q. (2020). Enhanced lipid accumulation and metabolism are required for the differentiation and activation of tumor-associated macrophages. *Cancer Research*, 80(7), 1438–1450. <https://doi.org/10.1158/0008-5472.CAN-19-2994>
- Sugimoto, H., Hayashi, H., & Yamashita, S. (1996). Purification , cDNA Cloning , and Regulation of Lysophospholipase from Rat Liver *. *The Journal of Biological Chemistry*, 271(13), 7705–7711.
- [REDACTED]
- [REDACTED]
- Swarthout, J. T., Lobo, S., Farh, L., Croke, M. R., Greentree, W. K., Deschenes, R. J., & Linder, M. E. (2005). DHHC9 and GCP16 constitute a human protein fatty acyltransferase with specificity for H- and N-Ras. *Journal of Biological Chemistry*, 280(35), 31141–31148. <https://doi.org/10.1074/jbc.M504113200>
- [REDACTED]
- [REDACTED]
- Tabaczar, S., Czogalla, A., Podkalicka, J., & Biernatowska, A. (2017). *Protein palmitoylation: Palmitoyltransferases and their specificity*. 1150–1157. <https://doi.org/10.1177/1535370217707732>
- [REDACTED]
- [REDACTED]
- Tai, L. H., De Souza, C. T., Bélanger, S., Ly, L., Alkayyal, A. A., Zhang, J., Rintoul, J. L., Ananth, A. A., Lam, T., Breitbach, C. J., Falls, T. J., Kirn, D. H., Bell, J. C., Makrigiannis, A. P., & Auer, R. A. (2013). Preventing postoperative metastatic disease by inhibiting surgery-induced dysfunction in natural killer cells. *Cancer Research*, 73(1), 97–107. <https://doi.org/10.1158/0008-5472.CAN-12-1993>
- [REDACTED]

Tan, B. T., Park, C. Y., Ailles, L. E., & Weissman, I. L. (2006). The cancer stem cell hypothesis: A work in progress. *Laboratory Investigation*, *86*(12), 1203–1207. <https://doi.org/10.1038/labinvest.3700488>

Tang, J., Peng, W., Feng, Y., Le, X., Wang, K., Xiang, Q., Li, L., Wang, Y., Xu, C., Mu, J., Xu, K., Ji, P., Tao, Q., Huang, A., Deng, C. X., Lin, Y., & Xiang, T. (2021). Cancer cells escape p53's tumor suppression through ablation of ZDHHC1-mediated p53 palmitoylation. *Oncogene*, February. <https://doi.org/10.1038/s41388-021-01949-5>

Tanimura, N., Nagafuku, M., Minaki, Y., Umeda, Y., Hayashi, F., Sakakura, J., Kato, A., Liddicoat, D. R., Ogata, M., Hamaoka, T., & Kosugi, A. (2003). Dynamic changes in the mobility of LAT in aggregated lipid rafts upon T cell activation. *Journal of Cell Biology*, *160*(1), 125–135. <https://doi.org/10.1083/jcb.200207096>

Tasdogan, A., Faubert, B., Ramesh, V., Ubellacker, J. M., Shen, B., Solmonson, A., Murphy, M. M., Gu, Z., Gu, W., Martin, M., Kasitnon, S. Y., Vandergriff, T., Mathews, T. P., Zhao, Z., Schadendorf, D., DeBerardinis, R. J., & Morrison, S. J. (2020). Metabolic heterogeneity confers differences in melanoma metastatic potential. *Nature*, *577*(7788), 115–120. <https://doi.org/10.1038/s41586-019-1847-2>

Teng, Y. Bin, Jing, H., Aramsangtienchai, P., He, B., Khan, S., Hu, J., Lin, H., & Hao, Q. (2014). Efficient demyristoylase activity of SIRT2 revealed by kinetic and structural studies. *Scientific Reports*, *5*, 1–8. <https://doi.org/10.1038/srep08529>

Tesfay, L., Paul, B. T., Konstorum, A., Deng, Z., Cox, A. O., Lee, J., Furdai, C. M., Hegde, P., Torti, F. M., & Torti, S. V. (2016). Steroyl-CoA Desaturase 1 (SCD1) protects ovarian cancer cells from ferroptotic cell death. *Cancer Research*, *176*(1), 139–148. <https://doi.org/10.1158/0008-5472.CAN-19-0369.Steroyl-CoA>

Thiele, C., Papan, C., Hoelper, D., Kusserow, K., Gaebler, A., Schoene, M., Piotrowitz, K., Lohmann, D., Spandl, J., Stevanovic, A., Shevchenko, A., & Kuerschner, L. (2012). Tracing fatty acid metabolism by click chemistry. *ACS Chemical Biology*, *7*(12), 2004–2011. <https://doi.org/10.1021/cb300414v>

Thul, P. J., Akesson, L., Wiking, M., Mahdessian, D., Geladaki, A., Ait Blal, H., Alm, T., Asplund, A., Björk, L., Breckels, L. M., Bäckström, A., Danielsson, F., Fagerberg, L., Fall, J., Gatto, L., Gnann, C., Hober, S., Hjelmare, M., Johansson, F., ... Lundberg, E. (2017). A subcellular map of the human proteome. *Science*, *356*(6340). <https://doi.org/10.1126/science.aal3321>

Tian, L., McClafferty, H., Knaus, H. G., Ruth, P., & Shipston, M. J. (2012). Distinct acyl protein transferases and thioesterases control surface expression of calcium-activated potassium channels. *Journal of Biological Chemistry*, *287*(18), 14718–14725. <https://doi.org/10.1074/jbc.M111.335547>

Tian, K., Xu, Y., Sahebkar, A., & Xu, S. (2020). CD36 in Atherosclerosis: Pathophysiological Mechanisms and Therapeutic Implications. *Current Atherosclerosis Reports*, *22*(10). <https://doi.org/10.1007/s11883-020-00870-8>

Tomatis, V. M., Trenchi, A., Gomez, G. A., & Daniotti, J. L. (2010). Acyl-protein thioesterase 2 catalyzes the deacylation of peripheral membrane-associated GAP-43. *PLoS ONE*, *5*(11). <https://doi.org/10.1371/journal.pone.0015045>

Tonn Eisinger, K. R., Woolfrey, K. M., Swanson, S. P., Schnell, S. A., Meitzen, J., Dell'Acqua, M., & Mermelstein, P. G. (2018). Palmitoylation of caveolin-1 is regulated by the same DHHC acyltransferases that modify steroid hormone receptors. *Journal of Biological Chemistry*, *293*(41), 15901–15911. <https://doi.org/10.1074/jbc.RA118.004167>

Tse, E., Helbig, K. J., Van Der Hoek, K., McCartney, E. M., Van Der Hoek, M., George, J., & Beard, M. R. (2015). Fatty acids induce a pro-inflammatory gene expression profile in Huh-7 cells that attenuates the anti-HCV action of interferon. *Journal of Interferon and Cytokine Research*, *35*(5), 392–400. <https://doi.org/10.1089/jir.2014.0165>

Tsutsumi, R., Fukata, Y., Noritake, J., Iwanaga, T., Perez, F., & Fukata, M. (2009). Identification of G Protein α Subunit-Palmitoylating Enzyme. *Molecular and Cellular Biology*, *29*(2), 435–447. <https://doi.org/10.1128/mcb.01144-08>

Tukachinsky, H., Kuzmickas, R. P., Jao, C. Y., Liu, J., & Salic, A. (2012). Dispatched and Scube Mediate the Efficient Secretion of the Cholesterol-Modified Hedgehog Ligand. *Cell Reports*, 2(2), 308–320. <https://doi.org/10.1016/j.celrep.2012.07.010>

Tutino, V., De Nunzio, V., Caruso, M. G., Veronese, N., Lorusso, D., Di Masi, M., Benedetto, M. L., & Notarnicola, M. (2019). Elevated aa/epa ratio represents an inflammatory biomarker in tumor tissue of metastatic colorectal cancer patients. *International Journal of Molecular Sciences*, 20(8), 1–11. <https://doi.org/10.3390/ijms20082050>

Ubellacker, J. M., Tasdogan, A., Ramesh, V., Shen, B., Mitchell, E. C., Martin-Sandoval, M. S., Gu, Z., McCormick, M. L., Durham, A. B., Spitz, D. R., Zhao, Z., Mathews, T. P., & Morrison, S. J. (2020). Lymph protects metastasizing melanoma cells from ferroptosis. *Nature*, 585(7823), 113–118. <https://doi.org/10.1038/s41586-020-2623-z>

Udenwobele, D. I., Su, R. C., Good, S. V., Ball, T. B., Shrivastav, S. V., & Shrivastav, A. (2017). Myristoylation: An important protein modification in the immune response. *Frontiers in Immunology*, 8(JUN), 1–16. <https://doi.org/10.3389/fimmu.2017.00751>

Van Der Weyden, L., Arends, M. J., Campbell, A. D., Bald, T., Wardle-Jones, H., Griggs, N., Velasco-Herrera, M. D. C., Tüting, T., Sansom, O. J., Karp, N. A., Clare, S., Gleeson, D., Ryder, E., Galli, A., Tuck, E., Cambridge, E. L., Voet, T., MacAulay, I. C., Wong, K., ... Adams, D. J. (2017). Genome-wide in vivo screen identifies novel host regulators of metastatic colonization. *Nature*, 541(7636), 233–236. <https://doi.org/10.1038/nature20792>

Vartak, N., Papke, B., Grecco, H. E., Rossmannek, L., Waldmann, H., Hedberg, C., & Bastiaens, P. I. H. (2014). The autodepalmitoylating activity of APT maintains the spatial organization of palmitoylated membrane proteins. *Biophysical Journal*, 106(1), 93–105. <https://doi.org/10.1016/j.bpj.2013.11.024>

Veglia, F., Tyurin, V. A., Blasi, M., De Leo, A., Kossenkov, A. V., Donthireddy, L., To, T. K. J., Schug, Z., Basu, S., Wang, F., Ricciotti, E., DiRusso, C., Murphy, M. E., Vonderheide, R. H., Lieberman, P. M., Mulligan, C., Nam, B., Hockstein, N., Masters, G., ... Gabrilovich, D. I. (2019). Fatty acid transport protein 2 reprograms neutrophils in cancer. *Nature*, 569(7754), 73–78. <https://doi.org/10.1038/s41586-019-1118-2>

Veglia, F., Tyurin, V. A., Mohammadyani, D., Blasi, M., Duperret, E. K., Donthireddy, L., Hashimoto, A., Kapralov, A., Amoscato, A., Angelini, R., Patel, S., Alicea-torres, K., Weiner, D., Murphy, M. E., Klein-seetharaman, J., Celis, E., Kagan, V. E., & Gabrilovich, D. I. (2017). Lipid bodies containing oxidatively truncated lipids in cancer. *Nature Communications*, 8(2122). <https://doi.org/10.1038/s41467-017-02186-9>

Verkruyse, L. A., & Hofmann, S. L. (1996). Lysosomal Targeting of Palmitoyl-protein Thioesterase. *The Journal of Biological Chemistry*, 271(26), 15831–15836.

Vessby, B., Uusitupa, M., Hermansen, K., Riccardi, G., Rivellese, A. A., Tapsell, L. C., Näslén, C., Berglund, L., Louheranta, A., Rasmussen, B. M., Calvert, G. D., Maffetone, A., Pedersen, E., Gustafsson, I. B., & Storlien, L. H. (2001). Substituting dietary saturated for monounsaturated fat impairs insulin sensitivity in healthy men and women: The KANWU study. *Diabetologia*, 44(3), 312–319. <https://doi.org/10.1007/s001250051620>

Viswanathan, V. S., Ryan, M. J., Dhruv, H. D., Gill, S., Eichhoff, O. M., Seashore-ludlow, B., Kaffenberger, S. D., Eaton, J. K., Aguirre, A. J., Viswanathan, S. R., Chattopadhyay, S., Javaid, S., Huang, C., Wu, X., Tseng, Y., Roider, E. M., Gao, D., Cleary, J. M., Wolpin, B. M., ... Schreiber, S. L. (2017). Dependency of a therapy-resistant state of cancer cells on a lipid peroxidase pathway. *Nature*, 547(7664), 453–457. <https://doi.org/10.1038/nature23007>.Dependency

Vivas-García, Y., Falletta, P., Liebing, J., Louphrasitthiphol, P., Feng, Y., Chauhan, J., Scott, D. A., Glodde, N., Chocarro-Calvo, A., Bonham, S., Osterman, A. L., Fischer, R., Ronai, Z., García-Jiménez, C., Hölzel, M., & Goding, C. R. (2020). Lineage-Restricted Regulation of SCD and Fatty Acid Saturation by MITF Controls Melanoma Phenotypic Plasticity. *Molecular Cell*, 77(1), 120-137.e9. <https://doi.org/10.1016/j.molcel.2019.10.014>

Vriens, K., Christe, S., Parik, S., Broekaert, D., Talebi, A., Dehairs, J., Escalona-noguero, C., Cornfield, T., Charlton, C., Romero-pérez, L., Rossi, M., Rinaldi, G., Orth, M. F., Boon, R., Kerstens, A., Kwan, S. Y., Faubert, B., Méndez-Lucas, A., Kopitz, C. C., ... Fendt, S. M. (2019). Evidence for an alternative fatty

- acid desaturation pathway increasing cancer plasticity. *Nature*, 566(7744), 403–406. <https://doi.org/10.1038/s41586-019-0904-1>
- Wan, J., Roth, A. F., Bailey, A. O., & Davis, N. G. (2007). Palmitoylated proteins: purification and identification. *Nature Protocols*, 2(7), 1573–1584. <https://doi.org/10.1038/nprot.2007.225>
- Wang, D., Eraslan, B., Wieland, T., Hallström, B., Hopf, T., Zolg, D. P., Zecha, J., Asplund, A., Li, L., Meng, C., Frejno, M., Schmidt, T., Schnatbaum, K., Wilhelm, M., Ponten, F., Uhlen, M., Gagneur, J., Hahne, H., & Kuster, B. (2019). A deep proteome and transcriptome abundance atlas of 29 healthy human tissues. *Molecular Systems Biology*, 15(2), 1–16. <https://doi.org/10.15252/msb.20188503>
- Wang, V. M. Y., Ferreira, R. M. M., Almagro, J., Evan, T., Legrave, N., Zaw Thin, M., Frith, D., Carvalho, J., Barry, D. J., Snijders, A. P., Herbert, E., Nye, E. L., MacRae, J. I., & Behrens, A. (2019b). CD9 identifies pancreatic cancer stem cells and modulates glutamine metabolism to fuel tumour growth. *Nature Cell Biology*, 21(11), 1425–1435. <https://doi.org/10.1038/s41556-019-0407-1>
- Wang, H., Franco, F., Tsui, Y. C., Xie, X., Trefny, M. P., Zappasodi, R., Mohmood, S. R., Fernández-García, J., Tsai, C. H., Schulze, I., Picard, F., Meylan, E., Silverstein, R., Goldberg, I., Fendt, S. M., Wolchok, J. D., Merghoub, T., Jandus, C., Zippelius, A., & Ho, P. C. (2020). CD36-mediated metabolic adaptation supports regulatory T cell survival and function in tumors. *Nature Immunology*, 21(3), 298–308. <https://doi.org/10.1038/s41590-019-0589-5>
- Wang, D., Fu, L., Wei, J., Xiong, Y., & DuBois, R. N. (2019c). PPAR δ mediates the effect of dietary fat in promoting colorectal cancer metastasis. *Cancer Research*, 79(17), 4480–4490. <https://doi.org/10.1158/0008-5472.CAN-19-0384>
- Wang, J., Hao, J. W., Wang, X., Guo, H., Sun, H. H., Lai, X. Y., Liu, L. Y., Zhu, M., Wang, H. Y., Li, Y. F., Yu, L. Y., Xie, C., Wang, H. R., Mo, W., Zhou, H. M., Chen, S., Liang, G., & Zhao, T. J. (2019d). DHH4 and DHH5 Facilitate Fatty Acid Uptake by Palmitoylating and Targeting CD36 to the Plasma Membrane. *Cell Reports*, 26(1), 209–221.e5. <https://doi.org/10.1016/j.celrep.2018.12.022>
- Wang, L., Li, C., Song, Y., & Yan, Z. K. (2020b). Inhibition of carnitine palmitoyl transferase 1A-induced fatty acid oxidation suppresses cell progression in gastric cancer. *Archives of Biochemistry and Biophysics*, 696(October). <https://doi.org/10.1016/j.abb.2020.108664>
- Wang, W., Runkle, K. B., Terkowski, S. M., Ekaireb, R. I., & Witze, E. S. (2015). Protein depalmitoylation is induced by Wnt5a and promotes polarized cell behavior. *Journal of Biological Chemistry*, 290(25), 15707–15716. <https://doi.org/10.1074/jbc.M115.639609>
- Wang, J., Wen, T., Li, Z., Che, X., Gong, L., Jiao, Z., Qu, X., & Lu, Y. (2021). Cd36 Upregulates Dek Transcription and Promotes Cell Migration and Invasion Via Gsk-3 β / β -Catenin-Mediated Epithelial-To-Mesenchymal Transition in Gastric Cancer. *Aging*, 13(2), 1883–1897. <https://doi.org/10.18632/aging.103985>
- Warburg, O., Wind, F., & Negelein, E. (1927). The metabolism of tumors in the body. *The Journal of General Physiology*, 8(6), 519–530.
- Warburg, O. (1956). On the origin of cancer cells. *Science*, 123(3191), 309–314. <https://doi.org/10.1126/science.123.3191.309>
- Wen, H., Gris, D., Lei, Y., Jha, S., Zhang, L., Huang, M. T., Brickey, W. J., & Ting, J. P. (2011). Fatty acid – induced NLRP3-ASC inflammasome activation interferes with insulin signaling. *Nature Immunology*, 12(5), 408–415. <https://doi.org/10.1038/ni.2022>
- Wen, J., Min, X., Shen, M., Hua, Q., Han, Y., Zhao, L., Liu, L., Huang, G., Liu, J., & Zhao, X. (2019). ACLY facilitates colon cancer cell metastasis by CTNNB1. *Journal of Experimental and Clinical Cancer Research*, 38(1), 1–12. <https://doi.org/10.1186/s13046-019-1391-9>
- Won, S. J., Cheung See Kit, M., & Martin, B. R. (2018). Protein depalmitoylases. *Critical Reviews in Biochemistry and Molecular Biology*, 53(1), 83–98. <https://doi.org/10.1080/10409238.2017.1409191>

Woodley, K. T., & Collins, M. O. (2019). S-acylated Golga7b stabilises DHHC 5 at the plasma membrane to regulate cell adhesion. *EMBO Reports*, 20(10), 1–19. <https://doi.org/10.15252/embr.201847472>

Wu, H., Han, Y., Rodriguez Sillke, Y., Deng, H., Siddiqui, S., Treese, C., Schmidt, F., Friedrich, M., Keye, J., Wan, J., Qin, Y., Kühn, A. A., Qin, Z., Siegmund, B., & Glauben, R. (2019). Lipid droplet-dependent fatty acid metabolism controls the immune suppressive phenotype of tumor-associated macrophages. *EMBO Molecular Medicine*, 11(11), 1–17. <https://doi.org/10.15252/emmm.201910698>

Xiang, S., Bai, W., Bepler, G., & Zhang, X. (2017). Activation of Ras by Post-Translational Modifications. *Conquering RAS: From Biology to Cancer Therapy*, 97–118. <https://doi.org/10.1016/B978-0-12-803505-4.00006-0>

Xu, S., Chaudhary, O., Rodríguez-Morales, P., Sun, X., Chen, D., Zappasodi, R., Xu, Z., Pinto, A. F. M., Williams, A., Schulze, I., Farsakoglu, Y., Varanasi, S. K., Low, J. S., Tang, W., Wang, H., McDonald, B., Tripple, V., Downes, M., Evans, R. M., ... Kaech, S. M. (2021). Uptake of oxidized lipids by the scavenger receptor CD36 promotes lipid peroxidation and dysfunction in CD8+ T cells in tumors. *Immunity*, 54(7), 1561–1577. <https://doi.org/10.1016/j.immuni.2021.05.003>

Xu, L. X., Hao, L. J., Ma, J. Q., Liu, J. K., & Hasim, A. (2020). SIRT3 promotes the invasion and metastasis of cervical cancer cells by regulating fatty acid synthase. *Molecular and Cellular Biochemistry*, 464(1–2), 11–20. <https://doi.org/10.1007/s11010-019-03644-2>

Yamamoto, Y., Chochi, Y., Matsuyama, H., Eguchi, S., Kawauchi, S., Furuya, T., Oga, A., Kang, J. J., Naito, K., & Sasaki, K. (2007). Gain of 5p15.33 is associated with progression of bladder cancer. *Oncology*, 72(1–2), 132–138. <https://doi.org/10.1159/000111132>

Yan, S. M., Tang, J. J., Huang, C. Y., Xi, S. Y., Huang, M. Y., Liang, J. Z., Jiang, Y. X., Li, Y. H., Zhou, Z. W., Ernberg, I., Wu, Q. L., & Du, Z. M. (2013). Reduced Expression of ZDHHC2 Is Associated with Lymph Node Metastasis and Poor Prognosis in Gastric Adenocarcinoma. *PLoS ONE*, 8(2). <https://doi.org/10.1371/journal.pone.0056366>

Yang, J., Brown, M. S., Liang, G., Grishin, N. V., & Goldstein, J. L. (2008). Identification of the Acyltransferase that Octanoylates Ghrelin, an Appetite-Stimulating Peptide Hormone. *Cell*, 132(3), 387–396. <https://doi.org/10.1016/j.cell.2008.01.017>

Yang, X., Chatterjee, V., Ma, Y., Zheng, E., & Yuan, S. Y. (2020). Protein Palmitoylation in Leukocyte Signaling and Function. *Frontiers in Cell and Developmental Biology*, 8(October), 1–19. <https://doi.org/10.3389/fcell.2020.600368>

Yang, X., Chen, L., Mao, Y., Hu, Z., & He, M. (2020b). Progressive and prognostic performance of an extracellular matrix-receptor interaction signature in gastric cancer. *Disease Markers*, 2020. <https://doi.org/10.1155/2020/8816070>

Yang, W., Di Vizio, D., Kirchner, M., Steen, H., & Freeman, M. R. (2010). Proteome scale characterization of human S-acylated proteins in lipid raft-enriched and non-raft membranes. *Molecular and Cellular Proteomics*, 9(1), 54–70. <https://doi.org/10.1074/mcp.M800448-MCP200>

Yang, X. H., Kovalenko, O. V., Kolesnikova, T. V., Andzelm, M. M., Rubinstein, E., Strominger, J. L., & Hemler, M. E. (2006). Contrasting effects of EWI proteins, integrins, and protein palmitoylation on cell surface CD9 organization. *Journal of Biological Chemistry*, 281(18), 12976–12985. <https://doi.org/10.1074/jbc.M510617200>

Yang, L., Moss, T., Mangala, L. S., Marini, J., Zhao, H., Wahlig, S., Armaiz-Pena, G., Jiang, D., Achreja, A., Win, J., Roopaimoole, R., Rodriguez-Aguayo, C., Mercado-Uribe, I., Lopez-Berestein, G., Liu, J.,

- Tsukamoto, T., Sood, A. K., Ram, P. T., & Nagrath, D. (2014). Metabolic shifts toward glutamine regulate tumor growth, invasion and bioenergetics in ovarian cancer. *Molecular Systems Biology*, *10*(5), 1–23. <https://doi.org/10.1002/msb.20134892>
- Yang, P., Su, C., Luo, X., Zeng, H., Zhao, L., Wei, L., Zhang, X., Varghese, Z., Moorhead, J. F., Chen, Y., & Ruan, X. Z. (2018). Dietary oleic acid-induced CD36 promotes cervical cancer cell growth and metastasis via up-regulation Src/ERK pathway. *Cancer Letters*, *438*(August), 76–85. <https://doi.org/10.1016/j.canlet.2018.09.006>
- Yao, H., Lan, J., Li, C., Shi, H., Brosseau, J., Wang, H., Lu, H., Fang, C., Zhang, Y., Liang, L., Zhou, X., Wang, C., Xue, Y., Cui, Y., & Xu, J. (2019). Inhibiting PD-L1 palmitoylation enhances T-cell immune responses against tumours. *Nature Biomedical Engineering*, *3*, 306–317.
- Ye, H., Adane, B., Khan, N., Sullivan, T., Minhajuddin, M., Gasparetto, M., Stevens, B., Pei, S., Balys, M., Ashton, J. M., Klemm, D. J., Woolthuis, C. M., Stranahan, A. W., Park, C. Y., & Jordan, C. T. (2016). Leukemic Stem Cells Evade Chemotherapy by Metabolic Adaptation to an Adipose Tissue Niche. *Cell Stem Cell*, *19*, 23–37.
- Ye, H., Minhajuddin, M., Krug, A., Pei, S., Chou, C.-H., Culp-Hill, R., Ponder, J., De Bloois, E., Schniedewind, B., Amaya, M. L., Inguva, A., Stevens, B. M., Pollyea, D. A., Christians, U., Grimes, H. L., D’Alessandro, A., & Jordan, C. T. (2021). The hepatic microenvironment uniquely protects leukemia cells through induction of growth and survival pathways mediated by LIPG. *Cancer Discovery*, *11*(2), 500–519.
- Yin, Y., Liu, L., Zhao, Z., Yin, L., Bauer, N., Nwaeburu, C. C., Gladkikh, J., Gross, W., Hackert, T., Sticht, C., Gretz, N., Strobel, O., & Herr, I. (2018). Simvastatin inhibits sonic hedgehog signaling and stemness features of pancreatic cancer. *Cancer Letters*, *426*, 14–24. <https://doi.org/10.1016/j.canlet.2018.04.001>
- Yokoi, N., Fukata, Y., Sekiya, A., Murakami, T., Kobayashi, K., & Fukata, M. (2016). Identification of PSD-95 depalmitoylating enzymes. *Journal of Neuroscience*, *36*(24), 6431–6444. <https://doi.org/10.1523/JNEUROSCI.0419-16.2016>
- Yoshida, T., Yokobori, T., Kuriyama, K., Sakai, M., Sano, A., Ogawa, H., Sohda, M., Saeki, H., Kuwano, H., & Shirabe, K. (2021). CD36 Expression Is Associated with Cancer Aggressiveness and Energy Source in Esophageal Squamous Cell Carcinoma. *Annals of Surgical Oncology*, *28*, 1217–1227. <https://doi.org/10.1245/s10434-020-08752-8>
- Yu, C., Niu, X., Du, Y., Chen, Y., Liu, X., Xu, L., Iwakura, Y., Ma, X., Li, Y., Yao, Z., & Deng, W. (2020). IL-17A promotes fatty acid uptake through the IL-17A/IL-17RA/p-STAT3/FABP4 axis to fuel ovarian cancer growth in an adipocyte-rich microenvironment. *Cancer Immunology, Immunotherapy*, *69*(1), 115–126. <https://doi.org/10.1007/s00262-019-02445-2>
- Yuan, M., Chen, X., Sun, Y., Jiang, L., Xia, Z., Ye, K., Jiang, H., Yang, B., Ying, M., Cao, J., & He, Q. (2020). ZDHHC12-mediated claudin-3 S-palmitoylation determines ovarian cancer progression. *Acta Pharmaceutica Sinica B*, *10*(8), 1426–1439. <https://doi.org/10.1016/j.apsb.2020.03.008>
- Zaoui, M., Morel, M., Ferrand, N., Fellahi, S., Bastard, J.-P., Lamazière, A., Larsen, A. K., Béréziat, V., Atlan, M., & Sabbah, M. (2019). Breast-Associated Adipocytes Secretome Induce Fatty Acid Uptake and Invasiveness in Breast Cancer Cells. *Cancers*, *11*(2012).
- Zhang, M., Di Martino, J. S., Bowman, R. L., Campbell, N. R., Baksh, S. C., Simon-Vermot, T., Kim, I. S., Haldeman, P., Mondal, C., Yong-Gonzales, V., Abu-Akeel, M., Merghoub, T., Jones, D. R., Zhu, X. G., Arora, A., Ariyan, C. E., Birsoy, K., Wolchok, J. D., Panageas, K. S., ... White, R. M. (2018). Adipocyte-derived lipids mediate melanoma progression via FATP proteins. *Cancer Discovery*, *8*(8), 1006–1025. <https://doi.org/10.1158/2159-8290.CD-17-1371>
- Zhang, J., Planey, S. L., Ceballos, C., Stevens, S. M., Keay, S. K., & Zacharias, D. A. (2008). Identification of CKAP4/p63 as a major substrate of the palmitoyl acyltransferase DHHC2, a putative tumor suppressor, using a novel proteomics method. *Molecular and Cellular Proteomics*, *7*(7), 1378–1388. <https://doi.org/10.1074/mcp.M800069-MCP200>
- Zhang, M. M., Tsou, L. K., Charron, G., Raghavan, A. S., & Hang, H. C. (2010). Tandem fluorescence imaging of dynamic S-acylation and protein turnover. *Proceedings of the National Academy of Sciences of the United States of America*, *107*(19), 8627–8632. <https://doi.org/10.1073/pnas.0912306107>
- Zhang, Q., Wang, H., Mao, C., Sun, M., Dominah, G., Chen, L., & Zhuang, Z. (2018b). Fatty acid oxidation contributes to IL-1 β secretion in M2 macrophages and promotes macrophage-mediated tumor cell migration. *Molecular Immunology*, *94*, 27–35. <https://doi.org/10.1016/j.molimm.2017.12.011>

- Zhang, B., Zhou, B. H., Xiao, M., Li, H., Guo, L., Wang, M. X., Yu, S. H., & Ye, Q. H. (2020). KDM5C Represses FASN-Mediated Lipid Metabolism to Exert Tumor Suppressor Activity in Intrahepatic Cholangiocarcinoma. *Frontiers in Oncology*, 10(June), 1–13. <https://doi.org/10.3389/fonc.2020.01025>
- Zhang, M., Zhou, L., Xu, Y., Yang, M., Xu, Y., Komaniecki, G. P., Kosciuk, T., Chen, X., Lu, X., Zou, X., Linder, M. E., & Lin, H. (2020b). A STAT3 palmitoylation cycle promotes TH17 differentiation and colitis. *Nature*, 586(7829), 434–439. <https://doi.org/10.1038/s41586-020-2799-2>
- Zhao, H., Yan, G., Zheng, L., Zhou, Y., Sheng, H., Wu, L., Zhang, Q., Lei, J., Zhang, J., Xin, R., Jiang, L., Zhang, X., Chen, Y., Wang, J., Xu, Y., Li, D., & Li, Y. (2020). STIM1 is a metabolic checkpoint regulating the invasion and metastasis of hepatocellular carcinoma. *Theranostics*, 10(14), 6483–6499. <https://doi.org/10.7150/thno.44025>
- Zheng Liua, Tangpo Yanga, Xin Lia, Tao Pengb, Howard C. Hangb, and X. D. L. X. D. L. (2015). Integrative chemical biology approaches to examine ‘erasers’ for protein lysine fatty-acylation. *Angew Chem Int Ed Engl*. 2015, 54(4), 1149–1152. <https://doi.org/10.1002/anie.201408763>. Integrative
- Zou, C., Ellis, B. M., Smith, R. M., Chen, B. B., Zhao, Y., & Mallampalli, R. K. (2011). Acyl-CoA:lysophosphatidylcholine acyltransferase I (Lpcat1) catalyzes histone protein O-palmitoylation to regulate mRNA synthesis. *Journal of Biological Chemistry*, 286(32), 28019–28025. <https://doi.org/10.1074/jbc.M111.253385>
- Zou, A. P., Ma, Y. H., Sui, Z. H., De Montellano, P. R. O., Clark, J. E., Masters, B. S., & Roman, R. J. (1994). Effects of 17-octadecynoic acid, a suicide-substrate inhibitor of cytochrome P450 fatty acid ω -hydroxylase, on renal function in rats. *Journal of Pharmacology and Experimental Therapeutics*, 268(1), 474–481.